INAUGURAL - DISSERTATION

zur
Erlangung der Doktorwürde
der
Naturwissenschaftlich-Mathematischen Gesamtfakultät
der
Ruprecht - Karls - Universität
Heidelberg

vorgelegt von

Carlo Dietl (Diplom-Geologe)

aus Mainz

2000

zum Thema:

Structural and Petrologic Aspects of the Emplacement of Granitoid Plutons:

Case Studies from the Western Margin of the Joshua Flat-Beer Creek-Pluton (White-Inyo Mountains, California) and the Flasergranitoid Zone (Odenwald, Germany)

Gutachter: Prof. Dr. Reinhard O. Greiling
PD Dr. Eckardt Stein

Table of contents

Introduction

General statement about pluton emplacement

About 75% of the earth's crust consist of igneous or metamorphosed igneous rocks. Therefore it cannot surprise that the origin and evolution of granitoid bodies is the subject of intense debate since the days of Abraham Gottlob Werner (1749 - 1817) and James Hutton (1726 - 1797). The ideas of "neptunism" and its younger relative "granitization" can be considered obsolate, but the argument goes on. Debate concentrates, however, on processes active during the ascent and emplacement of granitoid melts. Such "granite problems" were discussed only recently, following the recognition of the fundamental importance of magmatism in the evolution of the earth's crust and lithosphere (Paterson et al. 1996):

1) Magmatism is one of the most important heat transfer mechanisms in the earth's crust and has to be regarded as a significant driving force of metamorphism.
2) Igneous processes enable mantle material to be transported into the crust. Consequently, these processes make an eminent contribution to the evolution and growth of the earth's crust in general and the continents in particular. On the opposite, crustal material can be transferred into the mantle during pluton ascent and emplacement, where it can influence the chemistry of and physical processes in the mantle.
3) The high amount of igneous rocks in the continental crust controls its rheology and, therefore, also orogenic mechanisms.
4) The age of plutonic intrusions can be dated by several accurate geochronological methods. Granitoids, therefore, yield a kind of time schedule, in which orogenic processes can be quantified.

To interpret magmatic phenomena correctly, it is imperative to understand ascent and emplacement mechanisms of plutons and particularly, how space is made for a rising granitoid pluton. According to Paterson and Fowler (1993) only a few processes really make space for a pluton being emplaced into the crust:

1) Melting of magma generated in the crust and its ascent, provided that no material exchange across the Moho occurs and therefore addition of mantle material into the earth's crust by, for example, lowering of the Moho is prevented.
2) Deformation of the earth's surface, for example by updoming.
3) Volume loss, for example by cooling.
4) Elastic and plastic contraction of the host rock.

All the other so-called emplacement mechanisms, such as extensional tectonics or stoping, are actually material transfer processes, which do not lead to spacial expansion of the earth's crust by density or volume changes. Paterson and Fowler (1993) differentiate two main material transfer processes:

1) Near field processes, i.e. processes inside the contact aureole of a pluton due to direct interaction of magma and country rock.
2) Far field processes, i.e. processes outside the contact aureole, which make space for the rising pluton by wide-ranging material transport either to the earth's surface, or to the "magma kitchen".

The number of near field material transfer processes, which can remove host rock material from the pathway of the pluton, is limited:

- The pluton can stope blocks of host rock material from its roof and walls, which then either sink towards the floor of the pluton, or are assimilated by the magma.
- Dykes intrude by extension of propagating fractures (Hutton 1992).
- Shallowly intruding laccoliths can dome up their wall rocks or lift them along faults to make space for emplacement.
- The emplacement of a lopolith is accompanied by sinking of the floor of the magma chamber. This was just recently also even for bigger plutonic bodies (McNulty et al. 2000).
- The ascent and emplacement of diapirs requires ductile deformation of the country rocks. In the case of nested diapirs older, not yet entirely solidified magma pulses are pushed aside and downward due to the injection of a new pulse into the magma chamber. This downward flow can also involve the host rock of the diapirs.

- Ballooning (e.g. Ramsay 1989) is an emplacement process, during which several magma pulses intrude subsequently into the same magma chamber leading to its radial expansion and ductile flattening deformation of the host rock and former magma pulses.

Far field processes encompass all types of regional deformational processes, which can account for space making on a regional scale.

During granitoid magma emplacement material properties, especially those of the magma body itself, change dramatically: Temperature drops from at least 900 °C to the "normal" country rock temperature, viscosity and temperature gradients decrease over the range of several magnitudes. The rheology of both the host rock and the magma changes under the influence of temperature and volatile phases. All this happens over a relatively short period of time, some 10^5 to 10^6 years. Therefore, it cannot be expected, that any of the mentioned material transfer processes alone can be responsible for the intrusion of an entire pluton. Only a combination of several material transfer processes may lead to the successful ascent and final emplacement of a pluton. The question remains, which material transfer process is active at which time and place, respectively, during the rise of a pluton. To find a valid solution for the pluton of interest, it is necessary to do extensive field studies of the pluton / wall rock system accompanied by laboratory work, where a variety of methods, such as strain and shape orientation analyses as well as measurements of the anisotropy of the magnetic susceptibility (AMS) are applied. In addition, it is essential to investigate the intrusion conditions, i.e. pressure, temperature, oxygen fugacity, fluid availability and composition. All these parameters influence the viscosity, rheology and permeability of the individual parts of the entire pluton / wall rock system and, consequently, the emplacement mechanisms and their relative importance over space and time.

Overview of the investigated areas

Two areas were chosen to investigate emplacement conditions and mechanisms of granitoid plutons: the Inyo batholith in the White Inyo Range (California) as part of the Mesozoic Western Cordillera of North America and the Flasergranitoid zone in the Bergsträßer Odenwald (Germany) as part of the Variscan orogen. Both batholiths are part of a magmatic

arc (Bateman 1992, Henes-Klaiber 1992, Kreher 1994) and both are composed of several igneous lithologies, which probably were emplaced as nested diapirs in the same magma chamber. These examples also display several differences:

1) While the Inyo batholith can be regarded as a shallow- to mid-crustal pluton (sensu Paterson et al. 1996) intruding into a depth of c. 8 km (Ernst 1996), the plutons of the Flasergranitoid zone were emplaced in the middle to lower crust (sensu Paterson et al. 1996) at about 15 km (Henes-Klaiber 1992).
2) The Inyo batholith, although emplaced synorogenically during the Nevadan orogeny (Nelson et al. 1991) shows no signs of penetrative crystal plastic deformation. In contrast, most plutons of the Flasergranitoid zone show clear indicators for a magmatic origin of the fabric, but also an imprint of ductile crystal plastic deformation of at least the quartz fabric.
3) The third main difference between the Californian and Odenwald settings is the presence or lack of an extended pluton / wall rock system. The Inyo batholith intruded into a Lower Paleozoic metasedimentary sequence, which makes the investigation of processes in the aureole, such as structural evolution due to pluton emplacement and contact metamorphism possible. The Flasergarnitoidzone in the Odenwald, on the other hand, is an intimate assemblage of several small gabbroic to granitic, calk-alkaline plutons, with only minor amounts of metasedimentary country rock remaining.
4) The last main difference are the exposure conditions of both areas. While the White Inyo Mountains as part of the Great Basin and the Basin and Range Province are an arid mountain range with a high relief and therefore spectacular exposure of c. 90% of the rock surface with many three-dimensional sections, the Odenwald as a typical Central European low mountain range with low relief is covered with a rich vegetation and displays only poor exposure.

The study of these two different magmatic systems gives good insights into a number of emplacement mechanisms and conditions of plutons into an arc setting over a wide range of the earth's crust from lower- to upper-crustal conditions (sensu Paterson et al. 1996).

Overview of the contents of the individual chapters

The most important aspects of pluton emplacement at two different crustal levels of magmatic arcs are covered by the thesis, which is a compilation of six chapters and a number of data appendices. The six chapters are in the course of publication:

Chapter 1: Dietl, C. (1999): Emplacement of the Joshua Flat - Beer Creek - Pluton (White Inyo Mountains, California): a story of multiple material transfer processes [published in: Castro, A., Fernandez, C., and Vigneresse, J. L. (eds.) Understanding granites: Integrating new and classical techniques. Geological Society of London, Special Publication, **168**, 161-176.]

Chapter 2: Dietl, C.: Magma mingling and mixing in the Joshua Flat–Beer Creek Pluton: evidence for the interaction of mafic and felsic magmas from remote sensing, field and chemistry investigations [will be submitted to Geological Society of America, Bulletin]

Chapter 3: Dietl, C.: Evaluation of the PT*f* (fluid) conditions in and around a pluton: the intrusion of the Joshua Flat – Beer Creek Pluton (California) [will be submitted to International Journal of Earth Sciences]

Chapter 4: Kontny, A. & Dietl, C.: Relations between metamorphism and magneto-mineralogy in a contact aureole: a case study from the White Inyo Range, Eastern California [submitted to Geological Society of America, Bulletin]

Chapter 5: Dietl, C. & Stein, E. (2001, in press.): The diapiric emplacement and related magmatic fabrics of the porphyritic Ludwigshöhe granite, Central Odenwald (Germany). Mineralogy and Petrology, **72**.

Chapter 6: Stein, E. & Dietl, C. (2001, in press.): Implications of hornblende thermobarometry at granitoids for the meaning of shear zones in the Bergsträßer Odenwald (Germany) Mineralogy and Petrology, **72**.

Since the basic data cannot be presented in full in a normal publication, all the field and laboratory data are compiled in a sequence of appendices.

As a first and major part of the thesis, Chapters 1-4 present, discuss and interpret processes and conditions important for the emplacement of the Joshua Flat - Beer Creek – Pluton, which is the southern part of the Inyo batholith:

While Chapter 1 evaluates the importance of several emplacement processes for the intrusion of the upper- to mid-crustal pluton from the interpretation of field evidence, AMS, quartz c-axis and strain analyses, Chapter 2 deals with the interaction of magmas of different composition during intrusion into the magma chamber of the Joshua Flat–Beer Creek Pluton as nested diapirs. Chapter 3 tries to reconstruct the PT conditions and fluid compositions in this pluton and its aureole by combining phase petrology with geothermobarometry (amphibole-plagioclase and hornblende-clinopyroxene thermometry together with Al-in-hornblende barometry in the pluton; Na-in-cordierite thermometry in the aureole), infra-red spectroscopy at cordierites and one-dimensional numerical modelling. Additionally, this chapter gives insight into the use of amphiboles as thermobarometric index minerals in plutons intruding at different crustal levels by applying and comparing several calibrations of the amphibole-plagioclase thermometer and the Al-in-hornblende barometer. In Chapter 4 silicate and oxide assemblages from the aureole of the Joshua Flat–Beer Creek Pluton together with several geothermobarometers (Ti-in-biotite, Na-in-cordierite and chlorite thermometers, as well as the phengite barometer) are used to determine pressure, temperature and oxygen fugacity conditions during emplacement of the pluton. Moreover, the applicability of the individual thermobarometers is evaluated.

A second, minor part of the thesis is dedicated to different regional examples from the central Bergsträßer Odenwald as a comparison with the magmatic arc in California:

Chapters 5 and 6 are related to pluton emplacement in the Flasergranitoid zone. Both chapters proceed from a master thesis (Dietl 1995), but comprise new data and further results. Chapter 5 refers to magma mingling, as well as hyper- and subsolidus fabrics in the mid-crustal Ludwigshöhe pluton in the Flasergranitoid zone (Odenwald) and their importance for the interpretation of the emplacement of the so-called ”synkinematic Flasergranitoids“. Chapter 6 about plutonism in the Odenwald magmatic arc combines results of geothermobarometry presented by Dietl (1995) and Stein (2000) with newly calculated PT data. Similar to Chapter 3, the results for the individual calibrations of the amphibole-plagioclase thermometer and the

Al-in-hornblende barometer are compared and evaluated. Moreover, the PT data are used to assess the importance of two regional-scale shear zones (between the Frankenstein complex and the Flasergranitoid zone, on the one hand, and the Flasergranitoid zone and the Weschnitz pluton, on the other hand) in this Variscan magmatic arc.

Contributions of the individual authors to the co-authored manuscripts

Whereas the present author wrote most of the Chapters on the Joshua Flat-Beer Creek Pluton by himself, Chapters 4-6 are the product of cooperation with coauthors:
Chapter 4 "Relations between metamorphism and magneto-mineralogy in a contact aureole: a case study from the White Inyo Range, Eastern California" by A. Kontny and C. Dietl is based on silicate and oxide petrography, microprobe (mineral analyses) and XRF (whole rock) measurements, as well as on (temperature dependent) measurements of the magnetic susceptibility on samples by C. Dietl. Silicate petrography was done by C. Dietl, oxide petrography by A. Kontny. Microprobe measurements were carried out jointly by both authors. XRF measurements were done by H.P. Meyer, susceptibility measurements by A. Kontny. The following sections were written by A. Kontny: "Methods of investigation", "Whole rock geochemistry", "Chlorite thermometry", "Phengite barometry", "Oxide assemblages and their chemical composition", "Temperature-dependent magnetic susceptibility and its application for ferromagnetic phase identification". The following sections are by C. Dietl: "Abstract", "Geological setting", "Fe-Mg silicate assemblages", "Ti-in-biotite-thermometry" and "Na-in-cordierite-thermometry". C. 50% of the "Introduction" and 66% of "Discussion and conclusions" were written by A. Kontny and c. 34% by C. Dietl. Altogether A. Kontny contributed c. 65% to the manuscript and C. Dietl c. 35%.

The Chapter "The diapiric emplacement and related magmatic fabrics of the porphyritic Ludwigshöhe granite, Central Odenwald (Germany)" by C. Dietl and E. Stein is based on data, acquired by C. Dietl. The paragraphs "Mesostructures and microfabrics", "The anisotropy of the magnetic susceptibility (AMS)", and "Quartz-c-axes measurements" were entirely written by C. Dietl. Moreover, c. 50% of the paragraphs "Introduction", "Strain/shape orientation analyses", "Summary of the results" and "Conclusions and discussion" are from him. E. Stein wrote the "Summary", the "Zusammenfassung" and the

"Cathodoluminescence" sections, as well as half of the "Introduction", the methodological part of "Strain/shape orientation analyses" and about half of the "Summary of the results" and "Conclusions and discussion". Corrections, suggested by the two referees, were carried out by both authors together. Altogether C. Dietl contributed c. 75% to the manuscript and E. Stein c. 25%.

The Chapter "Implications of hornblende thermobarometry at granitoids for the meaning of shear zones in the Bergsträßer Odenwald (Germany)" by E. Stein and C. Dietl is based on the hypothesis of E. Stein that the two shear zones between the Frankenstein complex and the Flasergranitoid zone, on the one hand, and the Flasergranitoid zone and the Weschnitz pluton, on the other hand, which are generally regarded to seperate the Bergsträßer Odenwald into three major units are of different importance. This hypothesis was tested with thermobarometric data acquired by C. Dietl. E. Stein wrote the following sections of the manuscript: "Summary", "Zusammenfassung", "Regional setting of the Odenwald" (with all its paragraphs) and "Conclusions". C. Dietl wrote the entire "Amphiboles" section, providing all chemical and thermobarometric data. Corrections, suggested by the two referees, were carried out by both authors together. Each of the authors contributed c. 50% of the complete manuscript.

Summary of the results

Results for the Joshua Flat-Beer Creek Pluton

For the Joshua Flat-Beer Creek Pluton (JBP) is a perfectly exposed pluton of the Mesozoic Cordilleran magmatic arc, the pluton / wall rock system was investigated for almost all aspects of pluton emplacement. In the following at first the results for the pluton, such as composition, intrusion sequence, PT data etc., are described, followed by the description of the results for the aureole, including deformation structures, contact metamorphism, PT data etc..

Detailed field mapping at the southwestern rim of the JBP showed the pluton to consist of three distinct phases, probably intruding as nested diapirs: the Marble Canyon Diorite, the

Joshua Flat Monzonite and the Beer Creek Granodiorite. The Joshua Flat Monzonite and the Beer Creek Granodiorite make up *c.* 90 % of the JBP following a concentric pattern with the Joshua Flat Monzonite at the rim of the pluton and the Beer Creek Granodiorite in its center. The Marble Canyon Diorite (a medium- to coarse-grained, hornblende-rich diorite) was found only as xenoliths in the Joshua Flat Monzonite as well as in the Beer Creek Granodiorite; probably the result of brecciation through the latter two phases. Relations between the Joshua Flat Monzonite (a medium-grained monzonite to quartzmonzonite, characterized by hornblende crystals with pyroxene cores and macroscopically visible titanite) and the Beer Creek Granodiorite (a medium- to coarse-grained granodiorite with K-feldspar phenocrysts) are more complex and suggest both to intrude roughly simultaneously, with the granodiorite slightly later as the monzonite. A c. 3 km wide and 5 km long banding zone at the western rim of the JBP is the most impressive example for the complexity of this relationship. The banding zone was detected by remote sensing using thermal infra-red multispectral scanner (TIMS) data. Through detailed field work in the banding zone a wide range of magma interaction fabrics was established. Hybrid rocks with characteristic features of both main lithologies, such as hornblende crystals with pyroxene cores (monzonite) and K-feldspar phenocrysts (granodiorite), point to mixing between them. Bands, schlieren and enclaves of finegrained monzonite in the granodiorite and vice versa are hints for mingling between both. Finally, granodioritic dykes in the monzonite and monzonitic xenoliths in the granodiorite indicate brecciation of the Joshua Flat Monzonite by the Beer Creek Granodiorite. Major element mixing tests, according to the method established by Fourcade and Allegre (1981), carried out at rocks from the banding zone confirm the field observations of mixing between the two magmas. The different styles of magma interaction are explained by the increasing volume of granodiorite reacting with the monzonite over time: first, a high monzonite-granodiorite ratio led to mixing and the formation of hybrid magmas, while the increasing amount of felsic magma over time, and the consequentely increasing viscosity contrast, resulted in mingling followed by the brecciation of the Joshua Flat Monzonite by the Beer Creek Granodiorite.

A magmatic foliation was developed late during the magmatic history of the pluton in the two main igneous rock types of the JBP. This prominent fabric crosscuts intraplutonic contacts,

strikes generally NNW, dips steeply and is associated with a steep magmatic lineation made up by hornblende and/or mircrogranitoid enclaves. Close to the contact with the host rock the magmatic foliation turns into a concentric, contact-parallel pattern, what can be explained as an effect of deceleration flow close to the pluton´s wall. A subsolidus penetrative deformation inside the pluton was not observed. Mylonitic shear zones were found only locally at the pluton´s rim. Further intrusion processes observed inside the pluton or in the immediate contact to the wall rocks are diking and stoping. By these two, partly connected processes the pluton intrudes its own ductile structural aureole as is proven by stoped blocks with a ductile structural inventory.

Determination of the anisotropy of the magnetic susceptibilty (AMS) is a good tool to prove weak fabrics (Tarling and Hrouda 1993). AMS measurements carried out on oriented samples from the pluton give further insight into the wide spectrum of magmatic processes active in the JBP: All lithological units of the JBP are ferromagnetic. Consequently the main carrier of the magnetic susceptibility is magnetite, with biotite and hornblende as minor contributons. The magnetic foliation is oriented parallel with the magmatic foliation implying the simultaneous formation of both. Investigations regarding the viscosity contrast between the carrier of susceptibility (magnetite) and the magma (Hrouda & Lanza 1989) suggest the magnetic foliation, and therefore also the magmatic foliation, to have developed late in the magmatic state of the JBP. Steep magnetic lineations are interpreted to represent a magmatic flow fabric indicating magma transport from the pluton´s bottom or even its source region into the roof region. The much stronger anisotropy of the AMS ellipsoids measured in the JFM compared to the BCG as well as the increasing ellipticity of the indivudal AMS ellipsoids towards the contact between the two igneous phases are interpreted to be the products of the pluton's late stage inflation due to the intrusion of the BCG into the limited space of the magma chamber. The generally oblate character of all AMS ellipsoids, probably developed under coaxial flattening conditions, may support such a scenario.

Two geothermometers and one barometer were applied to determine the PT conditions in the Joshua Flat Monzonite and the Beer Creek Granodiorite during their emplacement: the amphibole-plagioclase-thermometer (Blundy and Holland 1990, Holland and Blundy 1994) and, because of clinopyroxene and hornblende occuring together in the monzonite, the

hornblende-clinopyroxene thermometer (Perchuk et al 1985). Since the Joshua Flat Monzonite and the Beer Creek Granodiorite contain the mineral assemblage quartz + K-feldspar + plagioclase ($an_{25–35}$) + biotite + Mg-hornblende + titanite + magnetite/ilmenite it was possible to apply the Al-in-hornblende barometer (Hammarstrom and Zen 1986, Hollister et al. 1987, Johnson and Rutherford 1989, Schmidt 1992, Anderson and Smith 1995). PT conditions for the crystallisation of the JBP, determined by these geothermobarometers, can be summarized as follows: The pluton intruded at a depth of c. 8 km (corresponding to a confining pressure of c. 0.24 GPa derived from Al-in-hornblende barometry) and over a temperature interval from c. 900 (upper limit of the temperature data derived from the hornblende-clinopyroxene thermometer) to c. 640°C (lower limit of the temperature data derived from the amphibole-plagioclase thermometer). Moreover, the application of several calibrations for both the amphibole-plagioclase thermometer and the Al-in-hornblende barometer allowed to evaluate the quality of the individual calibrations. All three calibrations of the thermometer yield about equivalent results for the indivdual samples. This observation matches the findings of Anderson (1996) that all three calibrations of the amphibole-plagioclase-thermometer give similar results when applied to relatively shallowly intruding plutons. Of the two applied calibrations of the Al-in-hornblende barometer the one of Anderson and Smith (1995) contains a temperature correction term. This term applies a correction to all pressure data, which were determined for amphiboles crystallizing above the wet granitic solidus (675°C according to Anderson and Smith 1995) and lowers these pressure data significantly. Application of this calibration gave good results, particularly for one sample from the Joshua Flat Monzonite, where hornblende crystallized at a temperature of c. 740°C. Application of the calibration by Schmidt (1992) to this sample resulted in pressure data averaging at 0.34 GPa, while pressure data for all other samples averaged around 0.24 GPa. Recalculation with the barometer of Anderson and Smith (1995) resulted in similar pressure data (c. 0.25 GPa) as for the other samples.

Several field and thin section observations, such as clinopyroxene in the monzonite and biotite inclusions in hornblende in all lithologies, as well as late magmatic pegmatites, indicate, that the pluton developed from H_2O-undersaturated to H_2O-saturated conditions.

Structures observed in the c. 2 km wide contact aureole document several emplacement mechanisms such as stoping and dyking, ductile downward flow, partial melting and magma chamber expansion. Steeply dipping strata, boudins with steeply plunging long axes and steeply plunging mineral lineations (partly by cordierite or andalusite) as well as kinematic indicators (σ- and δ-porphyroclasts and asymetrical shear folds) point to vertical movement of the country rocks relative to the JBP. For strata all around the entire pluton getting younger towars the intrusion, forming a funnel-like structure, it must assumed, that the aureole material was moved down relative to the rising pluton. From all these observations "ductile downward flow“ (Stein 2000) is proposed as one emplacement mechanism for the JBP. This material transfer process takes country rock from the area of the evolving magma chamber towards the pluton´s source region and makes space for the rising pluton. Other kinematic indicators show that synchronously with the ductile downward flow aureole material is transported horizontally parallel with the contact from zones. Ductile downward flow seems to be active already in the early evolution of the magma chamber. Later during the intrusion of further magma pulses the pluton expands and inflates in the horizontal, leading to a thinning of the aureole of about 30%. The field mapping shows clearly that a complex interplay of different emplacement mechanisms (ductile downward flow, stoping, diking and assimilation) was required to make the rise and the intrusion of the JBP possible. The relative importance of the different emplacement mechanisms through time is probably as follows: the Marble Canyon Diorite probably intruded as dyke or sill, whereas stoping and dyking, ductile downward flow together with assimilation acted during the emplacement of the Joshua Flat Monzonite. Magma chamber expansion represents only the latest stage of intrusion during the emplacement of the Beer Creek Granodiorite into the already existing magma chamber of the JBP.

Strain measurements using the Rf/ϕ-method (Ramsay 1967, Lisle 1985) were carried out along the same cross-section as the quartz-c-axes measurements. Pinitised cordierite porphyro-blasts were used as markers. Strain ellipsoids have a general prolate shape, indicating constrictional strain in the structural aureole. The x-axes of the individual ellipsoides plunge moderately to steep towards the SW, consistent with the ductile downward

flow of aureole material. The xy-planes of the individual strain ellipsoids lie parallel with the ss/s_1-planes of the aureole rocks and dip steeply towards the E or SE. High E_S values (Nadai 1963) close to the pluton and lower values further away from it point to the influence of the JBP´s forceful emplacement on the strain history of the aureole rocks. Moreover, the strain analyses show the influence of the pluton emplacement even on those strata which are not lying parallel with the pluton / wall rock contact.

Quartz-c-axes measurements carried out along a cross-section to the W of the JBP confirm the field observations, but also yield a much more detailed insight into the deformation processes in and near the contact aureole. In a c. 400 m wide zone at the contact to the JBP ductile downward flow (Stein 2000) under simple shear as well as pure shear is indicated by obliquely oriented yz girdles and Type II cross girdles. With increasing distance (a zone between 400 m and 700 m away from the pluton) to the pluton the quartz-c-axes fabric points at vertical as well as horizontal, dextral material transport parallel with the pluton contact. All measured quartz fabrics have medium to high temperature character (350 - 650°C), according to Passchier and Trouw (1996), and were built using basal and prism slip in <a>. Therefore these fabrics can be interpreted as being associated with the heating of the aureole rocks through the intrusion of the JBP. About 1 km away from the pluton the character of the quartz-c-axes fabrics changes. A weak high temperature influence can still be observed, but in general the crystallographic quartz fabrics are defined by external rotation. These fabrics can be correlated with the pre-intrusive deformation under greenschist facies conditions.

Detailed field and thin section petrography together with several geothermometers and the phengite geobarometer were used to get information about the PT conditions during contact metamorphism. The biotite zone (distance to JBP: > 2000 m) preserves the regional metamorphic history of the metasediments, while mineral assemblages in the andalusite-cordierite (distance to JBP: 2000-500 m), sillimanite (distance to JBP: 500-300 m) and cordierite-K-feldspar zone (distance to JBP: < 300 m) indicate increasing contact metamorphism with decreasing distance from the pluton up to incipient migmatisation in the innermost zone. Partial melting due to the dehydration reaction sillimanite + biotite + plagioclase + quartz --> cordierite + K-feldspar + melt (Le Breton and Thompson 1988) is

documented by numerous leucocratic veins in this zone. Na-in-cordierite thermometry (Mirwald 1986) yields peak temperatures of c. 730 °C for the highest contact metamorphic zone, whereas the Ti-in-biotite thermometer (Patiño Douce 1994) gives unreasonable temperatures of c. 555°C for the innermost aureole and of about 675°C for the external zones. This is explained by the stronger increase of Al relative to Ti with increasing contact metamorphic grade. Application of four different calibrations of chlorite thermometers (Cathelineau 1988; Kranidiotis and MacLean 1987, Jowett 1991, Walshe 1986) results in temperatures ranging from 280° to 420°C for the (hydrothermal) retrograde branch of the contact metamorphic path. Phengite barometry (Massonne & Schreyer 1987) indicates pressures between 0.2 and 0.3 GPa for retrograde assemblages.

To get information about the fluid conditions during contact metamorphism infra-red spectroscopy at cordierites was carried out. The measurements showed relatively low contents of channel volatiles in cordierite from pelites (H_2O: 0.76 to 0.85 wt.% and CO_2: 0.06 to 0.13 wt.%). This indicates that contact metamorphism took place under water undersaturated conditions (Jochum 1986, Carrington and Harley 1996).

Information about the evolution of oxygen fugacity with increasing contact metamorphism was obtained from magnetomineralogical investigations, such as oxide petrography and susceptibility measurements both at room temperature and temperature-dependent. According to petrographic research the regional metamorphic oxide assemblage ilmenite + rutile $\pm$ hematite observed in the biotite zone is overprinted during contact metamorphism and magnetite and ilmenite-hematite solid solutions are formed, which, according to Lindsley (1991), form a stable oxide assemblage at c. 600°C. In the cordierite-K-feldspar zone ilmenite together with white mica occurs. The observed prograde changes in magnetic mineralogy are related to (1) an increase of temperature from the biotite toward the cordierite-K-feldspar zone and (2) increasing log $f(O_2)$ conditions in the cordierite-K-feldspar zone. During retrograde metamorphism, oxygen fugacity declines towards the hematite-magnetite buffer line and eventually goes across this line into the field of magnetite at about 300°C. The magneto-mineralogical changes explain the behaviour of magnetic susceptibility and thermomagnetic curves. Susceptibilities in the biotite zone generally range from 200 – 500 x

10^{-6} SI units, typical for paramagnetic minerals. Samples from the andalusite-cordierite and transition zones give an inhomogeneous distribution of the magnetic susceptibility between 300 and 28000 x 10^{-6} SI units due to varying amounts of magnetite. Thermomagnetic curves for these zones give Curie temperatures of 590°, typical for pure magnetite, and 550° as well as 340°C that are related to Ti-bearing hematite phases (maghemite). Magnetic susceptibility measurements of samples from the cordierite-K-feldspar zone result in values suggesting a mixture of paramagnetic with small amounts of ferrimagnetic minerals (200 – 2000 x 10^{-6} SI units). Thermomagnetic investigations indicate that small amounts of magnetite are present in this zone but that most of the ferrimagnetic components were decomposed during a retrograde overprint by hydrothermal fluids probably associated with the cooling of the pluton. It is assumed that pre-existing magnetic isograde, which developed during the prograde contact metamorphism, are destroyed by these retrograde reactions.

Finally, the geothermobarometric results on rocks from the pluton and its aureole and the fluid investigations were combined with numerical modelling to get insight into the Tt path of the pluton / wall rock system. Application of the one-dimensional program ”CONTACT” (Peacock 1989) resulted in temperatures, which are too low relative to those determined by geothermometry, at least for the cordierite-K-feldspar zone. This discrepancy is explained by the complex geometry of the pluton, probably due to its diapiric nature, which cannot be modelled with the one-dimensional program.

Results for the Odenwald

The Bergsträßer Odenwald as part of the Mid-German Crystalline Rise comprises about 90% magmatic rocks of a calcalkaline suite (Henes-Klaiber 1992) and about 10% meta-sediments. The magmatic rocks show a general zonation from N to S with basic gabbros and diorites in the N (so called Frankenstein complex), intermediate granodiorites in the central part (Flasergranitoid zone) and acidic granites in the S (southern Bergsträßer Odenwald). Hornblende and biotite K/Ar-cooling ages (Kreuzer and Harre 1975, Kirsch et al. 1988) tie the intrusion of the plutons in a range between 363 Ma for the northern and 320 Ma for the southern Odenwald. The magmatic rocks are seperated by six narrow zones of metamorphic

rocks. These zones are oriented NE-SW. Characteristic mineral assemblages with sillimanite, andalusite and cordierite indicate a HT-LP-metamorphic imprint.

A zone of special interest is the so called Flasergranitoid-Zone in the Northcentral Odenwald. This zone is characterized by an intimate association of basic gabbros and diorites, intermediate granodiorites and acidic granites. Most of the magmatic rocks show a pronounced planar fabric which was interpreted either as tectonic in origin due to an intrusion in a transtensional regime (Krohe 1991, 1994) or as magmatic due to the successive emplacement of different plutons (Stein 1996, 2000). The porphyritic Ludwigshöhe granite, a very distinct, elliptical, 1 km^2 large, NE-SW striking pluton provides a lot of information concerning this problem. The porphyritic Ludwigshöhe granite is characterized by a NE-SW trending, steeply dipping planar fabric, which is due to the alignement of the mafic minerals biotite and hornblende as well as of about 2 cm large K-feldspar-phenocrysts (Fig. 9) lying in a middelgrained matrix. Furthermore this fabric is pronounced by finegrained, pancake shaped, microdioritic enclaves with their long axes oriented parallel to the foliation. Inclusions in different minerals point to a typical magmatic crystallization succession: ore minerals → plagioclase → hornblende → biotite → K-feldspar → quartz. Twinning in feldspars (albite and perikline twins in plagioclase and Karlsbad twins in K-feldspar) and hornblende is parallel to their long axes and parallel to the foliation, which is typical for the magmatic state (Paterson et al. 1989). No penetrative ductile solid state deformations can be observed in both the feldspars, as well as in hornblende and biotite. Quartz is the only mineral with ductile fabrics, ranging from undulous extinction, subgrain boundaries, chess board patterns to recrystallization. According to the findings of Kruhl (1996) on chess board patterns in quartz, the ductile quartz fabrics in the Ludwigshöhe granite probably developed at the solidus just before or immediately after the complete solidification of the granite and therefore are labeled as ”solid-state“. Cathodoluminescence investigations of quartz showing blue/violet colours give further evidence for the high temperature, probably magmatic nature of quartz (Zinkernagel 1978).

The strain/shape orientation analyses using the R_f/Φ-method (Ramsey 1967, Lisle 1985) was carried out at quartz, plagioclase, biotite and hornblende in thin sections, at K-feldspar in polished slices of three perpendicular orientations. These different minerals were used because they crystallized at different times and stages during the magma´s solidification history. Though quartz is strongly deformed it was possible to use it for strain analysis, because the cathodoluminescence made the old magmatic grains visible. To describe the magmatic strain history of the enclaves oriented pictures of an outcrop were used. While hornblende, plagioclase, K-feldspar show prolate ellipsoids plotting in the field of apparent constriction, biotite with an oblate ellipsoid plots in the field of apparent flattening. Most K-values range between 1.3 and 2.6. Only quartz has a significant higher K-value (335.13) due to its ductile solid state deformation. According to empirical data it can be assumed that K-values ≤ 1.5 are rather controlled by the mineral´s shape than by deformations. The strain ellipsoid of the microdioritic enclaves is oblate indicating a synmagmatic flattening during the emplacement of the granite. In the stereo net projection the xy-planes of the strain/shape orientation ellipsoids are parallel to the magmatic foliation pointing to the same magmatic origin.

The AMS measurements were carried out at the porphyritic granite and at the microdioritic enclaves. The mean susceptibility for the granite is about 10^{-2} SI which is typical for magnetite. In the enclaves the mean susceptibility ranges from 10^{-2} SI (typical for the ferrimagnetic mineral magnetite) to 10^{-4} SI (typical for the paramagnetic minerals hornblende, biotite and ilmenite). The low anisotropy factor P´ of about 1.1 in an enclave points to a magmatic flow texture, whereas P´-values ranging from 1.27 to 1.63 SI in the porphyritic granite are probably the result of ductile deformation in the magmatic state (Hrouda 1982). The AMS ellipsoids of all the samples are oblate problably due to deformation in the magmatic state. The magnetic and magmatic foliation are parallel one to another. The magnetic lineation (x-axis of the AMS ellipsoid) dips gently to the ENE or WSW.

Quartz-c-axes measurements were done within three samples of the Ludwigshöhe granite. In total 900 quartz-c-axes were measured, which were plotted in a stereo net with reference to the main axis of the average shape orientation ellipsoid. The resulting patterns are a pseudo-

two-girdle with an opening angle of 140° (Sander 1950) and subordinate a maximum V distribution (Sander 1950). The cone axes of both small circle distributions are shifted against each other by an angle of about 30°. The pseudo-two-girdle is oriented parallel to the xy-plane of the shape orientation ellipsoid and to the magnetic and magmatic foliatons. This is interpreted as evidence for their development under the same NW-SE directed stress field. A pseudo-two-girdle with a wide opening angle and forms during axial symmetric shortening under high temperature conditions and low strain rates (Tullis et al. 1973), what is in good accordance with the microstructural and cathodoluminescence observations. The measured pseudo-two-girdle appears in the Flinn diagram in the field of apparent flattening (Schmid and Casey 1986), again pointing to the cogenetic origin of the quartz fabric and the other observed and measured fabrics. The maximum V and its oblique orientation with respect to the pseudo-two-girdle can be interpreted as a result of a later solid state shear deformation (Vollbrecht 1981), which only affected the quartz fabric.
In conclusion the prevailing hyper- and near-solidus fabrics, which are preserved in the porphyritic Ludwigshöhe granite, are interpreted as the result of the contemperaneous intrusions of a lot of small plutons, which led to space problems resulting in a forcible emplacement with ballooning processes.

Another interesting problem in the Crystalline Bergsträßer Odenwald deals with the nature of the boundaries between its three major units (Frankenstein complex, Flasergranitoid zone and southern Bergsträßer Odenwald). According to literature, they are separated by two major shear zones. The importance of these sutures was evaluated by comparing own new hornblende geothermobarometry data from five plutons of the Flasergranitoid zone with published PT data from the entire Bergsträßer Odenwald. Temperatures were calculated with the three calibrations of the amphibole-plagioclase thermometer (Blundy and Holland 1990, Holland and Blundy 1994). Determinations of the intrusion depth was done with five calibrations of the Al-in-hornblende barometer (Hammarstrom and Zen 1986, Hollister et al. 1987, Johnson and Rutherford 1989, Schmidt 1992, Anderson and Smith 1995). The use of three different calibrations amphibole-plagioclase thermometer and of five different calibrations of the Al-in-hornblende barometer provides the opportunity to evaluate these

calibrations. All three calibrations of the thermometer yield temperature data differing significantly from each other. While the calibration of Blundy and Holland (1990) gave temperatures between 700 and 790°C for the investigated granitoids, thermometer A of Holland and Blundy (1994) resulted in temperature data in the range 640 to 740°C. Thermometer B of Holland and Blundy (1994) gives even lower temperatures ranging from 600 to 660°C. The observation of different calibrations giving significantly different temperatures is, according to Anderson (1996), typical for mid-crustal plutons. The mid-crustal nature of the plutons from the Flasergranitoid zone is verified by all five calibrations of the Al-in-hornblende barometer. All of them give reasonable results between 0.3 and 0.65 GPa (10 to 20 km) for the individual plutons, with the calibration of Johnson and Rutherford (1989) providing the lowest and the calibration of Schmidt 1992 providing the highest pressure data. Comparison of these new PT data with published PT data from the southern Bergstäßer Odenwald (Henes-Klaiber 1992), which range from 0.53 to 0.57 GPa, do not allow to postulate a major suture between the two zones. On the other hand, comparison of PT data from the Flasergranitoid zone and the Frankenstein complex (c. 0.15 to 0.2 GPa according to Kreher 1994) verify the importance of this shear zone. These findings are confirmed by the comparison of published radiometric, geochemical and structural data (e. g. Kreuzer and Harre 1975, Kirsch et al. 1988, Altherr et al. 1999, Stein 2000). Moreover, our PT data show, that the HT-LP metamorphism in the Bergsträßer Odenwald can also be interpreted as contact metamorphism and not necessarily as regional metamorphism.

References

Altherr, R., Henes-Klaiber, U., Hegner, E., Satir, M. & Langer, C. 1999. Plutonism in the Variscan Odenwald (Germany): from subduction to collision. International Journal of Earth Sciences, **88**, 422-443.

Anderson, J. L. 1996. Status of thermobarometry in granitic batholith. Transactions of the Royal Society of Edinburgh: Earth Sciences, **87**, 125-138.

Anderson, J. L. & Smith, D. R. 1995. The effects of temperature and f_{O2} on the Al-in-hornblende barometer. American Mineralogist, **80**, 549-559.

Bateman, P. C. 1992. Plutonism in the central part of the Sierra Nevada batholith, California. United States Geological Survey Professional Paper, **1483**.

Blundy, J. D. & Holland, T. J. B. 1990. Calcic amphibole equilibria and a new amphibole-plagioclase geothermometer. Contributions to Mineralogy and Petrology, **104**, 208-224.

Carrington, D. P. & Harley, S. L. 1996. Cordierite as a monitor of fluid and melt H_2O contents in the lower crust: An experimental calibration. Geology, **24**, 647-650.

Cathelineau, M. 1988. Cation site occupancy in chlorites as a function of temperature. Clay Minerals, **23**, 471- 485.

Dietl, C. 1995. Gefügeuntersuchungen und Mineralanalytik am porphyrischen Granit der Ludwigshöhe/Odw. Unpublished MSc thesis, TU Darmstadt.

Ernst, W. G. 1996. Petrochemical study of regional/contact metamorphism in metaclastic strata of the central White-Inyo Range, eastern California. Geological Society of America Bulletin, **108**, 1528-1548.

Fourcade, S. & Allegre, C. J. 1981. Trace elements behaviour in granite genesis: a case study the calc-alkaline plutonic association from the Querigut Complex (Pyrenees, France). Contributions to Mineralogy and Petrology, **76**, 177-195.

Hammarstrom, J. M. & Zen, E. 1986. Aluminium in hornblende: An empirical igneous geobarometer. American Mineralogist, **71**, 1297-1313.

Henes-Klaiber, U. 1992. Zur Geochemie der variszischen Granitoide des Bergsträßer Odenwaldes. Unpublished PhD thesis, TU Karlsruhe.

Holland, T. J. B. & Blundy, J. D. 1994. Non-ideal interactions in calcic amphiboles and their bearing on amphibole-plagioclase thermometry. Contributions to Mineralogy and Petrology, **116**, 433-447.

Hollister, L. S., Grissom, G. C., Peters, E. K., Stowell, H. H. & Sisson, V. B. 1987. Confirmation of the empirical correlation of Al in hornblende with pressure of solidification of calc-alkaline plutons. American Mineralogist, **72**, 231-239.

Hrouda, F. 1982. Magnetic anisotropy of rocks and its application in geology and geophysics. Geophysical Survey, **5**, 37-82.

Hrouda, F. & Lanza, R. 1989. Magnetocrystalline anisotropy of rocks and massiv ores: a mathematical model study and its fabric implications. Physics of the Earth and Planetary Interiors, **56**, 337-348.

Hutton, D. H. W. 1992. Granite sheeted complexes: evidence for the dyking ascent mechanism. Transactions of the Royal Society of Edinburgh: Earth Sciences, **83**, 377-382.

Jochum, C. 1986. Experimentelle Untersuchungen zum Wassereinbau und zur Kinetik der Hydratation und Dehydratation von synthetischen und natürlichen Cordieriten. Unpublished PhD thesis, University of Bochum.

Johnson, M. C. & Rutherford, M. J. 1989. Experimental calibration of the aluminium-in-hornblende geobarometer with applications to Long Valley caldera (California) volcanic rocks. Geology, **17**, 837-841.

Jowett, E.C. 1991. Fitting iron and magnesium into the hydrothermal chlorite geothermometer. GAC/AGC - MAC/AMC - SEG, program with abstracts, **16**, A62.

Kirsch, H., Kober, B. & Lippolt H. J. 1988. Age of intrusion and rapid cooling of the Frankenstein gabbro (Odenwald, SW-Germany) evidenced by $^{40}Ar/^{39}Ar$ and single-zircon $^{207}Pb/^{206}Pb$ measurements. Geologische Rundschau, **77**, 693-711.

Kranidiotis, P. & MacLean, W. H. 1987. Systematics of chlorite alteration at the Phelps Dodge Massive Sulphide Deposit, Matagami, Quebec: Economic Geology, **82**, 1898-1911.

Kreher, B. 1994. Petrologie und Geochemie der Gabbrointrusionen des Frankensteins (Odenwald). Geologisches Jahrbuch Hessen, **122**, 81-122.

Kreuzer, H. & Harre, W. 1975. K/Ar-Altersbestimmungen an Hornblenden und Biotiten des Kristallinen Odenwalds.- In: Amstutz, G. C., Meisl, S. & Nickel, E. (eds.) Mineralien und Gesteine im Odenwald. Aufschluß, Sonderband **27**, 71-77.

Krohe, A. 1991. Emplacement of synkinematic plutons in the Variscan Odenwald (Germany) controlled by transtensional tectonics. Geologische Rundschau, **80**, 391-409.

Krohe, A. 1994. Verformungsgeschichte in der mittleren Kruste eines magmatischen Bogens - der variszische Odenwald als Modellregion. Geotektonische Forschung, **80**, 1-147.

Kruhl, J. H. 1996. Prism- and basis-parallel subgrain boundaries in quartz: a microstructural geothermobarometer. Journal of Metamorphic Geology, **14**, 581-589.

Le Breton, N. & Thompson, A. B. 1988. Fluid absent (dehydration) melting of biotite in metapelites in the early stages of crustal anatexis: Contributions to Mineralogy and Petrology, **99**, 226-237.

Lindsley, D. H. 1991. Experimental studies of oxide minerals. Reviews in Mineralogy, **25**, 69-106.

Lisle, R. J. 1985. Geological strain analysis: A manual for the R_f/Φ method. Pergamon Press, Oxford.

Massonne, H.-J. & Schreyer, W. 1987. Phengite geobarometry based on the limiting assemblage with K-feldspar, phlogopite, and quartz: Contributions to Mineralogy and Petrology, **96**, 212-224.

McNulty, B. A., Tobisch, O. T., Cruden, A. R. & Gilder, S. 2000. Multistage emplacement of the Mount Gives pluton, Central Sierra Nevada batholith, California. GSA Bulletin, **112**, 119-135.

Mirwald, P. W. 1986. Ist Cordierit ein Geothermometer?. Fortschritte der Mineralogie, **64**, 119.

Nadai, A. 1963. Theory of flow and fracture of solids. McGraw-Hill, New York.

Nelson, C. A., Hall, C. A. Jr. & Ernst, W. G. 1991. Geologic history of the White-Inyo Range. - In: Hall, C. A. Jr. (ed.) Natural hitsory of the White-Inyo Range, California. University of California Natural History Guides, **55**, 42-47.

Passchier, C. W. & Trouw, R. A. J. 1996. Microtectonics. Springer, Berlin.

Paterson, S. R., Fowler, T. K. Jr. & Miller, R. B. 1996. Pluton emplacement in arcs: a crustal-scale exchange process. Transactions of the Royal Society of Edinburgh: Earth Sciences, **87**, 115-123.

Paterson, S. R. & Fowler, T. K. Jr. 1993. Re-examining pluton emplacement processes. Journal of Structural Geology, **15**, 781-784.

Paterson, S., Vernon, R. H. & Tobisch, O. T. 1989. A review of criteria for the identification of magmatic and tectonic foliations in granitoids. Journal of Structural Geology, **11**, 349-363.

Patiño Douce, A. E. 1994. Titanium substitution in biotite: an empirical model with applications to thermometry, O_2 and H_2O barometries, and consequences for biotite stability. Chemical Geology, **108**, 133-162.

Peacock, S. M. 1989. Thermal modeling of metamorphic pressure-temperature-time paths: a forward approach. - In: Spear, F.S. & Peacock, S. M. (eds.) Metamorphic Pressure-Temperature-Time Paths, **7**, 57-102.

Perchuk, L. L., Aranovich, L. Y., Podlesskii, K. K., Lavrant'eva, I. V., Gerasimov, V. Y., Fed'kin, V. V., Kitsul, V. I., Karsakov, L. P., Berdnikov, N. V. 1985. Precambrian granulites of the Aldan Shield, eastern Siberia, USSR. Journal of Metamorphic Geology, **3**, 265-310.

Ramsay, J.G. 1989. Emplacement mechanics of a granite diapir: the Chindamora batholith, Zimbabwe. Journal of Structural Geology, **11**, 191-210.

Ramsay, J. G. 1967. Folding and fracturing of rocks: McGraw-Hill, New York.

Sander, B. 1950. Einführung in die Gefügekunde der geologischen Körper. II. Teil. Springer, Wien.

Schmid, S. M. & Casey, M. 1986. Complete fabric analysis of some commonly observed quartz c-axis patterns. Mineral and Rock Deformation: Laboratory Studies The Paterson Volume. Geophysical Monograph, **36**, 263-286.

Schmidt, M. W. 1992. Amphibole composition in tonalite as a function of pressure: an experimental calibration of the Al-in-hornblende barometer. Contributions to Mineralogy and Petrology, **110**, 304-310.

Stein, E. 1996. Untersuchungen zur Genese der Flasergranitoid Zone des zentralen Odenwaldes - Magmatische und/oder tektonische Gefüge. Zeitschrift für geologische Wissenschaften, **24**, 573-583.

Stein, E. 2000. Zur Platznahme von Granitoiden - Vergleichende Fallstudien zu Gefügen und Platznahmemechanismen aus den White-Inyo Mountains, California, USA und dem Bergsträßer Odenwald. Geotektonische Forschung, **93**, 1-330.

Tarling, D. H. & Hrouda, F. 1993. The magnetic anisotropy of rocks. Chapman & Hall, London.

Tullis, J., Christie, J. M. & Griggs, D. T. 1973. Microstructures and preferred orientations of experimentally deformed quartzites. Geological Society of America Bulletin, **84**, 297-314.

Vollbrecht, A. 1981. Tektogenetische Entwicklung der Münchberger Gneismasse (Quarzkorngefüge-Untersuchungen und Mikrothermie an Flüssigkeitseinschlüssen). Göttinger Arbeiten zur Geologie und Paläontologie, **24**, 1-122.

Walshe, J. L. 1986. A six-component chlorite solid solution model and the conditions of chlorite formations in hydrothermal and geothermal systems: Economic Geology, **81**, 681-703.

Zinkernagel, U. 1978. Cathodoluminescence of quartz and its application to sandstone petrology. Contributions to Sedimentology, **8**, 1-69.

Emplacement of the Joshua Flat-Beer Creek Pluton (White Inyo Mountains, California): a story of multiple material transfer processes

CARLO DIETL
Ruprecht-Karls-Universität Heidelberg, Geologisch-Paläontologisches Institut, Im Neuenheimer Feld 234, D-69120 Heidelberg, Germany
(e-rnail: f16@ ix.urz.uni-heidelberg.de)

Abstract: The Joshua Flat-Beer Creek Pluton (JBP) in the White Inyo Mountains, California, is part of the Inyo batholith, which intruded a Neoproterozoic to Lower Cambrian metasedimentary sequence at about 180-160 Ma ago. Contact metamorphism around the JBP reached hornblende-hornfels- to lower amphibolite-facies conditions. The intrusion consists of three distinct phases. Field relations suggest an intrusion sequence Marble Canyon Diorite-Joshua Flat Monzonite Beer Creek Granodiorite as nested diapirs. In the Marble Canyon Diorite as well as the Joshua Flat Monzonite the subsequent intrusions led to brecciation and stoping, but also to mingling and mixing between the Joshua Flat Monzonite and the Beer Creek Granodiorite. Fabrics in the contact aureole document several emplacement mechanisms such as stoping and dyking, ductile downward flow, partial melting and magma chamber expansion. The relative importance of the different emplacement mechanisms through time is as follows: the Marble Canyon Diorite probably intruded as dyke/sill, whereas stoping and dyking, ductile downward flow together with assimilation acted during the emplacernent of the Joshua Flat Monzonite. Magma chamber expansion represents only the latest stage of intrusion during the emplacement of the Beer Creek Granodiorite into the already existing magma chamber of the JBP. AMS, quartz c-axis and strain measurements support the field observations.

Since the question about the origin of granitoids was decided for the 'plutonistic' faction in the 1950s, geoscientists argue about the main problem of pluton emplacement: which processes make space for a rising molten batch of rock? As one result of the debate two major schools were established, one preferring dyking the other diapirism as the main intrusion mode.

Magmatic overpressure acting in individual dykes together with an extensional regional stress regime and a final forceful expansion of the magma chamber are proposed by 'dykers' to be the major emplacement process for constructing an extended magma chamber. In contrast, to 'diapirists' buoyancy and vertical material transport are the most important features for the ascent and emplacement of plutons.

As already stated by Paterson & Fowler (1993) most emplacement processes do not really make space for a rising pluton, but lead to a replacement and redistribution of the wall rocks due to horizontal and vertical material-transfer processes. But, according to Buddington (1959), a combination of several material-transfer processes active at different times and places during the ascent and emplacement can enhance and accelerate the intrusion of a pluton.

Field observations in the aureole and the pluton provide information regarding the relative importance of individual material-transfer processes and the overall emplacement mode: dyking or diapirism. Clemens *et al.* (1997) suggest several field relations, although very simplified, which indicate if a pluton is a diapir or not. These are in the aureole: (l) narrow high temperature shear zones; (2) steep lineations; (3) rim synclines; (4) pluton-side-up kinematics; and in the pluton: (1) steeply plunging, high temperature, possibly radial, lineations; (2) margin parallel foliation. On the other hand dyking is indicated by (1) numerous dykes, (2) a pluton composed of sheeted complexes, (3) extensional fault zones bounding the pluton.

The JBP and its wall rocks are well exposed, which makes the JBP a perfect object to study material transfer and, possibly, space-making

From: CASTRO, A., FERNANDEZ, C. & VIGNERESSE, J. L. (eds) *Understanding Granites: Integrating New and Classical Techniques*. Geological Society, London, Special Publications, **168**, 161-176. 1-86239-058-4/99/$15.00

processes, their relative importance and, finally, to evaluate the ruling emplacement mode in this case study. In order to do that, detailed petrographic and structural mapping at the SW margin of this pluton in the Deep Springs Valley (DSV) area was complemented by laboratory studies such as AMS, quartz c-axis and strain measurements.

Regional setting

The JBP is situated at the southern end of the Inyo batholith in the White Inyo Mountains (Fig. 1), which is generally regarded as a precursor of the Sierra Nevada batholith. The alkaline to calc-alkaline Soldier Pass Intrusive Suite (Bateman 1992), consisting of granitoids with monzonitic, dioritic, granodioritic and granitic composition, occupies the southern part of the batholith. The Marble Canyon Diorite, Joshua Flat Monzonite and Beer Creek Granodiorite, making up the JBP, are part of this suite. According to U-Pb dating (Sylvester *et al*. 1978; Gillespie 1979; Stern *et a/*. 1981) the Soldier Pass Intrusive Suite intruded about 180-160 Ma ago into a Late Proterozoic to Cambrian sequence of carbonate and siliciclastic rocks, which was deposited at the western, then passive, continental margin of North America (Nelson *et a/*. 1991). This shelf sequence was deformed during the Antler (Late Devonian to Mississippian) and Sonoma orogeneses (Late Permian to Early Triassic) into N-S-trending (Antler) and NE SW-trending (Sonoma) folds (Dunne *et a/*. 1978; Bateman 19923, respectively, and metamorphosed under greenschist-facies conditions (Ernst 1996). The intrusion of the Inyo batholith coincides with the deformational events summarized as Nevadan orogenesis (Jurassic through Cretaceous; Dunne *et al*. 1978; Bateman 1792), although no structures related to this regional deformation phase were observed in and around the contact aureole of the JBP. The Nevadan orogenesis is characterized by thrust tectonics (Dunne *et a/*. 1978), which can be distinguished from deformations related to the intrusion leading to tight or isoclinal folds (parallel to the contact with the plutons), boudinage and thinned strata around the plutons of the Inyo batholith (Stein & Paterson 1996). According to *P-T* data from aureole rocks, the intrusion took place at a depth of about 10 km (Ernst 1996). In the thermal aureoles of the intrusive bodies contact metamorphism reached hornblende-hornfels up tolower amphibolite-facies conditions (Ernst 1996). According to U-Pb (Gillespie 1979 Hanson *et ai*. 1987) and K-Ar and $^{40}Ar/^{39}Ar$ dating (McKee & Conrad 1996), further plutons intruded into the batholith during two later periods of igneous activity ranging from 145 to 140 Ma and from 100 to 80 Ma. The Cenozoic era (especially the last 5 Ma) in the White Inyo Mountains is marked by extensional tectonics typical for the Basin and Range Province, accompanied by a bimodal basaltic-rhyolitic volcanism (Nelson *et a/*. 1991).

Field and microscopic observations

Petrography of the pluton

Mapping and thin section investigations (Figs 2 and 3) prove the JBP to consist of three distinct intrusions:.the Marble Canyon Diorite, the Joshua Flat Monzonite and the Beer Creek Granodiorite. The Marble Canyon Diorite is a medium- to coarse-grained, isotropic honblenderich diorite with biotite, titanite and magnetite as accessories. The Joshua Flat Monzonite, a medium-grained monzonite to quartzmonzonite, is characterized by a strong magmatic foliation made up by hornblende (typically with pyroxene cores) and the high amount of titanite, visible even with an unaided eye. The Beer Creek Granodiorite, a medium- to coarse-grained, biotite- and hornblende-bearing granodiorite contains 1-3 cm long alkali feldspar phenocrysts, which make up a weak magmatic foliation together with dark fine grained, monzonitic enclaves.

Field relationships and structures inside the JBP

The Joshua Flat Monzonite and the Beer Creek Granodiorite make up c. 90% of the JBP following a concentric pattern with the Joshua Flat Monzonite at the rim of the pluton and the Beer Creek Granodiorite in its center. In the entire pluton the Marble Canyon Diorite is abundant as xenoliths in the Joshua Flat Monzonite as well as in the Beer Creek Granodiorite (Fig. 3a). Moreover, stoped blocks of the Joshua Flat Monzonite appear in the Beer Creek Granodiorite all over the working area. In addition to these monzonitic xenoliths, characterized by sharp edges and an internal magmatic foliation discordant with the external magmatic foliation in the Beer Creek Granodiorite, monzonitic enclaves with smooth edges and internal magmatic fabrics concordant with the external fabrics, interpreted to be derived from the Joshua Flat Monzonite, occur in the Beer Creek Granodiorite. A third kind of contact

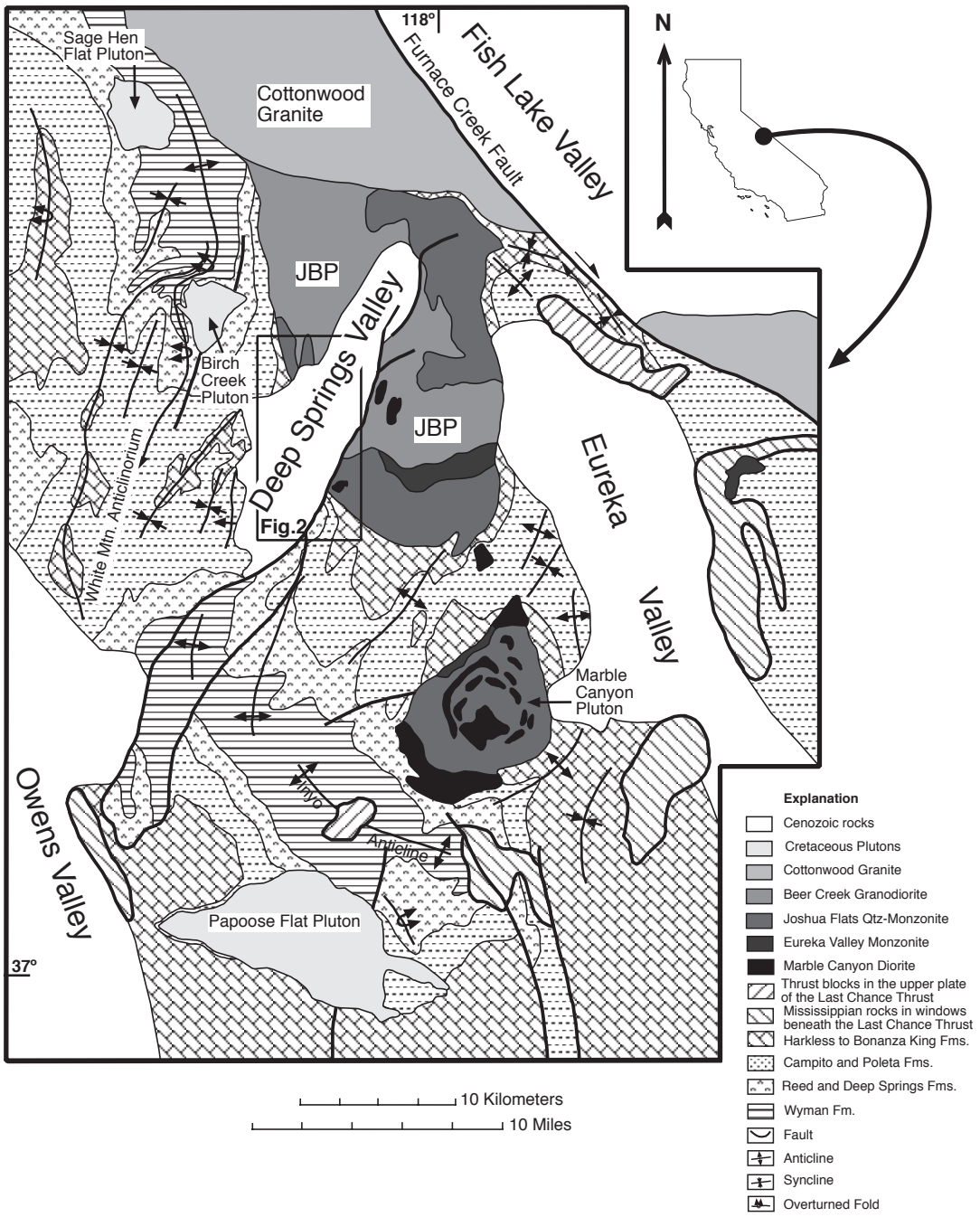

Fig. 1. Generalized geological map of the central portion of the White Inyo Range (modified after Nelson *et al.* 1991); rectangle refers to Fig. 2, arrow on the map of California shows the location of the White Inyo Range.

between the Joshua Flat Monzonite and the Beer Creek Granodiorite is characterized by mixing and mingling of both magmas. Mingling: led to schIieren of Joshua Flat Monzonite in Beer Creek Granodiorite and vice versa, whereas sheets of an igneous material (1-l00 m wide), characterized by porphyritic alkali feldspar as well as hornblende with pyroxene cores lying between the Joshua Flat Monzonite and the Beer Creek Granodiorite are interpreted as a result of magma mixing between the monzonite and the granodiorite (Fig. 3d). The magmatic foIiation in

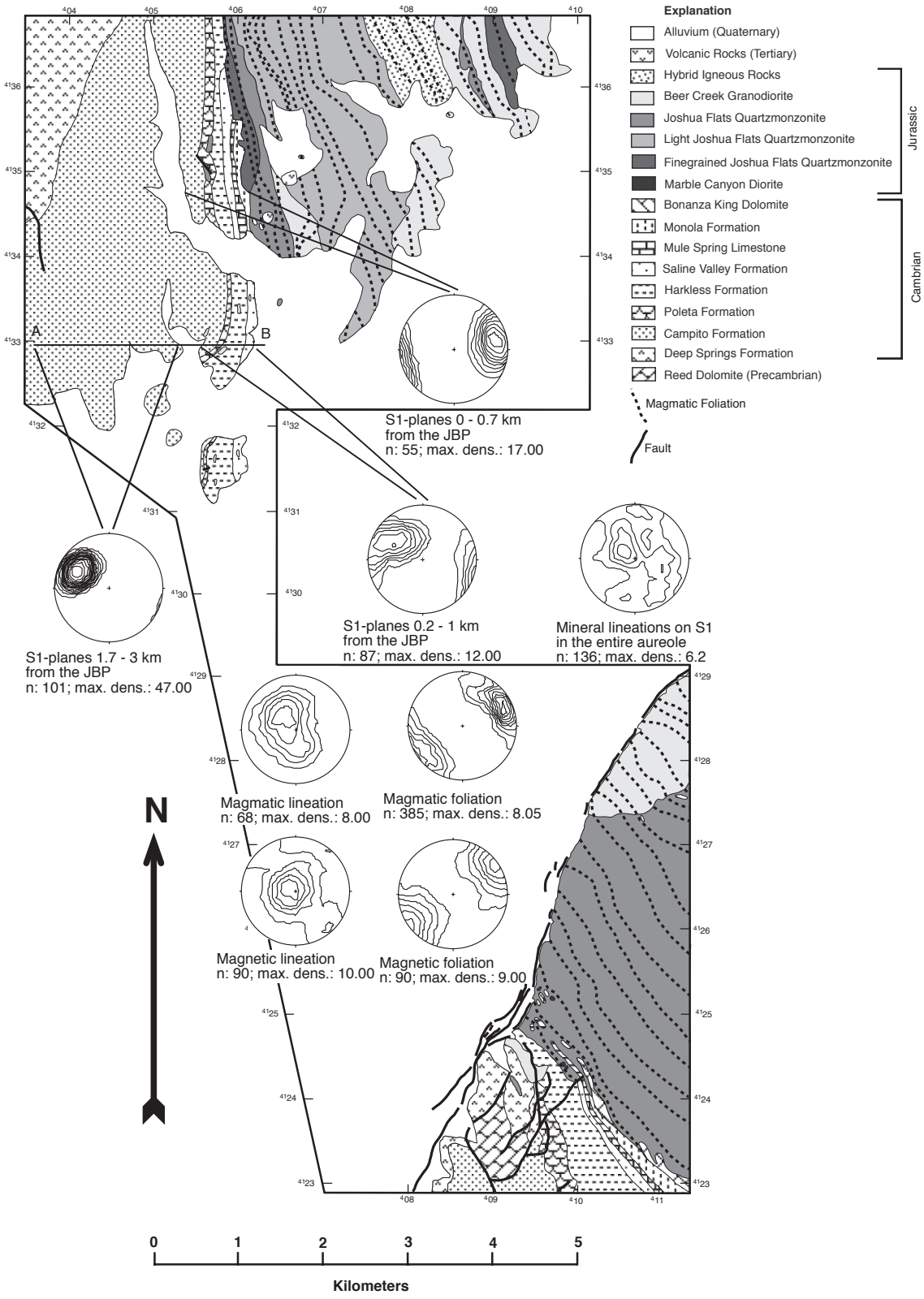

Fig. 2. Schematic geological map of the field area at the SW rim of the:JBP; line A-B represents profile along which samples for the strain and quartz c-axis measurements were taken. Included are also stereoplots of the magmatic and magnetic fabrics in the JBP, as well as stereoplots showing the orientation of Sl planes in several parts of the mapping area NW of DSV.

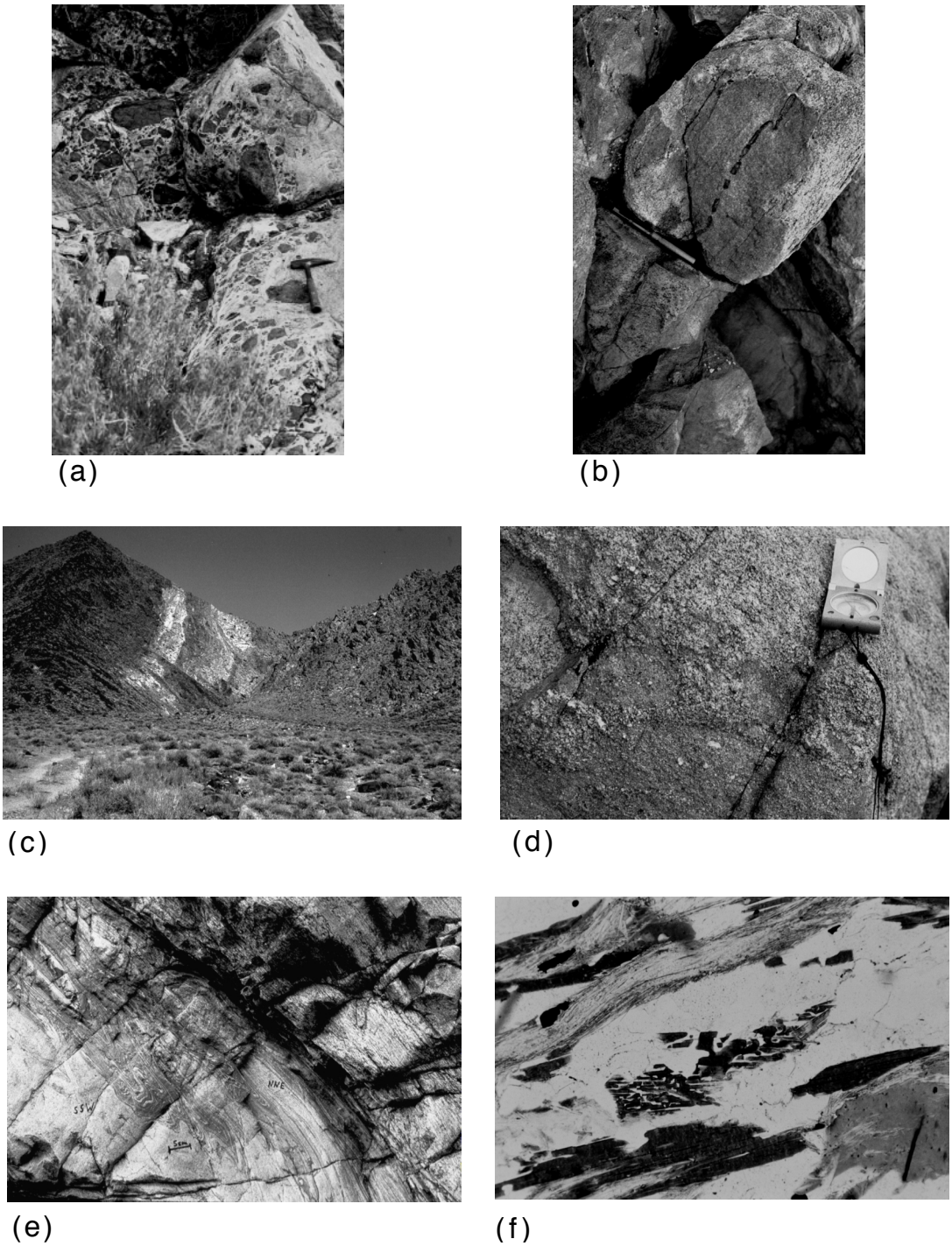

Fig. 3. Field and microscopic observations in and around the JBP. (a) Brecciated blocks of the Marble Canyon Diorite in the Joshua Flat Monzonite. (b) Asymmetrical shear foId and boudins in a marble of the Deep Springs Formation indicating ductile downward flow (left NNE, right SSW). (c) Pluton-wall rock contact near Birch Creek with overturned strata (left W, right E). (d) Diffuse contact between the fine-grained Joshua Flat Monzonite and the Beer Creek Granodiorite both still in the magmatic state: alkali feldspar being transferred from the Beer Creek Granodiorite into the Joshua Flat Monzonite. (e) Interisively folded stoped block with smooth edges, indicating partiai melting at its rims. (f) Reaction fabric between biotite, sillimanite, andalusite, plagioclase and quartz on one side and cordierite, alkali feldspar on the other side (long edge: 2 mm, PPL).

the JBP is oriented concentrically along the steep contact to the wall rocks; therefore it strikes NNW in the mapping area (Fig. 2), where it cross-cuts even intraplutonic contacts. Stoped blocks of aureole material are common not only at the rim of the JBP, but also in its centre. Many of these xenoliths show fabrics typical for intense ductile deformation, such as isoclinal folds (Fig. 3e) and chocolate-tablet boudins.

Petrography of the aureole rocks

The JBP intruded a sequence of carbonatic and psammopelitic rocks which had suffered only a weak regional metamorphism in greenschist facies with biotite as a kind of index mineral. This greenschist facies is overprinted by a later contact metamorphism up to lower amphibolitefacies conditions. Three contact metamorphic zones could be distinguished according to the occurrence of index minerals in the metapelites. The andalusite-cordierite zone (1.8-0.5 km distance from the pluton) is characterized by the mineral reaction chlorite + muscovite + ilmenite -> biotite + cordierite + andalusite + H_2O. The transition into the next zone, the sillimanite zone (0.5 0.25 km) is indicated by the overgrowth of biotite and coexisting andalusite by sillimanite. Although the deduced polymorphic transition from andalusite to sillimanite is the only observable mineral reaction, additional reactions might have also taken place at the andalusite-cordierite zone-sillimanite zone boundary. In the immediate contact area (<0.25 km) a cordierite-alkali-feldspar zone is characterized by leucocratic veins, probably the products of dehydration melting due to the mineral reaction sillimanite/andalusite + biotite + quartz -> cordierite + alkali feldspar + melt + H_2O (Fig. 3f). At least two reactions are dehydration reactions. Therefore water must have been present during and after the emplacement of the JBP, probably not only from dehydration reactions, but also water from the pluton, released during the continuous crystallization of the melt. The influence of fluids is visible all around and inside the pluton: The retrograde chloritization of andalusite and biotite as well as the extensive pinitization of cordierite in pelitic rocks, skarns, copper mineralizations at the contact between the JBP and marbles and numerous epidote veins, all observed in the innermost aureole, prove that fluids were present during the ascent and emplacement of the JBP.

Structures and field relations in the contact aureole

The most prominent fabric in the country rocks is an E-: to NE-striking cleavage (S1), which developed parallel to the bedding planes, probably as a pressure-solution cleavage. Regional deformation associated with the greenschistfacies regional metamorphism deformed this fabric into open E- to NE-trending folds. Inside the mapped part of the contact aureole along the western rim of the JBP the S1 cleavage is continuously rotated into a contact parallel direction. The dip of the stratigraphic units continuously steepens towards the contact, they even may be overturned next to the pluton (Figs 2 and 3c). The same observations can be made at the northern and southern rim of the JBP (Stein & Paterson 1996). Thanks to the detailed stratigraphic work of Nelson (1962, 1966) it was possible to correlate the strongly metamorphosed and deformed layers in the contact aureole with only regionally deformed strata outside the aureole. The strata become younger when approaching the pluton. Preserved sedimentary structures, such as ripple marks and cross bedding, indicate that the stratigraphic younging is directed toward the pluton. Therefore, the aureole of the JBP can be regarded as a funnel-like structure (Fig. 1). Moreover, a comparison of the thickness of the same stratigraphic units outside and inside the aureole, using Nelson's stratigraphic column (Nelson 1962), shows that the stratigraphic units have been thinned from 30% in the outer part of the aureole up to 80% in the inner part of the aureole. The Poleta formation has a thickness of c. 400 m outside the aureole but just 100 m inside; i.e. it has been thinned by 75%. :

Discordant contacts along large sections with the pluton are common. This feature corresponds very well with the numerous stoped blocks observed in the JBP. The structural inventory of the inner aureole (up to 500 m away from the JBP) is characterized by ductile deformational structures. Chocolate-tablet boudins confirm the amount of strain deduced from the strata's thickness and are very often associated with small scale asymmetrical shear folds with horizontal fold axes and axial planes dipping toward the pluton (Fig. 3b). Moreover, isoclinal, cylindrical folds in the centimetre- to metre-scale, often with moderately to steeply plunging fold axes parallel to mineral stretching lineations, can be found. The axial planes of these folds strike NNE and dip steeply to the WSW or ENE. The moderate to steep mineral lineations lie on the Sl planes and show a similar trend as those: they

steepen continuously toward the pluton, moreover, they increase in number. The mineral stretching lineations consist partly of elongated black spots, interpreted as the remnants of the typical contact metamorphic mineral cordierite. In the cordierite-alkali-feldpar zone mylonite zones can be found, where sillimanite forms S-C fabrics, which indicate upward movement of the stratigraphic hanging wall, i.e. the pluton side. Most other kinematic indicators in shear zones of the inner aureole, as σ- and δ-porphyroclasts and asymmetrical shear folds, show the same transport direction: pluton-side up relative to the rest of the aureole (Fig. 3b). In the outer part of the aureole (0.5-1.8 km away from the JBP) ductile structures ttat can be related with the emplacement of the JBP are missing and only extensional kink bands can be found. Moreover, monzonitic and granodioritic dykes at all scales—millimetres to metres wide—were observed in the inner part of the aureole.

Measurements of the anisotropy of the magnetic susceptibility (AMS)

According to Tarling & Hrouda (1993) the AMS is a good tool to measure weak fabrics, e.g. magmatic foliations and lineations as well as the intensity of magmatic fabrics very easily and quickly. Here only a short description of the important parameters for the AMS ellipsoid shall be given. Hrouda (1982) proposed the following parameters to describe the AMS ellipsoid:

foliation factor $F = k_y/k_z$;
lineation factor $L = k_x/k_y$;
anisotropy factor $P = k_x/k_z$;
corrected anisotropy factor $P' = \exp\{2(\ln k_x - \ln k_m)^2 + 2(\ln k_y - \ln k_m)^2 + 2(\ln k_z - \ln k_m)^2\}^{1/2}$
with km (mean susceptibility) $= (k_x + k_y + k_z)/3$;
form factor $T = (\ln F - \ln L)/(\ln F + \ln L)$.

P' describes the degree of ellipticity/anisotropy of the AMS ellipsoid. Flattening AMS ellipsoids are characterized by T values > 0, whereas constrictional AMS ellipsoids have T values < 0. The most useful graphical depiction to describe and interpret AMS measurements is the Jelinek diagram (Hrouda 1982), where P' is plotted against T.

Measuring conditions

Measurements were carried out with a Kappabridge KLY-2. The measuring conditions were as follows: temperature = 20 °C, magnetic field = 300 Am^{-1} (weak magnetic field). Cylinders with a height of 2.08 cm and a diameter of 2.54 cm were used as samples. Their magnetic susceptibility is measured in 15 positions and the AMS ellipsoid calculated with the ANISO14g computer program. Measurements were done at 90 samples: 53 from the Joshua Flat Monzonite and 37 from the Beer Creek Granodiorite). Each sample consists of 4 to 10 cylinders. Only in one case a single cylinder was measured, due to the small size of the hand specimen.

Magnetic susceptitility and AMS in the JBP

Lithological units of the JBP are mostly ferromagnetic with susceptibilities between 20 000 and 30 000 x 10^{-6} SI. Only 10% of all samples lie below 10000 x 10^{-6} SI and are, therefore, paramagnetic. Consequently, the main carrier of the magnetic susceptibility is magnetite, with biotite and hornblende as minor contributors. The orientation of the magnetic lineations and foliations are fairly consistent for all samples (Fig. 2) and therefore for all lithologies. For both the poles of the magnetic foliation and the magnetic lineation eigenvalues and eigenvectors were calculated (Scheidegger 1965). The eigenvector of the largest normalized eigenvalue represents the average magnetic foliation and the average magnetic lineation, respectively. In case the largest normalized eigenvalue is higher than 0.5 the corresponding eigenvector can be regarded as well defined. Accordingly the average magnetic foliation is oriented 237/90 (dip direction/dip angle) with an eigenvalue of 0.6688. The mean magnetic lineation has the orientation 300/84 (trend/plunge), the eigenvalue is 0.5644. Therefore, both lie parallel to the magmatic foliations and lineations respectively (Fig. 2) and imply the contemporaneous formation of both magmatic and magnetic fabrics.

The anisotropy of the AMS ellipsoids (Fig. 4) measured in the Joshua Flat Monzonite lies between 2.5% (P' = 1.025) and 59.3% (P' = 1.593) with an average value P'= 1.212 ± 0.114 and is much stronger t han the anisotropy of those in the Beer Creek Granodiorite, where P' ranges between 1.049 and 1.285 (average P' = 1.127 ± 0.056). The broad range in P' for the AMS ellipsoids of the Joshua Flat Monzonite has two reasons: of the ten ellipsoids with P' < 1.1 six are paramagnetic, the two ellipsoids with P' > 1.4 were measured in samples that had suffered ductile subsolidus deformation. The samples from the Beer Creek Granodiorite are much more consistent with respect to their magnetology and structural inventory: only one sample is paramagnetic, none showed: signs of subsolidus deformation. Most AMS ellipsoids have an oblate shape. Only 14 of all samples are prolate.

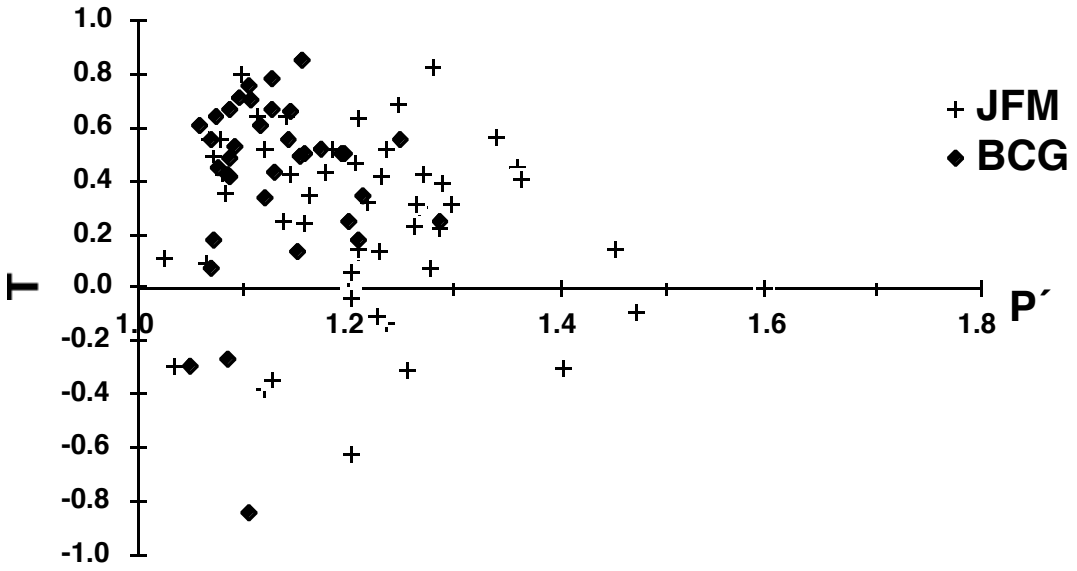

Fig. 4. Jelinek diagram for AMS results from the JBP. The ellipsoids in the Joshua Flat Monzonite (JFM) have a much stronger anisotropy (indicating stronger deformation) than those measured in the Beer Creek Granodiorite (BCG). Ellipsoids in both lithologies are generally oblate, probably due to flattening deformation.

The average *T* for the Joshua Flat Monzonite is 0.258 ± 0.321 and 0.414 ± 0.328 for the Beer Creek Granodiorite.

Investigations regarding the viscosity contrast between the carrier of susceptibility (magnetite) and the magma according to Hrouda & Lanza (1989) suggest the magnetic foliation, and therefore also the magmatic foliation, to have developed late in the magmatic state of the JBP: Hrouda & Lanza established a relation between the anisotropy factor *P*', the strain, the viscosity ratio magnetite:magma, the pluton's radius and the intrusion depth. They introduced a graphical solution for this question. As already stated, *P*' in the Beer Creek Granodiorite lies between 1.049 and 1.285 equivalent to 4.928.5% anisotropy and between 1.025 (=2.5% anisotropy) and 1.593 (=59.3% anisotropy) in the Joshua Flat Monzonite. The intrusion depth is about 10 km and the pluton's radius amounts to 15-20 km. Plotting these values in the diagram of Hrouda & Lan.za shows that the viscosity ratio between the carrier of susceptibility, magnetite, and its matrix, the magma, is 20: 1 to 10: 1. That is, both magmas were already very viscous when the magnetic and, thus, the magmatic foliation were developed, i.e. the most important fabrie in the JBP originated late in the near solidus magmatic state of the pluton, confirming the field observations.

Strain measurements in the aureole of the JBP

Samples and measurement method

The strain/shape orientation analyses were carried out with a VIDS image analysis equipment and the program VIDS V, using the Rf/ϕ-method (Ramsay 1967). The computer program RS PLOT, which is based on the geological strain analysis of Lisle (1985), was used for data processing and their evaluations. The triaxial strain ellipsoids were calculated by the computer program TRISEC. Strain measurements were carried out at six samples collected along one profile W of the JBP (Fig. 2). Samples were taken at 500 m, 550 m, 600 m, 1700 m, 2000 and 2200 m away from the pluton. The samples are part of the Harkless and Campito Formations and have pelitic composition. Black spots, in thin sections identified as partly altered cordierite porphyroblasts, were used as strain markers.

Shape and orientation of the strain/fabric ellipsoids

All but one of the measured strain ellipsoids have a prolate shape indicating a more linear than planar character of the cordierite strain fabrics. Neither R_{xy} nor R_{yz} are higher than 2.1 and the

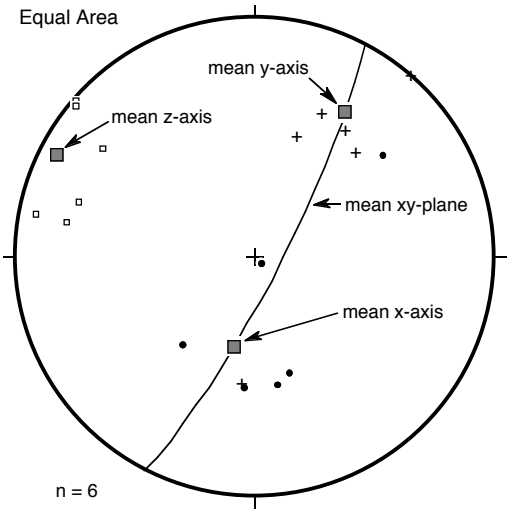

Fig. 5. Stereoplot for the six strain measurements, including the orientation of the xy plane and the three principle axes of the average strain ellipsoid.

E_S value (Nadai 1963) also does not exceed 0 944 The strain is therefore surprisingly low, even in the immediate contact with the pluton. Again, as already done for the AMS ellipsoids, the orientation tensors for the three main axes of all measured ellipsoids were computed to get the average *x*, *y* and *z* axes for an average ellipsoid. The largest normalized eigenvalue represents the average x (y or z) axis with its eigenvector representing its orientation. All three axes are very well defined (Fig. 5). The mean x axis with its moderately steep plunge to the S (eigenvalue: 0.7415, eigenvector: 178/58) indicates oblique, subvertical material transport, supporting the kinematics observed in the field. The mean *x* axis together with the mean *y* axes (eigenvalue: 0.7653, eigenvector: 032/30) defines the mean *xy* plane of the strain ellipsoid, which lies, as expected, parallel to the foliation of the samples. Therefore, the mean *z* axis (eigenvalue: 0.9217, eigenvector: 296/15), as the pole of the xy plane, lies parallel to the poles of the foliation planes measured-in the field.

Quartz c-axis measurements

Quartz *c*-axis measurements were carried out on ten samples from a cross-section on the west side of the JBP. The profile extended about 3 km away from the pluton-wall rock contact. In each sarnple 300 measurements were carried out on a four-axis Zeiss U-stage on one oriented thin section. The data obtained were plotted in a stereonet. with reference to the lineation and foliation measured at the individual samples. The N-S direction of the stereonets corresponds to the pole of the foliation and the E-W direction to the lineation. To make the *c*-axis fabrics (Fig. 6) clearer the lineations are shown either as lines or, if a shear sense could be deduced from the *c*-axis patterns, as arrows. The description of the individual quartz *c*-axis fabrics follows the classification of Hofmann (1974). He distinguishes seven different maxima: maximum I—in the centre of the stereonet; maximum II—between the centre and the poles of the stereonet; maximum III—between the poles and the equator along the rim of the stereonet, maximum IV—in the centre of each quadrant of the stereonet; maximum V—at both poles of the stereonet; maximum VI—on the equator of the stereonet, halfway between the centre of the stereonet and its rim; maximum VII—at the E and W end of the equator of the stereonet.

Description and interpretation of the quartz c-axis fabrics in the aureole rocks of the JBP

Quartz *c*-axis measurements confirm the field observations, but also yield a much more detailed insight into the deformation processes in and near the contact aureole. The following different features can be observed with increasing distance from the pluton (Fig. 6). In a *c*. 500 m wide zone directly at the contact to the JBP obliquely oriented *yz* girdles (composed of maxima I or II and V) and type II cross girdles (consisting of maxima I and III) are the dominant quartz *c*-axis fabrics. According to Paschier & Trouw (1996) maxima V are due to basal slip in ⟨*a*⟩ and maxima I can be referred to prism slip in ⟨*a*⟩. The combined activation of basal and prism slip systems is typical for medium to high temperature conditions, i.e. 350-650°C (Paschier & Trouw 1996). Tullis *et al.* (1973) emphasize the direct relation between the opening angle of type II cross girdles and their formation temperatures: the higher the temperature, the higher the opening angle. The opening angles of the measured type II cross girdle lie between 750 and 90°, indicating formation temperatures of at: least 550°C. This temperature is too high for the regional greenschist-facies metamorphism present in the White Inyo Mts, but matches perfectly the contact metamorphism related to the emplacement of the JBP. All observed quartz c-axis fabrics in the innermost aureole can therefore be related to this event. Several authors (Carter *et al.* 1964, Green *et a/.* 1970; Tullis *et a/.* 1973; Schmid & Casey

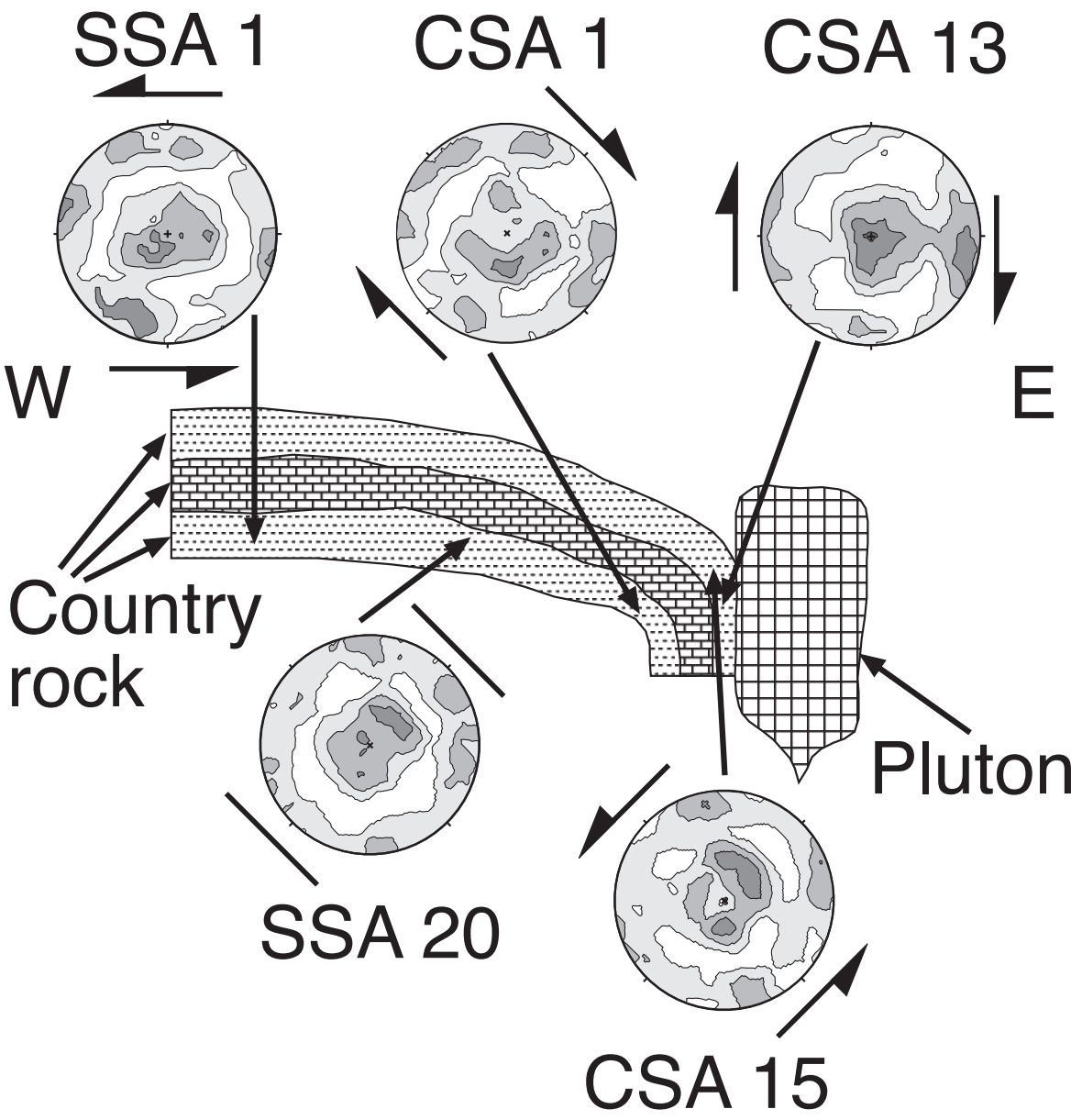

Fig. 6. Typical quartz *c*-axis fabrics from the aureole at the western rim of the JBP. Arrows represent the shear sense deduced from the quartz *c*-axis fabrics and, as arrows or lines, the orientation of the lineations on the individual samples. Sample CSA 13 was taken 250 m away from the pluton, maximum density is 5.00; CSA 15: 350 m/4.325; CSA 1: 950 m/5.00; SSA :20: 2300 m/5.00; SSA 1 3000 m/4.67.

1986) relate type II cross girdles to coaxial, constrictional strain or interpret them at least as linear fabrics. Other linear features as the strain ellipsoids, plotting within the field of apparent constriction, or the numerous moderate to steep mineral stretching lineations are confirmed by the quartz *c*-axis measurements. The oblique orientation of the crystallographic quartz fabrics to the tectonic *x*, *y* and *z* coordinates and their dependence on steep mineral lirieations indicates the presence of a component of rotational deformation. Unfortunately this rotational deformation shows contradictory shear senses even in samples from locations close to each other, so that, for example, sample CSA 13 (250 m away from the JBP) shows a dextral shear sense (pluton-side down relative to the aureole) and sample CSA 15 (350m away from the JBP) indicates a sinistral shear sense (pluton-side up relative to the aureole).

With increasing distance to the pluton, within a zone between 500 m and 1000 m away from the pluton, the quartz *c*-axis fabrics are still dominated by a combination of maxima I or II and V.

The difference is that part of them are now not related to moderately steep but also to horizontal mineral lineations. Tho-se related to half steep lineations (especially CSA 1, 950 m away from the JBP) indicate transport of the aureole down relative to the rest of the host rock. Those related to horizontal lineations show dextral shear sense indicating material transport parallel to the pluton contact.

About 1 km away from the pluton the character of the quartz *c*-axis fabrics changes. Instead of type II cross girdles and yz girdles, xy girdles consisting of maxima I and obliquely oriented maxima VIII become the dominant fabrics. 0nly one sample (SSA12: *c*. 1.7 km away from the contact) shows a weak type II cross girdle additional to the maxima VIII and another sample (SSA20:*c*. 2 km away from the pluton) has a maximum I and a maximum II as the dominant fabric. Sample SSA 1 (*c*. 3 km away from the pluton) is dominated by oblique maxima VIII. The weak type II cross girdle in SSA 12 and the Maxima I/II in SSA 20 can still be related to combined basal and prism slip due to the intrusion of the JBP. The necessary temperatures for the construction of those fabrics (350-650 •C) were attained even *c*. 2 km from the contact as is proved by the occurrence of cordierite even 1.8 km from the pluton (cordierite growth needs *c*. 500•G according to Seifert (1970)). It is more difficult to explain the maxima VIII, which can be found inside (SSA 12) as well as outside (SSA 1) the thermal aureole. According to Paschier & Trouw (1996) obliquely oriented maxima VIII should be interpreted as shear fabrics, originated at temperatures higher than 650 •C. Because of the distance of those samples from the pluton this assumption does not seem to be very probable; at least the fabrics should not indicate higher temperatures than those taken closer to the pluton. A better solution might be to interpret the maximum VIII dominated fabrics as the results of external rotation. Fairbairn (1949) and Griggs *et al*. (1960) proposed this process to produce lower grade quartz fabrics. It remains unclear, if the maxima VIII is older or younger than the other observed fabrics. The fact that maxima VIII are found also outside the aureole and assuming that the stress exerted from the JBP on the country rocks at a distance > 1 km is not high enough to obliterate an older quartz *c*-axis fabrics, the maxima VIII can be related to the pre-intrusive regional deformation, which is a low-temperature (greenschist-facies) event and would fit to the 'external rotation' interpretation.

Discussion

Field observations as evidence for diapirism or dyking

I will try to follow the field criteria of Clemens *et al*. (1997), although they seem to be too simple and fit modelled hot-Stokes diapirs better than composite, viscoelastic diapirs. Therefore, the field observations do not match fully the criteria of Clemens *et al*. (1997). Clemens *et al*. (1997) demand narrow, high-temperature shear zones directly at the pluton-wall rock interface or, in the case of deeper seated plutons, in the aureole together with steep lineations as hints for large scale downward movement of aureole material relative to the ascending diapir. No narrow high-temperature shear zones were found directly at the contact between the wall rocks and the pluton, but in the inner aureole mylonite zones with S-C fabrics consisting of fibrolitic sillimanite were observed. These mylonites show a pluton-side up kinematic and prove downward movement of aureole material relative to the pluton at the peak of the contact metamorphism and therefore during the emplacement of the JBP. Steep mineral lineations in the inner aureole support this interpretation. The observed funnel structure is not the rim syncline that Clemens *et al*. (1997) postulate, but is an argument as good as a rim syncline for diapirism, because in the 'funnel' country rock material is transferred downward, what makes space for the suggested JBP diapir. There is no way to produce such a funnel by dyking. Moreover both criteria, which should, according to Clemens *et al*. (1997), be observed inside the pluton to call it a diapir, are fulfilled for the JBP: steep magmatic and magnetic lineations were observed and a magmatic/magnetic foliation parallel to the pluton-wall rock contact was found. On the other hand none of the general criteria for dyking are fulfilled by the JBP. The observed dykes radiate from the already constructed magma chamber into the host rock and do not construct the entire chamber. No major sheeted complexes were found, but two big batches of magma, the Joshua Flat Monzonite and the Beer Creek Granodiorite make the pluton. No extensional fault zones of Jurassic age or older occur at either side of the JBP. Therefore, the JBP can be regarded as a diapir, or better as a batch of nested diapirs, because three distinct igneous phases could be established.

Field relationships and AMS: arguments for an intrusion of nested diapirs and magma chamber expansion

One of the intrusions, the Marble Canyon Diorite, was found as xenoliths only in the other two igneous phases and is therefore regarded as the oldest intrusive. Idiz (1981) observed the same rock type in the Marble Canyon Pluton, about 10 km south of the JBP (Fig. 1). There it makes up about 30% of the exposed pluton and lies as a ring-like structure in a matrix of Joshua Flat Monzonite and at the rim of this pluton. Idiz (1981) interpreted the Marble Canyon Diorite as a precursor of the Joshua Flat Monzonite as well. He interpreted the Marble Canyon Diorite as a sill which was later intruded and brecciated by the Joshua Flat Monzonite. Because the Marble Canyon Diorite was found only as disconnected blocks in the JBP, no interpretation of the intrusion mode of the Marble Canyon Diorite is possible. As described above the relations between the Joshua Flat Monzonite and the Beer Creek Granodiorite are much more complicated, but the presence of monzonitic xenoliths in the granodiorite and the lack of granodioritic xenoliths in the monzonite lead to the conclusion that the Joshua Flat Monzonite represents the second and the Beer Creek Granodiorite the third and last intrusive phase. What makes the relation between the Joshua Flat Monzonite and the Beer Creek Granodiorite more complicated is the existence of mingling and mixing structures between both (Fig. 3d). This means that the granodiorite intruded the monzonite in a partly molten state. It might be that during the intrusion of the Beer Creek Granodiorite into the still melt containing Joshua Flat Monzonite, magma chamber expansion took place. Magma chamber expansion may be an explanation for the strong magmatic foliation in the monzonite relative to the weak magmatic foliation in the granodiorite as well as for the high anisotropy of the AMS ellipsoids measured in the monzonite relative to those of the granodiorite (Fig. 4). Moreover, it can be responsible for the concentric foliation pattern at the pluton's rim, for oblate fabrics in the inner aureole (namely the chocolate-tablet boudins) and for the generally oblate character of the AMS ellipsoids. Although all structures described can be explained by late-stage magma chamber expansion, the last three arguments are not necessarily connected with it. The concentric pattern made up by the magmatic foliation at the rim of the JBP can also be due to boundary-layer effects such as the wall, Magnus and Bagnold effects (Barriere 1981), which all can align crystals parallel to the pluton-wall rock interface or either to a cooling front propagating from the contact into the pluton. Oblate fabrics, such as the chocolate-tablet boudins in the inner aureole and the AMS ellipsoids, indicate a flattening event during the emplacement and deformation history of the JBP, but do not necessarily require late-stage magma chamber expansion. Nevertheless late-stage magma chamber expansion seems to be the only way to produce the observed intensity differences of the magmatic and magnetic fabrics in the monzonite and granodiorite, respectively.

The meaning of fabrics and foliations: implications for vertical material transfer

Emplacement-related structures indicate that multiple processes played a role during the emplacement of the JBP. Most of these structures and features have one thing in common: they are steeply or even vertically oriented. This is so in the aureole for all vertical lineations and the steepening of stratigraphic units towards the pluton and, in the pluton, for steep magmatic and magnetic lineations and for stoped blocks, which indicate vertical, downward directed material transport as all other features referred to before. Moreover, all structures in the inner part of the aureole are ductile high-temperature structures and very often associated with the typical contact metamorphic minerals cordierite and sillimanite, and are related to the emplacement of the JBP and not part of the much colder and older regional metamorphic events. Because the cordierite lineations appear on the Sl planes, which are bent down around the pluton to form the funnel structure, it is suggested that this structure developed during the emplacement of the JBP. A further argument for the coeval character of the funnel is the occurrence of sillimanite in mylonite zones, which lie parallel to steeply dipping Sl planes and can be related to the construction of the funnel. A possible explanation for the funnel is found in the steep mineral stretching lineations (cordierite), which indicate ductile vertical material transport in the contact aureole. To originate the observed funnel, country rock material has to flow ductilely from the roof region of the ascending pluton towards its source region, a process recently discovered by Stein (pers. comm.) and named by him as 'ductile downward flow'. This vertical material transfer process could also solve the space problem during the ascent and emplacement of the pluton. Ductile downward flow seems to be a space

making process, which is active during the entire ascent and emplacement history of a pluton or even a batholith. As soon as enough magma has accumulated in a pluton's source region in the lower crust or the upper mantle, it rises buoyantly and leaves virtually a cavity behind that has to be filled imrnediately due to the high lithostatic pressure in that depth. The easiest way to fill this 'hole' is to transfer material vertically, i.e. from the sides and the roof regions of the ascending pluton into the area the magma batch has just left. Material transfer takes place by ductile flow. Host rock material is 'sucked' into a funnel-like megastructure around the pluton, which is constructed as the pluton rises. Other observed structures in the aureole fit in this scenario. The heat necessary for the duclile behaviour of the wall rocks is supplied by the pluton, heat transfer occurred by conduction as well as by convection with fluids derived from the pluton and from the aureole due to dehydration reactions during the prograde contact metamorphism. As demonstrated by the melt-producing reaction sillimanite + biotite + quartz -> cordierite + alkali feldspar + melt + H_2O temperatures in the immediate contact area reached c. 730°C (Le Breton & Thompson 1988). Therefore, partial melting also played a role for the ductile downward flow, although only in a 250 m wide zone around the pluton. According to Norton & Knight (1977) fluids originating during contact metamorphic dehydration reactions are transferred towards the pluton, where they are heated up and transported to the pluton's roof region. Obviously the roof region could be weakened by these fluid flow processes and become more sensitive for the ductile downward flow as long as fluid transport takes place through the bulk volume of country rocks and not on discrete shear zones or similar anisotropies. Fluids can also be helpful in enhancing the effectiveness of the shear movements (McNulty l995) necessary to transport country rock along the sides of the rising pluton downward.

Some observed structures do not fit into the scenario of ductile downward flow. Especially moderately steep or even horizontal lineations, as well as the moderately steep axes of the strain ellipsoids, do not fit very well to this clearly vertically oriented material-transfer process. But also isoclinal, cylindrical folds with steep axes parallel to mineral lineations are hard to explain by a process where stretching, but not pure constriction, is an important ingredient. Furthermore, chocolate-tablet boudins require flattening. All these structures could have been produced during a transpressiorial deformation phase, which could succeed the phase of pure ductile downward flow. Stein & Paterson (1996) already proposed this conclusion for similar synintrusional structures at the southern rim of the JBP. Due to the changing geometry of the rising pluton over time the downward moving aureole material at a: certain level (e.g. the level of recent exposure) is exposed to a changing strain field, where not only rotation, stretching and thinning of strata, but oblique arid horizontal, contact-parallel strike-slip transport accompanied by flattening, i.e. transpression, plays an important role. On the other hand, flattening type structures, such as the chocolate-tablet boudins, could also be produced by late-stage magma chamber expansion during the intrusion of later magma batches, i.e. the Beer Creek Granodiorite. Another remaining problem could be solved assuming that several structures were layed out late during ductile downward flow: most kinematic indicators in the inner aureole, including part of the quartz *c*-axis fabrics and even the S-C fabrics by sillimanite show the pluton side to move up and the rest of the aureole to move down. This makes a coupling of the pluton with its host rock necessary, which seems to be very unlikely considering the high viscosity contrast between the pluton and the country rock. In case all these structures are late during ductile downward flow it can be assumed that the rim portion of the JBP was already near or even below the solidus. That means that the viscosity contrast between the pluton and its aureole was not very high and a coupling between both would be possible. The steep magmatic and magnetic lineations in the JBP could be incorporated in the ductile downward flow and interpreted as a magmatic flow fabric that indicates the vertical buoyancy-driven magma transport, which caused the downward movement of the aureole material.

The observation of discordant contacts, numerous country rock xenoliths in the JBP and dykes radiating from the pluton into its host rocks can be explained only by stoping. Moreover, the relative low E_s values computed even for those strain measurements close to the pluton (e.g. 0.899 at 500 m away from the contact) may point to the fact that the innermost, strongest deformed aureole was removed by stoping. At the interface between the magma and its host rocks the thermal gradient is very steep. This forces the relatively cool country rock to expand very rapidly and to break open so that dykes from the pluton can propagate into the surrounding material and get out blocks of the country rock. The blocks fall into the magma chamber, where they either become assimilated or, depending on the magma viscosity, sink to

the bottom of the magma chamber and make some space for the rising pluton (Paterson & Miller 1998). One observation in the stoped blocks is of particular importance for the role stoping played during the emplacement of the JBP. Many of the xenoliths contain isoclinal folds (Fig. 3e) and boudin structures related to ductile deformation connected with late stages during ductile downward flow. The fact that these ductile structures were found in stoped blocks means that the pluton intruded its own ductile aureole and that stoping was active late during the emplacement of the JBP. If stoping still works even late during the magmatic history, when the thermal gradient between pluton and wall rock is already shallow and the viscosity of the magma relatively high, it must be even more productive during the early stages of emplacement.

Summary: time sequence of emplacement processes

It was shown that numerous emplacement processes played a role during the intrusion of the JBP: dyking and stoping, ductile downward flow accompanied by fluid release from the host rock and the pluton and partial melting of aureole material. Because the intrusion of the JBP occurred in three stages, I tried to define timing and relative importance of these processes during the stages of emplacement.

Stage 1: Intrusion of the Marble Canyon Diorite. Because the Marble Canyon Diorite was found only as xenoliths in the other two intrusive phases, no emplacement process was observed directly for this stage of the intrusion history.

Stage 2: Intrusion of the Joshua Flat Monzonite. Stoping followed by dyking is proved to be an important material transfer process for the emplacement of the Joshua Flat Monzonite by the existence of discordant contacts between the monzonite and the aureole rocks, numerous stoped blocks, found as far as 2-3 km away from the wall rock contact and numerous monzonitic dykes. Ductile downward flow played an important role during the entire emplacement history of the JBP and especially during the intrusion of the Joshua Flat Monzonite. Obviously this stage is the phase, during which the funnel around the pluton was established together with sillimanite-bearing mylonite zones and steep cordierite lineations. The steep magnetic and magmatic lineations are interpreted as representing vertical magma transport during the rise of the diapir. Evidence for partial melting that accompanied and enhanced the ductile downward flow was observed in the innermost aureole (up to 250 m away from the pluton-wall rock contact)

Stage 3: Intrusion of the Beer Creek Granodiorite. Stoping accompanied by dyking appears to be still important as is evidenced by numerous granodioritic to granitic dykes and stoped blocks. Country rock xenoliths with a ductile structural inventory prove that the JBP intruded its own ductilely deformed (i.e. by ductile downward flow) aureole. During the intrusion of the Beer Creek Granodiorite the ductile downward flow probably moved from the aureole into the Joshua Flat Monzonite. As the granodiorite ascended into the already constructed magma chamber the monzonite was forced downward, but also displaced towards the sides and the top of the magma chamber, what led to magma chamber expansion. The successive intrusion of nested diapirs supplied additional heat to the aureole and supported vertical material transfer there.

Conclusions

Field observations and laboratory data (AMS, quartz *c*-axes, strain) show that the JBP consists of nested diapirs, which intruded in the sequence Marble Canyon Diorite-Joshua Flat Monzonite-Beer Creek Granodiorite. The emplacement of the pluton was possible only because multiple material-transfer processes, such as stoping and dyking, ductile downward flow, partial melting and magma chamber expansion vvere working together at different times. Two of these space-making processes contributed to the rise of diapirs into the magma chamber: ductile downward flow and stoping acting during the entire emplacement history of the pluton. Ductile downward flow was assisted and enhanced by partial melting in the innermost aureole and increased ductility due to the convective and conductive heat flow induced by the ascending pluton. Magma chamber expansion played a role only during the last stage of the JBP emplacement. The JBP shows that diapirism is a model for pluton emplacement, because it involves many space-making material transfer processes, which can have a positive feedback on each other. Ductile downward flow and stoping, especially, seem to be very powerful material-transfer processes, which might be responsible for major crustal recycling during ascent and emplacement of the Sierra Nevada batholith.

The research was supported by grants of the DAAD, the Landesgraduiertenförderung Baden-Württemberg and the DFG. Special thanks go to T. Fink, R. B. Miller and S. R. Paterson, who put their field data at my disposal, to R. O. Greiling, E. Stein and S. R. Paterson for discussion and comments, to C. Fernandez and A. Castro for their helpful reviews and to S. Hetzler for his personal support.

References

BARRJERE, M. 1981. On curved laminae, graded layers, convection currents and dynamic crystal sorting in the Ploumanac'h (Brittany) subalkaline granite. *Contributions to Mineralogy and Petrology,* **77**, 214-224.

BATEMAN, P. C. 1992. *Plutonism in the central part of the Sierra Nerada batholith, California*. United States Geological Survey Professional Paper, **1483.**

BUDDINGTON, A. F. 1959. Granite emplacement with special reference to North America. *Geological Society of America Bulletin,* **70**, 671-747.

CARTER, N. L., CHRJSTIE, J. M. & GRIGGS, D. T. 1964. Experimental deformation and recrystallisation of quartz. *Journal of Geology,* **72**, 687-733.

CLEMENS, J. D., PETFORD, N. & MAWER, C. K. 1997. Ascent mechanisms of granitic magmas: causes and consequences. *In:* HOLNESS, M. B. (ed.) *Deformation-enhanced Fluid Transport in the Earths Crust and: Mantle*. Chapman & Hall, London, 144-171.

DUNNE, G. C., GULLIVER, R. M. & SYLVESTER, A. G. 1978. Mesozoic evolution of rocks of the White, Inyo, Argus and Slate ranges, eastern California. *In:* HOWELL, D. G. & MCDOUGALL, K. (eds) *Mesozoic paleogeography of the western United States*. Society of Economic Paleontologists and Mineralogists, Los Angeles, 89-207.

ERNST, W. G. 1996. Petrochemical study of regional / contact metamorphism in metaclastic strata of the central White-Inyo Range, eastern California. *Geological Society of America Bulletin,* **108**, 1528-1548.

FAIRBAIRN, H. B. 1949. *Structural petrology of deformed rocks*. Addison-Wesley Press Inc., Cambridge, Mass.

GILLESPIE, J. G. 1979. U-Pb and Pb-Pb ages of primary and detritial zircons from the White Mountains, eastern California. *Geological Society of America Abstracts with Programs,* **11**, 79.

GREEN, H. W., GRIGGS, D. T. & CHRISTIE, J. M. 1970. Syntectonic and annealing recrystallisation of fine-grained quartz-aggregates. *In:* PAULITSCH, P. (ed.) *Experimental and natural rock deformation*. Springer, Berlin, 272-335.

GRIGGS, D. T., TURNER, F. J. & HEARD, H. C. 1960. Deformation of rocks at 500°-800°C. *In:* GRIGGS, D. T & HANDIN, J. W. (eds) *Rock Deformation*. Geological Society of America Memoirs, **79**, 39-104.

HANSON, R. B., SALEEBY, J. B. & FATES, D. G. 1987. Age and tectonic setting of Mesozoic metavolcanie and metasedimentary rocks, northern White Mountains, California. *Geology,* **15**, 1074-1078.

HOFMANN, J. 1974. *Das Quarzteilgefüge von Metamorphiten und Anatexiten, dargestellt am Beispiel des Osterzgebirges*. Freiberger Forschungshefte, **C297**.

HROUDA, F. 1982. Magnetic anisotropy of rocks and its application in geology and geophysics. *Geophysical Survey, 5,* 37-82.

------ & LANZA, R. 1989. Magnetocrystalline anisotropy o rocks and massiv ores: a mathematical model study and its fabric implications. *Physics of Earth and Planetary Interiors,* **56**, 337-348.

IDIZ, E. F. 1981. *Geology of the Marble Canyon Plutonic Complex*. PhD thesis, University of California, Los Angeles, USA.

LE BRETON, N. & THOMPSON, A. B. 1988. Fluid absent (dehydration) melting of biotite in metapelites in the early stages of crustal anatexis. *Contributions to Mineralogy and Petrology,* **99**, 226-237.

LISLE, R. J. 1985. *Geological strain analysis: A manual for the Rf/φ method*. Pergamon Press, Oxford.

McKEE, E. H. & CONRAD, J. E. 1996. A tale of 10 plutons—revisited: Age of granitic rocks in the White Mountains, California and Nevada. *Geological Society of America Bulletin,* **108**, 1515-1527.

McNULTY, B. A. 1995. Shear zone development during magmatic arc construction: The Bench Canyon shear zone, central Sierra Nevada, California. *Geological Society of Americ a Bulletin,* **107**, 1094-1107.

NADAI, A. 1963. *Theory of flow and fractures of solids*. McGraw-Hill, New York.

NELSON, C. A. 1962. Lower Cambrian-Precambrian sueeession, White-Inyo Mountains, California. *Geological Society of America Bulletin,* **73**, 139-144.

------ 1966. *Geologic map of the Blanco Mountain quadrangle, Inyo and Mono Counties, California*. United States Geologieal Survey Geologic Quadrangle Map, GQ-529, Scale I :62 500.

------ , HALL C. A. JR. & ERNST, W. G. 1991. Geologie history of the White-Inyo Range. *In:* HALL, C. A. JR. (ed.) *Natural History of the White-lnyo Range, California*. University of California Natural History Guides, **55**, 42-47.

NORTON, D. & KNIGHT, J. 1977. Transport phenomena in hydrothermal systems: cooling of plutons. *American Journal of Science,* **277**, 937-981.

PASCHIER, C. W. & TROUW, R. A. J. 1996. *Microtectonics*. Springer, Berlin.

PATERSON, S. R. & FOWLER, T. K. JR. 1993. Reexamining pluton emplacement proeesses. *Journal of Structural Geology,* **15**, 781-784.

------ & MILLER, R. B. 1998. Stoped blocks in plutons: paleo-plumb blobs, viscometers, or chronometers. *Journa/ of Structural Geology,* **20**, 1261-1272.

RAMSAY, J. G. 1967. *Folding and fracturing of rocks*. McGraw-Hill, New York.

SCHEIDEGGER, A. E. 1965. On the statistics of the orientation of bedding planes, grain axes, and similar sedimentological data. *United States Geological Survey Professional Paper,* **525c**, 164-167.

SCHMID, S. M. & CASEY, M. 1986. Complete fabric analysis of some commonly observed quartz c-axis patterns. *In: Mineral and Rock Deformation: Laboratory Studies. AGU* Geophysical Monographs, **36**, 263-286.

SEIFERT, F. 1970. Low-temperature compatibility relations of cordierite in haplopelites of the system K_2O-MgO-Al_20_3-SiO_2-H_2O. *Journal of Petrology,* **11**, 73-99.

STEIN, E. & PATERSON, S. R. 1996. Country rock displacement during emplacement of the Joshua Fiat Pluton, White-Inyo mountains, California *In:* ONCKEN, O. & JANSSEN, C. (eds) *Basement Tectonics*. Kluwer Academic Publishers Dordrecht, **11**, 35-49.

STERN, T: W., BATEMAN, P. C., MORGAN, B. A., NEWELL, M. F. & PECK, D. L. 1981. *Isotopic U-Pb ages of zircon from the granitoids of the central Sierra Nevada, California*. United States Geological Survey Professional Paper, **1185**.

SYLVESTER, A. G., MILLER, C. F. & NELSON, C. A. 1978. Monzonites of the White-Inyo Range, California, and their relation to the calc-alkalic Sierra Nevada batholith. *Geological Society of America Bulletin,* **89**, 1677-1687.

TARLING, D. H. & HROUDA, F. 1993. *The magnetic anisotropy of rocks*. Chapman & Hall, London.

TULLIS, J., CHRISTIE, J. M. & GRIGGS, D. T. 1973. Microstructures and preferred orientations of experimentally deformed quartzites. *Geological Society of America Bulletin,* 84, 297-314.

Magma mingling and mixing in the Joshua Flat–Beer Creek Pluton: Evidence for the interaction of mafic and felsic magmas from remote sensing, field and chemistry investigations

C. Dietl[*] *Department of Geology and Paleontology, Ruprecht-Karls-University Heidelberg, Im Neuenheimer Feld 234, D-69120 Heidelberg, Germany*

ABSTRACT

The Middle Jurassic Joshua Flat–Beer Creek Pluton at the southern rim of the Inyo Batholith (eastern California) is part of the Mesozoic magmatic arc at the active western margin of the North American continent. The pluton consists mainly of two distinct rock types, the Joshua Flat Monzonite and the Beer Creek Granodiorite. A banding zone at the margin of the pluton, which is characterized by an intimated association of these two lithologies, was detected by remote sensing using thermal infrared multispectral scanner (TIMS) data. Through detailed field work in the banding zone a wide range of magma interaction fabrics was established. Hybrid rocks with characteristic features of both main lithologies, such as hornblende crystals with pyroxene cores (monzonite) and K-feldspar phenocrysts (granodiorite), point to mixing between them, while bands, schlieren and enclaves of finegrained monzonite in the granodiorite and vice versa are hints for mingling between both; finally granodioritic dykes in the monzonite and monzonitic xenoliths in the granodiorite indicate brecciation of the Joshua Flat Monzonite by the Beer Creek Granodiorite. Major element mixing tests confirm the field observations of mixing between the two magmas. The different styles of magma interaction

[*] e-mail: carlo.dietl@urz.uni-heidelberg.de

are explained by the increasing volume of granodiorite reacting with the monzonite over time: first, a high monzonite-granodiorite ratio led to mixing and the formation of hybrid magmas, while the increasing amount of felsic magma over time, and the consequentely increasing viscosity contrast, resulted in mingling followed by the brecciation of the Joshua Flat Monzonite by the Beer Creek Granodiorite.

INTRODUCTION

Numerous plutons display structures, which can be associated with the interaction of different magmas with distinct physical and chemical properties, such as viscosity, temperature, composition and H_2O content. These structures range from finegrained mafic igneous inclusions in felsic magma, so called “enclaves” (Vernon, 1983), via alternating bands of mafic and felsic material of variable thickness (Bacon, 1986) to hybrid rocks formed by the mixture of mafic and silicic educts (Castro et al., 1995) and cover, therefore, a wide field of interactions from mingling to mixing. *Mingling* was defined by Frost and Mahood (1987) as the quenching of one magma by another one due to high viscosity and/or temperature differences. It results in the formation of enclaves in case of an extremely high viscosity/temperature contrast or in the formation of a banding in case of a moderate viscosity/temperature contrast. If the viscosity/temperature contrast is low or even neglible, *mixing* of the magmas occurs and a new hybrid magma with petrological and geochemical properties of both its “parent magmas” is generated. According to Sparks and Marshall (1984) the question, if mingling or mixing occurs also depends on the amount of felsic and mafic magma interacting with each other and on the degree of physical mixing in the magma chamber. Therefore, the observed relationships between the individual lithologies can give informations on the viscosities and temperatures of the participating magmas and about flow conditions, mechanical mixing etc. in the magma chamber.

The Joshua Flat – Beer Creek – Pluton (JBP) of the White Inyo Mountains (California) shows examples of extensive interaction between monzonitic and granodioritic magmas, which encompass the entire range of interplays possible, i.e. enclaves, banding and even hybridisation. They can be observed on all scales: banding was detected on remote sensing imagery (TIMS data) and confirmed by subsequent field work. Swarms of enclaves as well as hybrid rocks were also found during mapping, hybridisation was then confirmed then by geochemical (XRD) investigations.

The paper presents the observed structures, which are related to the interaction of different magmas, at all scales and discusses the physical and chemical properties of magmas in the magma chamber of the JBP.

REGIONAL SETTING

The JBP is situated at the southern end of the Inyo batholith in the White Inyo Mountains, California (Fig. 1), the westernmost range of the Basin and Range Province. The Inyo batholith is composed of alkaline and calc-alkaline plutons, which, according to K-Ar- and $^{40}Ar/^{39}Ar$ datings by McKee and Conrad (1996), intruded in three stages at 180-160 Ma, 145-140 Ma and 100-80 Ma ago into metasedimentary rocks of Precambrian to Triassic age (Nelson et al., 1991).The aureole rocks of the JBP itself are made up of a sequence of Precambrian and Cambrian pelites and carbonates, which were deformed and metamorphosed under greenschist facies conditions during the Antler and Sonoma orogenic events (Ernst 1996). The JBP is part of the oldest intrusive sequence (U-Pb dating by Sylvester et al., 1978; Gillespie, 1979; Stern et al., 1981) and is composed of four lithologic units: the Eureka Valley Monzonite, the Marble Canyon Diorite, the Joshua Flat Monzonite and the Beer Creek Granodiorite (Nelson et al., 1991; Bateman, 1992).

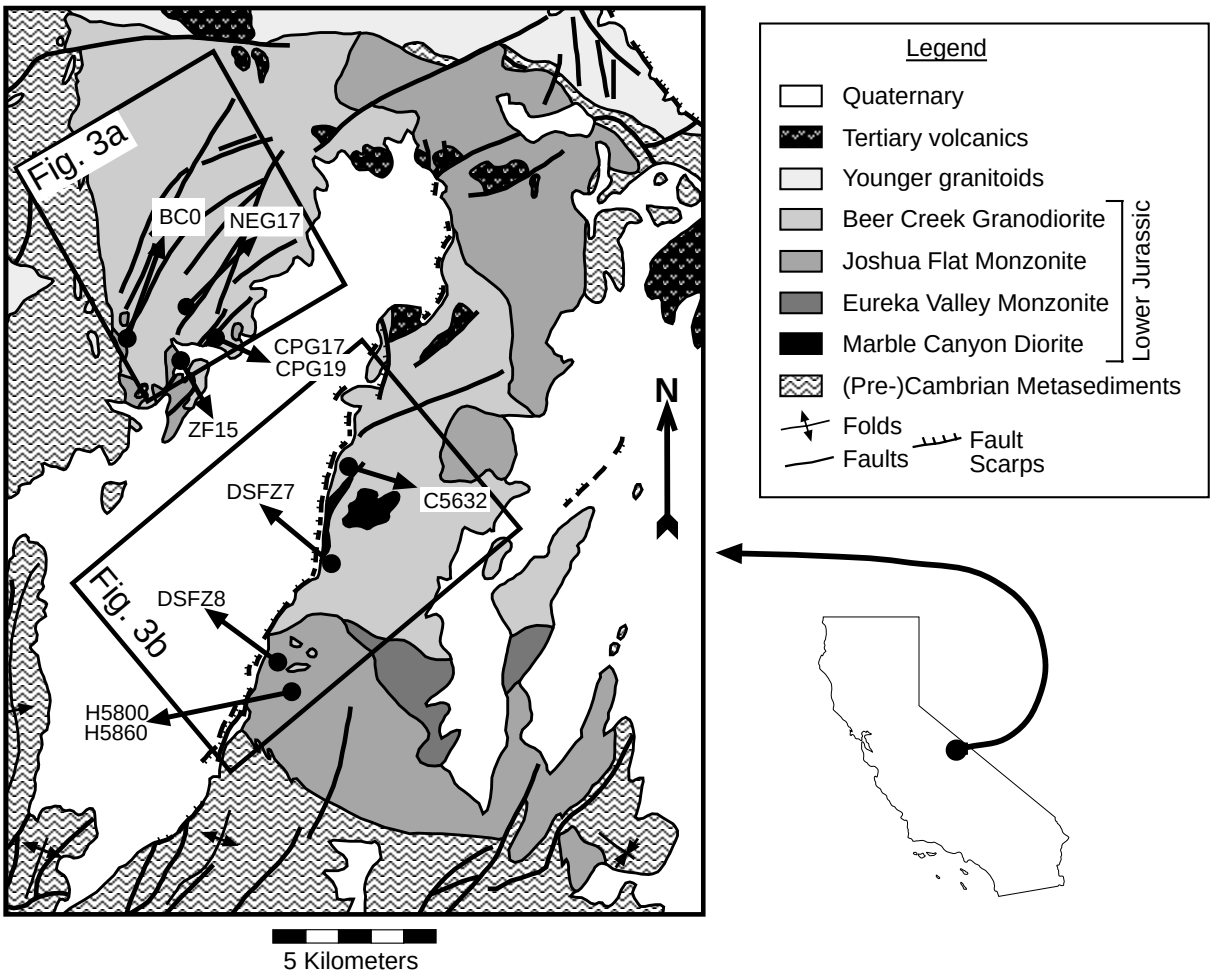

Fig. 1: *Generalized map of the JBP and its vicinity on the base of the maps by Nelson (1966), McKee and Nelson (1967) and Nelson et al. (1991). Also shown are the sample locations and the position of the White Inyo Mountains in California.*

The Eureka Valley Monzonite and the Marble Canyon Diorite form isolated bodies of different size. The margin of the JBP is built up of the Joshua Flat Monzonite, while its centre is made up of the Beer Creek Granodiorite (Fig. 1). According to Al-in-hornblende- (Dietl, in prep.) and phengite-barometry (Ernst, 1996) they intruded at a depth of 8-10 km and heated their host rock to temperatures of up to 735°C as is indicated by Na-in-cordierite-thermometry (Kontny and Dietl, in prep.) and the mineral assemblage K-feldspar + cordierite + plagioclase + quartz in the innermost aureole (Dietl, 1999). During Tertiary and Quaternary times the White Inyo Range was subjected to the typical extensional Basin and Range tectonics accompanied by bimodal basaltic-rhyolithic volcanism.

REMOTE SENSING

Remote sensing data are useful to get a first impression of the overall structure of an unmapped area, but they can also open the eyes of a field geologist for structures overlooked during earlier mapping. In the case of the central White Inyo Mountains the last detailed mapping was done more than 30 years ago by Nelson (1966) and McKee and Nelson (1967). In the meantime several remote sensing studiess were carried out by the Jet Propulsion Laboratory of the NASA. Results of these studies have the potential to complete and improve the published maps and, consequently, our understanding of the intrusion mechanisms of the plutons of this region.

Theoretical background

Most geologic remote sensing studies work with data acquired in the spectral wavelength range from 0.4-2.5 µm due to the high availability of data from this spectral region. One possible method to discriminate granitoid rocks is the determination of the Fe^{2+} content using the reflectivity ratio of band 6 to band 4 of NS-001 Thematic Mapper simulator (TMS) data (Blom, 1986). These two bands are, according to Baird (1984), particularly sensitive for minerals containing ferrous iron. Nevertheless, their usefulness for mapping of silicate rocks is limited, because discrimination of lithologies is based on the presence of iron-bearing silicates, iron oxides, clay minerals and carbonates and not on the bulk chemistry of silicate rocks. The thermal infrared region from 8 to 12 µm provides an opportunity to close this gap, because spectral variations in this range depend on Si-O bonding and therefore on the silicate mineralogy of the rocks. The thermal infrared spectra of silicate minerals have been

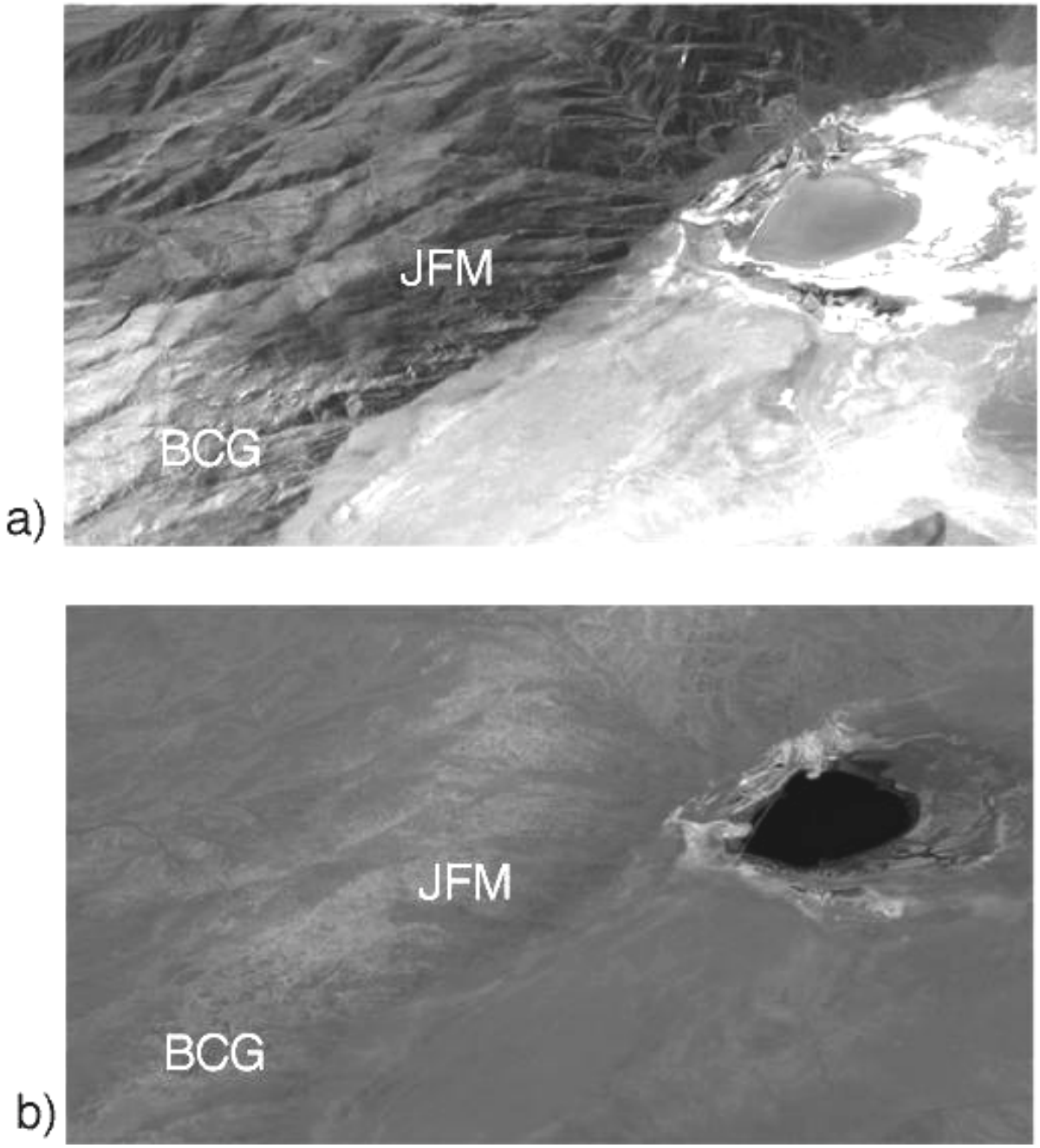

Fig. 2: *NS-001 images of the SW corner of the JBP. Images were not corrected for displacement and distortion introduced by the scanning geometry. North is to the top.* ***Fig. 2a*** *is composed of band 7, 4 and 2. The boundary between the Joshua Flat Monzonite (JFM, dark) and the Beer Creek Granodiorite (BCG, light) is obvious. For comparison with the geologic maps of Nelson (1966), McKee and Nelson (1967) and Nelson et al. (1991). see Fig. 1.* ***Fig. 2b*** *shows the spectral reflectivity ratio between bands 6 and 4, which is indicative for the abundance of ferrous minerals. Again the the two main igneous litholigies can be distinguished by their brightness: the Beer Creek Granodiorite is less bright than the Joshua Flat Monzonite, pointing to its lower* Fe^{2+} *content relative to the latter. Moreover the monzonite seems to be zoned with a brighter, i.e. more ferrous core and a less bright, i.e.* Fe^{2+} *poor rind.*

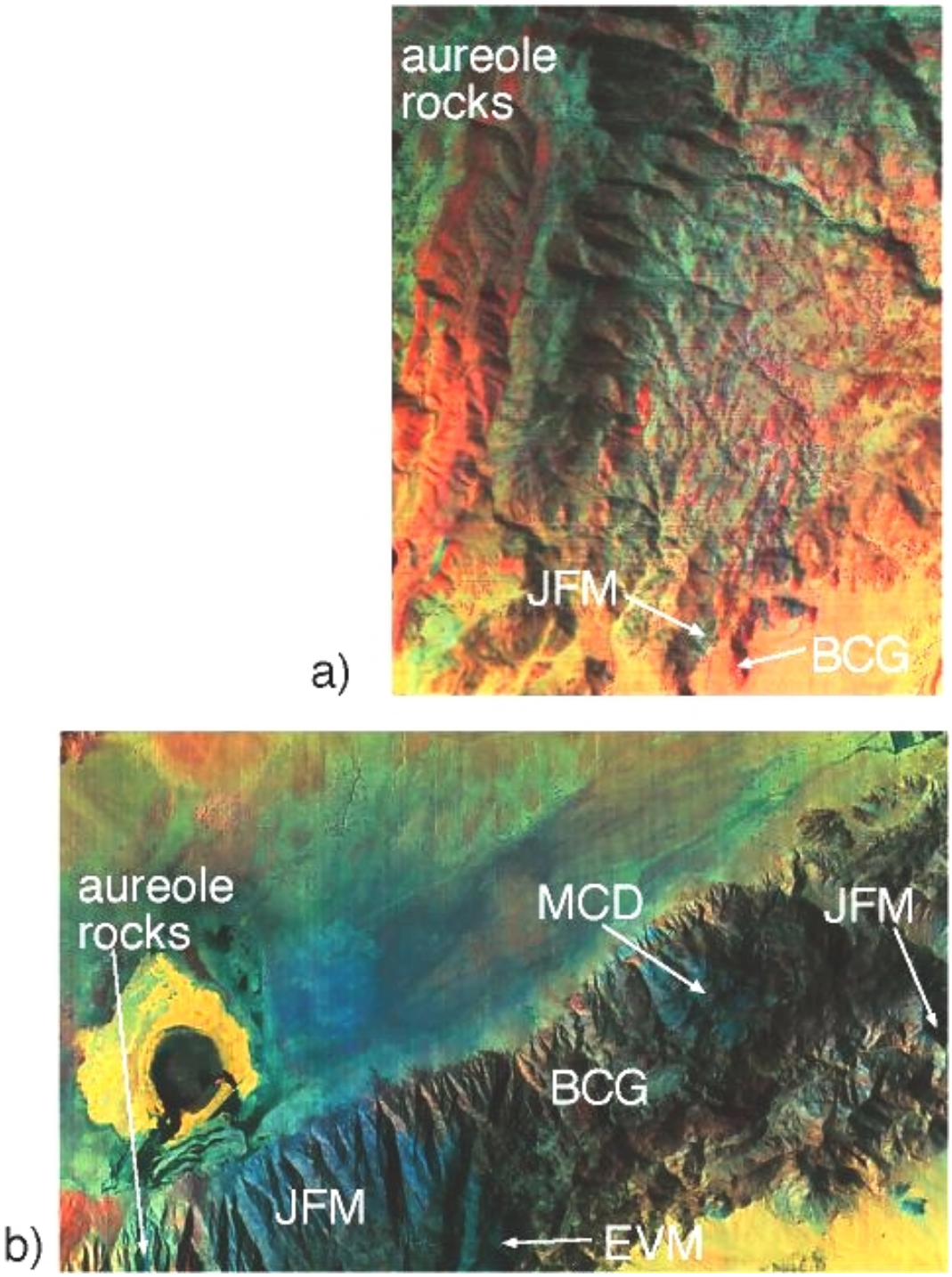

Fig. 3: *Decorrelation stretched TIMS images of the SW part of the JBP with band 5 as red, band 3 as green and band 1 as blue. Images were not corrected for displacement and distortion introduced by the scanning geometry. North is to the top.* ***Fig. 3a*** *shows the so called banding zone north of Deep Springs Valley with granodioritic layers (BCG) in red and monzonitic layers (JFM) in green. The westernmost part of the image is occupied by the aureole rocks: carbonates and metapelites. Short side of the image is c. 7 km long.****Fig. 3b*** *shows the part of the pluton south of Deep Springs Valley. The blue colours correlate with more mafic rocks (Marble Canyon Diorite, MCD, Eureka Valley Monzonite, EVM, and Joshua Flat Monzonite, JFM), while the Beer Creek Granodiorite (BCG) appears red-brown. Short side of the image is c. 7.5 km long. For comparison with the geologic maps of Nelson (1966), McKee and Nelson (1967) and Nelson et al. (1991). see Fig. 1.*

investigated for almost 50 years (Launer, 1952; Salisbury et al. 1987) and led to the conclusion, that the Reststrahlen emissivity minimum is directly related to the Si-O stretching vibration frequency and shifts from longer (11 µm) to shorter wavelengths (9 µm) with increasing strength of the Si-O bonds. Si-O bonds are weak in nesosilicates with isolated tetrahedra and become stronger with increasing connectivity between the individual tetrahedra, i.e. are strongest in tectosilicates (Hunt, 1980). Although whole rock spectra are composed of spectra of individual minerals and are, consequently, more complex the latter (Salisbury et al. 1987), it can be assumed, that Reststrahlen spectra of igneous rocks shift from longer wavelengths for mafic rocks, which contain more neso- and inosilicates, to shorter wavelengths for felsic rocks, which consist mainly of tectosilicates.

For a comprehensive information of the composition and general structure of the JBP data sets from both spectral regions, the near (0.76-1.75 µm) and the middle infrared (8-12 µm) were used.

Data acquisition and processing

Data were acquired with an airborne NS-001 TMS and a six-channel thermal infrared multispectral scanner (TIMS) aboard a NASA Lear jet.

TABLE 1. NS-001 TMS CHANNELS

Channel	Wavelength (µm)
1	0.45-0.52
2	0.52-0.60
3	0.63-0.69
4	0.76-0.90
5	1.00-1.30
6	1.55-1.75
7	2.08-2.35
8	10.4-12.5

TABLE 2. PEAK POSITIONS OFTIMS CHANNELS

Channel	Wavelength (µm)
1	8.3
2	8.8
3	9.2
4	10.05
5	10.7
6	11.5

NS-001 data were taken during flights on March 25, 1987 under minor cloud coverage. For the spectral width of the individual bands see Table 1. Image processing was done with the UNIX computer program “Imagine” at the Department of Geology, Geophysics and

Geoinformatic of the Free University Berlin. The images presented here are composed of band 7, 4 and 2 (Fig. 2a) and show the spectral reflectivity ratio between bands 6 and 4 (Fig. 2b).

TIMS images were taken during two flights on March 25, 1987 and August 18, 1994 under almost cloud-free conditions by the NASA Jet Propulsion Laboratory at the California Institute of Technology, Pasadena. The peak positions of the six spectral bands collected by the individual channels of the TIMS are shown in Table 2. TIMS imagery derived from the scans presented here (Fig. 3) are decorrelation stretched images with band 5 as red, band 3 as green and band 1 as blue. Images were not corrected for displacement and distortion introduced by the scanning geometry. Processing was carried out by the Jet Propulsion Laboratory.

Image analysis

Analysis and interpretation of the remote sensing data are mainly based on the comparison of the TIMS imagery with the published geologic maps of the central White Inyo Range, shown here as a simplified sketch map (Fig. 1), (Nelson, 1966; McKee and Nelson, 1967) and the results of my own field work. The comparison with the maps of Nelson (1966) and McKee and Nelson (1967) shows clearly, that certain lithologies can be distinguished and mapped on the base of these images in good detail (comparison of Figs. 1, 2 and 3).

The NS-001 images, the composite one (Fig. 2a) as well as the ratio image (Fig. 2b), show the border between the Beer Creek Granodiorite and the Joshua Flat Monzonite as a clear break in gray shades (Fig. 2a) and brightness (Fig. 2b) in the same position as on the map of Nelson (1966) (Fig. 1). The monzonite appears much darker and brighter than the granodiorite due to its higher Fe^{2+} content. Moreover, the reflectivity ratio image shows a zonation inside the Joshua Flat Monzonite with an iron-poor margin and a core rich in ferrous iron.

Also on the TIMS images the big spherical body composed of the Joshua Flat Monzonite (and to a smaller degree also of the Eureka Valley Monzonite, which was not mapped during field work for this project) at the SW corner of the JBP south of Deep Springs Valley (Fig. 3b) can be clearly identified by means of the blue colours, which are, according to Sabine et al. (1994), typical for mafic rocks. In the same image a smaller body of Joshua Flat Monzonite at the northeastern margin and the dioritic xenoliths, which were mapped by Nelson (1966) and McKee and Nelson (1967) (Fig. 1) and verified by own field work can also be detected by remote sensing. The rock type, which includes the dioritic xenoliths and appears in red-brown colours on the TIMS image, should be, according to Sabine et al. (1994), of intermediate to felsic composition. Again, the geologic map of Nelson (1966) and McKee and Nelson (1967) (Fig. 1) and own field work confirm this assumption and identify this lithological unit as Beer Creek Granodiorite. Moreover, the entire host rock-pluton-contact can be seen in the images and even the origin of alluvial sediments in the Deep Springs Valley can be deduced from their colour: the bluish and reddish sediments in the valley, for example, are probably derived from mafic and felsic igneous rocks, respectively, in the surrounding mountains. A structure in the JBP not present on the geologic maps by Nelson (1966) (Fig. 1) and not mentioned by mapping geologists until now is the banding shown in Fig. 3a north of Deep Springs Valley. Interpreting this TIMS image according to the colours displayed, the reddish stripes should represent felsic, possibly granodioritic or granitic material, while the green stripes should be composed of more mafic material, such as diorite or monzonite. The area covered by the banding (in the following called “banding zone”) is 3 km wide and 8 km long and is, consequently, an important feature of the entire, 15 km by 20 km wide pluton, which had not been recognized without the TIMS data. This banding zone appeared to be of particular importance for the intrusion of the JBP and was therefore investigated in detail.

FIELD OBSERVATIONS

Petrography

Of all four lithologic units of the JBP only three, the Marble Canyon Diorite, the Joshua Flat Monzonite and the Beer Creek Granodiorite, respectively, are present in the mapping area described here.

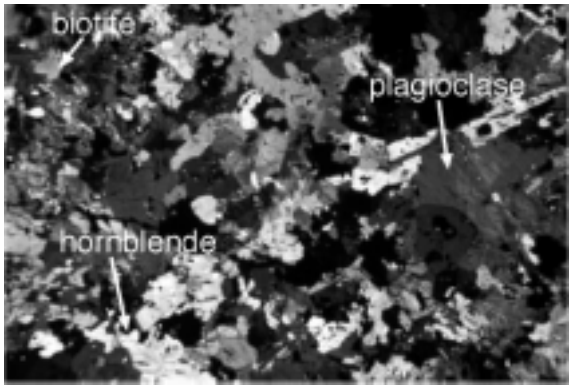

Fig. 4a: *Microphotograph of the Marble Canyon Diorite (XPL, long side: 7 mm).*

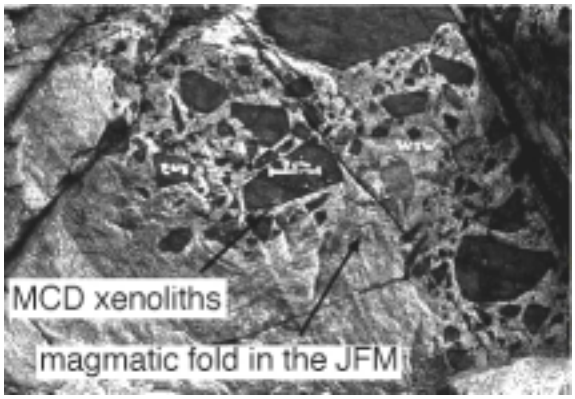

Fig. 4b: *Xenoliths of the Marble Canyon Diorite (MCD) in the Joshua Flat Monzonite (JFM). The monzonite describes a magmatic fold between two xenoliths in the left half of the photograph. The fold is probably a result of magmatic flow.*

The Marble Canyon Diorite is a medium- to coarse-grained, structurally isotropic diorite to monzodiorite, rich in hornblende (60 vol%) and plagioclase (25 vol%). K-feldspar (5 vol%), biotite and quartz (5 vol%) are rare; titanite, apatite, hematite and magnetite occur as accessories (Fig. 4a). This diorite was found only as xenoliths in the Joshua Flat Monzonite (Fig. 4b) and the Beer Creek Granodiorite. The Joshua Flat Monzonite is characterized by hornblende aligned in a steep NNW-SSE striking, magmatic foliation. It is composed of oligoclasic to andesitic plagioclase (c. 50 vol%), K-feldspar (up to 30 vol%), quartz (5-10 vol%), hornblende (10-40 vol%), biotite (up to 10 vol%), clinopyroxene (up to 10 vol%) and titanite (up to 5 vol%) (Fig. 5a). Three varieties of the monzonite were found: a medium-

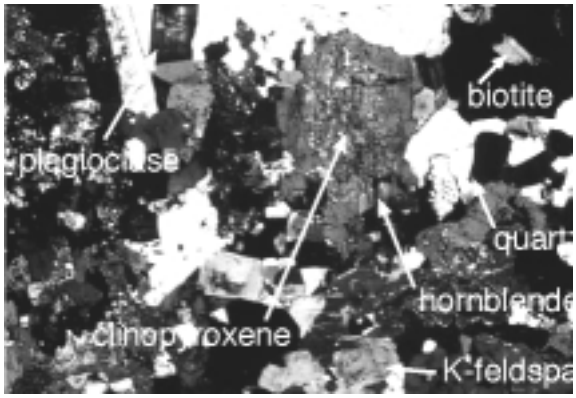

Fig. 5a: *Microphotograph of the Joshua Flat Monzonite (XPL, long side: 5 mm).*

Fig. 5b: *The light variety of the Joshua Flat Monzonite with a slight, subhorizontal, magmatic banding.*

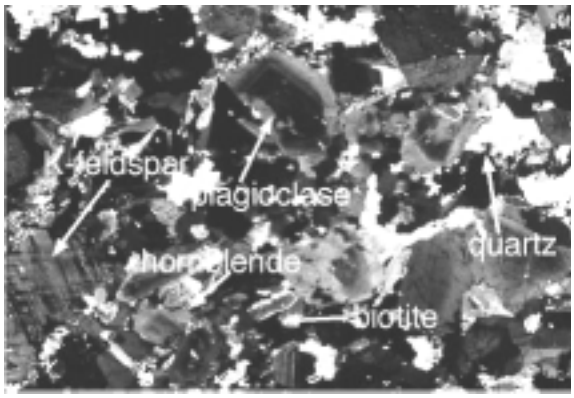

Fig. 6a: *Microphotograph of the Beer Creek Granodiorite (XPL, long side: 5 mm).*

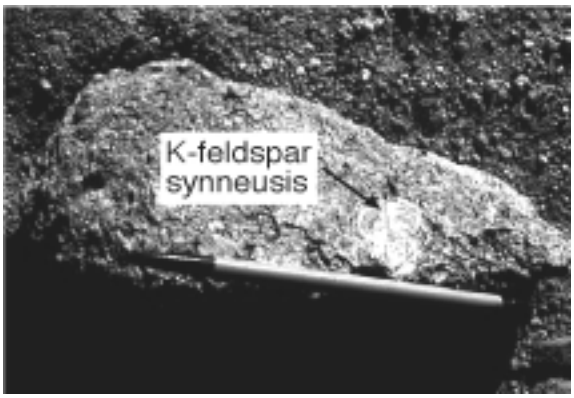

Fig. 6b: *Synneusis of K-feldspar phenocrysts in the Beer Creek Granodiorite.*

grained and hornblende-rich one (the “normal” variety; Fig. 4b), a second, light-coloured, K-feldspar-rich variety with a foliation, which is only weakly developed due to the scarcity of the foliation-forming mineral hornblende (Fig. 5b) and, finally, a dark, finegrained, biotite- and hornblende-rich variety (Fig. 7a), which was found only in the immediate neighbourhood of the Beer Creek Granodiorite, in particular in the banding zone. All three varieties have two features in common: the occurence of hornblendes with pyroxene cores and large titanite crystals visible even macroscopically. The Beer Creek Granodiorite is a coarse-grained, light-coloured granodiorite and consists of quartz (10-20 vol%), oligoclasic plagioclase (40 vol%), K-feldspar (30 vol%), biotite (15-25 vol%) and hornblende (5-15 vol%); titanite, epidote, zircon, apatite and magnetite occur as accessories (Fig. 6a). The most characteristic feature of

the Beer Creek are the idiomorphic and up to 3 cm long K-feldspar phenocrysts, which are often aligned in a weak, steeply dipping and NNW-SSE trending magmatic foliation, but can also form other typical magmatic fabrics such as tiling or synneusis (Fig. 6b). Microgranular enclaves of monzonitic composition also follow this foliation (Fig. 8a). At the contacts between the latter two lithologies and especially in the banding zone granitoids with properties of both the monzonite and the granodiorite were observed: they show K-feldspar phenocrysts typical for the Beer Creek Granodiorite as well as hornblendes with pyroxene cores typical for the Joshua Flat Monzonite (Fig. 7b).

Field relationships in the banding zone

A number of different contact relationships between the Joshua Flat Monzonite and the Beer Creek Granodiorite can be observed.

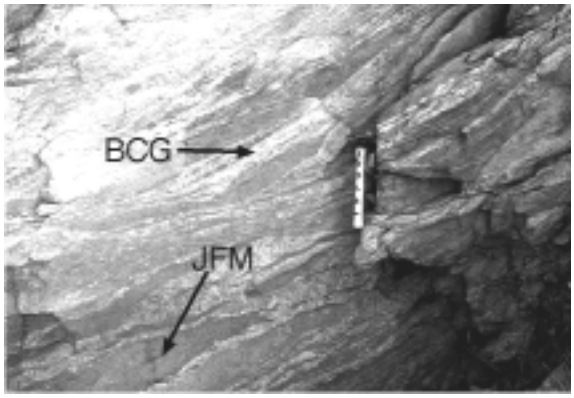

Fig. 7a: *Schlieren of finegrained Joshua Flat Monzonite (JFM) intercalated with Beer Creek Granodiorite (BCG).*

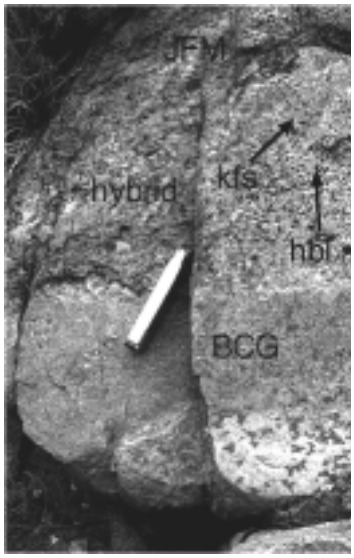

Fig. 7b: *K-feldspar (kfs) xenocrysts derived from the Beer Creek Granodiorite (BCG) together with hornblende (hbl) from the Joshua Flat Monzonite (JFM) point to the hybridic nature of the igneous rock in this photograph.*

The first type of contact is represented by diffuse injection zones, with monzonitic and granodioritic bands and schlieren close together. Schlieren of monzonitic material (the finegrained as well as the normal variety) lie in a granodioritic matrix and vice versa (Fig. 7a). The banding occurs on all scales. Schlieren, only a few decimeters long occur next to bands hundreds of meters long. Generally, the bands are oriented parallel with the magmatic

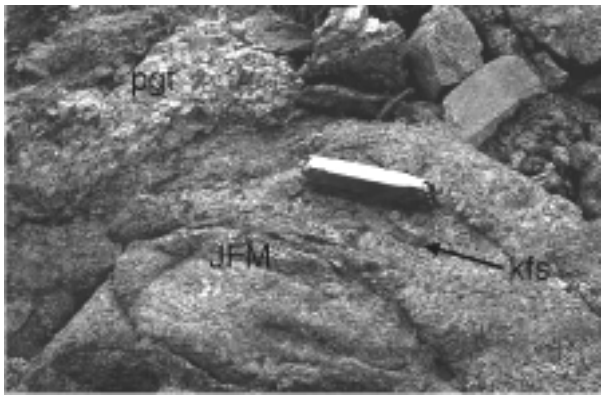

Fig. 7c: *The large K-feldspar (kfs) xenocrysts in Joshua Flat Monzonite (JFM) come originally from the neighbouring pegmatite (pgt) and indicate the liquid-liquid-contact of both the magmas, as well as mingling between both.*

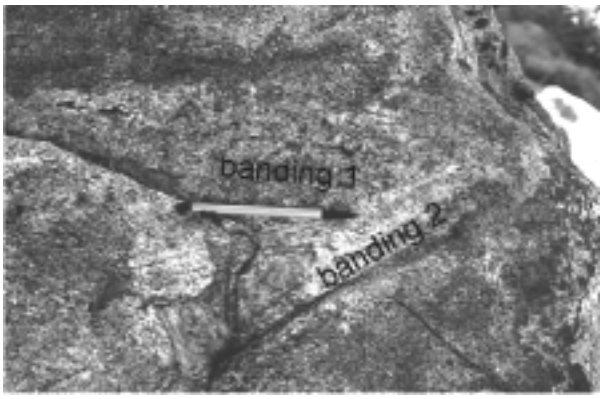

Fig. 7d: *Two magmatic bandings, one crosscutting the other one.*

foliation; they strike NNW and dip steeply to the ESE or WNW. Bands dominate, but also elliptical bodies of Beer Creek Granodiorite of several square metres of outcrop size in the finegrained Joshua Flat Monzonite can be observed. Not all bands can easily be identified as Beer Creek Granodiorite or Joshua Flat Monzonite: some show characteristics of both, such as K-feldspar phenocrysts (Beer Creek Granodiorite) and hornblende crystals with pyroxene cores or large titanite crystals (Joshua Flat Monzonite), (Fig. 7b). These bands are interpreted as the products of magma mixing and therefore as hybrid rocks. In one place even mixing between the monzonite and a pegmatite was found: a pegmatite with K-feldspar phenocrysts up to 5 cm long lies parallel with a band of the normal Joshua Flat Monzonite. At the immediate contact the monzonite bears 4 cm long K-feldspar phenocrysts, which are interpreted as xenocrysts derived from the pegmatite, indicating a simultaneous intrusion of both (Fig. 7c). The observation of lobate contacts between layers of different composition, which are convex toward the more mafic band, indicates a liquid-liquid contact and points to the hypersolidus origin of the banding (Castro et al., 1995). Lobate interfaces between fluids of differing viscosities are a common feature in nature with the convex shape usually on the less viscous side (e. g. contacts between oil and water). In one place two banding generations

are developed with the one cutting across the other one (Fig. 7d). Some schlieren have a

Fig. 7e: *Cumulatic schliere consisting of hornblende and titanite.*

Fig. 7f: *Intensely deformed magmatic banding with schlieren deformed to tight and even isoclinal folds.*

cumulate-like character with the composition K-feldspar + hornblende ± titanite (Fig. 7e). In some places the banding was folded into asymmetrtial shear or isoclinal folds (Fig. 7f). These deformational structures can be regarded as the product of magmatic flow under a simple shear regime close to or even beneath the rheological critical melt percentage (RCMP) of c. 25% (Arzi, 1978).

Enclaves of finegrained Joshua Flat Monzonite are the second type of contacts between monzonite and granodiorite. They are the most common feature in the banding zone. Most of them occur in the Beer Creek Granodiorite, but they were also found in the normal Joshua Flat Monzonite and pegmatite dykes. Three different types of shapes can be distinguished: (1) elongated, ellipsoidal enclaves, which build enclave swarms (Fig. 8a); (2) elongated, but irregular, schlieren-like enclaves (Fig. 8b), which are particularly common, where bands of monzonitic, granodioritic and hybrid material are intimately associated; (3) pillow-like, globular bodies of all sizes from centimetres to the metre-scale (Fig. 8c).

Fig. 8a: *Swarm of elongated, ellipsoidal enclaves.*

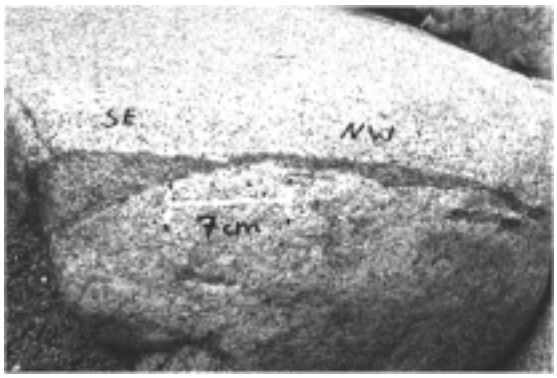

Fig. 8b:*Elongated, irregular and almost disintegrated enclave.*

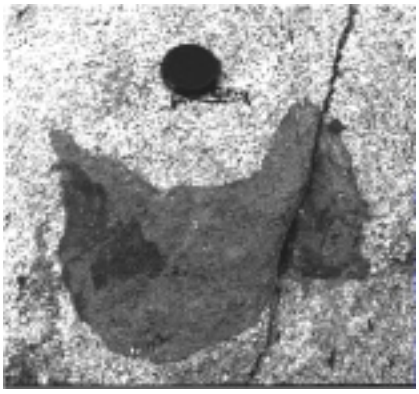

Fig. 8c: *Pillow-like, globular enclave with a partly smooth, partly lobate, dark and extremey finegrained magin, regarded as the product of chilling of the finegrained, monzonitic enclave material.*

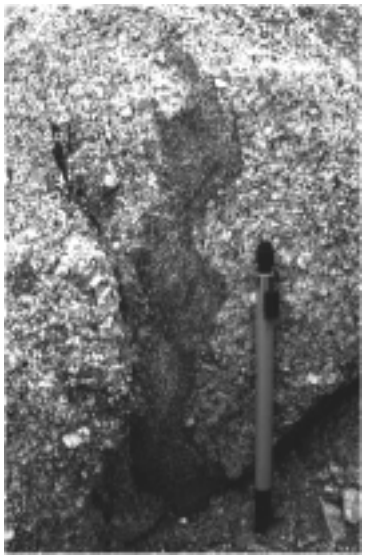

Fig. 8d: *Elongate enclave with clearly lobate contacts with its host, the Beer Creek Granodiorite, indicating liquid-liquid contacts and unstable flow between both magmas.*

Fig. 8e: *Enclave with a pegmatoidal, quartzofeldspathic margin (pgt rim). This margin might be due to chilling of the H_2O-rich enclave, what led to the expulsion of the water into the hosting granodiorite (BCG) and to the formation of a pegmatitic granodiorite rind around the monzonitic enclave.*

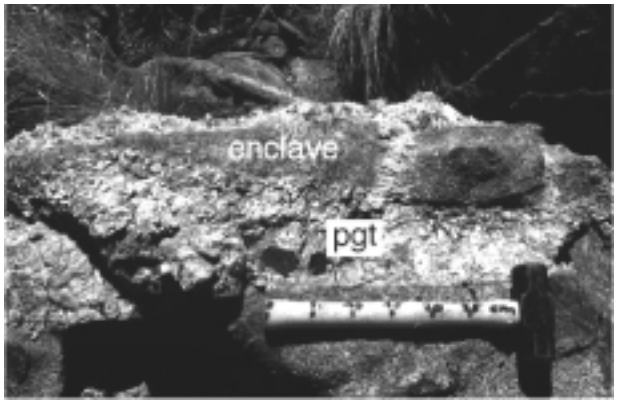

Fig. 8f: *Finegrained, monzonitic enclave disrupted by a pegmatitic dyke (pgt).*

Fig. 8g: *Enclave, deformed to a sigmoidal body by magmatic defor-mation, with an isotropic, disor-dered internal*

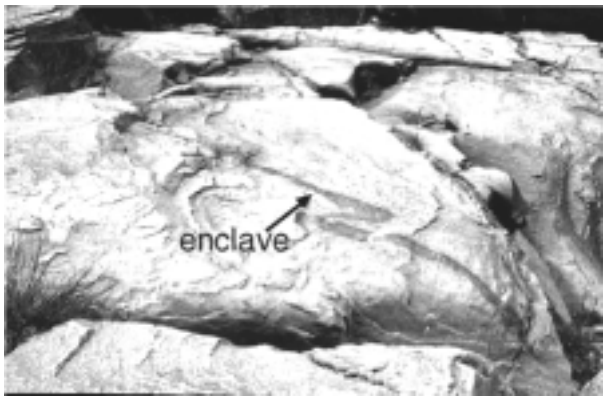

Fig. 8h: *Large enclave deformed to an asymmetrical shear fold due to deformation in the maamatic state.*

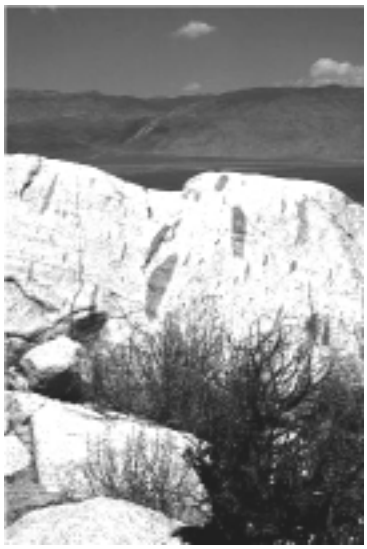

Fig. 8i: *Enclave swarm aligned in a kind of magmatic sc-fabric.*

Fig. 8j: *Microgranular enclave, deformed to tight folds, whose axial planes are parallel to the magmatic foliation.*

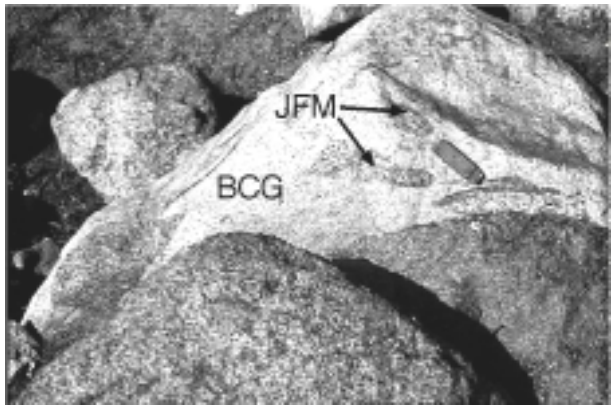

Fig. 8k: *Enclaves of the normal Joshua Flat Monzonite (JFM) hosted by the Beer Creek Granodiorite (BCG).*

All three types can be found next to each other. Aside from smooth enclave rims also lobate margins were observed (Fig. 8d), which are, as stated earlier in this section, typical for a liquid-liquid contact, a low viscosity contrast and unstable flow between the two interacting magmas (Castro et al., 1990a). Some of the enclaves have finer grained, darker, probably chilled, margins (Fig. 8c), other enclaves have pegmatoidal, quartzofeldspathic margins (Fig. 8e). The finegrained enclaves are “intruded” and eventually disrupted by the Beer Creek Granodiorite and related pegmatites (Fig. 8f). Feldspar phenocrysts in the microgranular enclaves are probably due to physical interaction with the felsic lithologies. The internal fabric of the enclaves, mainly a magmatic foliation defined by hornblende and biotite, is in the most cases concordant with the external fabric. However, such enclaves were also found where the internal fabric lies discordant to the external fabric or the crystals in the enclave are totally disordered (Fig. 8g). In both these cases the external foliation is cut by the contact between enclave and host. Some enclaves are deformed into asymmetrical shear folds (Fig. 8h) and sigmoidal shear bodies (Fig. 8g), indicating simple shear in the magmatic state. One enclave swarm seems to be aligned in a kind of magmatic S-C fabric (Fig. 8i). Other enclaves form tight and isoclinal folds (Fig. 8h and j) with the internal fabric being also folded. The axial surface of these folds is lying parallel with the external magmatic foliation and may also be refolded. Again, all these fabrics are interpreted as the result of magmatic flow close to or even beneath the RCMP. Generally, the number of microgranular enclaves increases close to the contacts between the Joshua Flat Monzonite and the Beer Creek Granodiorite. In addition to the microgranular enclaves elongated, ellipsoidal enclaves of the normal Joshua Flat Monzonite were found in the Beer Creek Granodiorite (Fig. 8k) and a pegmatitic enclave in the Joshua Flat Monzonite were found.

A third kind of contact between the two litholgies is made up by dykes: granodioritic dykes crosscut the monzonite (Fig. 9a), disrupt and brecciate it and and seperate small stoped blocks

as well as pillow-like enclaves (Fig. 9b). In other places, dykes of the light-coloured Joshua Flat Monzonite intrude the Beer Creek Granodiorite.

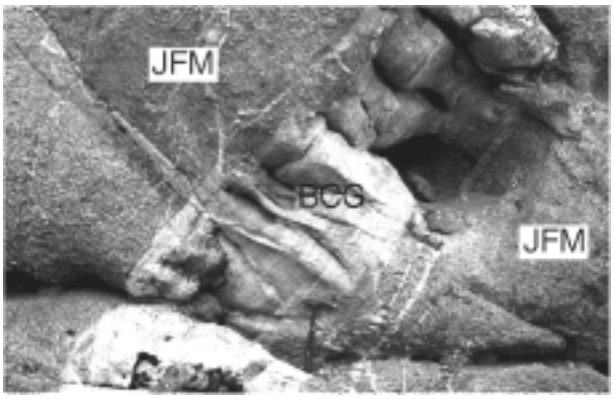

Fig. 9a: *Dykes of the Beer Creek Granodiorite (BCG) intrude, disrupt and brecciate the finegrained Joshua Flat Monzonite (JFM).*

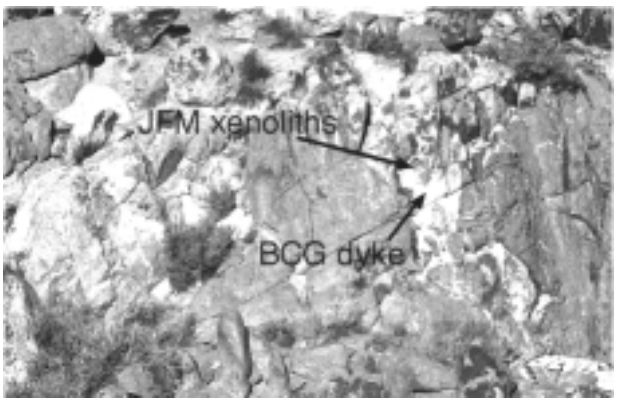

Fig. 9b: *Enclaves and xenoliths of the finegrained Joshua Flat Monzonite (JFM) in a granodioritic dyke as the results of brecciation of the monzonite by the Beer Creek Granodiorite (BCG).*

WHOLE ROCK GEOCHEMISTRY

All igneous rock types appearing in the mapped area, including the Marble Canyon Diorite (sample C5632), the normal (H5860, DSFZ8), finegrained (CPG17) and light Joshua Flat Monzonite (ZF15), the Beer Creek granodiorite (CPG19, DSFZ7), hybrid rocks according to field observations (NEG17, BC0) and a mafic, coarsegrained enclave (H5800), were analyzed for major elements by X-ray fluorescence. The sample locations are sho wn in Fig. 1 and results in Table 3. The aim of these examinations was a) to characterize the individual rock types distinguished earlier by petrographic methods and b) to find out, if the observed mixing can be confirmed by geochemical data. For this purpose the major element mixing test proposed by Fourcade and Allegre (1981) was applied.

Major elements

Almost all investigated rocks belong to the alkalic suite. Only one of the two samples from the Beer Creek granodiorite and sample C5632 (Marble Canyon Diorite) plot in the sub-alkalic field in the nomenclature diagram (Fig. 10) of Cox et al. (1979) and are of calc-

alkaline nature. All other samples are alkaline rocks and belong to the K-series, besides sample H5800, which is part of the high-K series. The most mafic rocks are the mafic, coarsegrained enclave (H5800), which is of monzogabbroic to monzodioritic composition, and the sample from the Marble Canyon Diorite (C5632), which plots in the diorite field in Fig. 10. All the samples from the normal and finegrained Joshua Flat Monzonite, as well as the hybrid samples plot in the monzonite field. Smple ZF15 from the light-coloured Joshua Flat Monzonite occurs as a syenite in Fig. 10. The Beer Creek Granodiorite samples are, according to Cox et al. (1979) of granitic (CPG19) and alkali granitic composition (DSFZ7).

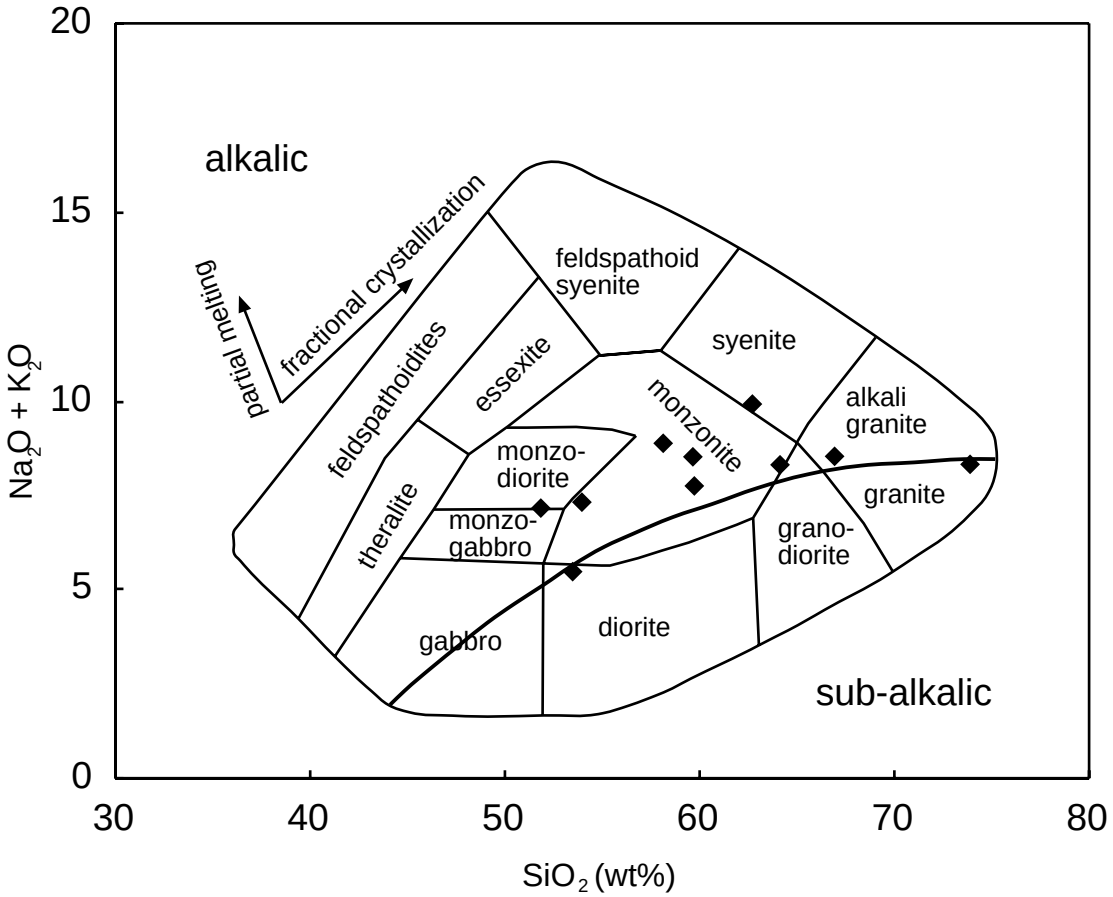

Fig. 10: *Nomenclature diagram for plutonic rocks according to Cox et al. (1979) with the composition of the individual samples from the JBP. For discussion see text.*

Major elements of almost all samples display good linear trends in SiO_2 variation diagrams (Fig. 11). Only diorite C5632 and monzogabbro H5800 differ significantly, indicating that they are not related to the rest of the suite.

TABLE 3. MAJOR ELEMENT ANALYSES FOR THE INDIVIDUAL ROCK TYPES FROM THE JBP. FOR SAMPLE LOCATIONS SEE FIG. 1

Sample	SiO_2	TiO_2	Al_2O_3	FeO	MnO	MgO	CaO	Na_2O	K_2O	P_2O_5	LOI	Total
Enclave												
H5800	51.84	1.60	13.22	7.92	0.18	8.99	8.10	1.97	5.15	0.32	0.90	100.18
MCD												
C5632	53.46	1.62	12.74	7.99	0.13	6.95	10.13	3.23	2.20	1.41	0.42	100.27
Finegrained JFM												
CPG17	53.83	1.00	18.12	6.94	0.12	2.91	7.81	3.97	3.30	0.84	0.45	99.30
Normal JFM												
DSFZ8	59.54	0.82	17.11	5.73	0.11	3.25	5.90	3.71	4.02	0.32	0.24	100.74
H5860	58.03	1.05	17.22	5.88	0.10	2.78	6.11	4.78	4.02	0.44	0.35	100.77
Light-coloured JFM												
ZF15	62.66	0.66	16.78	3.53	0.06	1.26	3.56	4.71	5.15	0.43	0.26	99.06
BCG												
DSFZ7	66.84	0.52	15.76	3.16	0.05	1.15	2.89	4.21	4.31	0.20	0.47	99.55
CPG19	73.77	0.19	14.27	1.30	0.02	0.39	1.41	3.77	4.49	0.04	0.24	99.89
Hybrid rocks												
NEG17	59.60	0.76	17.73	4.58	0.07	2.34	4.90	4.44	4.01	0.36	0.48	99.27
BC0	64.15	0.74	16.48	3.93	0.05	1.63	3.82	4.10	4.14	0.32	0.39	99.75

MCD: Marble Canyon Diorite
JFM: Joshua Flat Monzonite
BCG: Beer Creek Granodiorite

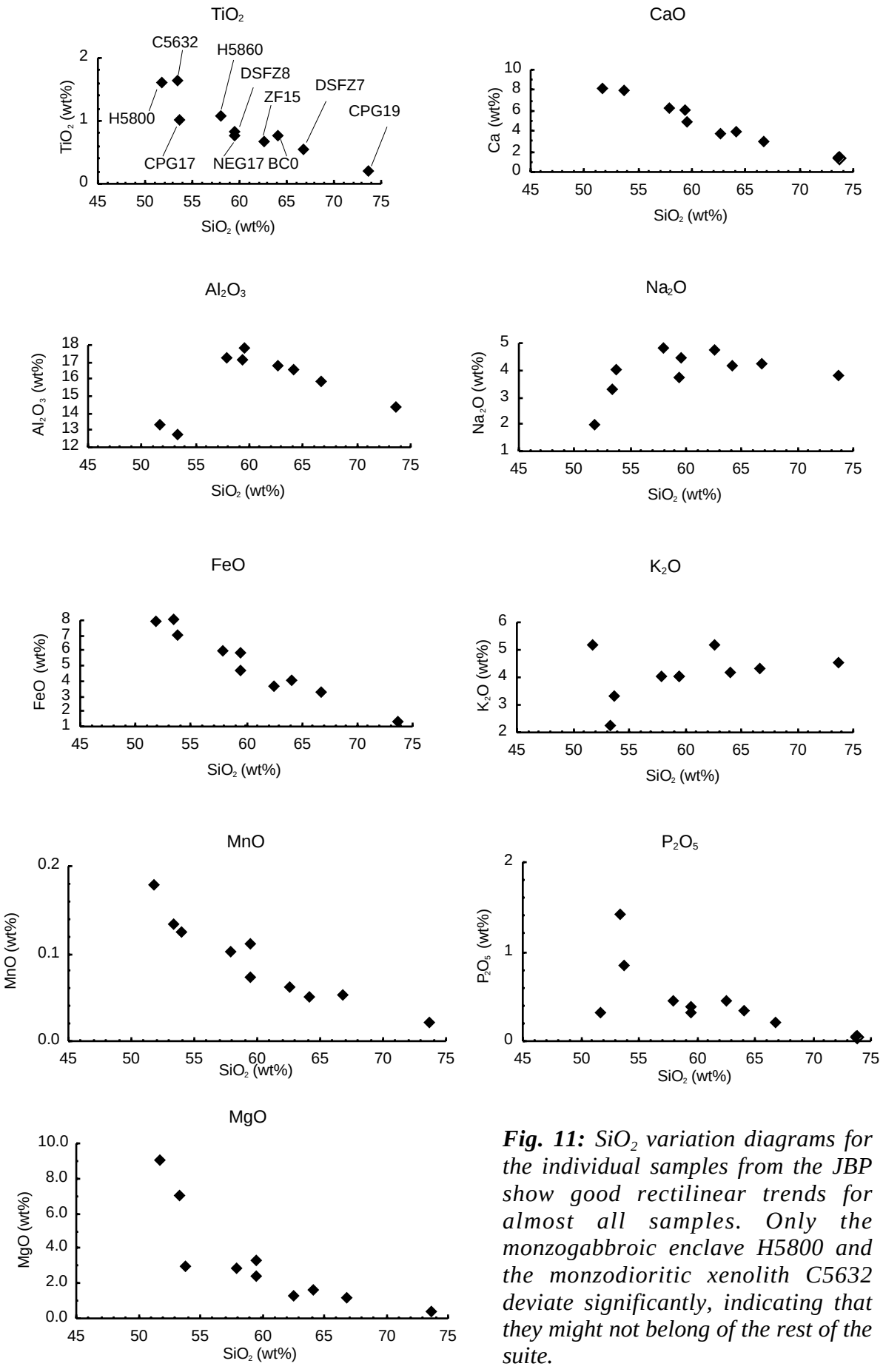

Fig. 11: *SiO_2 variation diagrams for the individual samples from the JBP show good rectilinear trends for almost all samples. Only the monzogabbroic enclave H5800 and the monzodioritic xenolith C5632 deviate significantly, indicating that they might not belong of the rest of the suite.*

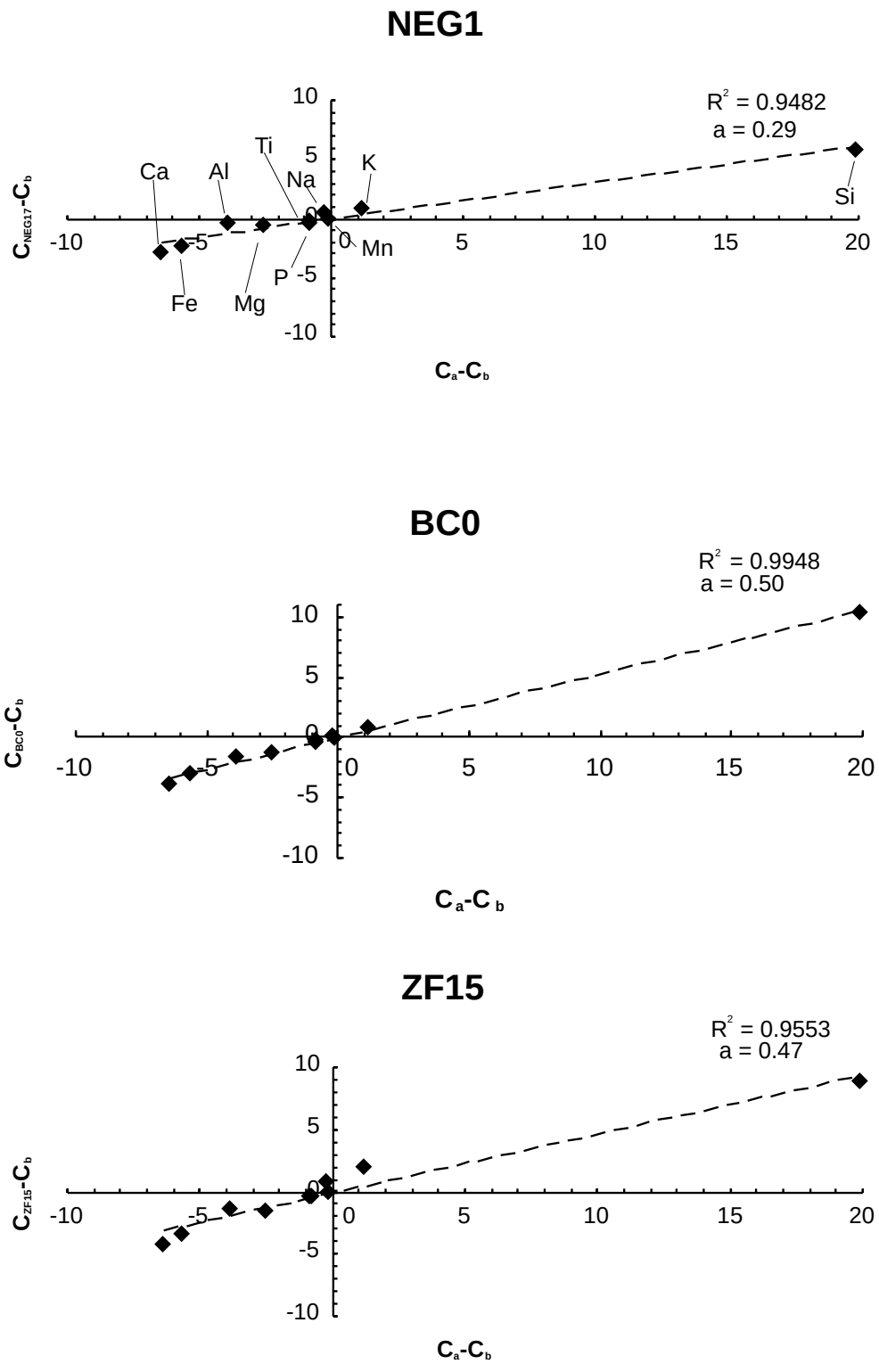

Fig. 12: *Mixing tests according to Fourcade and Allegre (1981) for samples NEG17, BC0 and ZF15. Mafic and felsic end members are CPG17 and CPG19, respectively. C_a is the cation oxide content of the felsic end member, C_b the cation oxide content of the mafic end member and C_{NEG17} C_{BC0} and C_{ZF15} the cation oxide content of the hybrids. R^2 is the correlation coefficient and a the slope of the regression straight line. The slope also gives the portion of felsic magma taking part in the mixing process. For brevity, element symbols are shown instead of oxides.*

Mixing test

The mixing hypothesis, which is based on the observed structures in the banding zone NW of Deep Springs Valley was checked by applying the mixing test of Fourcade and Allegre (1981) to the samples from this area. The mixing test is done by plotting the difference in all major element oxides between the felsic and mafic end members on the x-axis versus the same difference between one of the supposed hybrids and the mafic end member on the y-axis (Fig. 12). The regression straight line for this data set gives two informations: the correlation coefficient (R^2) indicates, if the "hybrid" can be regarded as the product of mixing. This can be assumed, if R^2 is close to 1. Only in this case the slope gives the relative proportion of the felsic magma end member in the hybrid.

Sample CPG19 (Beer Creek Granodiorite) and CPG17 (finegrained Joshua Flat Monzonite) constitute the felsic and mafic end members, respectively. All three sa mples picked for the mixing test (NEG17, BC0 and ZF15) display very good correlation coefficents (0.9482 for NEG17, 0.9948 for BC0 and 0.9553 for ZF15) pointing to their hybrid origin. It is surprising, that even the light-coloured Joshua Flat Monzonite appears as a hybrid rock, but the results of the mixing test makes this very probable. The slopes of the regression lines for the individual samples show the proportion of the Beer Creek Granodiorite in the single hybrids to be 29% (NEG17), 50% (BC0) and 47% (ZF15).

DISCUSSION AND CONCLUSIONS

Detailed field work documented different styles of interaction between the Beer Creek Granodorite and the Joshua Flat Monzonite, ranging from mixing of both parent magmas via mingling and formation of monzonitic, microgranular enclaves to dyking of the granodiorite associated with brecciation of the monzonite. Geochemical investigations showed that from two end members, the Beer Creek Granodiorite and the finegrained Joshua Flat Monzonite, several stages of hybridisation with different proportions of both end members in the hybrid

products can be derived. The finegrained Joshua Flat Monzonite is the least “contaminated” variety of the monzonite. The fine grain size indicates rapid cooling and chilling. This variety, therefore, does not show any signs of interaction with the granodiorite.

Although a wide spectrum of relations between the two main lithologies was observed, most features indicate the Beer Creek Granodiorite to intrude the Joshua Flat and not vice versa. (1) Most enclaves are of monzonitic composition, occur mainly in the Beer Creek Granodiorite and increase in number towards the contacts between the Beer Creek Granodiorite and the individual varieties of the Joshua Flat Monzonite. (2) Only a few enclaves have chilled margins. Microgranular enclaves with chilled margins are usually regarded as the remnants of basaltic dykes, which intruded a colder, more felsic magma, crystallized rapidly and were subsequently disrupted (Castro et al., 1990b). Therefore, most, if not all enclaves can not originate from mafic dykes. (3) All but two dykes are granodioritic and intrude the Joshua Flat Monzonite. The two monzonitic dykes intruding the granodiorite can be regarded, according to Castro et al. (1995) as the results of back-veining. (4) Only stoped blocks of Joshua Flat Monzonite in Beer Creek Granodiorite were observed, but never the inverse relationship.

The homogeneous and heterogeneous bands of hybrid rocks as well as the K-feldspar xenocrysts in the monzonite band close to the K-feldspar-rich pegmatite can only be regarded as the products of magma-magma interaction above the solidus. Enclaves and bands with lobate margins and interfaces, respectively, support strongly the hypersolidus nature of these contacts (Castro et al., 1995; Fernandez et al. 1997). From these observations it is clear, that the intrusion of the Beer Creek Granodiorite into the Joshua Flat Monzonite started, when both rocks were still in a molten state, probably above the RCMP. The crenulate and lobate interfaces provide a potential explanation for the developement of hybrid magmas without extensive turbulent flow in the magma chamber of the JBP: According to experimental work of Blake and Campell (1986) lobate, convex margins of enclaves and similar contacts

between magmatic bands are interpreted as the result of a slight viscosity contrast between both the magmas, which can lead to local destabilization of the magma-magma interface and to turbulent, unstable flow directly at the interface. Unstable flow between magmatic bands makes mingling and, as long as the viscosity contrast between the magmas is not too high (Frost and Mahood, 1987), even mixing possible, without turbulent flow in the entire magma chamber (Castro et al. 1995). On the other hand, brittle contacts - dykes of Beer Creek Granodiorite brecciating the Joshua Flat Monzonite – were observed. Is there a way to explain the contradictory observations of magma mixing and brittle fracturing next to each other in the JBP?

Frost and Mahood (1987) gave constraints, which control the intrusion of a hot, mafic magma into a cooler felsic one. According to their results magma mixing is only probable, if a mafic magma intrudes a felsic magma of similar volume. In any other case the viscosity contrast between both will increase rapidly as soon as both the magmas come into contact with each other. Magma mingling or even brecciation will occur depending on the temperature and viscosity contrast. In the case of the JBP a more felsic magma intruded a more mafic one and not vice versa. Consequently, it must be considered, that a relative small volume of Beer Creek Granodiorite is allowed to intrude the Joshua Flat Monzonite to reach hybridization. With ongoing intrusion of the granodiorite the mafic : felsic ratio decreases and the granodiorite has to interact with a monzonitic magma, which is becoming more and more viscous. Therefore the style of interaction changes with time early from mixing with homogeneous hybridization over mixing with heterogeneous hybridization to mingling associated with the formation of microgranular, monzonitic enclaves and finally to dyking of the Beer Creek Granodiorite and brecciation of the Joshua Flat Monzonite. The hybrid rocks identified in the field and the so called light-coloured Joshua Flat Monzonite probably developed during an early phase of homogeneous hybridization due to the mixing of monzonite and granodiorite at different ratios. The finegrained variety of the Joshua Flat

Monzonite is regarded as the product of undercooling and subsequent rapid crystallization of the monzonite. This explains the finegrained nature of this variety. Undercooling of the monzonite probably happened, when the relative volume of granodiorite to it was already high, but before granodioritic dykes invaded the finegrained monzonite, because the finegrained variety was found as bands in mingling zones, as enclaves and brecciated by dykes of Beer Creek Granodiorite.

In conclusion, the observed variety of rock types and structures appears to be the product of the continuous intrusion of an increasing amount of Beer Creek Granodiorite into the magma chamber of the Joshua Flat Monzonite. As a consequence, the viscosity contrast between both increased during this process.

One question remains: has the intrusion of the Beer Creek Granodiorite and the formation of the banding zone to be regarded as due to dyking or diapirism? As a product of dyking the pluton as a whole should consist of sheets. Famous examples of sheeted plutons are the Ox Mountain Granite, Ireland (McCaffrey, 1992), the Great Tonalite Sill, Alaska and British Columbia (Hutton and Ingram, 1992) and the Jackass Lake Pluton, California (McNulty et al. 1996). All these plutons are characterized by extended sheets, which essentially build up the pluton. This is not the case for the JBP, a more or less concentrical pluton, with the Joshua Flat Monzonite at its rim and the Beer Creek Granodiorite in its centre. Even the Joshua Flat Monzonite, at least according to the NS001 data, seems to be a concentric body. As can be seen on the TIMS images, the banding zone covers an oblong area of 24 km^2, but not the entire contact zone between both rock types. It has to be regarded as a special part of the contact zone between two nested diapirs, where mixing and mingling happend to be much more extensive than elsewhere, e.g. south of Deep Springs Valley. The banding zone might represent the lower part of the magma chamber, where hotter and therefore less viscous magmas could interact with each other and form mixing and mingling structures. On the other hand, the area south of Deep Springs Valley, also investigated by remote sensing (Fig. 1-3)

with its sharp contacts can be interpreted as a region closer to the roof of the magma chamber, where the already cooler and less viscous magmas were not able to mix and to mingle. These two different levels of the JBP's magma chamber might have been juxtaposed during the opening of Deep Springs Valley as a result of the extensional Basin and Range tectonics in the Neogene and Quaternary.

ACKNOWLEDGEMENTS

The research was supported by grants of the DAAD, the Landesgraduiertenförderung Baden-Württemberg and the DFG. Special thanks go to H.-P. Meyer and I. Glass for X-ray fluorescence analyses and to R. O. Greiling and E. Stein for discussion and comments.

REFERENCES

Arzi, A. A., 1978, Critical phenomena in the rheology of partially melted rocks: Tectonophysics, v. 44, p. 173-184.

Bacon, C. R., 1986, Magmatic inclusions in silicic and intermediate volcanic rocks: Journal of Geophysical research, v. 91B, p. 6091-6112.

Bateman, P.C., 1992, Plutonism in the central part of the Sierra Nevada batholith, California: U.S. Geological Survey Professional Paper, v. 1483, 186 p.

Baird, A. K., 1984, Iron variation within a granitic pluton as determined by near-infrared reflectance: Journal of Geology, v. 92, p. 344-350.

Blake, S., and Campell, I. H., 1986, The dynamics of magma-mixing during flow in volcanic conduits: Contributions to Mineralogy and Petrology, v. 94, p. 72-81.

Blom, R. G., 1986, Iron content of granitic rocks estimated from Landsat thematic mapper type spectral reflectrance data: Geological Society of America Abstracts with Programs, v. 18, no. 6, p. 543.

Castro, A., Moreno-Ventas, I., and De la Rosa, J. D., 1990a, Microgranular enclaves as indicators of hybridization processes in granitoid rocks, Hercynian belt, Spain: Geological Journal, v. 25, p. 391-404.

Castro, A., De la Rosa, J. D., and Stephens, W. E., 1990b, Magma mixing in the subvolcanic environment; petrology of the Gerena interaction zone near Seville, Spain: Contributions to Mineralogy and Petrology, v. 105, p. 9-26.

Castro, A., De la Rosa, J. D., Fernandez, C., and Moreno-Ventas, I., 1995, Unstable flow, magma mixing and magma-rock deformation in a deep-seated conduit: the Gil-Márquez Complex, south-west Spain: Geologische Rundschau, v. 84, p. 359-374.

Cox, K. G., Bell, J. D., and Pankhurst, R. J., 1979, The interpretation of igneous rocks: London, Allen and Unwin.

Dietl, C., 1999, Emplacement of the Joshua Flat-Beer Creek Pluton (White Inyo Mountains, California): a story of multiple material transfer processes, *in* Castro, A., Fernandez, C., and Vigneresse, J. L., eds., Understanding granites: Integrating new and classical techniques: Geological Society, London, Special Publications, v. 168, p. 161-176.

Ernst, W.G., 1996, Petrochemical study of regional/contact metamorphism in metaclastic strata of the central White-Inyo Range, eastern California: Geological Society of America Bulletin, v. 108, p. 1528-1548.

Fernandez, C., Castro, A., De la Rosa, J. D., and Moreno-Ventas, I., 1997, Rheological aspects of magma transport inferred from rock structures, *in* Bouchez, J. L., Hutton, D. W., and Stephens, W. E., eds., Granites: From Segregation of Melt to Emplacement Fabrics: Amsterdam, Kluwer, p. 75-91.

Fourcade, S., and Allegre, C. J., 1981, Trace elements behaviour in granite genesis: a case study the calc-alkaline plutonic association from the Querigut Complex (Pyrenees, France). Contributions to Mineralogy and Petrology, v. 76, p. 177-195.

Frost, T. P., and Mahood, G. A., 1987, Field, chemical, and physical constraints on mafic-felsic magma interaction in the Lamarck Granodiorite, Sierra Nevada, California: Geological Society of America Bulletin, v. 99, p. 272-291.

Gillespie, J. G., 1979, U-Pb and Pb-Pb ages of primary and detritial zircons from the White Mountains, eastern California: Geological Society of America Abstracts with Programs, v. 11, no. 30, p. 79.

Hunt, G. R., 1980, Electromagnetic radiation: The communication link in remote sensing, *in* Siegal, B. S., and Gillespie, A. R., eds., Remote Sensing in Geology: New York, John Wiley, p. 5-45.

Hutton, D. H. W., and Ingram, G. M., 1992, The Great Tonalite Sill of southeastern Alaska and British Columbia: emplacement into an active contractional high angle reverse shear zone (extended abstract): Transactions of the Royal Society of Edinburgh: Earth Sciences, v. 83, p. 383-386.

Launer, P. J., 1952, Regularities in the infrared absorption spectra of silicate minerals: American Mineralogist, v. 37, p. 764-784.

McCaffrey, K. J. W., 1992, Igneous emplacement in the transpressive shear zone; Ox Mountain igneous complex: Journal of the Geological Society, London, v. 149, p. 221-235.

McKee, E. H., and Conrad, J. E., 1996, A tale of ten plutons – Revisited: Age of granitic rocks in the White Mountains, California and Nevada: Geological Society of America Bulletin, v. 108, p. 1515-1527.

McKee, E. H., and Nelson, C. A., 1967, , Geologic map of the Soldier Pass quadrangle, Inyo and Mono Counties, California: U.S. Geological Survey Geologic Quadrangle Map, GQ-654, scale 1:62500, 1 sheet.

McNulty, B. A., Tong, W., Tobisch, O. T., 1996, Assembly of a dike-fed magma chamber: The Jackass Lakes pluton, central sierra Nevada, California: Geological society of America Bulletin, v. 108, p. 926-940.

Nelson, C. A., 1966, Geologic map of the Blanco Mountain quadrangle, Inyo and Mono Counties, California: U.S. Geological Survey Geologic Quadrangle Map, GQ-529, scale 1:62500, 1 sheet.

Nelson, C.A., Hall, C.A., Jr., and Ernst, W.G., 1991, Geologic history of the White-Inyo Range, *in* Hall, C.A.,Jr., ed., Natural history of the White-Inyo Range, California: University of California Natural History Guides, v. 55, p. 42-74.

Sabine, C., Realmuto, V. J., and Taranik, J. V., 1994, Quantitative estimation of granitoid composition from thermal infrared multispectral scanner (TIMS) data, Desolation Wilderness, northern Sierra Nevada, California: Journal of Geophysical Research, v. 99, p. 4261-4271.

Salisbury, J. W., Walter, L. S., and Vergo, N., 1987, Mid-infrared (2.1 to 25 μm) spectra of minerals: First edition: U.S. Geological Survey Open File Repository, p. 87-263.

Sparks, R. S. J., and Marshall, L., 1986, Thermal and mechanical constraints on mixing between mafic and silicic magmas: Journal of Volcanology and Geothermal Research, v. 29, p. 99-124.

Stern, T. W., Bateman, P. C., Morgan, B. A., Newell, M. F., and Peck, D. L., 1981, Isotopic U-Pb ages of zircon from the granitoids of the central Sierra Nevada, California: U.S. Geological Survey Professional Paper, v. 1185, 17 p.

Sylvester, A. G., Miller, C. F.; and Nelson, C. A. 1978, Monzonites of the White-Inyo Range, California, and their relation to the calc-alkalic Sierra Nevada batholith: Geological Society of America Bulletin, v. 89, p. 1677-1687.

Vernon, R. H., 1983, Restite, xenoliths and microgranitoid enclaves in granites: Royal Society of New South Wales Journal and Proceedings, v. 116, p. 77-103.

Carlo Dietl

Evaluation of the PT*ƒ* (fluid) conditions in and around a pluton: the intrusion of the Joshua Flat – Beer Creek Pluton (California)*

Carlo Dietl

Geologisch-Paläontologisches Institut, Ruprecht-Karls-Universität Heidelberg, Im Neuenheimer Feld 234, D-69120 Heidelberg, Germany

Tel: +49-6221-546050, Fax: +49-6221-545503

e-mail: f16@ix.urz.uni-heidelberg.de

Key words Emplacement conditions · Hornblende-plagioclase thermometry · Al-in-hornblende barometry · Na-in-cordierite thermometry · Fluids in cordierite · Numerical modelling

* Evaluation of the PT*ƒ* (fluid) conditions in and around a pluton

Abstract

Geothermobarometry on rocks from the Middle Jurassic Joshua Flat - Beer Creek Pluton and its aureole was combined with fluid investigations and numerical modelling. The pluton is composed of distinct bodies of diorites, monzonites and granodiorites. Several field and thin section observations indicate, that the pluton developed from H_2O-undersaturated to H_2O-saturated conditions. Geothermobarometry with the hornblende-plagioclase and amphibole-clinopyroxene thermometers and the Al-in-hornblende barometer give cooling temperatures between 664 and 900 °C and pressures of about 0.25 GPa. In the contact aureole three metamorphic zones were distinguished with decreasing distance from the pluton: the andalusite-cordierite, sillimanite, and cordierite-K-feldspar zones, respectively. In the immediate contact area partial melting due to the dehydration reaction sillimanite + biotite + plagioclase + quartz --> cordierite + K-feldspar + melt is documented by numerous leucocratic veins. The Na-in-cordierite thermometer gave c. 730 °C as the peak metamorphic temperature in the innermost aureole. Infra-red spectroscopy measurements showed relatively low contents of channel volatiles in cordierite from pelites (H_2O = 0.76 - 0.85 weight % and CO_2 = 0.06 - 0.13 weight %). This indicates that the intrusion and related contact metamorphism took place under water undersaturated conditions. Numerical modelling of the Tt path of the pluton / wall rock system with the program ”CONTACT” resulted in temperatures, which are too low relative to those determined by geothermometry. This discrepancy is explained by the complex geometry of the

pluton, probably due to its diapiric nature, which cannot be modelled with the one-dimensional program.

Introduction

Plutons, together with their contact aureoles provide the opportunity to study many important geologic processes. For example, material transfer within the crust or from the mantle to the crust (e.g. Buddington 1959; Paterson and Fowler 1993) can be studied in detail and the examination of intrusions yields a key for the understanding of processes, which control heat transfer in the earth's crust.

Case studies of PT*f* (fluid) conditions during pluton intrusion and the evolution of contact aureoles are numerous (e.g. Cotkin and Medaris 1993; Symmes and Ferry 1995; Kalt et al. 1998) as are publications on numerical simulations of intrusion events (e.g. Norton and Knight 1977; Kukowski 1992). However, only rarely both approaches are combined (e. g. Zulauf and Helferich 1997). Therefore in the present work, geothermobarometry is linked with numerical modelling. The aim of this study is to understand the PT*f* (fluid) conditions during pluton emplacement and to control the obtained geothermobarometric data by a numerical model, which gives also insight into the temperature history of the pluton / wall rock system.

The Joshua Flat – Beer Creek – Pluton (JBP) at the southern rim of the Inyo batholith in the White-Inyo Mountains (Eastern California, USA, Fig. 1) is particularly suitable for this attempt, because the batholith and its host rocks are well studied (e.g. Knopf 1918; Krauskopf 1968; Sylvester et al. 1978;

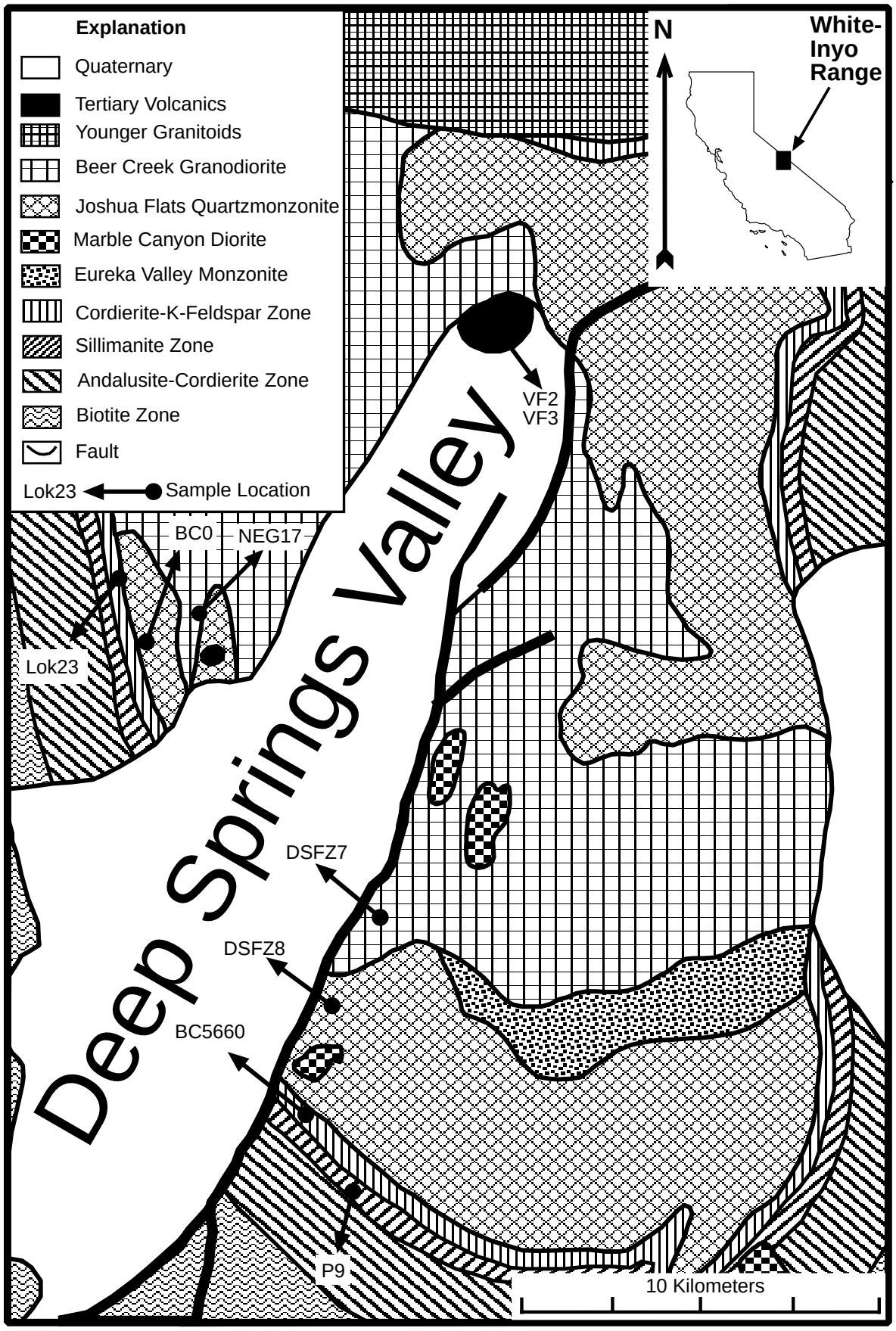

Fig. 1: *Geologic map of the JBP and its aureole with the sample locations. Also shown is the position of the White Inyo Range in California.*

McKee and Conrad 1996; Ernst 1996; Stein and Paterson 1996; Stein 2000). Moreover, the JBP and its aureole are well exposed and both contain mineral assemblages suitable for the application of several geothermobarometers: the amphibole-plagioclase thermometer (Blundy and Holland 1990; Holland and Blundy 1994), the hornblende-clinopyroxene thermometer (Perchuk et al. 1985) and the Al-in-hornblende barometer (Schmidt 1992; Anderson and Smith 1995) can be applied to rocks from this pluton. The Na-in-cordierite thermometer (Mirwald 1986) can be used on metapelites from the aureole and PT conditions estimated from mineral parageneses.

In the earth's crust heat can be transferred by conduction or by convection. The most suitable and most widespread medium available for heat transport in the crust are volatiles and fluids, in particular. For information about fluids in the entire magmatic system, i. e. the JBP and its aureole, field observations and detailed thin section studies were combined with infra-red spectroscopy on cordierites.

These data formed the base of numerical models of the (P)Tt path and the intrusion conditions. For this purpose the one-dimensional computer program "CONTACT" (Peacock 1989) was applied.

Geological setting

The JBP is situated in the White-Inyo Mountains, the westernmost mountain range of the Basin and Range Province, at the southern end of the Inyo batholith (Bateman 1992) and consists of plutons of dioritic, monzonitic and granodioritic

composition. According to U-Pb and $^{40}Ar/^{39}Ar$ datings (Sylvester et al. 1978, Gillespie 1979, Stern et al. 1981, McKee and Conrad 1996) the JBP was emplaced in middle Jurassic times between 180 and 165 Ma ago, into a Proterozoic to Cambrian siliciclastic to carbonatic sedimentary sequence, which was deformed and metamorphosed under lower greenschist facies conditions during the late Paleozoic (Bateman 1992, Ernst 1996). The batholith is regarded as part of the magmatic arc, which formed in the White-Inyo Mountains during the Jurassic and Cretaceous as a result of the subduction of the Pacific plate beneath the North American plate (Nelson et al. 1991). Phengite barometry (Ernst 1996, Kontny and Dietl in prep.) shows that the plutons intruded at a depth of 8-10 km. Ernst (1996) also investigated mineral assemblages and mineral compositions in the thermal aureole of the Inyo batholith and estimated contact metamorphic conditions to reach hornblende-hornfels- up to lower amphibolite conditions (T = 500-600 °C; P = 0.2-0.3 GPa).

Petrography and sample description

Petrography of the JBP and sampling

The pluton is composed of four lithologic units (Fig. 1), three of which are exposed in the actual area and described here. The *Marble Canyon Diorite* (Fig. 2 a) is a medium to coarse grained diorite to monzodiorite and consists mainly of hornblende (60 vol%), plagioclase (25 vol%), K-feldspar (5 vol%), quartz (5 vol%) and biotite (5 vol%). Titanite, epidote, apatite, hematite and magnetite are accessories.

sample	DSFZ8	BC0	VF2	VF3	DSFZ7	NEG17
n	36	5	8	8	7	8
SiO_2	60.79 (1.34)	63.00 (0.45)	64.78 (0.49)	63.73 (0.61)	63.58 (0.75)	62.08 (1.05)
TiO_2	0.02 (0.07)	0.00 (0.00)	0.00 (0.00)	0.00 (0.00)	0.00 (0.00)	0.00 (0.00)
Al_2O_3	24.30 (3.27)	23.84 (0.28)	22.51 (0.42)	23.36 (0.41)	22.90 (0.39)	23.99 (0.48)
Cr_2O_3	0.01 (0.02)	0.00 (0.00)	0.00 (0.00)	0.00 (0.00)	0.00 (0.00)	0.00 (0.00)
Fe_2O_3	0.42 (1.40)	0.16 (0.04)	0.23 (0.03)	0.21 (0.08)	0.16 (0.05)	0.19 (0.06)
MgO	0.24 (1.41)	0.00 (0.00)	0.00 (0.00)	0.00 (0.00)	0.00 (0.00)	0.00 (0.00)
MnO	0.02 (0.05)	0.00 (0.00)	0.00 (0.00)	0.00 (0.00)	0.01 (0.02)	0.00 (0.00)
CaO	6.59 (0.54)	4.55 (0.36)	2.98 (0.40)	3.93 (0.47)	3.54 (0.33)	4.71 (0.65)
Na_2O	7.60 (1.22)	9.01 (0.22)	10.05 (0.28)	9.48 (0.32)	9.77 (0.18)	8.84 (0.36)
K_2O	0.21 (0.37)	0.17 (0.04)	0.17 (0.05)	0.18 (3.93)	0.12 (0.02)	0.18 (0.02)
Total	100.20 (0.38)	100.73 (0.18)	100.73 (0.35)	100.89 (0.29)	100.06 (1.00)	99.98 (0.71)
Cations on the basis of 8 O						
Si	2.70 (0.07)	2.77 (0.02)	2.84 (0.02)	2.79 (0.02)	2.81 (0.01)	2.75 (0.03)
Al	1.27 (0.17)	1.24 (0.02)	1.16 (0.02)	1.21 (0.02)	1.19 (0.01)	1.25 (0.03)
Fe^{3+}	0.01 (0.05)	0.01 (0.00)	0.01 (0.00)	0.01 (0.00)	0.01 (0.00)	0.01 (0.00)
Ti	0.00 (0.00)	0.00 (0.00)	0.00 (0.00)	0.00 (0.00)	0.00 (0.00)	0.00 (0.00)
Mn	0.00 (0.00)	0.00 (0.00)	0.00 (0.00)	0.00 (0.00)	0.00 (0.00)	0.00 (0.00)
Mg	0.02 (0.09)	0.00 (0.00)	0.00 (0.00)	0.00 (0.00)	0.00 (0.00)	0.00 (0.00)
Ca	0.31 (0.03)	0.21 (0.02)	0.14 (0.02)	0.18 (0.02)	0.17 (0.01)	0.22 (0.03)
Na	0.65 (0.10)	0.77 (0.02)	0.85 (0.02)	0.81 (0.03)	0.84 (0.02)	0.76 (0.03)
K	0.01 (0.02)	0.01 (0.00)	0.01 (0.00)	0.01 (0.00)	0.01 (0.00)	0.01 (0.00)
Total	4.99 (0.05)	5.00 (0.01)	5.01 (0.01)	5.01 (0.01)	5.02 (0.01)	5.00 (0.01)
An content	33.30 (9.32)	21.81 (1.73)	14.10 (1.96)	18.66 (2.36)	16.67 (1.54)	22.76 (3.13)

Tab. 1: *Average plagioclase compositions of the inividual samples from the pluton (numbers in brackets are standard deviations).*

The *Joshua Flat Monzonite* (Fig. 2 b), a fine or medium grained monzonite to quartzmonzonite (Streckeisen 1976), is composed of plagioclase of oligoclase to andesine composition (c. 50 vol%, Tab. 1), K-feldspar (up to 30 vol%), quartz (5 to 10 vol%), hornblende (10 to 40 vol%), biotite (up to 10 vol%), clinopyroxene (up to 10 vol%) and titanite (up to 5 vol%). It is characterized by a strong magmatic foliation caused by hornblende, hornblende with clinopyroxene cores and titanite crystals, which are macroscopically visible. The *Beer Creek Granodiorite* (Fig. 2 c) is a coarse grained, light-coloured granodiorite with euhedral K-feldspar phenocrysts up to 3 cm long. It contains 10 to 20 vol% quartz, 20 to 40 vol% plagioclase (oligoclase) (Tab. 1), c. 30% K-feldspar, 15 to 25 vol% biotite and 5 to 15 vol% hornblende. Titanite,

epidote, zircon, apatite and magnetite occur as accessories. Only a weak magmatic foliation caused by the alignement of the long axes of K-feldspar phenocrysts and microgranular enclaves is observed.

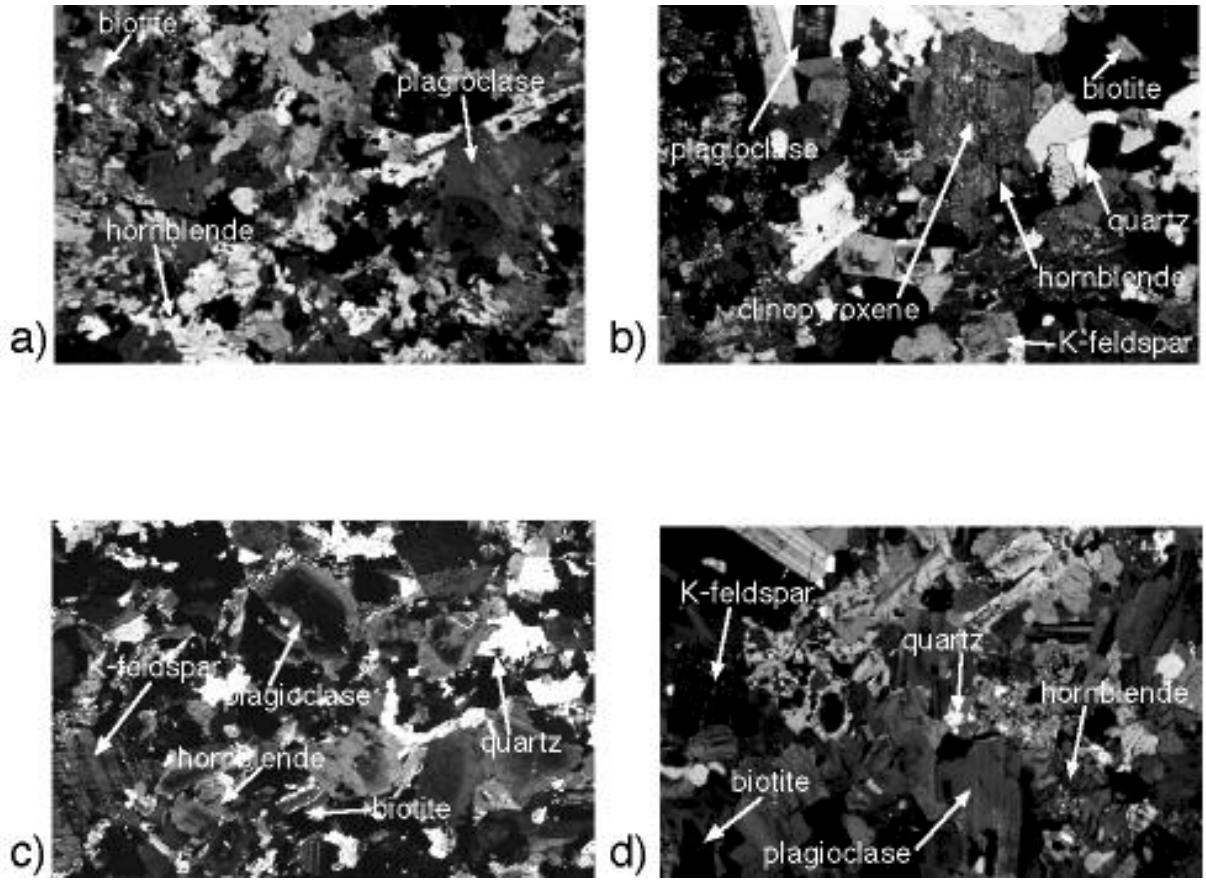

Fig. 2: *Photomicrographs of the intrusives the JBP is composed of:* ***a)*** *Marble Canyon Diorite (XPL, long edge: 7 mm);* ***b)*** *Joshua Flat Monzonite with hornblendes with pyroxene core (XPL, long edge: 5 mm);* ***c)*** *Beer Creek Granodiorite (XPL, long edge: 5 mm);* ***d)*** *hybrid between the monzonite and the granodiorite (XPL, long edge: 5.6 mm).*

Mineral inclusions and mineral intergrowth showed a nearly identical crystallization sequence for all three rock types: magnetite, apatite --> clinopyroxene (only in the Joshua Flat Monzonite) --> biotite --> hornblende --> quartz --> K-feldspar --> titanite. Hematite and epidote are regarded as subsolidus phases growing at the expense of magnetite (hematite) and plagioclase (epidote).

The Marble Canyon Diorite is present only as xenoliths within the Joshua Flat Monzonite and the Beer Creek Granodiorite, respectively. Field relations between the latter two lithologies range from mixing and mingling to brecciation of the monzonite by the granodiorite. Mixing is indicated by the presence of hybrid rocks (Fig. 2 d) with characteristics of both the monzonite (hornblende crystals with pyroxene cores) and the granodiorite (K-feldspar phenocrysts). Typical mingling structures are enclaves and schlieren, mainly of the Joshua Flat Monzonite in the Beer Creek Granodiorite, but also vice versa. Xenoliths of the Joshua Flat Monzonite in the Beer Creek Granodiorite and granodioritic dykes crosscutting the monzonite point to brecciation of the monzonite by the granodiorite. The juxtaposition of all these different features is interpreted as the result of the intrusion of more and more Beer Creek Granodiorite into a magma chamber filled with Joshua Flat Monzonite. As long as only a small volume of relative cool granodiorite intruded into the monzonite, the latter was able to heat up the first. Consequently, both magmas had a low viscosity and mixing was possible. The increasing volume of granodiorite cools down the monzonite and lowers its viscosity, preventing mixing, but not mingling. Finally, a viscosity contrast between both magmas is reached, where only brecciation of the Joshua Flat Monzonite by the Beer Creek Granodiorite is possible (for a more detailed discussion see also Dietl in prep.). From the described observations an intrusion sequence Marble Canyon Diorite --> Joshua Flat Monzonite --> Beer Creek Granodiorite is suggested with the Joshua Flat Monzonite intruding an already solidified Marble Canyon Diorite and the Beer Creek Granodiorite following only shortly after the Joshua Flat Monzonite. A

last magmatic stage is indicated by the presence of monzonitic, granodioritic and granitic pegmatite dykes, some of them with K-feldspar megacrysts (up to 5 cm long), as well as tourmaline and fluorite. The observation K-feldspar xenomegacrysts in the Joshua Flat Monzonite, which were derived from a neighbouring pematite, point to the occurence of the first pegmatites before the complete solidification of the monzonite.

The field and thin section observations together with previously published work give hints to the fluid evolution of the JBP. According to Cotkin and Medaris (1993) the presence of clinopyroxene in the quartz diorite of the Russian Peak Intrusive Complex points to a H_2O content < 4 wt%. Probably, the clinopyroxene cores in hornblende from the Joshua Flat Monzonite indicate a similar low H_2O content for the monzonite during the growth of clinopyroxene. However, the overgrowth of clinopyroxene by hornblende points to an increase in H_2O during the evolution of the monzonitic melt. Naney (1983) carried out experiments with a synthetic granodiorite at 0.2 GPa (close to the pressure, under which the JBP was emplaced according to Ernst 1996) and found out, that hornblende crystallizes only from a melt with at least 4 wt% H_2O and forms before biotite only at a water content > 4 wt%. From these findings and the observation of biotite inclusions in hornblende (and never vice versa) in all lithologies of the JBP it can be concluded that all magmas of the JBP contained about 4 wt% H_2O when hornblende and biotite crystallized. According to Clarke (1992) at 0.2-0.3 GPa (corresponding to the confining pressure during emplacement of the JBP according to Ernst, 1996) c. 5 wt% water are necessary to saturate a silicate melt with water. However, a further increase of the water

content of the pluton is shown by the pegmatitic dykes described above: such dykes are only formed when a free fluid phase is present (Cotkin and Medaris 1993). Other indicators for the presence of a free fluid phase during the late and post magmatic stages are epidote veins in both the pluton and the contact aureole, copper mineralizations and skarns in the immediate contact area, and the intense retrograde overprint of biotite to chlorite and plagioclase to sericite in the pluton and the aureole rocks. However, these phenomena do not necessarily have to be related to the emplacement of the JBP, but can also belong to other Jurassic or Cretaceous magmatic events (Nelson et al. 1991).

Alltogether six samples, four from the NNW-side of Deep Springs Valley (NEG17, BC0, VF2 und VF3) and two from the SSE-side of the valley (DSFZ7 und DSFZ8), were studied (Fig. 1). DSFZ8, BC0 and VF2 are of monzonitic composition, while VF3 and DSFZ7 come from the Beer Creek Granodiorite. NEG17 is a hybridic rock, a mixture between the monzonite and the granodiorite as indicated by the occurence of K-feldspar phenocrysts (typical for the Beer Creek Granodiorite) in a monzonitic matrix. VF2 and VF3 are samples from granitoid xenoliths found in a tertiary rhyolithic tuff at the northern end of Deep Springs Valley. During microprobe measurements care was taken to examine only fresh and primary (igneous) hornblende.

Petrography of the aureole and sampling

A more detailed description of the contact metamorphic mineral assemblages in the aureole is given by Dietl (1999) and Kontny and Dietl (in prep.). These

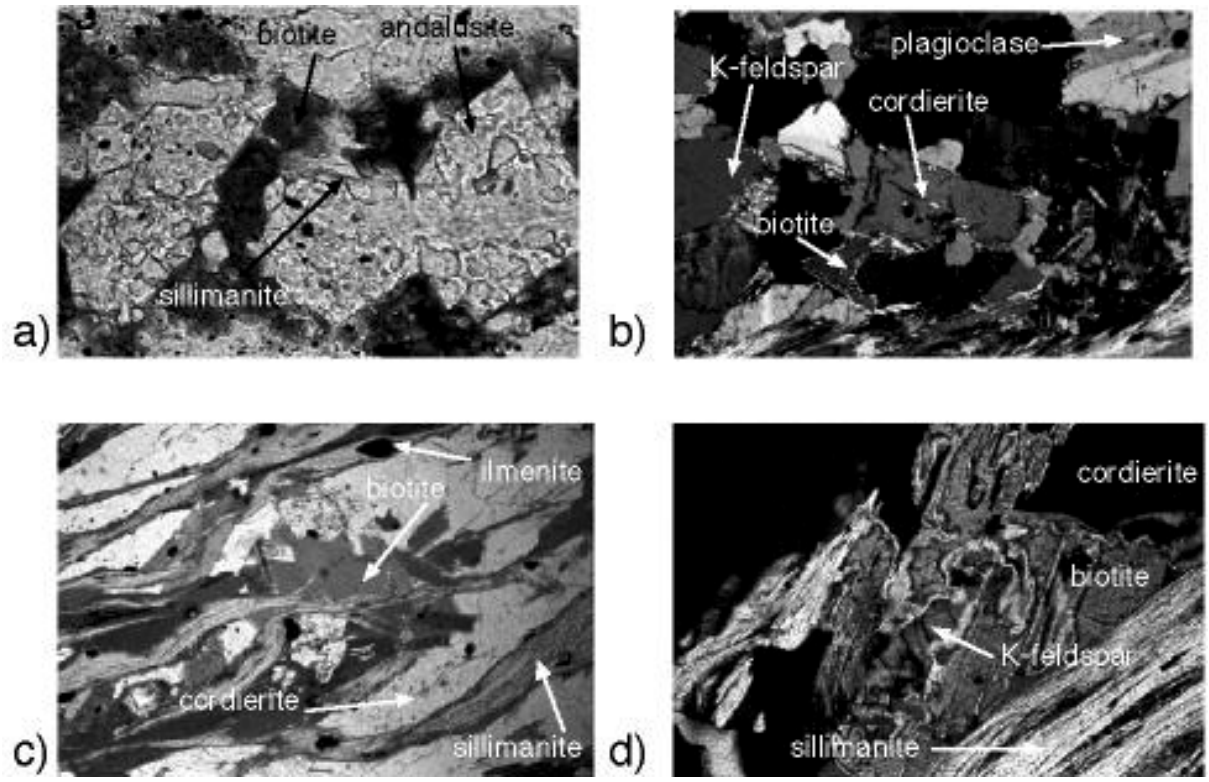

Fig. 3: *Photomicrographs showing phase relations from the individual metamorphic zones in the contact aureole:* ***a)*** *sillimanite overgrows biotite and andalusite (PPL, long edge: 1.4 mm);* ***b)*** *leucosome in the cordierite - K-feldspar zone with quartz, cordierite, K-feldspar and plagioclase (XPL, long edge: 2.2 mm);* ***c)*** *typical melanosome in the cordierite – K-feldspar zone with biotite, sillimanite, andalusite and cordierite (PPL, long edge: 2.2 mm);* ***d)*** *reaction relation between biotite and K-feldspar as part of the reaction quartz + plagioclase + biotite + sillimanite = cordierite + K-feldspar + ilmenite + HO + melt (XPL, long edge: 0.6 mm).*

data are briefly reviewed here: three contact metamorphic zones were separated and named according to the newly formed minerals, based on petrographic examinations of metapelites. The outermost part of the aureole (1800 – 500 m away from the JBP, see also Fig. 1) is in the *andalusite-cordierite zone*, characterized by the mineral reaction chlorite + muscovite + ilmenite --> biotite + cordierite + andalusite + H_2O. Between 500 and 250 m distance from the pluton sillimanite occurs, establishing the *sillimanite zone* . Sample P9 (500 m away from the contact, see also Figs. 1) comes from the border between the andalusite-cordierite and sillimanite zones. In this sample the assemblage biotite + cordierite + andalusite + quartz was found, while sillimanite overgrows biotite

and andalusite at one spot (Fig. 3 a). The immediate contact area (< 250 m from the pluton) is occupied by the *cordierite-K-feldspar zone*. Samples Lok23 (150 m away from the contact, see also Fig. 1) and BC5660 (100 m away from the contact, see also Fig. 1) were derived from this zone. Here many leucocratic, frequently lit-par-lit oriented dykes, as well as diffuse, schlieren-like areas were observed, which are interpreted as leucosomes and therefore as products of partial melting. Indicators for the migmatic nature of the leucosomes are their larger grain size as well as their composition – they consist nearly entirely of plagioclase, quartz and K-feldspar (Fig. 3 b). In BC5660 also leucosomes built of quartz and cordierite can be found – in contrast to mafic patches and areas rich in biotite, alumosilicates and cordierite, which are regarded as melanosomes (Fig. 3 c). The dehydration reaction sillimanite + biotite + quartz -> cordierite + K-feldspar + melt + H_2O (Fig. 3 d) may be responsible for partial melting.

Geothermobarometry

Methods of investigation

Electron microprobe examinations were carried out with an CAMECA SX51 instrument at the Mineralogical Institute of the University of Heidelberg. Standards used were albite (Na), periclase (Mg), Al_2O_3 (Al), wollastonite (Si, Ca), orthoclase (K), TiO_2 (Ti), Cr_2O_3 (Cr), rhodonite (Mn), and hematite (Fe).. The raw data were corrected with the PAP program of Pouchou and Pichoir (1984). An acceleration voltage of 15 kV and a sample current of 20 nA were used.

Amphibole thermobarometry

Nomenclature of amphiboles

Mineral formulas (including Fe^{3+}) were calculated using the computer program "Formelcalc (incl hbl)" on the basis of 23 oxygens and normed for 13 cations (without Ca, Na and K).

sample	DSFZ8	BC0	VF2	VF3	DSFZ7	NEG17
n	85	17	19	20	21	27
SiO_2	46.91 (1.61)	46.75 (0.59)	48.61 (2.04)	47.70 (0.44)	46.59 (0.68)	46.79 (1.08)
TiO_2	1.04 (0.27)	0.96 (0.14)	0.32 (0.13)	0.67 (0.15)	1.03 (0.17)	0.92 (0.21)
Al_2O_3	7.14 (0.83)	6.58 (0.34)	4.96 (1.35)	5.81 (0.27)	6.36 (0.38)	6.59 (0.63)
Cr_2O_3	0.04 (0.05)	0.01 (0.01)	0.02 (0.02)	0.01 (0.01)	0.01 (0.01)	0.02 (0.02)
FeO	10.43 (1.18)	11.84 (0.52)	12.06 (0.58)	11.21 (0.34)	12.02 (0.91)	11.51 (0.57)
Fe_2O_3	4.45 (1.86)	4.64 (0.46)	3.93 (0.80)	4.87 (0.45)	4.20 (0.89)	4.56 (0.62)
MgO	13.13 (0.94)	12.35 (0.37)	13.08 (0.92)	12.93 (0.22)	12.37 (0.47)	12.60 (0.46)
MnO	0.45 (0.05)	0.45 (0.04)	0.51 (0.07)	0.71 (0.05)	0.64 (0.09)	0.44 (0.05)
CaO	11.88 (0.81)	11.56 (0.08)	11.75 (0.19)	11.55 (0.14)	11.44 (0.10)	11.70 (0.13)
Na_2O	1.19 (0.22)	1.31 (0.09)	1.21 (0.33)	1.41 (0.12)	1.54 (0.10)	1.23 (0.17)
K_2O	0.85 (0.18)	0.78 (0.06)	0.66 (0.20)	0.72 (0.04)	0.82 (0.06)	0.74 (0.13)
Total	97.51 (1.66)	97.23 (0.48)	97.10 (0.43)	97.59 (0.33)	97.02 (0.77)	97.12 (0.56)
Cations on the basis of 23 O						
Si	6.91 (0.19)	6.95 (0.07)	7.20 (0.23)	7.05 (0.05)	6.96 (0.06)	6.95 (0.13)
Al^{IV}	1.09 (0.13)	1.05 (0.07)	0.80 (0.23)	0.95 (0.05)	1.04 (0.06)	1.05 (0.13)
Al^{VI}	0.15 (0.02)	0.10 (0.03)	0.07 (0.02)	0.06 (0.02)	0.08 (0.06)	0.11 (0.03)
Ti	0.11 (0.03)	0.11 (0.02)	0.04 (0.01)	0.07 (0.02)	0.12 (0.02)	0.10 (0.02)
Fe^{2+}	1.29 (0.16)	1.47 (0.07)	1.50 (0.09)	1.39 (0.05)	1.50 (0.12)	1.43 (0.08)
Fe^{3+}	0.49 (0.20)	0.52 (0.05)	0.44 (0.09)	0.54 (0.05)	0.47 (0.10)	0.51 (0.07)
Cr	0.00 (0.01)	0.00 (0.00)	0.00 (0.00)	0.00 (0.00)	0.00 (0.00)	0.00 (0.00)
Mn	0.06 (0.01)	0.06 (0.01)	0.06 (0.01)	0.09 (0.01)	0.08 (0.01)	0.06 (0.01)
Mg	2.88 (0.17)	2.74 (0.08)	2.89 (0.18)	2.85 (0.04)	2.75 (0.10)	2.79 (0.09)
Ca	1.87 (0.13)	1.84 (0.01)	1.87 (0.02)	1.83 (0.02)	1.83 (0.02)	1.86 (0.02)
Na	0.34 (0.06)	0.38 (0.03)	0.35 (0.10)	0.40 (0.04)	0.45 (0.03)	0.35 (0.05)
K	0.16 0.03)	0.15 (0.01)	0.13 (0.04)	0.14 (0.01)	0.16 (0.01)	0.14 (0.02)
Total	15.36 (0.11)	15.37 (0.04)	15.34 (0.13)	15.37 (0.04)	15.43 (0.05)	15.36 (0.07)

***Tab. 2**: Average hornblende compositions of the inividual samples from the pluton (numbers in brackets are standard deviations).*

Almost all measured hornblendes are Mg-hornblendes (Tab. 2) according to the classification of Leake et al. (1997). Only three measurements from sample VF2, with blue-green amphiboles, plot in the actinolite field. These actinolites were probably formed when the (Jurassic) monzonite came in contact with the

(Tertiary) rhyolithic magma either as a new mineral, or as a retrograde reaction product from the Mg-hornblendes and can therefore not be used for thermobarometric purposes.

The amphibole-plagioclase thermometer

Of the three calibrations of the thermometer two are based on the edenite-tremolite-reaction: 4 quartz + edenite --> albite + tremolite, the third on the edenite-richterite-reaction: edenite + albite --> richterite + anorthite.

The empirical thermometer of Blundy and Holland (1990), hereafter called "BH90", is based on the first reaction. It can be used for quartz-bearing, intermediate to felsic igneous rocks with An 92% and Si in hornblende 7.8 p.f.u.:

$$T[\pm 311K] = \frac{0.677P[kbar] - 48.98}{-0.0429 - 0.0083144 \ln\left\{\left(\frac{Si-4}{8-Si}\right) X_{Ab}^{Plag}\right\}}$$

with Si as p.f.u. and the entire formula already adapted to the observed plagioclase chemistry, i. e. the albite component > 50% (see also Tab. 1).

Holland and Blundy (1994) developed two other calibrations, which take into account not only the Si content of hornblende and the Ab content of plagioclase, but also the components involved in the edenite-tremolite- and edenite-richterite-reactions, respectively. Thermometer HB94A, based on the edenite-tremolite-reaction, is applicable also to quartz-bearing mafic metamorphic rocks:

$$T[\pm 313K] = \frac{-76.95 + 0.79P[kbar] + 39.4X_{Na}^{A} + 22.4X_{K}^{A} + (41.5 - 2.89P[kbar])X_{Al}^{M2}}{-0.0650 - 0.0083144 \ln\left(\frac{27X_{vac}^{A}X_{Si}^{T1}X_{Ab}^{Plag}}{256X_{Na}^{A}X_{Al}^{T1}}\right)}$$

and thermometer HB94B, based on the edenite-richterite-reaction, can be applied to quartz-free igneous and metamorphic rocks:

$$T[\pm 313K] = \frac{81.44 - 33.6X_{Na}^{M4} - (66.8 - 2.92P[kbar])X_{Al}^{M2} + 78.5X_{Al}^{T1} + 9.4X_{Na}^{A}}{0.0721 - 0.0083144 \ln\left(\frac{27X_{Na}^{M4}X_{Si}^{T1}X_{An}^{Plag}}{64X_{Ca}^{M4}X_{Al}^{T1}X_{Ab}^{Plag}}\right)}$$

Measurements were carried out on amphibole-plagioclase pairs, which share grain boundaries, and on cores of neighbouring amphibole and plagioclase crystals, which were assumed to have grown contemporaneously and which were therefore expected to yield (higher) temperatures from an earlier stage of crystallization than measurements at the rims of amphibole-plagioclase pairs. Because the calculation of temperatures with the amphibole-plagioclase-thermometer is based on a pressure assumption, a pressure of 0.3 GPa was estimated. This is the average pressure Ernst (1996) calculated as the result of phengite barometry applied to regional and contact metamorphic assemblages in the central White-Inyo Range. In the following, the temperatures calculated with BH90 will be presented first and then compared with the results achieved with HB94A and HB94B. Nearly all results from BH90 are within a range from 640 to 732°C at or close to the H_2O-saturated solidus of granodiorite, which lies at 0.3 GPa and 680°C (Piwinskii and Wyllie 1968; Piwinskii 1968). Also the standard error ± 5 to 15°C is acceptable. Temperatures from the two xenolithic samples VF2 and VF3 are 20 to 30°C lower than the average temperatures from

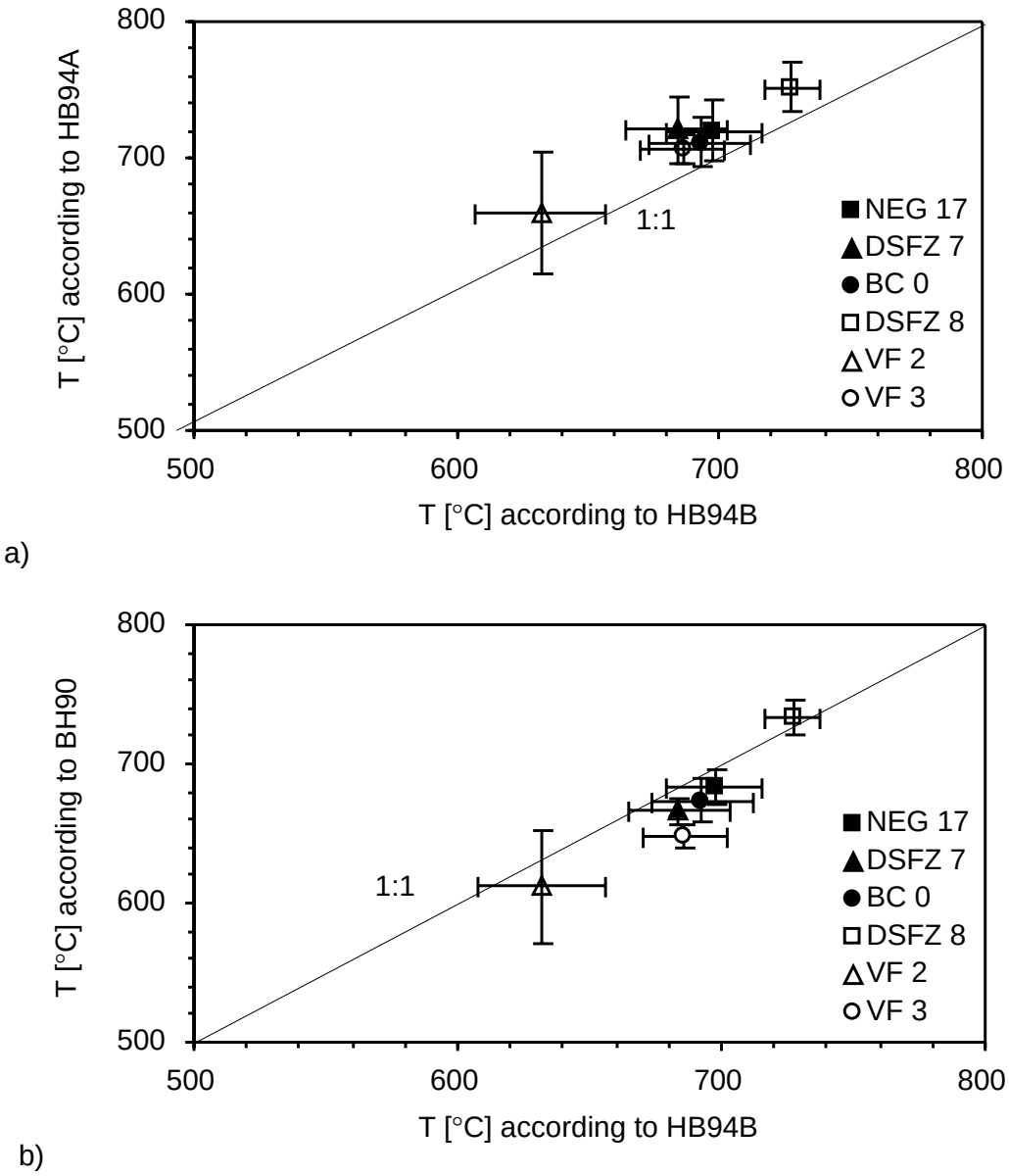

Fig. 4: *Comparative plot of the temperature calculations carried out with the three different calibrations of the amphibole-plagioclase-thermometer.*

the other samples. This can be explained with a reequilibration of the hornblendes due to the heat of the rhyolithic magma. Sample DSFZ8 yields 733°C, a clearly higher temperature than all other samples, i. e. the hornblende-plagioclase-pairs crystallized above the H_2O-saturated solidus of granodiorite. A possible key for this behaviour lies in the much more mafic nature of DSFZ8 compared to all other samples. Therefore the solidus for this monzonite is at higher temperatures than for the quartzmonzonitic and granodioritic samples.

The amphiboles and coexisting plagioclases from DSFZ8 also crystallized at higher temperatures. Temperatures obtained for cores of neighbouring plagioclase and hornblende grains cannot be distinguished from temperatures derived from rim pairs. For sample NEG17 core temperatures lie between 676 and 690°C. The average temperature is 684°C. The same is true for sample VF3, where the only temperature calculated for a core pair is 656°C and the average temperature is 649°C. Finally in sample DSFZ8 two core measurements lie at 719 and 747°C, respectively, with an average of all measurements at 733°C.All three calibrations give similiar results to HB94A, with HB94B yielding slightly higher temperatures than BH90. Calculations using HB94A are about 40 - 60°C higher, while results from HB94B tend to lie c. 20°C above the temperatures calculated with BH90. In Fig. 4 results from BH90 and HB94A, respectively, are plotted on the y-axis versus HB94B on the x-axis. It becomes clear from this graph that the differences between the individual calibrations are not significant. Only HB94A yields slightly higher temperatures as compared with the two other calibrations.

The hornblende-clinopyroxene thermometer

Perchuk et al (1985) calibrated an empirical thermometer for clinopyroxene and amphibole bearing rocks, based on the Fe/Mg exchange between these two minerals. It correlates the Mg-# (Mg/{Mg+Fe}) of clinopyroxene and coexisting hornblende. The thermometer is not very exact, because only a solution is only graphical, on the base of empirical microprobe data and all there are uncertainties regarding the determination of Fe^{2+} and Fe^{3+}. Nevertheless it can be

sample	DSFZ8
n	50
SiO_2	52.55 (0.86)
TiO_2	0.35 (0.22)
Al_2O_3	1.95 (1.17)
Cr_2O_3	0.07 (0.04)
FeO	7.04 (1.52)
Fe_2O_3	1.16 (0.72)
MgO	13.95 (0.36)
MnO	0.51 (0.08)
CaO	21.75 (2.42)
Na_2O	0.55 (0.16)
K_2O	0.11 (0.17)
Total	99.96 (0.45)
Cations on the basis of 6 O	
Si	1.95 (0.03)
Al^{IV}	0.05 (0.03)
Al^{VI}	0.04 (0.02)
Ti	0.01 (0.01)
Cr	0.00 (0.00)
Fe^{2+}	0.22 (0.04)
Fe^{3+}	0.03 (0.02)
Mg	0.77 (0.02)
Mn	0.02 (0.00)
Ca	0.87 (0.10)
Na	0.04 (0.01)
K	0.01 (0.01)
Total	4.00 (0.00)

Tab. 3: *Average clinopyroxene composition of sample DSFZ8 (numbers in brackets are standard deviations).*

used to verify the results of the amphibole-plagioclase-thermometry and, in this special case, to get temperatures closer to the liquidus, because according to pyroxene inclusions in hornblende, pyroxenes from the examined samples crystallized early in the melt. Of all investigated samples only DSFZ8 contains clinopyroxene. It has augitic to diopsidic composition (Tab. 3) and was found in the cores of hornblende. It cannot be excluded that hornblende grew at the expense of clinopyroxene as a consequence of coexistence with a melt, which was progressively enriched in H_2O over the course of crystallisation. Therefore, it is not quite clear if neighbouring hornblende and clinopyroxene crystals can be regarded as coexisting with each other. These data must be used with caution and should be interpreted only together with the much more reliable results of the amphibole-plagioclase thermometry. The Mg-# of clinopyroxenes in sample DSFZ8 ranges from 0.7 to 0.8 (only one value is significantly lower with 0.64), those for hornblende lie between 0.56 and 0.7.

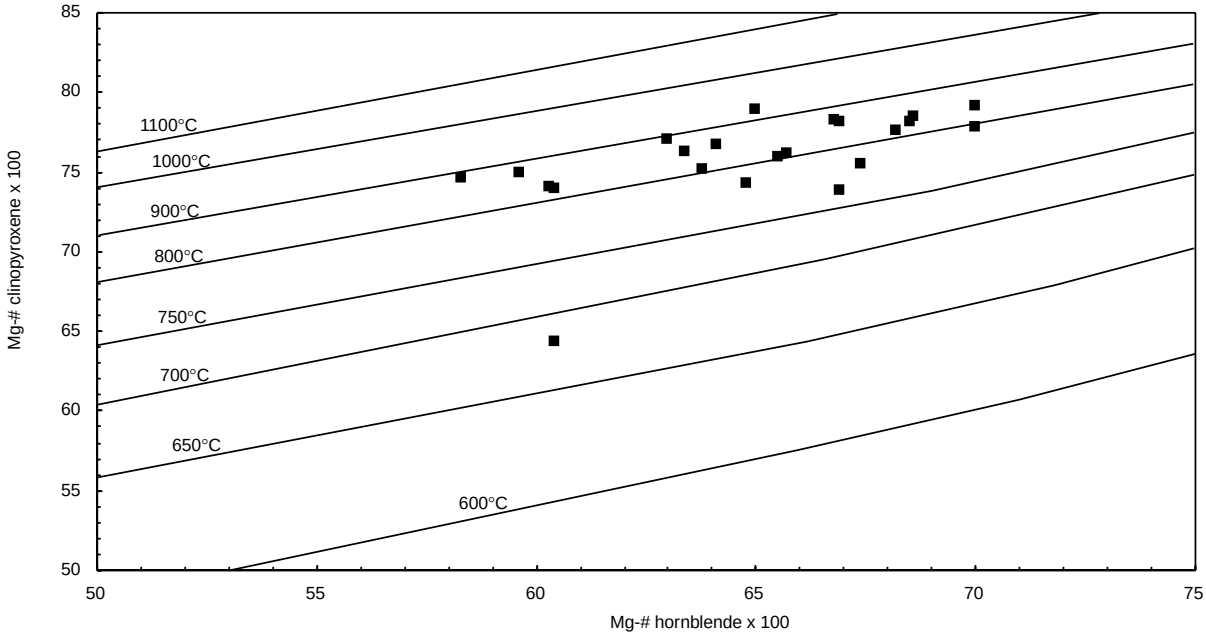

Fig. 5: *Graphically determined results of the hornblende-clynopyroxene-thermometer by Perchuk et al. (1985) applied to the Joshua Flat Monzonite.*

The graphical solution of the thermometer (Fig. 5) gives temperatures between 750 and 900°C for sample DSFZ8. Only for one mineral pair the resulting temperature below 700°C is lower than the average temperature obtained with the amphibole-plagioclase-thermometer (733°C). All other temperatures range between those of the amphibole-plagioclase-thermometry and liquidus temperatures for intermediate magmatic systems, which are c. 1000°C (Piwinskii and Wyllie 1968; Cotkin and Medaris 1993). The spread of temperature data over a range of c. 250°C probably reflects crystallization of hornblende-clinopyroxene pairs over a wide range of the hypersolidus history of the JBP. Application of the hornblende-clinopyroxene together with the amphibole-plagioclase thermometer allows a reasonable estimation of the temperature interval for the crystallisation of the JBP between somewhat in the range of 900 and 675°C. This temperature interval will become important later for the modelling of the PTt path of the JBP and its aureole. Moreover, the

amphibole-plagioclase temperatures are important for the Al-in-hornblende barometry.

The Al-in-hornblende barometer

The barometer was calibrated by Hammarstrom and Zen (1986), Hollister et al. (1987), Johnson and Rutherford (1989), Schmidt (1992) and Anderson and Smith (1995). It can be applied to granitoids crystallized at pressures between 0.2 and1.3 GPa with the mineral assemblage quartz + K-feldspar + plagioclase ($an_{25–35}$) + biotite + hornblende + titanite + magnetite/ilmenite. All authors but Anderson and Smith (1995) based their calibrations on a direct relation between Al_{tot} in hornblende and the confining pressure during crystallization.. Anderson and Smith (1995) showed that the Al-content of hornblende is controlled not only by pressure, but also by temperature. Consequently, they formulated a new barometer on the base of the calibration by Schmidt (1992) and introduced a temperature correction term, in order to make the barometer applicable also to hornblende, which crystallized above the H_2O-saturated granite solidus (c. 675°C). To determine the confining pressure, under which the JBP crystallized, the calibrations by Schmidt (1992)

$$P[\pm 0.6 kbar] = -3.01 + 4.76 Al_{tot}$$

and Anderson and Smith (1995)

$$P[\pm 0.6 kbar] = -3.01 + 4.76 Al_{tot} - \left\{\frac{(T[°C] - 675)}{85}\right\} \times \left\{0.53 Al_{tot} + 0.005294 \times (T[°C] - 675)\right\}$$

were used. The first one was applied, because it is the base for the second applied calibration of Anderson and Smith (1995). The Anderson and Smith (1995) barometer was used, because the hornblende at least of sample DSFZ8

crystallized at temperatures above the H_2O-saturated granite solidus and a temperature correction seems to be necessary. For the variable ”T” the temperatures calculated with the amphibole-plagioclase-thermometer by Blundy and Holland (1990) were inserted. The resulting pressures for both the calibrations are shown in Fig. 6. Because hornblendes of almost all samples

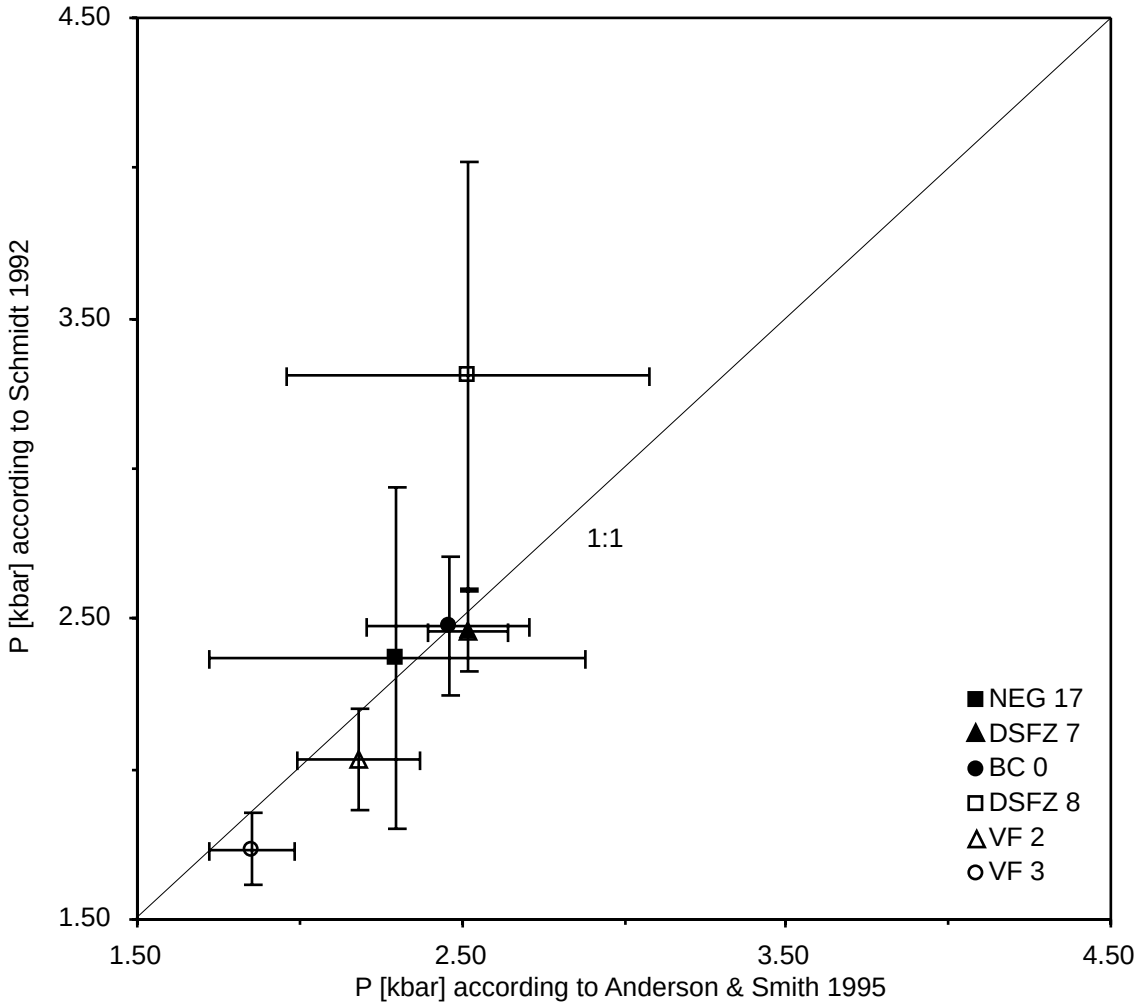

Fig. 6: *Comparative plot of the pressures calculated with the two applied calibrations of the Al-in-hornblende-barometer by Schmidt (1992) and Anderson and Smith (1995).*

crystallized close to the solidus, both versions of the barometer yield very similar pressures. Only for sample DSFZ8, with amphiboles crystallizing at c. 730°C, the temperature correction lowers the pressure significantly from 0.33 to 0.25 GPa. After application of the temperature correction to all samples they all fall into a tight interval from 0.23 to 0.25 GPa. This is in good agreement with

the phengite barometry on pelites from contact aureole rocks by Ernst (1996). The example of DSFZ8 shows how useful the temperature correction by Anderson and Smith (1995) is, because it explains the neighbourship of rocks, which crystallized under apparently different conditions. Only hornblendes from samples VF2 and VF3 yield clearly lower pressures from 0.22 and 0.19 GPa, respectively. Both samples are xenoliths in a probably Tertiary rhyolitic tuff. Consequentely, the deviating pressure data are probably the result of a reequilibration of hornblende in these two xenolithic samples due to the heat of the rhyolitic magma, which brought them into their present-day position.

Summary of the results of amphibole thermobarometry

PT conditions for the crystallisation of the JBP, determined by hornblende thermobarometry, can be summarized as follows: The pluton intruded at a depth of c. 8 km (corresponding to a confining pressure of c. 0.24 GPa) and over a temperature interval from c. 900 (upper limit of the temperature data derived from the hornblende-clinopyroxene thermometer) to c. 640°C (lower limit of the temperature data derived from the amphibole-plagioclase thermometer).

Na-in-cordierite thermometry

Structure and chemistry of cordierite

Cordierite is a tectosilicate and occurs usually as orthorhombic or pseudohexagonal low temperature variety or, more rarely as the hexagonal high temperature variety indalite. The polymorphic transition occurs for Mg-cordierite at 1450°C, for Fe-cordierite at c. 900°C and for intermediate compositions at c. 700°C (Deer et al. 1992). The lower temperature stability of Mg-cordierite is at 450°C (Deer et al. 1992). The simplified mineral formula is:

$$[(Mg,Fe)_2Si_5Al_4O_{18}]*n(H_2O, CO_2)$$

4 Si and 2 Al atoms occupy 6 tetrahedral lattice positions in the ring structure, the remaining Si and Al atoms build a framework of tetrahedra, which is tied to the ring structures. All bivalent atoms, such as Fe and Mg, also substituted by Mn or Li (Cerny et al. 1997), take octahedral positions between the ring channels. In three dimensions, the ring structures build channels parallel with the crystallographic c-axis (Armbruster and Bloss 1980), where, for example H_2O, CO_2, Na and K can be found (Armbruster and Bloss 1980; Mirwald 1986; Schreyer et al. 1990). Natural cordierite may incorporate up to 1 mol fluid p.f.u., corresponding to 2.99 wt% H_2O or 6.99 wt% CO_2 (Johannes and Schreyer 1981).

Methodology

The Na-in-cordierite thermometer was developed by Mirwald (1986) based on experiments in the systems Mg-cordierite - NaOH and Mg-cordierite - NaOH – albite at pressures between 0.1 and 0.8 GPa and temperatures between 650 and

850°C. The experimental results showed an inverse correlation between temperature and the Na-content in cordierite, which can be expressed either graphically (Mirwald 1986) or by the following formula:

$$T[\pm 30°C] = -2744.8X_{Na} + 897.36$$

with X_{Na} = atoms per formula unit as calculated for the structural formula. According to Kalt et al. (1998) the Na-in-cordierite-thermometer is applicable to natural Mg-Fe-cordierites as long as they coexist with plagioclase (An_{10-40}), K-feldspar, biotite and quartz. No other parameters than temperature were found to influence the Na-content of cordierite.

sample	Lok23	BC5660	P9
n	281	293	38
SiO_2	46.77 (1.63)	47.11 (0.65)	47.77 (1.35)
TiO_2	0.02 (0.05)	0.01 (0.03)	0.02 (0.01)
Al_2O_3	32.09 (1.74)	31.79 (0.46)	31.78 (1.00)
Cr_2O_3	0.01 (0.02)	0.01 (0.01)	0.01 (0.01)
FeO	12.64 (1.05)	11.10 (0.43)	11.53 (0.49)
Fe_2O_3	0.00 (0.00)	0.00 (0.00)	0.00 (0.00)
MgO	5.05 (0.44)	5.72 (0.28)	5.79 (0.39)
MnO	0.49 (0.08)	0.50 (0.09)	0.51 (0.08)
CaO	0.03 (0.06)	0.02 (0.04)	0.07 (0.24)
Na_2O	0.25 (0.04)	0.55 (0.08)	0.26 (0.05)
K_2O	0.07 (0.37)	0.05 (0.42)	0.02 (0.03)
Total	97.42 (2.82)	96.86 (0.83)	97.75 (1.40)
Cations on the basis of 18 O			
Si	4.98 (0.09)	5.01 (0.04)	5.03 (0.11)
Al^{IV}	1.02 (0.09)	0.99 (0.04)	0.97 (0.11)
Al^{VI}	3.00 (0.10)	2.99 (0.03)	2.98 (0.02)
Ti	0.00 (0.00)	0.00 (0.00)	0.01 (0.01)
Cr	0.00 (0.00)	0.00 (0.00)	0.00 (0.00)
Fe^{2+}	1.12 (0.09)	0.99 (0.04)	1.02 (0.04)
Fe^{3+}	0.00 (0.00)	0.00 (0.00)	0.00 (0.00)
Mg	0.80 (0.08)	0.91 (0.04)	0.91 (0.06)
Mn	0.04 (0.01)	0.04 (0.01)	0.05 (0.01)
Ca	0.00 (0.01)	0.00 (0.00)	0.01 (0.03)
Na	0.05 (0.01)	0.11 (0.02)	0.05 (0.01)
K	0.01 (0.05)	0.01 (0.06)	0.00 (0.00)
Total	11.04 (0.04)	11.06 (0.04)	11.02 (0.06)

Tab. 4: *Average cordierite compositions of the inividual samples from the aureole (numbers in brackets are standard deviations).*

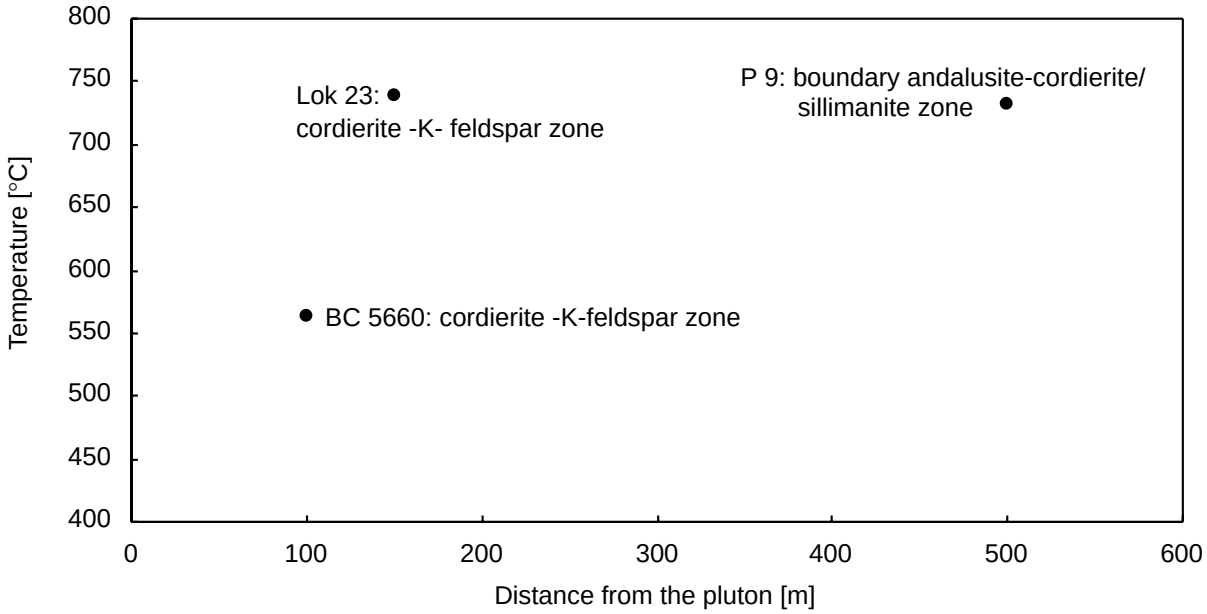

Fig. 7: *Temperatures obtained with the Na-in-cordierite-thermometer plotted on the y-axis versus distance from the pluton of the examined samples.*

Results of the Na-in-cordierite thermometry

In this paper only a short overview of the results is given. For a more detailed discussion see Kontny and Dietl (in prep.).Measurements were carried out at samples BC5660 and Lok23 (cordierite-K-feldspar zone) and P9 (transition andalusite-cordierite to sillimanite zone). In all samples only fresh, not pinitized cordierite with K below the detection limt (0.02 wt %) were measured. Average Na-contents can be found in Tab. 4 and related temperatures (plotted versus distance from the pluton) are shown in Fig. 7.The mean Na content of sample Lok 23 is 0.052 (±0.008) p.f.u. corresponding to an average temperature of 738°C. This agrees well with the observed dehydration melting reaction sillimanite + biotite + plagioclase ⇒ cordierite + K-feldspar + melt, which, according to Le Breton and Thompson (1988), takes place at 0.2 GPa and 730°C and confirms the interpretation of the leucosomes as results of partial melting. Also the average temperature for sample P9 of 731°C (Na content: 0.054

(±0.010) p.f.u.) matches the presence of sillimanite, which appears at 0.23 GPa and 600°C (Holdaway and Mukhopadhyay 1993). Only sample BC 5660 has an average Na content of 0.113 (±0.016) p.f.u. and yields therefore a temperature of 570°C, too low for the cordierite-K-feldspar zone.The most probable explanation for that observation lies in the sampling locality: sample BC 5660 comes from the immediate vicinity of a c. 30 m thick granite dyke. The intrusion of the dyke may have caused the Na-content of cordierite to reequilibrate. This idea is supported by the higher mean variation of the data compared to the other two samples. The scatter can be explained with the fact, that not all, but only a part of the cordierites reequlibrated due to the heat flux from a hot, but rapidly cooling dyke in its immediate neighbourhood (c. 5 m distance).

Infra-red spectroscopy at cordierites

Methodology

As already stated, cordierite can incorporate alkalis and volatiles, such as H_2O, CO_2, Ar, N_2 and hydrocarbons (HCs) in its channel structures (Damon and Kulp 1958; Armbruster and Bloss 1980; Johannes and Schreyer 1981; Vry et al. 1990; Santosh et al. 1993). H_2O, CO_2 and HCs produce peaks in the infra-red spectrum of cordierite between 2300 and 3700 cm^{-1}: The CO_2 peak is situated at 2349 cm^{-1}, HCs can be found around 2900 cm^{-1} and H_2O generates 3 peaks at 3574, 3632 and 3689 cm^{-1} (Aines and Rossmann 1984). CO_2 occurs in the channel sectors with the widest diameter and is oriented normal to the crystallographic c-axis of cordierite and parallel with the crystallographic a-axis

(Armbruster and Bloss 1980). The 3 H_2O peaks can be assigned to 2 orientations of water molecules: for H_2O I (3689 cm^{-1}) the H-H vector lies parallel with the crystallographic c-axis, while for H_2O II (3574 and 3632 cm^{-1}), which is tied to the presence of alkalies and occupies the narrowest parts of the channels, the H-H vector is oriented parallel with the crystallographic b-axis (Wood and Nassau 1967). Measurements were done at individual cordierite crystals in thick sections (200 µm thick) at the Mineralogical Department of the University of Hannover, Germany under the direction of Harald Behrens with the infra-red microscope A590, which is coupled with the FTIR spectrometer Bruker IFS 88 in the middle infra-red (spectral resolution: 2 cm^{-1}). The aperture of the microscope was 0.6 or 0.75 mm, corresponding to focal radii of 20 and 25 µm, respectively. Light source was a Glowbar pin. A KBr radiation separator and a MCT detector with NIR equipment (measuring range: 600-10000 cm^{-1}) were used for the investigations. One spectrum consists of 50 to 100 individual measurements. H_2O and CO_2 contents were calculated from the spectra based on the calibration by Vry et al. (1990).

Results of the infra-red spectroscopy

sample	Lok23	BC5660	P9
n	27	8	4
H_2O I	0.29 (0.05)	0.36 (0.05)	0.25 (0.04)
H_2O II	0.31 (0.06)	0.43 (0.05)	0.28 (0.10)
CO_2	0.06 (0.02)	0.08 (0.01)	0.03 (0.01)
Total	0.66 (0.09)	0.85 (0.10)	0.56 (0.15)

Tab. 5: *Average volatile contents in the channel structures of cordierite from Lok23, BC5660 and P9 (numbers in brackets are standard deviations).*

Generally in all 3 samples H_2O I, H_2O II, CO_2 and HC peaks were observed. The HC peaks are neglectibly small or are overlapped by a broad peak

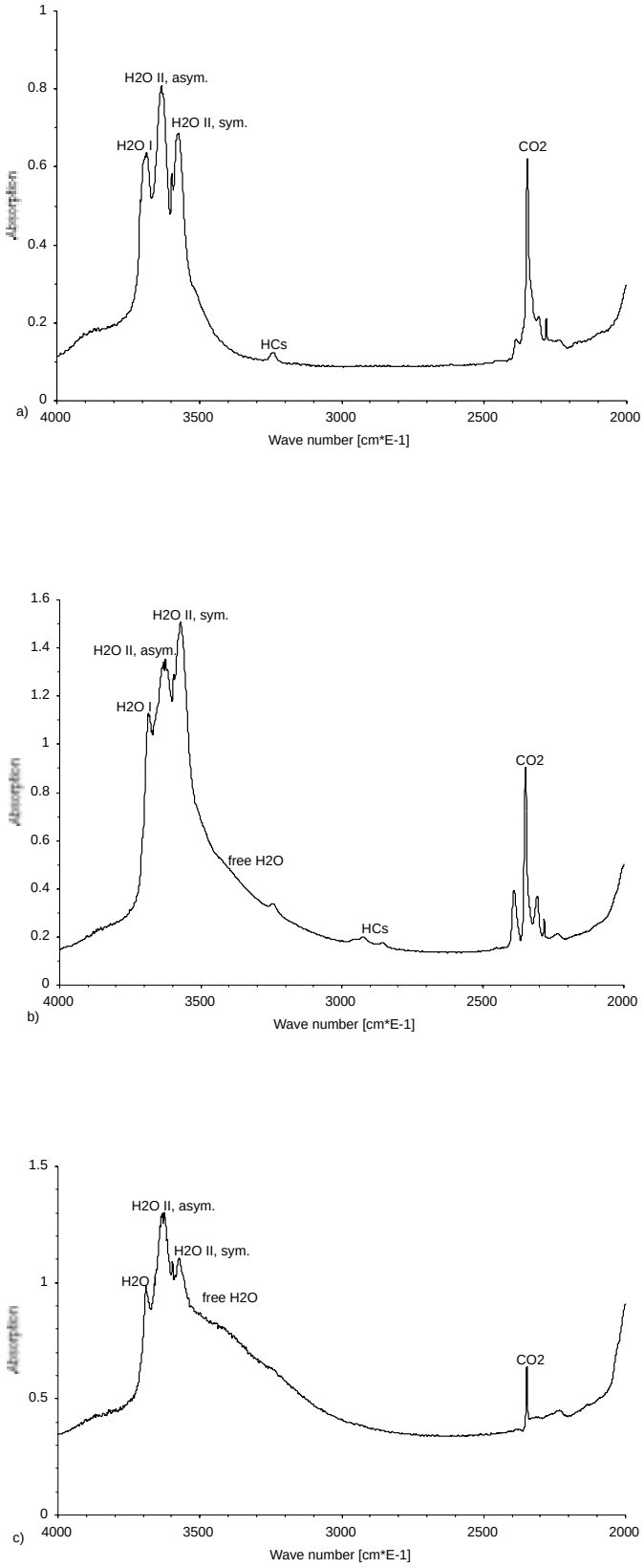

Fig. 8: *Typical infra-red spectra of the individual samples:* ***a)*** *Lok23;* ***b)*** *BC5660;* ***c)*** *P9.*

made by free water probably from fluid inclusions (Fig. 8). Cordierite from sample P9 are not really suitable for infra-red spectroscopy, because they are very rich in mineral and fluid inclusions. Therefore only 4 measurements were carried out at this sample. At samples Lok23 and BC5660 32 and 9 measurements, respectively, were made. In all samples fluid contents are very low. H_2O is never higher than 1.0 wt%. It ranges in sample Lok23 between 0.4 and 0.8 wt%, in sample BC5660 between 0.6 and 0.9 wt% and in sample P9 between 0.3 and 0.7 wt% (Tab. 5). CO_2 is also very low: cordierites from Lok23 contain between 0.03 and 0.1 wt%, those from BC5660 have 0.05 to 0.1 wt% CO_2 and the 4 cordierites measured in sample P9 only between 0.02 and 0.04 wt% (Tab. 5).This is far below the equilibrium water content under water saturated conditions: Jochum (1986) established H_2O contents of 1.25 wt% for Na-free Mg-cordierite and 1.53 wt% for Mg-cordierite with 0.4 Na p.f.u. at P = 0.2 GPa and T = 700, close to the formation conditions of the investigated cordierites. Although Vry et al. (1990) suggest postmetamorphic volatile loss to be responsible for low fluid contents in the channel structures of cordierite. Jochum (1986) showed that natural cordierites do not tend to loose volatiles extensively after their formation. Accordingly, secondary dehydration causing the low H_2O contents of the examined cordierites can be excluded and it is probable that cordierite grew under water undersaturated conditions as suggested by Carrington and Harley (1996). This, together with the petrographic observations and the results of the Na-in-cordierite-thermometry, implies that partial melting as observed in the cordierite-K-feldspar zone occured in the absence of a free, aqueous fluid phase.

Modelling of the intrusion of the JBP with ”CONTACT”

”CONTACT” (Peacock 1989) calculates one-dimensional, conductive heat transfer from a pluton to its host rock by using a finite difference algorithm. Several thermal parameters can be chosen to simulate the Tt-path during the intrusion and cooling of a pluton. The parameters for the intrusion of the JBP are as follows (for each parameter one value can be chosen): half width of intrusion: 10000 m, country rock temperature: 300°C (corresponding to the temperature of the pre-intrusive regional metamorphism as determined by Ernst (1996)), intrusion temperature: 900°C (as the upper temperature limit of the hornblende-clinopyroxene-thermometry), temperature interval of crystallization: 225°C (starting from the assumed intrusion temperature 900°C down to the average crystallisation temperature of hornblende-plagioclase pairs of 675°C), heat of crystallization: 200 kJ/kg (Peacock 1989), thermal conductivity: 2.75 (W/m-K) (England and Thompson 1984), heat capacity: 1000 (J/kg-K) (Peacock 1989),density: 2750 kg/m^3. Modelling was carried out for a time span of 5 Ma in time steps of 50 ka. The graphics window of ”CONTACT” shows every tenth time step. Fig. 9 a shows the temperature evolution in the pluton (y-axis) and its aureole with increasing distance from the centre of the pluton (x-axis). The individual curves show the temperature evolution in time steps of 500 Ka. In Fig. 9 b temperature (y-axis) is plotted versus time (x-axis). The individual curves show the temperature evolution with time at certain points in the pluton and its aureole.

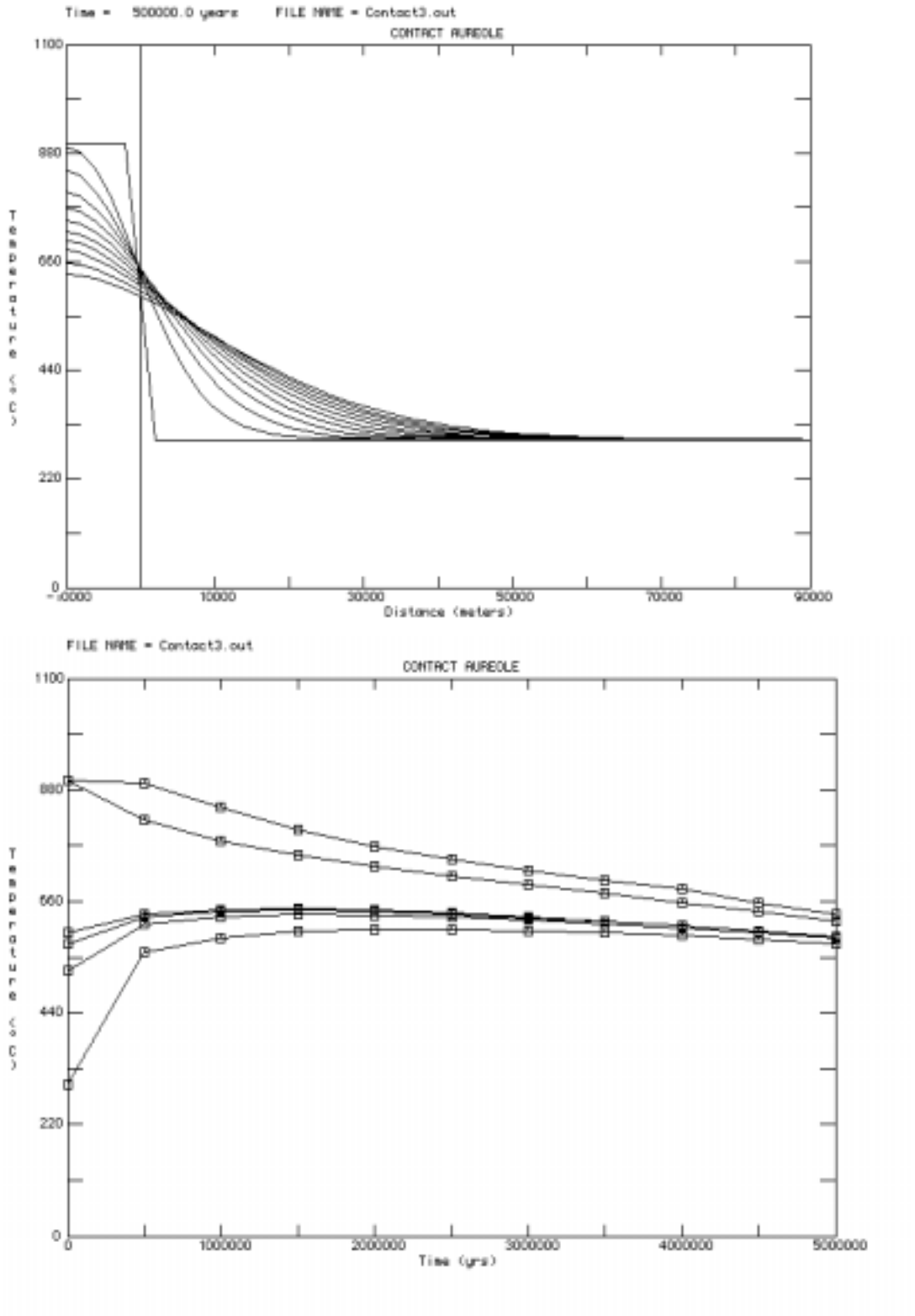

Fig. 9: *Graphical results of the model created with "CONTACT". In* ***a)*** *the temperature evolution in the pluton and its aureole on the y-axis versus distance from the centre of the pluton on the x-axis are shown. The vertical line depicts the contact between pluton and host rock. In* ***b)*** *temperature on the y-axis is plotted versus time on the x-axis. The individual curves show the temperature evolution with time at certain points in the pluton and its aureole. A: centre of the JBP; B: halfway between the centre of the pluton and the contact with the country rocks; C: direct at the pluton/wall rock contact; D: 150 m away from the JBP; E: 500 m away from the JBP; F: 2000 m away from the JBP.*

Points of interest are the centre of the intrusion (”A”), halfway between the centre of the pluton and the contact with the country rocks (”B”), direct at the contact itself (”C”), and within the aureole, 150, 500 and 2000 m away from the JBP (”D”, ”E” and ”F”, respectively). The choice of spots in the aureole corresponds to the locations of samples (Lok23 and BC5660 c. 150 m, P9 c. 500 m) and to the outer edge of the thermal aureole at 2000 m. Modelling shows the JBP to reach its solidus not until 4.5 Ma after the intrusion. In the aureole at a distance of 2000 m the simulated maximum temperature of 570°C is sufficient for the growth of andalusite and cordierite. There, temperature stays clearly above 450°C for c. 4 Ma, the lower thermal stability of Mg-cordierite. During this long time span, cordierite and andalusite were able to form large porphyroblasts. At a distance of 500 m the simulation yields 600°C and a maximum temperature at the contact of 650°C. These temperatures occur at a pressure of c. 0.24 GPa and are insufficient for the growth of sillimanite as observed in rocks of the inner aureole. However, the Na-in-cordierite-temperatures are significantly higher than the model temperatures. The low temperatures derived from a simulation based on conductive heat transfer only, indicate that heat transfer in the contact aureole happened convectively or that the geometry of the pluton affects the thermal field significantly. However, infra-red spectroscopy has shown, that cordierite grew without a free fluid phase. Therefore, there was no fluid, which could have served as a medium for convective heat transfer. All other indicators for the presence of a free fluid phase, such as skarns, epidote veins and chloritized biotite belong to the late and post magmatic stage of the history of the JBP and cannot be related directly to

the high temperatures deduced from mineral assemblages in the cordierite-K-feldspar zone, as well as from Na-in-cordierite-thermometry. Therefore, a good way to explain the elevated temperatures in the inner aureole is to assume the existence of more pluton material below the present-day level of the aureole.

Conclusions

The combination of several different methods such as field geology, thin section petrography, geothermobarometry, infra-red spectroscopy and numerical modelling provide valuable information about the PT*f* (fluid) conditions and their changes over time. The temperatures calculated with the amphibole-plagioclase and hornblende-clinopyroxene thermometers (Blundy and Holland 1990, Holland and Blundy 1994, Perchuk et al. 1985) show the Joshua Flat Monzonite and the Beer Creek Granodiorite to crystallize over a temperature interval probably starting at 900 ranging to 650˚C. These temperatures are in good agreement with the intrusion and solidus temperatures of a monzonitic to granodioritic pluton (Piwinskii and Wyllie 1968; Piwinskii 1968). The average confining pressure during the intrusion of 0.25 GPa, determined with the Al-in-hornblende barometer (Anderson and Smith 1995) corresponds very well with the pressure established by Ernst (1996) with phengite barometry. The peak metamorphic temperature, established with the Na-in-cordierite thermometer (Mirwald 1986) in the contact aureole of the JBP is 730˚C. At this temperature and a pressure of c. 0.25 GPa dehydration melting takes place in metapelites due to the mineral reaction sillimanite + biotite + plagioclase + quartz --> cordierite + K-feldspar + melt (Le Breton and Thompson 1988). Fabrics related to this

reaction were observed in the innermost aureole, the so called cordierite-K-feldspar zone. There, leucocratic veins, either lit-par-lit parallel with the foliation or as diffuse schlieren, were also found. These facts point to partial dehydration melting in the cordierite-K-feldspar zone. Melting under water-undersaturated conditions is supported by the low fluid contents in the channel structures of cordierite, determined with infra-red spectroscopy. Moreover, the observation of hornblende crystallizing after biotite in all three igneous rock types and the occurence of clinopyroxene in the Joshua Flat Monzonite indicate slightly H_2O-undersaturated conditions also in the JBP. The presence of pegmatites, epidote veins, skarns and copper mineralisations point to water saturation only for the late and post magmatic history of the pluton / wall rock system. Consequentely, conductive heat flow seems to be the only heat transfer mechanism in the contact aureole during peak metamorphism. For this reason it should be allowed to use the computer program ”CONTACT” (Peacock 1989) for numerical modelling. Nevertheless, the peak temperature (650˚C) resulting from modelling is far below the peak temperature determined with the Na-in-cordierite thermometer. A good reason for this discrepancy is the geometry of the pluton, which cannot be modelled with the one-dimensional program. Only if plutonic material was present also below the studied part of the contact aureole (and not only next to it) during the peak of contact metamorphism, the JBP could have supplied enough heat to induce partial dehydration melting of its host rock. The assumption of igneous material next to and below the present-day level of the contact aureole may point to the diapiric shape and nature of the

JBP. To test this hypothesis it is necessary to apply at least a two-dimensional modelling program. This will be the subject of further research.

Acknowledgements

This research was funded by the Graduiertenkolleg 273 ”Fluid-rock interactions” of the German Science Foundation (DFG). Special thanks go to H. Behrens and H. P. Meyer for assistance with obtaining infra-red spectroscopy and electron microprobe analyses, respectively. I am grateful to R. O. Greiling, S. Hurter, A. Kalt and E. Stein for the helpful and constructive discussions and reviews.

References

Aines RD, Rossmann, GR (1984) The high-temperature behaviour of water and carbon dioxide in cordierite and beryl. Am Mineral 69: 319-337

Anderson JL, Smith DR (1995) The effects of temperature and f_{O2} on the Al-in-hornblende barometer. Am Mineral 80: 549-559

Armbruster T, Bloss FD (1980) Channel CO_2 in cordierites. Nature 286: 140-141

Bateman PC, (1992) Plutonism in the central part of the Sierra Nevada batholith, California: US Geol Surv Prof Paper 1483: pp 1-186

Blundy JD, Holland TJB (1990) Calcic amphibole equilibria and a new amphibole-plagioclase geothermometer. Contrib Mineral Petrol 104: 208-224

Buddington AF (1959) Granite emplacement with special reference to North America. Geol Soc Am Bull 70: 671-747

Carrington DP, Harley SL (1996) Cordierite as a monitor of fluid and melt H_2O contents in the lower crust: An experimental calibration. Geology 24: 647-650

Cerny P, Chapman R, Schreyer W, Ottolini L, Bottazi P, McCammon CA (1997) Lithium in sekaninaite from the type locality, Dolni Bory, Czech Republic. Can Mineral 35: 167-173

Clarke DB (1992) Granitoid rocks. Chapman and Hall, London, 1-283

Cotkin SJ, Medaris LG (1993) Evaluation of the crystallization conditions for the calcalkaline Russian Peak intrusive complex, Klamath Mountains, northern California. J Petrol 34: 543-571

Damon PE, Kulp JL (1958) Excess helium and argon in beryl and other minerals. Am Mineral 62: 67-78

Deer WA, Howie RA, Zussman J (1992) An introduction to the rock-forming minerals. Longman, Essex, 1-696

Dietl C (1999) Emplacement of the Joshua Flat-Beer Creek Pluton (White Inyo Mountains, California): a story of multiple material transfer processes. In: Castro A, Fernandez C, Vigneresse JL (eds) Understanding granites: Integrating new and classical techniques. Geol Soc Lond Spec Publ 168: pp 161-176

England PC, Thompson AB (1984) Some thermal and tectonic models for crustal melting in continental collision belts. In: Coward MP, Ries AC (eds) Collision tectonics. Geol Soc Lond Spec Publ 19: pp 83-94

Ernst WG (1996) Petrochemical study of regional/contact metamorphism in metaclastic strata of the central White-Inyo Range, eastern California. Geol Soc Am Bull 108: 1528-1548

Gillespie JG (1979) U-Pb and Pb-Pb ages of primary and detrital zircons from the White Mountains, eastern California: Geol Soc Am Abstr Prog 11 (30): 79

Hammarstrom JM, Zen E (1986) Aluminium in hornblende: An empirical igneous geobarometer. Am Mineral 71: 1297-1313

Holdaway MJ, Mukhopadhyay, B (1993) A reevaluation of the stability relations of andalusite: Thermodynamical data and phase diagram for the aluminum silicates. Am Min 78: 298-315

Holland TJB, Blundy JD (1994) Non-ideal interactions in calcic amphiboles and their bearing on amphibole-plagioclase thermometry. Contrib Mineral Petrol 116: 433-447

Hollister LS, Grissom GC, Peters EK, Stowell HH, Sisson VB (1987) Confirmation of the empirical correlation of Al in hornblende with pressure of solidification of calc-alkaline plutons. Am Mineral 72: 231-239

Jochum C (1986) Experimentelle Untersuchungen zum Wassereinbau und zur Kinetik der Hydratation und Dehydratation von synthetischen und natürlichen Cordieriten. Unpubl PhD thesis, University of Bochum, pp 1-235

Johannes W, Schreyer W (1981) Experimental introduction of CO_2 and H_2O into Mg-cordierite. Am J Sci 281: 299-317

Johnson MC, Rutherford MJ (1989) Experimental calibration of the aluminium-in-hornblende geobarometer with applications to Long Valley caldera (California) volcanic rocks. Geology 17: 837-841

Kalt A, Altherr R, Ludwig T, (1998) Contact metamorphism in pelitic rocks on the island of Kos (Greece, Eastern Aegean Sea): a test for the Na-in-cordierite thermometer. J Petrol 39: 663-688

Knopf A (1918) A geologic reconnaissance of the Inyo Range and the eastern slope of the southern Sierra Nevada, California. : US Geol Surv Prof Paper 110: pp 1-130

Krauskopf KB (1968) A tale of ten plutons. Geol Soc Am Bull 79: 1-18

Kukowski N (1992) Plutonische hydrothermale Systeme in der kontinentalen Kruste: Numerische Modellrechnungen zu räumlichen Dimensionen und zeitlichen Variationen von Quelle und Umfeld. Unpubl PhD thesis, University of Bonn, pp 1-118

Leake BE, Woolley AR, Arps CES, Birch WD, Gilbert MC, Grice JD, Hawthorne FC, Kato A, Kisch HJ, Krivovichev VG, Linthout K, Laird J, Mandarino J, Maresch WV, Nickel EH, Rock NMS, Schumacher JC, Smith DC, Stephenson NCN, Ungaretti L, Whittaker EJW, Youzhi, G (1997) Nomenclature of amphiboles. Report of the Subcommittee on Amphiboles of the International Mineralogical Association Commission on New Minerals and Mineral Names. Eur J Mineral 9: 623-651

Le Breton N, Thompson AB, (1988) Fluid absent (dehydration) melting of biotite in metapelites in the early stages of crustal anatexis: Contrib Mineral Petrol 99: 226-237

McKee EH, Conrad JE (1996) A tale of ten plutons – Revisited: Age of granitic rocks in the White Mountains, California and Nevada. Geol Soc Am Bull 108: 1515-1527

Mirwald PW (1986) Ist Cordierit ein Geothermometer?. Fortsch Mineral 64: 119

Nelson CA, Hall CA Jr, Ernst WG (1991) Geologic history of the White-Inyo Range. In: Hall CA Jr (ed) Natural history of the White-Inyo Range, California. University of California Natural History Guides 55: pp 42-74

Naney MT (1983) Phase equilibria of rock rock-forming ferromagnesian silicates in granitic systems. Am J Sci 283: 993-1033

Norton D, Knight J (1977) Transport phenomena in hydrothermal systems: cooling of plutons. Am J Sci 277: 937-981

Paterson SR, Fowler TK Jr (1993) Re-examining pluton emplacement processes. J Struct Geol 15: 781-784

Peacock SM (1989) Thermal modeling of metamorphic pressure-temperature-time paths: a forward approach. In: Spear FS, Peacock SM (eds) Metamorphic Pressure-Temperature-Time Paths 7: pp 57-102

Perchuk LL, Aranovich LY, Podlesskii KK, Lavrant'eva IV, Gerasimov VY, Fed'kin VV, Kitsul VI, Karsakov LP, Berdnikov NV (1985) Precambrian granulites of the Aldan Shield, eastern Siberia, USSR. J Metamorph Geol 3: 265-310

Piwinskii AJ (1968) Experimental studies of igneous rock series, central Sierra Nevada batholith, California. J Geol 76: 548-570

Piwinskii AJ, Wyllie PJ (1968) Experimental studies of igneous rock series: a zoned pluton in the Wallowa batholith, Oregon. J Geol 76: 205-234

Pouchou JL Pichoir F (1984) A new model for quantitative X-ray microanalysis; Part I: Application to the analysis of homogeneous samples. La Recherche Aérospatiale 3: 167-192

Santosh M, Jackson DH, Harris NBW (1993) The significance of channel and fluid inclusion CO_2 in cordierite: evidence from carbon isotopes. J Petrol 34: 233-258

Schmidt, MW (1992) Amphibole composition in tonalite as a function of pressure: an experimental calibration of the Al-in-hornblende barometer. Contrib Mineral Petrol 110: 304-310

Schreyer W, Maresch WV, Daniels P, Wolfsdorff P(1990) Potassic cordierites: characteristic minerals for high-temperature, very low-pressure environments. Contrib Mineral Petrol 105: 162-172

Stein E (2000) Zur Platznahme von Granitoiden - Vergleichende Fallstudien zu Gefügen und Platznahmemechanismen aus den White-Inyo Mountains, California, USA und dem Bergsträßer Odenwald. Geotekt Forsch 93: 1-330

Stein E, Paterson SR (1996) Country rock displacement during emplacement of the Joshua Flat Pluton, White-Inyo mountains, California. In: Oncken O, Janssen C (eds) Basement Tectonics 11. Kluwer, Dordrecht, pp 35-49

Stern TW, Bateman PC, Morgan BA, Newell MF, Peck DL (1981) Isotopic U-Pb ages of zircon from the granitoids of the central Sierra Nevada, California: US Geol Surv Prof Paper 1185: pp 1-17

Streckeisen A (1976) To each plutonic rock its proper name. Earth Sci Rev 12: 1-33

Sylvester AG, Miller CF, Nelson CA (1978) Monzonites of the White-Inyo Range, California, and their relation to the calc-alkalic Sierra Nevada batholith. Geol Soc Am Bull 89: 1677-1687

Symmes GH, Ferry JM (1995) Metamorphism, fluid flow and partial melting in pelitic rocks from the Onawa contact aureole, central Maine, USA. J Petrol 36: 587-612

Vry JK, Brown PE, Valley JW (1990) Cordierite volatile content and the role of CO_2 in high-grade metamorphism. Am Mineral 75: 71-88

Wood DL, Nassau K (1967) Infrared spectra of foreign molecules in beryl. J Chem Physics 47: 2220-2228

Zulauf G, Helferich S (1997) Strain and strain rate in a synkinematic trondhjemitic dike: evidence for melt-induced strain softening during shearing (bohemian Massif, Czech Republic). J Struct Geol 19: 639-652

Relations between metamorphism and magneto-mineralogy in a contact aureole: a case study from the White Inyo Range, Eastern California

A. Kontny*, C. Dietl

Geologisch-Paläontologisches Institut, Ruprecht-Karls-Universität Heidelberg, Im Neuenheimer Feld 234, D-69120 Heidelberg

Abstract

The relations between Fe-Ti oxides and Fe-Mg silicates in metapelites and their changes in magnetic susceptibility with increasing LP-HT metamorphism were investigated in the contact metamorphic aureole of the Jurassic Joshua Flat-Beer Creek pluton at the southern rim of the Inyo batholith (White Inyo Mountains, Eastern California). Several geothermometers and the phengite geobarometer were applied to get information on the P-T conditions of the regional and contact metamorphic zones. The biotite zone preserves the regional metamorphic history of the metasediments, while mineral assemblages in the andalusite-cordierite, transition and cordierite-K-feldspar zone indicate increasing contact metamorphism with decreasing distance from the pluton up to incipient migmatisation in the innermost zone. Na-in-cordierite thermometry yields peak temperatures of c. 730 °C for the highest contact metamorphic zone, whereas the Ti-in-

* Corresponding author. Tel.:+49 (6221) 54-6053, Fax: +49 (6221) 54-5503; E-mail: agnes.kontny@urz.uni-heidelberg.de

biotite thermometer gives unreasonable temperatures of c. 555°C for the innermost aureole and of about 675°C for the external zones. This is explained by the stronger increase of Al relative to Ti with increasing contact metamorphic grade. Application of four different calibrations of chlorite thermometers results in temperatures ranging from 280° to 420°C for the (hydrothermal) retrograde branch of the contact metamorphic path. Phengite barometry indicates pressures between 0.2 and 0.3 GPa for retrograde assemblages. The regional metamorphic oxide assemblage ilmenite + rutile ± hematite observed in the biotite zone is overprinted during contact metamorphism and magnetite and ilmenite-hematite solid solutions are formed. In the cordierite-K-feldspar zone ilmenite together with white mica occurs. The observed prograde changes in magnetic mineralogy are related to (1) an increase of temperature from the biotite to the cordierite-K-feldspar zone and (2) increasing log $f(O_2)$ conditions in the cordierite-K-feldspar zone. During retrograde metamorphism, log $f(O_2)$ conditions decline towards the hematite-magnetite buffer line and eventually go across this line into the field of magnetite at about 300°C.

The magneto-mineralogical changes explain the behaviour of magnetic susceptibility and thermomagnetic curves. Susceptibilities in the biotite zone generally range from 200 – 500 x 10^{-6} SI units, typical for paramagnetic minerals. Samples from the andalusite-cordierite and transition zones give an inhomogeneous distribution of the magnetic susceptibility between 300 and 28000 x 10^{-6} SI units due to varying amounts of magnetite. Thermomagnetic curves for these zones give Curie temperatures of 590°, typical for pure magnetite, and 550° as well as 340°C that are related to Ti-bearing hematite phases (maghemite). Magnetic susceptibility measurements of samples from the cordierite-K-feldspar zone result in values suggesting a mixture of paramagnetic with small amounts of ferrimagnetic minerals (200 – 2000 x 10^{-6} SI units). Thermomagnetic

investigations indicate that small amounts of magnetite are present in this zone but that most of the ferrimagnetic components were decomposed during a retrograde overprint by hydrothermal fluids probably associated with the cooling of the pluton. It is assumed that pre-existing magnetic isograde, which developed during the prograde contact metamorphism, are destroyed by these retrograde reactions.

Keywords: contact metamorphism; Fe-Mg silicate and oxide assemblage; geothermobarometry; magnetic volume susceptibility; temperature-dependent susceptibility; oxygen fugacity

1. Introduction

Systematic magnetic–petrologic studies of different metamorphic rock types have shown that their magnetic susceptibility sometimes varies as a function of metamorphism (e.g. Warner and Wasilewski, 1995; Shive et al., 1988a and 1988b; Rochette, 1987). The changes in magnetic susceptibility are controlled by the Fe distribution among paramagnetic Fe-Mg silicates as well as para- and ferromagnetic (s.l.) Fe-Ti oxides and Fe-sulphides. The understanding of the interrelations between silicate-oxide/sulphide minerals, their chemical composition and the magnetic susceptibility are important for the interpretation of crustal magnetic anomalies.

For this study, metasediments with a relatively high modal content of iron oxides (magnetite-ilmenite around 5 vol% of the rock; Robigou, 1986), in association with phyllosilicates were selected. These were sampled in the contact aureole of the Joshua Flat – Beer Creek pluton (JBP) from the Central White Inyo Range / California composed of monzonitic to granodioritic rocks.

The metamorphic evolution of the metasediments was controlled by episodic deformational and igneous events that resulted in lower greenschist grade metamorphism (chlorite / biotite zone; Ernst, 1996) and an increasing contact metamorphic overprint towards the intrusive body up to conditions of the cordierite-andalusite and cordierite-K-feldspar zone (Dietl, 1999). The contact metamorphic zonation is obscured by retrograde metamorphism, which is either related to a late- or post-intrusive hydrothermal event.

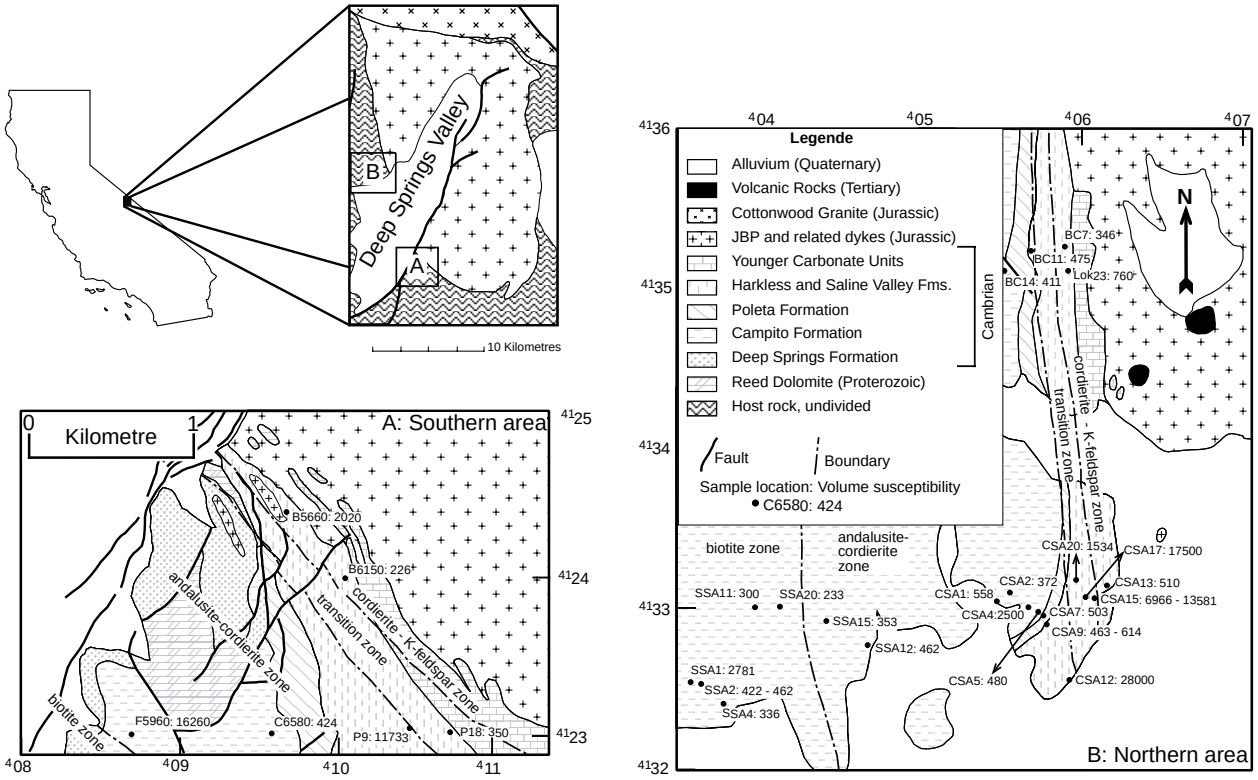

Fig. 1. *Simplified geologic map of the working area south (A) and north (B) of the Deep Springs Valley with sample localities and magnetic susceptibilities (in 10^{-6} SI units). Also shown is the location of the Central White Inyo Range in California and the position of area A and B in the contact aureole of the JBP.*

We investigated the effects of prograde contact metamorphism and later retrogression on the distribution of Fe among different para- and ferrimagnetic minerals and the related changes in magnetic mineralogy. Applied were a combination of microscopic descriptions (rock fabrics and opaque mineralogy), electron microprobe analyses of Fe-Mg silicates and oxides, whole rock

geochemistry and measurements of the volume and temperature-dependent magnetic susceptibility on samples taken at different distances to the pluton. Several semiquantitative and quantitative geothermometers (Ti-in-biotite, chlorite- and Na-in-cordierite-thermometer) and the phengite geobarometer were applied to constrain the conditions of the different metamorphic zones. Magnetic susceptibility measurements were carried out in order to investigate its use as indicator of magnetic isograde (according to Rochette 1987) in such a geologic setting.

Three lithologic units were sampled: the Lower Cambrian Campito, Harkless and Saline Valley Formations. All three consist of metapelites of similar geochemical composition (see below). Therefore, from here on, the samples are not assigned to the stratigraphic formations, but are treated according to their mineralogical composition and metamorphic grade. 22 samples north of Deep Springs Valley, which divides the JBP and its aureole into two parts (Fig. 1), and 6 samples south of it were taken and investigated with respect to their silicate and oxide mineralogy as well as their magnetic susceptibility.

2. Geological setting

The White-Inyo Range in eastern California is characterised by Mesozoic plutons, which intruded as part of the Cordilleran magmatic arc into an early Palaeozoic sedimentary sequence consisting of carbonates and psammopelites, partly with volcanic detritus (Nelson et al., 1991). This sequence was metamorphosed during the late Palaeozoic Antler and Sonoma orogeneses under greenschist facies conditions (Ernst, 1996). According to $^{40}Ar/^{39}Ar$ dating by McKee and Conrad (1996) three major plutonic stages can be recognised at 180-165 Ma, 150-140 Ma and 90-75 Ma, respectively. The largest assemblage of igneous rocks is the Inyo batholith in the White Mountains. The Joshua Flat - Beer Creek - Pluton (JBP) is situated at the southern end of the

batholith. It belongs to the magnetite-series of the Cordilleran batholith (Bateman, 1992). According to U-Pb dating (Sylvester et al., 1978; Gillespie, 1979; Stern et al., 1981) the JBP intruded during the first igneous stage around 170 Ma. Phengite barometry (Ernst, 1996) and Al-in hornblende barometry (Stein, 2000; Dietl, in prep.) show the plutons to intrude into a depth of 8 - 10 km. Ernst (1996) investigated mineral assemblages and mineral compositions in the thermal aureole of the Inyo batholith, and estimated contact metamorphic conditions to be in the hornblende-hornfels up to lower amphibolite facies (peak metamorphism: T = 500-600 °C; P = 0.3 GPa).

3. Methods of investigation

3.1 Mineralogical methods

The chemical compositions of Fe-Ti oxides and Fe-Mg silicates were determined with an electron microprobe (CAMECA SX51) at the Mineralogical Institute of the University of Heidelberg. Standards used were albite (Na), periclase (Mg), Al_2O_3 (Al), wollastonite (Si, Ca), orthoclase (K), TiO_2 (Ti), Cr_2O_3 (Cr), rhodonite (Mn), and hematite (Fe). The raw data were corrected with the PAP algorithm of Pouchou and Pichoir (1984). An acceleration voltage of 15 kV and a sample current of 20 nA were used. Whole rock analyses of major elements were performed with an X-ray fluorescence spectrometer (Siemens SRS 303).

3.2. Magnetic methods

The temperature-dependence of low-field (300 A/m) magnetic susceptibility was measured in the temperature range of –192° to 700°C using a KLY-2 Kappabridge combined with the CS-

2/CS-L furnace apparatus of AGICO (Hrouda 1994) at the Geological Institute of the University of Heidelberg. Thermomagnetic heating/cooling cycles from room temperature to 700°C were performed in argon (purity >99.998 vol.%, <0.003vol% oxygen) with a heating/cooling rate of 10°C/minute. Bulk susceptibilities were obtained by measuring the susceptibility at room temperature and normalising it to a sample volume of 10 cm^3. As the pore space in the metamorphic rocks investigated is negligible the density can be simply determined from Archimedes principle.

4. Whole rock geochemistry

The major element concentration in the metasediments were determined in order to reveal any correlation between the Fe content (calculated as FeO) of Fe-Mg silicates, and / or the magnetic susceptibility, respectively.

	Northern profile							Southern profile		
zone	bio		and-crd			trans	crd-kfs	and-crd	trans	crd-kfs
sample	SSA1	SSA2	SSA15	CSA9	CSA12	CSA15	LOK23	F5920	P18	B5660
SiO_2	66.07	79.48	65.52	67.14	68.55	70.66	54.65	51.70	61.96	65.28
TiO_2	1.42	0.48	0.87	0.85	1.32	0.91	1.05	2.13	0.87	0.71
Al_2O_3	13.68	10.76	16.47	15.57	12.32	13.30	26.57	21.72	18.06	19.35
FeO_{tot}	7.61	1.26	6.19	5.65	8.06	4.41	8.63	9.60	5.84	7.37
MnO	0.06	0.00	0.05	0.06	0.05	0.08	0.19	0.05	0.05	0.14
MgO	1.96	0.29	2.29	2.56	1.79	1.36	2.38	2.76	1.87	2.18
CaO	0.61	0.62	0.58	0.82	0.62	1.10	0.33	0.63	0.47	0.36
Na_2O	4.77	2.13	0.95	1.18	1.93	1.75	0.57	2.04	0.96	0.55
K_2O	2.55	4.31	5.23	3.19	3.63	3.95	3.46	5.47	5.64	2.53
P_2O_5	0.16	0.16	0.08	0.13	0.12	0.02	0.08	0.31	0.06	0.19
LOI	0.64	0.57	1.79	2.35	0.98	1.03	1.04	3.01	2.62	1.15
Total	100.37	100.19	100.70	100.13	100.26	99.06	99.92	100.50	99.05	100.63
X_{FeO}	0.80	0.81	0.73	0.69	0.82	0.77	0.79	0.78	0.76	0.78
κ	483	79	394	360	511	283	557	608	371	474

Table 1. *Major element bulk rock composition of metasediments in wt% from the contact aureole of the JBP pluton (from left to right towards the pluton; X_{FeO} = FeO/(FeO+MgO)). κ is the calculated paramagnetic volume susceptibility from FeO content according to the formula κ = (2.096 x concentration (FeO) + 2.542 x concentration (MnO)) x density from Zapletal (1985; ρ = 3000 kg/m^3).*

The whole rock composition of the metasediments investigated in this study is listed in Table 1. FeO_{tot} contents range between 1.3 and 9.6 wt%. All samples display chemical compositions typical of a clastic sedimentary rock suite, with shales (e.g. LOK23 and F5920), greywackes (CSA9, CSA12), and sandstones (SSA2.1). All samples show $K_2O > Na_2O$, which is typical for metasediments, except for sample SSA1 with $Na_2O > K_2O$, denoting an igneous contribution (Mason and Moore 1985). Therefore, volcanic detritus is sometimes intercalated with the sedimentary rocks.

5. Fe-Mg silicate assemblages

The *biotite zone* (distance to JBP: > 2000 m) is characterised by the presence of quartz, K-feldspar, albite and the beginning growth of green biotite (Fig. 2a) or colourless to greenish white

mica, depending on the bulk rock chemistry of the sediments. The size of these phyllosilicates ranges from 10 to 100 µm. In the biotite zone an annealed, statically recrystallized fabric is typical.

The *andalusite-cordierite zone* (distance to JBP: 2000-500 m) is macroscopically characterised by black spots that mostly consist of white mica (either as coarse individual crystals or as fine-grained sericitic aggregates) pseudomorphosing the contact metamorphic cordierite. Fresh cordierite together with fresh andalusite was only observed in sample P9, which comes directly from the border between the *andalusite-cordierite* and the *transition zone*. Andalusite, which is partly replaced by chlorite, was observed only in sample F5920 (Fig. 2b) and white mica growing pseudomorphically after andalusite occurs in sample CSA9. Brown biotite up to 200 µm in size is aligned in a pronounced foliation, which sometimes is crenulated (Fig. 2b). The prograde silicate assemblage further consists of quartz and albitic plagioclase. A possible mineral reaction leading

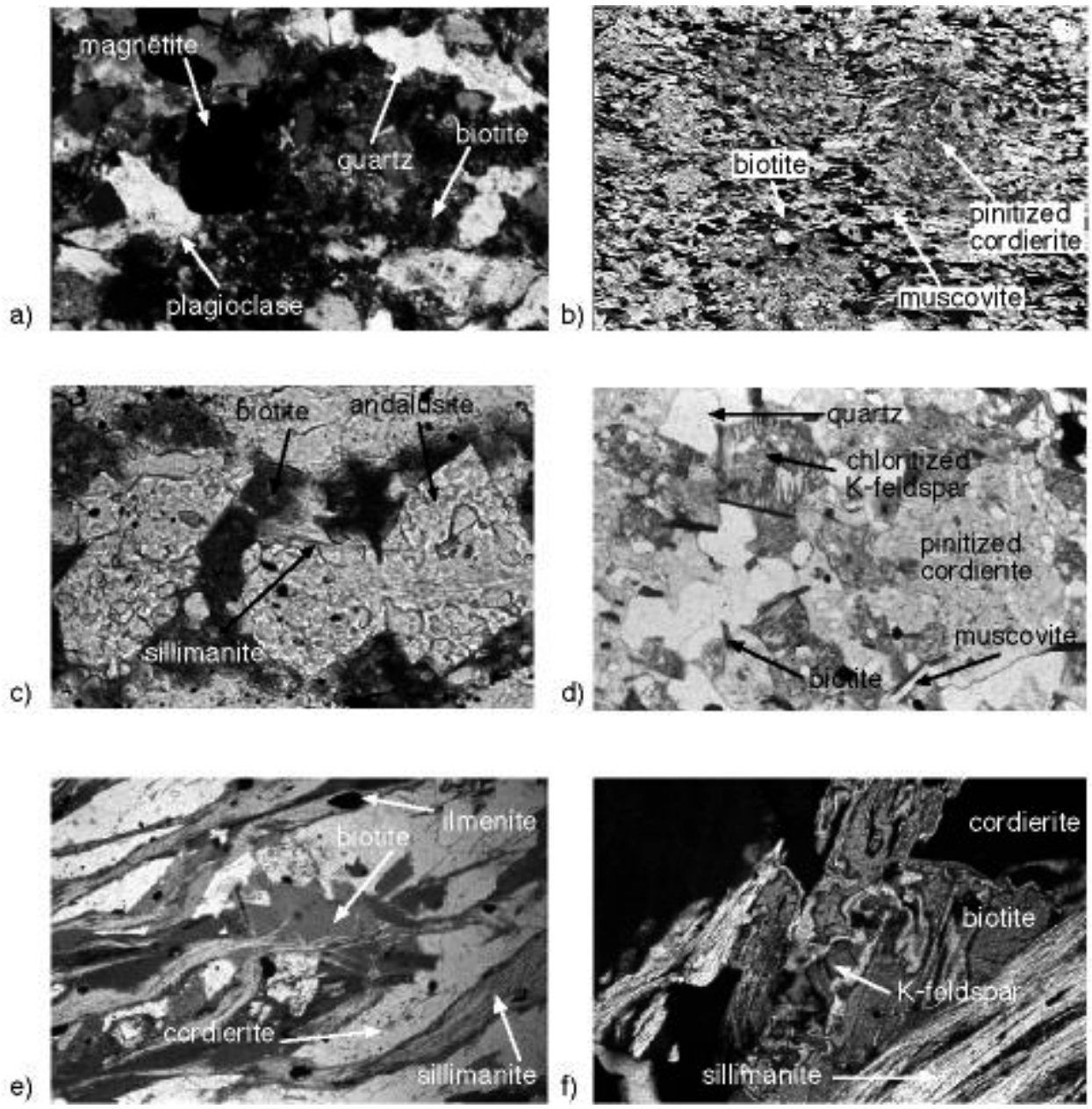

Fig. 2. *Photomicrographs (transmitted light) of typical assemblages and textures of the different metamorphic zones: a) Typical equilibrated fabric in the biotite zone between plagioclase, quartz, biotite and magnetite (sample SSA1, XPL, long side 1.4 mm). b) Crenulation cleavage in the andalusite-cordierite zone by biotite and white mica around strongly pinitized cordierite porphyroblasts (sample F5920, PPL, long side 1.4 mm). c) In the transition zone fibrolitic sillimanite overgrows andalusite and biotite (sample P9, PPL, long side 1.4 mm). d) Retrograde overprint of cordierite and K-feldspar in the transition zone by white mica and chlorite, probably due to hydrothermal alteration (sample P18, PPL, long side 1.4 mm). e) Microfabric from a shear zone in the cordierite-K-feldspar zone. A wavy cleavage is built of biotite and fibrolite. Cordierite forms elongated shear bodies (sample LOK23, PPL, long side 2.2 mm). f) Reaction fabric between biotite + sillimanite on the educt side and cordierite + K-feldspar on the product side (sample LOK23, XPL, long side 0.6 mm).*

to the growth of cordierite, andalusite and biotite is white mica + chlorite + ilmenite = biotite + andalusite + cordierite + H_2O (Symmes and Ferry, 1995). White mica, chlorite and K-feldspar app as part of a retrograde probably hydrothermally overprinted assemblage. White mica occurs as clusters of fine-grained, sericitic aggregates, restricted to the black spots. Chlorite is mostly found intergrown with biotite and sometimes andalusite and is therefore regarded as a retrograde reaction product of these prograde minerals.

In the *transition zone* (distance to JBP: 500-300 m), sillimanite and/or K-feldspar occur, depending on the whole rock chemistry of the protoliths. In sample P9 fibrolitic sillimanite is overgrowing andalusite and biotite (Fig. 2b). Some samples (CSA17 and P18) are rich in K-feldspar, mostly perthite, indicating temperatures of probably >600°C (Symmes and Ferry, 1995). Quartz, plagioclase, biotite, andalusite and cordierite accompany sillimanite and K-feldspar. All investigated samples are coarse-grained and show a well-developed foliation made up of biotite. In sample CSA17 a second crenulation cleavage also formed by biotite and a statically recrystallized fabric was observed. As already displayed in the andalusite-cordierite zone, retrograde hydrothermal reactions also play an important role in the transition zone. In sample P18 all cordierites are pinitized (Fig. 2d). They can be identified as former cordierites only from their idiomorphic to hypidiomorphic shape and the numerous quartz and ilmenite inclusions, which can also be observed in fresh cordierites from sample P9. Moreover, most of the K-feldspars are overgrown by chlorite (Fig. 2d). Rutile needles are common in biotite.

The innermost and highest grade zone of the aureole is built up by the *cordierite-K-feldspar zone* (distance to JBP: <300 m). Metapelites from this zone are rich in cordierite, K-feldspar, plagioclase, fibrolitic sillimanite, relictic andalusite, biotite and quartz. Fibrolite formed along c-planes of sheared rocks and is intergrown with biotite that forms a wavy cleavage (Fig. 2e). Biotite shows "myrmekitic" structures with quartz and K-feldspar at its rims (Fig. 2f). This points to a reaction, in which biotite is consumed and K-feldspar produced. Numerous leucosomes (K-feldspar, plagioclase, quartz and cordierite), partly lying lit-par-lit parallel with the cleavage planes and partly irregularly distributed through the rock, are typical for this zone and are regarded as products of the melting reaction sillimanite + biotite + quartz = cordierite + K-feldspar + melt + H_2O. The increased grain size of the leucosomes relative to the melanosomes (biotite, sillimanite, andalusite and cordierite) together with inclusion relations (e. g. plagioclase inclusions in quartz) and the eutectic composition of the leucosomes suggest a melt origin. Again, retrograde reactions can be observed. Biotite and andalusite are overgrown by chlorite, while white mica and chlorite substitute cordierite and K-feldspar.

6. Mineral chemistry and quantitative / semi-quantitative approaches for temperature and pressure estimation

6.1 Ti-in-biotite-thermometry

Biotite of all zones is of eastonitic to phlogopitic composition. The ratio $Fe_{tot}/(Fe_{tot}+Mg)$ (X_{Fe}) of biotite from the biotite and andalusite-cordierite zones is between 0.52 - 0.59 and Ti is 0.12-0.14 atoms per formula unit (p.f.u.; Table 2). In the transition and the cordierite-K-feldspar zone, increased Fe- (X_{Fe} = 0.7) and Ti-contents (up to 0.16 p.f.u.) indicate higher grade contact

metamorphic conditions (Patiño Douce 1994). However, the Ti increase is not very significant and lower Ti contents of biotites from the cordierite-K-feldspar (0.13 p.f.u.) than those from the transition zone (0.16 p.f.u.) were found.

	Northern profile							Southern profile			
zone	bio	and-crd			trans		crd-kfs	and-crd	trans		crd-kfs
sample	SSA1	SSA15	CSA9	CSA12	CSA17	CSA15	LOK23	F5920	P9	P18	B5660
n	4	17	12	12	10	12	31	7	19	21	20
SiO_2	35.39	34.36	34.10	34.29	35.31	35.77	33.71	34.05	33.22	33.80	33.71
TiO_2	2.34	1.64	2.00	2.52	2.67	2.38	2.18	2.07	2.29	2.78	1.71
Al_2O_3	16.77	17.61	17.89	16.67	16.64	15.92	20.21	17.16	19.01	19.39	20.40
Cr_2O_3	0.03	0.06	0.06	0.03	0.03	0.07	0.03	0.02	0.10	0.11	0.05
FeO	20.78	21.45	20.76	22.23	19.54	20.08	23.90	21.99	24.05	22.44	23.16
MgO	9.27	8.85	9.23	8.51	10.16	9.93	5.41	8.81	6.24	6.09	5.83
MnO	0.16	0.16	0.18	0.14	0.25	0.27	0.17	0.05	0.13	0.10	0.14
CaO	0.01	0.04	0.01	0.01	0.01	0.29	0.04	0.03	0.04	0.02	0.04
Na_2O	0.05	0.06	0.08	0.08	0.08	0.05	0.13	0.05	0.14	0.11	0.28
K_2O	9.53	9.17	9.38	9.53	9.59	9.54	8.60	9.59	8.66	8.68	8.72
Total	94.33	93.40	93.69	93.99	94.27	94.31	94.37	93.81	93.87	93.50	94.03
	on the basis of 11 O, all Fe as Fe^{2+}										
Si	2.75	2.71	2.67	2.71	2.74	2.78	2.64	2.69	2.63	2.66	2.64
Al(IV)	1.25	1.29	1.33	1.29	1.26	1.22	1.36	1.31	1.37	1.34	1.36
Al(VI)	0.29	0.34	0.33	0.26	0.26	0.24	0.51	0.28	0.41	0.46	0.53
Ti	0.14	0.10	0.12	0.15	0.16	0.14	0.13	0.12	0.14	0.16	0.10
Cr	0.00	0.00	0.00	0.00	0.00	0.00	0.00	0.00	0.01	0.01	0.00
Fe^{2+}	1.35	1.41	1.36	1.47	1.27	1.30	1.57	1.45	1.59	1.48	1.52
Mg	1.08	1.04	1.08	1.00	1.17	1.15	0.63	1.04	0.74	0.72	0.68
Mn	0.01	0.01	0.01	0.01	0.02	0.02	0.01	0.00	0.01	0.01	0.01
Ca	0.00	0.00	0.00	0.00	0.00	0.02	0.00	0.00	0.00	0.00	0.00
Na	0.01	0.01	0.01	0.01	0.01	0.01	0.02	0.01	0.02	0.02	0.04
K	0.95	0.92	0.94	0.96	0.95	0.95	0.86	0.97	0.88	0.87	0.87
Fe/Mg	1.26	1.36	1.26	1.47	1.08	1.13	2.48	1.40	2.16	2.07	2.23
X_{Fe}	0.56	0.58	0.56	0.59	0.52	0.53	0.71	0.58	0.68	0.67	0.69
T(°C)		607	640	744	746	747	573	679	625	621	538

Table 2. *Average chemical composition of biotite in wt% oxide, calculated structural formula, and temperatures calculated using the Ti-in-biotite geothermometer (Patiño Douce, 1994; n is number of single analyses).*

According to Patiño Douce (1994) the Ti contents of biotite in metapelites with the mineral assemblage biotite + alumosilicate + ilmenite + quartz is mainly temperature-controlled due to

the substitution reactions at octahedral sites $Al^{3+} + Fe^{3+} \Rightarrow Ti^{4+} + Fe^{2+}$ and Ti^{4+} + vacancy $\Rightarrow$ $2Fe^{2+}$. Based on these two reactions a thermodynamic thermometer was developed (Patiño Douce, 1994), which was applied to all samples in which biotite, andalusite/sillimanite and ilmenite were considered to be in equilibrium.

Ti-in-biotite-temperatures were determined using average biotite and ilmenite compositions over the sample and a pressure of 0.2 GPa corresponding to the intrusion depth of the JBP (Dietl, in prep.).

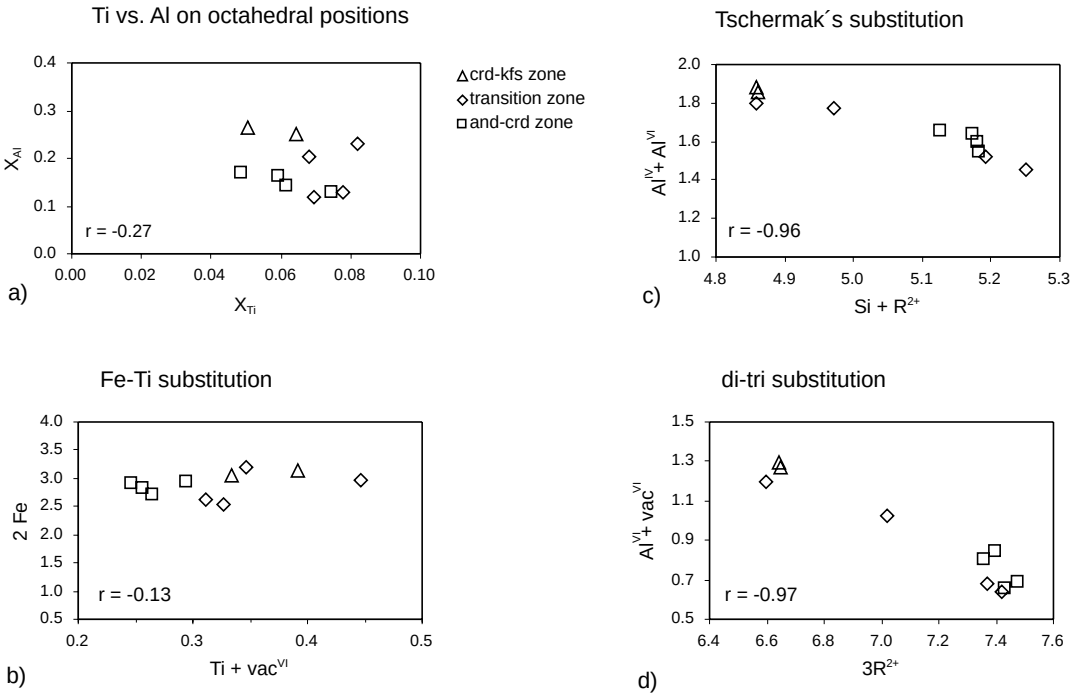

Fig. 3. *Correlation diagrams for different substitution reactions in biotite from the andalusite-cordierite, transition and cordierite-K-feldspar zone. Correlation coefficients (r) close to -1 for the Tschermak´s and di-tri substitution in biotite indicate their significance relative to the Ti vs. Al and Ti vs. Fe substitution showing low correlation coefficients (mean values of atoms per formula unit, see Table 2; $X_{Al} = Al^{VI}/2$ and $X_{Ti} = Ti/2$). For interpretation see text.*

Temperatures for the individual contact metamorphic zones are shown in Table 2. They seem to be unrealistic, because samples from the cordierite-K-feldspar zone yield much lower

temperatures than samples from metamorphic zones further away from the pluton. Moreover, temperatures of only 550 °C in the cordierite-K-feldspar zone appear much too low for the observed assemblage cordierite + K-feldspar + plagioclase + quartz + ilmenite, which should become unstable below 730 °C at 0.2 GPa (Le Breton and Thompson, 1988). The same holds for the samples from the transition and the andalusite-cordierite zones, where calculated temperatures are between 607 °C (sample SSA15) and 746 °C (sample CSA17). This is much too high for the observed mineral assemblage andalusite + cordierite (stable at T > 550°C at 0.2 GPa; Symmes and Ferry, 1995), and sillimanite should grow at the expense of andalusite at T ≥ 675 °C at 0.2 GPa (Holdaway, 1971).

There can be a number of reasons for the unreliable nature of the Ti-in-biotite-temperature data. One possible explanation is the assumption of ideality for activity-composition relationships in biotite made by Patiño Douce (1994). Our observations indicate that other explanations also have to be considered. The Ti-in-biotite-thermometer is based on the substitution reaction Al^{3+} + Fe^{3+} = Ti^{4+} + Fe^{2+} (Ti-Al-substitution on octahedral sites), and X_{Al} vs. X_{Ti} as well as Fe vs. Ti should show a good correlation. However the Ti-Al and Fe-Ti substitutions for all our samples show no well-developed correlation (correlation coefficient r = –0.27 and r = – 0.13; Fig. 3a, b).

Samples closest to the JBP have increased Al contents (around 0.5 p.f.u.) relative to those further away from the pluton (between 0.2 and 0.4 p.f.u.), while Ti contents for all samples range between 0.1 and 0.16 p.f.u.. Neither Ti, nor Fe^{2+} in biotite are related to the distance from the pluton. Looking at the Tschermak's substitution Si + R^{2+} = Al^{IV} + Al^{VI} and the di-tri substitution 3 (Fe + Mg) = $2Al^{VI}$ + vacancy (Fig. 3c, d), a good correlation (-0.96 and –0.95) is found for all data. All samples from the immediate contact area (high-grade cordierite-K-feldspar zone) show

increased Tschermak´s- and di-tri substitutions relative to those from the more distant (lower-grade) contact metamorphic zones. Assuming nearly isobaric conditions for the JBP and its contact aureole, temperature should control these substitution reactions. Therefore, all substitution reactions involving Al^{VI} in biotite seem to be influenced by temperature and not only by pressure as proposed by Patiño Douce et al. (1993). An increase in Al contents as it is

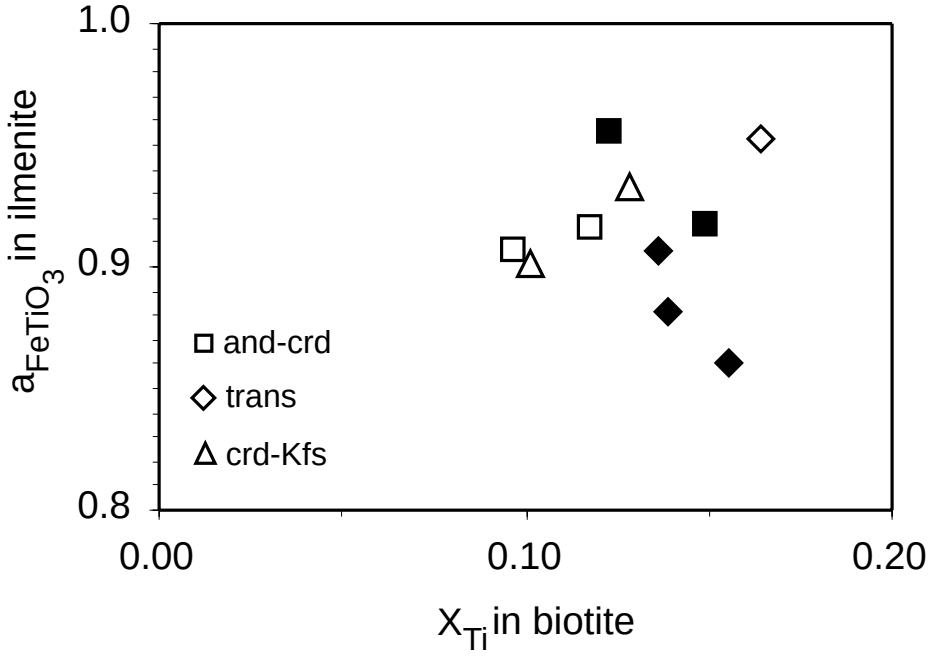

observed in our samples has a contrary effect on the calculated temperature values.

Fig. 4. *Correlation between a_{FeTiO3} in ilmenite and X_{Ti} in biotite (mean values) indicate no simple relation between the two parameters required by the model of Patiño Douce (1994). Only the magnetite-bearing samples (filled symbols) show the trend proposed by Patiño Douce (1994). Those only with ilmenite (open symbols) follow a positive trend contrary to the trend required for the Ti-in-biotite thermometer.*

The Patiño Douce model (1994) assumes a negative correlation between the $FeTiO_3$ component in ilmenite and the Ti content in biotite. However, of the investigated samples only those containing ilmenite *and* magnetite follow the postulated trend (r = -0.78, Fig. 4), whereas samples containing *only* ilmenite show a positive correlation (r= 0.98) between a_{FeTiO3} in ilmenite and X_{Ti} in biotite (Fig. 4). In our case, this relationship is only observed in the presence of

magnetite, which appears to influence the incorporation of Ti into the biotite lattice. Since oxide minerals are the only indicator for the Fe^{3+}/Fe^{2+} ratio in the samples, the presence of the Fe^{3+}-bearing magnetite indicates a relative high oxygen fugacity. Obviously, $f(O_2)$ rules the incorporation of Ti into the biotite lattice.

According to Patiño Douce (1994) the assemblage biotite + Fe-Ti-oxide can also be used to estimate the oxygen fugacity. Applying this model to our data, log $f(O_2)$ calculations resulted in unrealistically low values, below the wuestite-magnetite buffer. This is not in accordance with the observed oxide assemblages containing Fe^{3+}-bearing phases.

6.2 Na-in-cordierite-thermometry

Cordierite is of intermediate composition (Fe-Mg-cordierite) with X_{Fe} of 0.53 in the andalusite-cordierite zone, and higher X_{Fe} of 0.58 in the cordierite-K-feldspar zone. All investigated cordierites are fresh as indicated by low K contents below 0.01 p.f.u.. Zn is below the detection limit (0.02 wt%; Table 3).

The Na-in-cordierite-thermometer was developed by Mirwald (1986) on the basis of experiments in the systems Mg-Cordierite - NaOH and Mg-Cordierite - NaOH – Albite at conditions in the range 0.1-0.8 GPa and 650-850 °C. The experimental results showed an inverse correlation between temperature and the Na-contents in cordierite.

Mirwald (1986) developed only a graphical solution for the thermometer, but the negative correlation between temperature and Na-contents of cordierite can be also expressed by the following formula:

$$T\left[\pm 30°C\right] = -2744.8X_{Na} + 897.36$$

with X_{Na} = atoms per formula unit as calculated for the structural formula.

zone	trans	crd-kfs	
sample	P9	B5660	LOK23
n	38	293	281
SiO_2	46.77	47.11	47.77
TiO_2	0.02	0.01	0.02
Al_2O_3	32.09	31.79	31.78
Cr_2O_3	0.01	0.01	0.01
FeO	12.64	11.10	11.53
MgO	5.05	5.72	5.79
MnO	0.49	0.50	0.51
CaO	0.03	0.02	0.07
Na_2O	0.25	0.55	0.26
K_2O	0.07	0.05	0.02
Total	97.42	96.86	97.75
on the basis of 18 O, all Fe as Fe^{2+}			
Si	4.98	5.01	5.03
Al^{IV}	1.02	0.99	0.97
Al^{VI}	3.00	2.99	2.98
Ti	0.00	0.00	0.01
Cr	0.00	0.00	0.00
Fe^{2+}	1.12	0.99	1.02
Mg	0.80	0.91	0.91
Mn	0.04	0.04	0.05
Ca	0.00	0.00	0.01
Na	0.05	0.11	0.05
K	0.01	0.01	0.00
Fe/Mg	1.40	1.09	1.12
X_{Fe}	0.58	0.52	0.53
T(°C)	731	570	738
s	25	47	25

Table 3.Chemical composition of cordierite in wt%, calculated structural formula, and temperatures with standard deviation (s; sigma1), calculated with the Na-in-cordierite-thermometer (Mirwald, 1986) , n is number of single analyses.

According to Kalt et al. (1998), the Na-in-cordierite-thermometer is applicable to natural Mg-Fe-cordierites as long as they coexist with plagioclase (An_{10-40}), K-feldspar, biotite and quartz. In their studies, no other parameters than temperature were found to influence the Na-content of cordierite.

Na-contents (p.f.u.) and temperatures were determined for three metapelitic samples from two metamorphic zones of the aureole: Sample P9 stems from the boundary of the andalusite-cordierite to the sillimanite zone, 480 m away from the contact with the JBP. The other two samples, LOK23 and B5660, are from

the cordierite - K-feldspar zone 120 and 100 m away from the pluton, respectively. Sample B5660 was taken from the immediate vicinity of a 30 m thick, granitic dyke. The average Na-contents of cordierite and the derived temperatures are shown in Fig. 5 and Table 3.

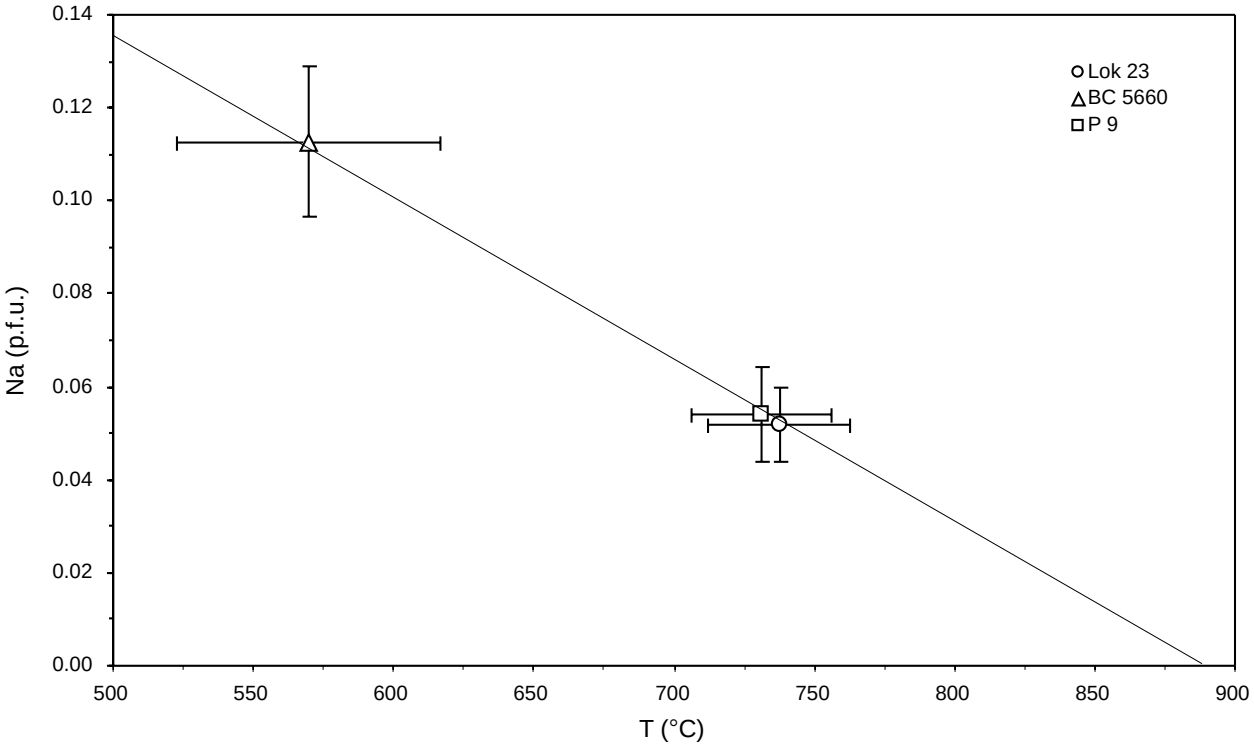

Fig. 5. *Formation temperatures of cordierite calculated using the Na-in-cordierite geothermometer of Mirwald (1986). Na in atoms per formula unit (see Table 3).*

The average temperature for sample LOK23 of 738°C correlates well with the observed migmatitic fabrics. The migmatisation is controlled by the mineral reaction sillimanite + biotite + plagioclase = cordierite + K-feldspar + melt. This reaction, according to Le Breton and Thompson (1988), takes place at 0.2 GPa and 730 °C. The average temperature for sample P9 of 731°C also matches with the presence of sillimanite, which appears at T ≥ 675°C at 0.2 GPa (Holdaway, 1971). Only sample B5660 yields temperatures that are too low for the cordierite - K-feldspar zone: only 570 °C , compared with 730°C for sample LOK23, which shows the same mineral assemblage and the same fabrics. One possible explanation for the increased Na-contents

in the cordierites of sample B5660 might be a beginning pinitisation of the cordierites. The crystals look fresh and unaltered under the microscope, but only chemical analyses would show, whether cordierite has already started to disintegrate or not. The main indicator for beginning pinitisation is an increased K-content that might be accompanied by an increased Na-content. Cordierite in all three samples shows K-contents below the detection limit; pinitisation can therefore be excluded. Obviously the high Na-content in B5660 represents real, lower temperatures. The most probable explanation for the lower temperatures of sample B5660 is its proximity to a c. 30 m thick late magmatic granite dyke. During the intrusion of this dyke the Na-content of cordierite could have been reequilibrated around an average value of 0.113 p.f.u. corresponding to a temperature of 570 °C. The reequilibration hypothesis is supported by the higher mean variation of the data compared with LOK23 and P9. The scattering can be explained with the fact that not all but only some of the cordierite crystals reequilibrated due to the heat flux from a hot, but rapidly cooling dyke in its immediate neighbourhood. Rapid heating and cooling did not allow the cordierites in B5660 to reequilibrate fully with the new temperature conditions, and lead to the observed scattering of the Na-contents. On the other hand, the low mean variation of Na in LOK23 and P9 requires a widespread and long-term heat flux through the entire contact aureole, which was produced by the intrusion of the JBP. Moreover, the preservation of the high temperature fabric in sample B5660 shows that the imprint of the thermal effect of the granite dyke was not complete.

6.3 Chlorite thermometry

Chlorite contains 2.54-2.87 Si p.f.u. and 2.51-2.93 Al p.f.u.. It shows X_{Fe} values between 0.46 and 0.62 (Table 4). Manganese contents are slightly higher in the northern profile (0.31- 0.37 wt%) than in the southern profile (0.15 wt%). According to the classification of Bailey (1986) the chlorites can be classified as Fe-clinochlore ($X_{Fe} < 0.5$, CSA9) and Mg-chamosites ($X_{Fe} > 0.5$, CSA13, F5920, and P18). The value of Al^{VI} is always higher than Al^{IV} indicating that in addition to the Tschermak´s exchange ($R^{2+}Si^{IV} = Al^{VI}Al^{IV}$) the exchange reaction $3(Mg, Fe^{2+}) = 2(Al^{3+}) +$ $vacancy^{VI}$ occurs at octahedral sites. It has to be mentioned that we calculated all formulae with Fe_{tot} as Fe^{2+} and therefore the substitution reactions do not consider the effect of Fe^{3+}.

All observed chlorites were found to overgrow the prograde index minerals and are related to the retrograde overprint of the contact metamorphic metasediments. Different empirical chlorite geothermometers and a geothermometer based on a thermodynamic model were applied to constrain the conditions of this retrograde overprint. The empirical geothermometers are based on calibrations between tetrahedral occupancy in chlorite and measured temperatures in geothermal systems (Cathelineau, 1988) and modifications of this approach taking into account the variation in Fe/(Fe+Mg) in chlorite (Kranidiotis and McLean, 1987; Jowett, 1991). The six-component chlorite solid solution model of Walshe (1986) uses five exchange reactions (see De Caritat et al., 1993; Table 1) and can be applied for chlorite that formed in equilibrium with quartz and an aqueous solution. This model uses thermodynamic properties extracted from data from geothermal and hydrothermal systems and works best at temperatures between 300-350°C. The fluid composition is lying between the quartz-pyrophyllite and the K-feldspar-white mica buffer, but does not include the latter one (De Caritat et al., 1993).

	Northern profile		Southern profile	
zone	and-crd	crd-kfs	and-crd	trans
sample	CSA9	CSA13	F5920	P18
n	12	13	6	18
SiO_2	24.83	23.20	25.62	25.45
TiO_2	0.15	0.47	0.14	0.04
Al_2O_3	21.49	22.73	19.76	19.53
Cr_2O_3	0.02	0.04	0.01	0.02
FeO	24.86	30.02	25.93	30.39
MgO	14.71	10.15	14.52	10.62
MnO	0.32	0.37	0.16	0.15
CaO	0.02	0.01	0.04	0.04
Na_2O	0.01	0.08	0.02	0.01
K_2O	0.07	0.02	0.25	0.13
Total	86.48	87.02	86.44	86.38
	on the basis of 14 O, all Fe as Fe^{2+}			
Si	2.66	2.54	2.76	2.81
Al^{IV}	1.35	1.46	1.24	1.20
Al^{VI}	1.36	1.47	1.26	1.34
Ti	0.01	0.04	0.01	0.00
Cr	0.00	0.00	0.00	0.00
Fe^{2+}	2.22	2.75	2.33	2.80
Mg	2.34	1.66	2.33	1.75
Mn	0.03	0.04	0.01	0.01
Ca	0.00	0.00	0.00	0.00
Na	0.00	0.00	0.00	0.00
K	0.01	0.00	0.03	0.02
Vac^{VI}	0.02	0.04	0.00	0.07
Fe/Mg	0.94	1.63	1.00	1.60
X_{Fe}	0.48	0.62	0.50	0.61
$T\ (°C)_{C8}$	371	409	338	323
s	7	11	14	22
$T\ (°C)_{KL87}$	375	420	356	363
s	5	8	9	15
$T\ (°C)_{J91}$	376	(417)*	343	(332)*
s	7	11	14	22
$T\ (°C)_{W86}$	321	347	277	234
s	11	17	21	22
log $f(O_2)$	-29.3	-27.9	-34.6	-41.6
s	1.2	1.8	2.6	3.1
Δlog MH	0.21	-0.34	-1.63	-4.73

*modification of Jowett can only be used for chlorite with $X_{Fe} < 0.6$

Table 4. *Chemical composition of chlorite in wt%, calculated structural formula and temperatures from different chlorite geothermometers as well as log $f(O_2)$ from the thermodynamic model using the CHLORITE computer program after Walshe (C88: Cathelineau 1988; KL87: Kranidiotis and MacLean 1987, J91: Jowett 1991, W86: Walshe 1986; s: standard deviation, sigma1; Δlog MH: difference between calculated log $f(O_2)$ and log $f(O_2)$ of the hematite-magnetite buffer at calculated temperature, n: number of single analyses.).*

Table 4 lists the mean values of the temperatures obtained for chlorites from the White Inyo metasediments and Fig. 6 shows all single analyses in a temperature versus Al^{IV} diagram. The thermodynamic model (Walshe 1986) was applied using the computer program CHLORITE

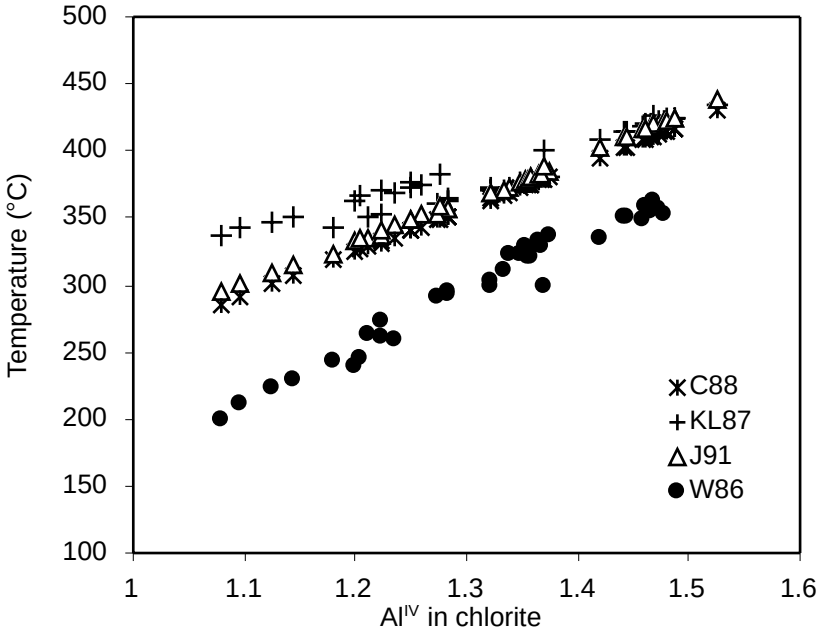

***Fig. 6**. Al^{IV} in chlorite vs. temperature, calculated with different chlorite geothermometers for single analyses in different samples (C88: Cathelineau (1988), KL: Kranidiotis and MacLean (1987), J91: Jowett (1991), W86: Walshe*

(modified PC version after Walshe 1986). Calculations were performed at 0.1 GPa, because the program calculates temperatures only at 1 atmosphere, 0.05 and 0.1 GPa. The empirical Al^{IV} geothermometers yield similar temperatures ranging between 320° and 420°C (Table 4 and Fig. 6). The temperatures calculated with the thermodynamic model reveal distinctly lower values between 230° and 350°C (Table 4 and Fig. 6). In the samples CSA9, CSA13 and F5920 $Al^{IV} \approx Al^{VI}$, and the differences between the empirical and thermodynamic approaches are in an acceptable range between 55° and 70°C. In sample P18 a maximum temperature difference of 130°C between the results of the empirical and thermodynamic approaches was observed. According to our data, the Tschermak's substitution, as well as the octahedral di-tri substitution in chlorite (Fig. 7) is temperature-sensitive. This is confirmed by all geothermometers as long as

$Al^{IV} \approx Al^{VI}$, i. e. the Tschermak´s substitution dominates. High variations in temperature estimation between the different approaches arise if $Al^{VI} > Al^{IV}$. The highest temperature deviation was obtained for sample P18 with higher Si (and Al^{VI}) contents, increased vacancies and

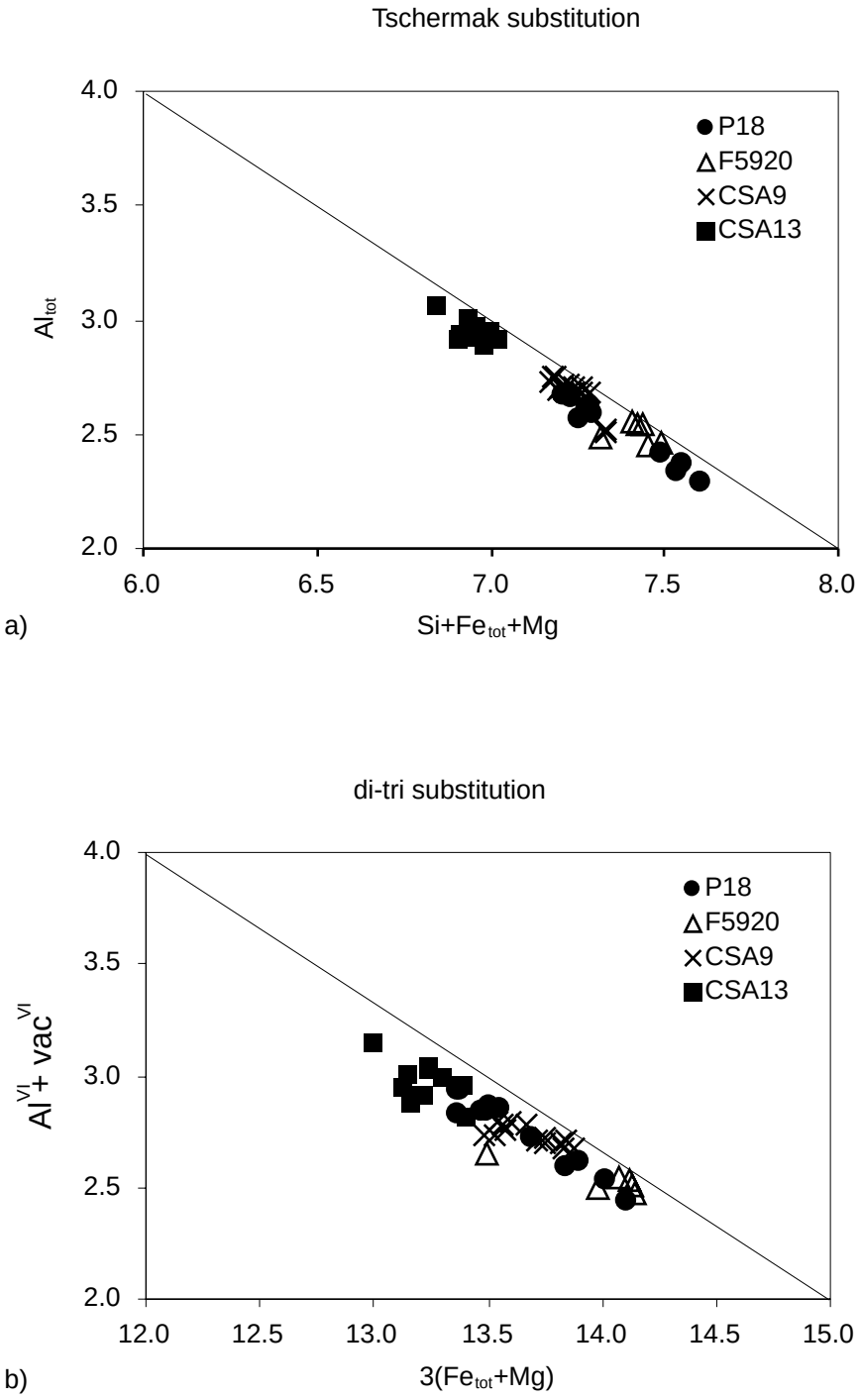

Fig. 7. *Plots of Al_{tot} vs. Si + R^{2+} (Tschermak's substitution) and Al^{VI} + vacancies^{VI} versus 3 (Fe_{tot} + Mg) (di-tri substitution). Both plots show a good correlation close to the 1:1 substitution line indicating the significance of both substitutions (single analyses of atoms per formula unit, see Table 4).*

high X_{Fe} values. This result indicates that if only Al^{IV} and X_{Fe} are considered, temperatures are overestimated especially with the modified empirical geothermometers. On the other hand, the thermodynamic model seems to underestimate temperatures of formation or reequilibration for chlorites with $Al^{VI} > Al^{IV}$.

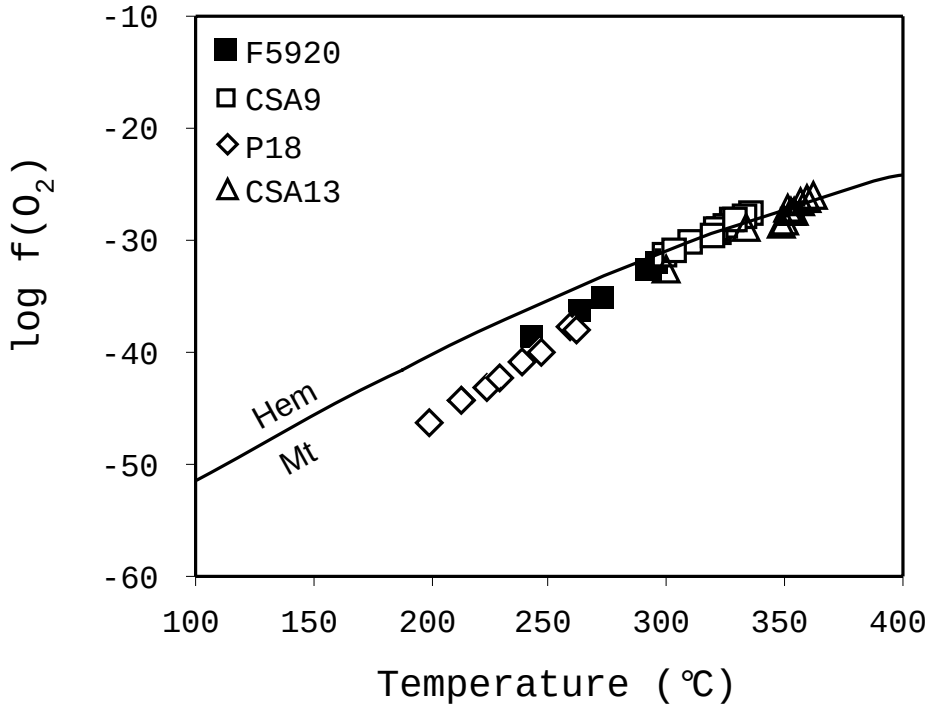

Fig. 8. *Log f(O_2) vs. temperature diagram show redox conditions close to the hematite-magnetite buffer during chlorite formation or reequilibration (parameters were calculated from single analyses with the program CHLORITE;).*

The oxygen fugacity was calculated with the thermodynamic model of Walshe (1986) and is illustrated in Fig. 8. From the oxide assemblages redox conditions for chlorite formation are close to the hematite-magnetite boundary. This is consistent with results obtained for sample CSA13 and CSA9 with mean log $f(O_2)$ values of –28 and –29 which are very close to the hematite-magnetite boundary. These samples show the assemblage ilmenite, hematite and/or goethite. Sample F5920 shows an average log $f(O_2)$ value of –35 that indicates more reducing conditions. This is consistent with the oxide assemblage including magnetite and ilmenite. The calculated

$f(O_2)$ values for sample P18 are assumed to be much too low, because hematite is observed in the polished sections and detected by magnetic methods (see below). Again, we assume the redox conditions in this sample, like the temperature estimations, to be underestimated with the thermodynamic model. Caritat et al. (1993) also mention this problem and point out that, in practice, the thermodynamic model is only valid over a narrow range of $a\mathrm{Al}^{3+}/(a\mathrm{H}^{+})$.

Plots of Al_{tot} versus $\mathrm{Si} + \mathrm{R}^{2+}$ (Tschermak's substitution) and Al^{VI} + vacancies versus 3 (Fe + Mg; di-tri substitution) seem to be a useful method to decide whether chlorite reached equilibrium in the sample or not. Samples CSA9, CSA13 and F5920 show clusters in Fig. 7a and b, indicating that equilibrium may be reached, but sample P18 scatters over a wide range. Therefore temperature and log $f(O_2)$ conditions of this sample will not be further considered.

6.4 Phengite barometry

Analysed white micas represent muscovite – celadonite solid solutions (phengite) with Si contents ranging between 3.05 and 3.2, based on 11 oxygens (Table 5). The highest Si value is observed in sample SSA2, which was taken from about 3 km away of the plutonic contact (Table 5). X_{Fe} varies from 0.56 to 0.78 and Ti is below 0.07 p.f.u..

White micas coexist in some samples with quartz, K-feldspar and biotite (X_{Fe} = 0.53-0.71), which is the limiting assemblage for the phengite geobarometer of Massonne & Schreyer (1987). This assemblage occurs in the andalusite-cordierite zone (sample SSA15, CSA12) and in retrograde samples from the transition zone (CSA15 and P18). In nearly all samples of these zones, biotite-phengite pairs show K_D-values for Fe and Mg in a narrow range between 0.47 and 0.64 (Table 6) indicating an attainment of equilibrium. Only in sample P18, in which alteration effects are much stronger than in sample CSA17 and CSA15, the K_D-values for Fe and Mg

	Northern profile							Southern profile		
zone	bio	and-crd			trans		crd-kfs	trans		crd-kfs
sample	SSA2	SSA15	CSA9	CSA12	CSA17	CSA15	LOK23	P9	P18	B5660
n	20	16	14	13	12	10	9	2	13	5
SiO_2	47.08	46.38	45.22	45.83	47.10	46.97	45.16	48.41	47.15	44.97
TiO_2	0.67	0.88	0.47	0.41	1.38	0.73	0.13	0.28	0.09	0.12
Al_2O_3	30.53	34.03	31.99	31.09	30.81	32.22	33.58	35.78	32.80	34.95
Cr_2O_3	0.03	0.03	0.03	0.02	0.02	0.05	0.01	0.01	0.01	0.02
FeO	4.55	2.95	5.11	5.28	4.44	4.37	3.90	2.64	3.30	2.59
MgO	1.53	0.68	2.10	1.35	1.36	1.04	0.91	0.41	1.47	0.45
MnO	0.01	0.02	0.04	0.02	0.02	0.03	0.03	0.02	0.02	0.02
CaO	0.03	0.00	0.01	0.13	0.01	0.01	0.02	0.00	0.01	0.02
Na_2O	0.17	0.41	0.36	0.21	0.19	0.29	0.46	0.51	0.19	0.94
K_2O	9.98	10.10	9.62	10.16	9.79	10.12	10.25	7.11	10.11	9.79
Total	94.57	95.48	94.94	94.48	95.12	95.84	94.44	95.16	95.14	93.87
	on the basis of 11 O, all Fe as Fe^{2+}									
Si	3.20	3.10	3.08	3.14	3.18	3.15	3.08	3.16	3.16	3.05
Al(IV)	0.80	0.90	0.92	0.86	0.82	0.85	0.92	0.84	0.84	0.95
Al(VI)	1.64	1.78	1.64	1.65	1.63	1.70	1.77	1.92	1.75	1.85
Ti	0.03	0.04	0.02	0.02	0.07	0.04	0.01	0.01	0.00	0.01
Cr	0.00	0.00	0.00	0.00	0.00	0.00	0.00	0.00	0.00	0.00
Fe^{2+}	0.26	0.16	0.29	0.30	0.25	0.25	0.22	0.14	0.19	0.15
Mg	0.16	0.07	0.22	0.14	0.14	0.10	0.09	0.04	0.15	0.05
Mn	0.00	0.00	0.00	0.00	0.00	0.00	0.00	0.00	0.00	0.00
Ca	0.00	0.00	0.00	0.01	0.00	0.00	0.00	0.00	0.00	0.00
Na	0.02	0.05	0.05	0.03	0.03	0.04	0.06	0.07	0.02	0.12
K	0.87	0.86	0.84	0.89	0.84	0.87	0.89	0.59	0.86	0.85
Fe/Mg	1.67	2.44	1.36	2.20	1.84	2.35	2.41	3.63	1.26	3.26
X_{Fe}	0.64	0.71	0.60	0.69	0.65	0.71	0.71	0.78	0.56	0.77

***Table 5**. Average chemical composition of white mica in wt% oxide and calculated structural formula; n is number of single analyses.*

	Northern profile					Southern profile		
zone	and- crd		trans		crd-kfs	trans		crd-kfs
sample	CSA9	CSA12	CSA17	CSA15	LOK23	P9	P18	B5660
K_D crd-bio					0.520	0.531		0.496
K_D bio-mus	0.916	0.598	0.544	0.466	0.806	0.540	1.791	0.643
K_D bio-chl	1.340						1.375	

***Table 6.** Distribution coefficients ($K_D = (Mg/Fe)_{min1} / (Mg/Fe)_{min2}$, all Fe calculated as Fe^{2+}) between cordierite-biotite, biotite-white mica and biotite-chlorite pairs, respectively. K_D from bio-mus and bio-chl pairs of samples CSA9 and P18 are related to retrograde metamorphism, whereas all other pairs represent prograde assemblages. Numbers of K_D pairs are given in parentheses.*

between biotite and white mica are much higher (1.54-1.84). According to Ernst (1996) iron seems to be enriched in white mica relative to biotite at higher temperatures, but in biotite relative to phengite at lower temperatures. This is in agreement with our observations, which indicate higher (retrograde) temperatures for samples SSA15, CSA12, CSA17, and CSA15, and lower temperatures in sample P18 where chlorite occurs as a retrograde alteration product together with phengite, biotite, K-feldspar and quartz. Even if chlorite geothermometry gives a wide range of temperatures, an average temperature of about 300°-350°C can be assumed for the retrograde conditions of this sample. Taking this temperature into account, a pressure of 0.2 GPa can be estimated from an average Si content of 3.16 p.f.u. in coexisting phengites.

Pressures estimated for phengites from the andalusite-cordierite zone range between 0.2 and 0.3 GPa (average Si-content 3.15). They were obtained below 400°C and therefore indicate that the assemblage phengite + biotite + K-feldspar + quartz also belongs to the retrograde branch of the contact metamorphic PT path. Pressure estimations for metasediments of the White Inyo Range from Ernst (1996) using the phengite geobarometer of Massonne and Schreyer (1987) are also reported with 0.2 ± 0.1 GPa.

7. Oxide assemblages and their chemical composition

The most distant (3 km away from the pluton) and less metamorphosed sample SSA1 from the *biotite zone* shows the oxide assemblage ilmenite (8.8 wt% MnO, Table 7), pseudobrookite$_{ss}$, hematite and magnetite (Fig. 9a). The oxide aggregates are about 150 µm or less in size. Magnetite occurs as tiny grains of about 10-20 µm and as submicron aggregates together with titanite. Ilmenite-inclusions in pseudobrookite (Fig. 9a) suggest pseudobrookite formation to be related to high temperature deuteric oxidation of primary ilmenite (Haggerty 1991).

	Northern profile											Southern profile				
zone	bio	and-crd				trans					crd-kfs	and-crd		trans		
sample	SSA1	SSA 1	SSA 15	CSA9	CSA 12	CSA 17	CSA 17	CSA 15	CSA 15	CSA 15	Lok23	F5960	F5920	P 9	P 9	P 18
mineral	il	hm	il	il	il	il	hm	il	hmil	hm	il	il	ilhm	il	hm	il
n	10	2	4	10	9	7	2	11	3	4	9	13	1	6	2	10
SiO_2	0.08	0.04	0.01	0.02	0.03	0.06	0.38	0.08	0.17	0.27	0.01	0.01	0.00	0.04	0.03	0.04
TiO_2	51.09	0.20	53.06	52.17	49.27	51.54	3.03	50.17	14.12	0.92	49.06	50.23	32.11	50.06	0.07	52.26
Al_2O_3	0.00	0.02	0.00	0.00	0.00	0.00	0.11	0.00	0.00	0.05	0.03	0.00	0.00	0.00	0.18	0.00
Cr_2O_3	0.02	0.01	0.01	0.02	0.01	0.02	0.25	0.03	0.22	0.40	0.08	0.01	0.02	0.17	1.60	0.02
Fe_2O_3	2.25	97.86	0.18	0.24	4.88	2.35	93.18	3.33	72.39	96.37	5.49	2.98	37.32	5.84	98.54	0.00
FeO	36.98	0.15	42.61	43.38	42.12	40.55	2.86	40.20	12.53	0.91	43.10	44.12	28.12	43.04	0.00	44.30
MnO	8.81	0.04	3.42	2.68	1.89	5.15	0.17	4.56	0.21	0.06	0.78	0.91	0.53	1.52	0.04	1.70
MgO	0.01	0.01	0.02	0.03	0.04	0.07	0.02	0.06	0.02	0.01	0.08	0.03	0.01	0.12	0.02	0.03
Total	99.29	98.33	99.38	98.59	98.30	99.83	100.05	98.43	99.71	99.06	98.65	98.33	98.15	100.88	100.48	98.39
Si	0.00	0.00	0.00	0.00	0.00	0.00	0.01	0.00	0.00	0.01	0.00	0.00	0.00	0.00	0.00	0.00
Ti	0.98	0.00	1.01	1.00	0.96	0.98	0.06	0.97	0.28	0.02	0.95	0.97	0.63	0.94	0.00	1.01
Al	0.00	0.00	0.00	0.00	0.00	0.00	0.00	0.00	0.00	0.00	0.00	0.00	0.00	0.00	0.01	0.00
Cr	0.00	0.00	0.00	0.00	0.00	0.00	0.01	0.00	0.00	0.01	0.00	0.00	0.00	0.00	0.03	0.00
Fe^{3+}	0.04	1.99	0.00	0.00	0.08	0.04	1.85	0.06	1.43	1.94	0.09	0.06	0.74	0.12	1.96	0.00
Fe^{2+}	0.79	0.00	0.90	0.93	0.91	0.86	0.06	0.86	0.28	0.02	0.93	0.95	0.62	0.90	0.00	0.95
Mn	0.19	0.00	0.07	0.06	0.04	0.11	0.00	0.10	0.00	0.00	0.02	0.02	0.01	0.03	0.00	0.04
Mg	0.00	0.00	0.00	0.00	0.00	0.00	0.00	0.00	0.00	0.00	0.00	0.00	0.00	0.00	0.00	0.00

Table 7. Chemical composition of ilmenite-hematite solid solution in wt% oxide (means of n single analyses). Fe_2O_3, FeO and formula are calculated assuming stochiometry (2 cations, 3 oxygen).

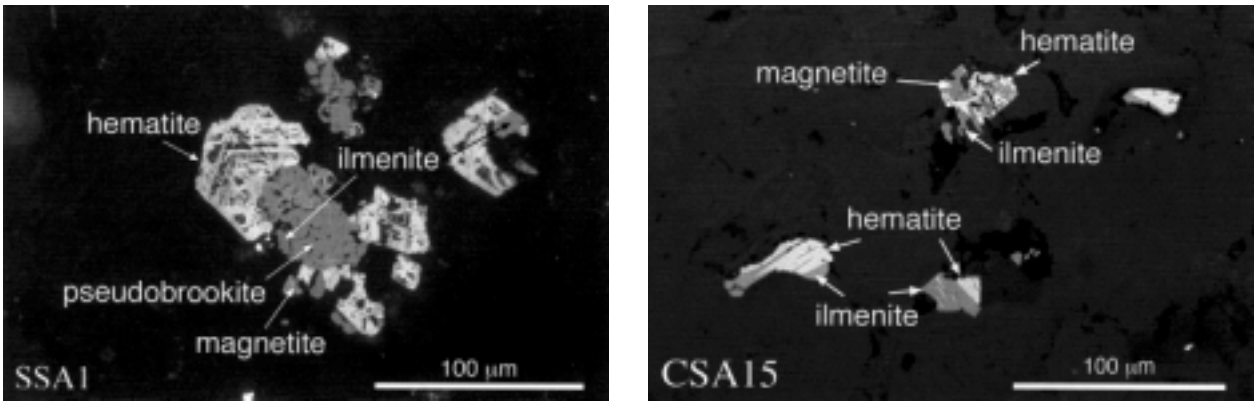

Fig. 9. *Photomicrographs (reflected light) of oxide minerals showing a) magnetite-bearing assemblage with pseudobrookite, ilmenite and hematite from the biotite zone, and b) complex Fe-Ti oxide assemblage from the transition zone with martitized magnetite and hematite$_{ss}$ with exsolved lenses of ilmenite$_{ss}$ and vice versa.*

	Northern	**profile**		**Southern**	**profile**
zone	and-crd	trans		and-crd	trans
sample	CSA 12	CSA 17	CSA 15	F5920	P9
n	5	7	4	2	8
SiO_2	0.02	0.01	0.02	0.02	0.03
TiO_2	0.12	0.09	0.08	0.07	0.20
Al_2O_3	0.03	0.05	0.04	0.04	0.25
Cr_2O_3	0.13	0.14	0.68	0.06	0.89
Fe_2O_3	67.76	68.26	67.40	68.20	66.42
FeO	30.72	30.84	30.63	30.77	30.68
MnO	0.03	0.04	0.04	0.01	0.06
MgO	0.01	0.02	0.01	0.00	0.01
Total	98.85	99.47	98.94	99.19	98.60
Si	0.00	0.00	0.00	0.00	0.00
Ti	0.00	0.00	0.00	0.00	0.01
Al	0.00	0.00	0.00	0.00	0.01
Cr	0.00	0.00	0.02	0.00	0.03
Fe^{3+}	1.98	1.99	1.97	1.99	1.95
Fe^{2+}	1.00	1.00	1.00	1.00	1.00
Mn	0.00	0.00	0.00	0.00	0.00
Mg	0.00	0.00	0.00	0.00	0.00

Table 8. *Chemical composition of magnetite in wt% oxide (means of n single analyses). Fe_2O_3, FeO and formula are calculated assuming stochiometry (3 cations, 4 oxygen).*

Generally, metasediments of the *biotite zone* are characterised by the oxide assemblage hematite + rutile and/or ilmenite (Fig. 10b) with grain sizes less than 300 µm. Ilmenite contains 2.8 wt% MnO and no hematite component. Sometimes goethite occurs instead of hematite.

Within the *andalusite-cordierite* and *transition zones*, magnetite and ilmenite are the major oxide minerals in metasediments and hematite, rutile and ilmenite-hematite solid solutions (ss) are common (Tables 8, 9). In sample CSA15, ilmenite-hematite$_{ss}$ appears mostly as isometric grains with grain sizes between 10 and 50 µm. Ilmenite also forms porphyroblasts (Fig. 9b). Magnetite shows always some degree of martitization. Grain sizes of magnetite and ilmenite are less than 100 µm. Aggregates of ilmenite-hematite$_{ss}$ are partly altered: the hematite-rich parts decompose to a mixture of pure hematite and different Ti-bearing products like titanite and leucoxene. In sample P9, small ilmenite, magnetite and hematite grains (up to 50 µm) are disseminated within the rock. Ilmenite from this metamorphic zone contains between 4 and 10 mol% of the hematite component and 1-5 wt% MnO (Table 7). Magnetite displays low Cr_2O_3-contents of about 0.9 wt% (Table 8). On the basis of experimental phase relations in the FeO-TiO_2-Fe_2O_3 system (Lindsley 1991), the most Fe^{3+}-rich ilmenite and the most Ti-rich hematite together with magnetite form a stable assemblage at about 600°C (Fig. 10). However, the observed compositions towards the pure rhombohedral end-members probably indicate a retrograde overprint.

Within the *cordierite-K-feldspar zone*, ilmenite is the major oxide component. In sample LOK23, however, magnetite was not observed microscopically. The hematite-component in ilmenite is 9 mol% and the MnO content is low (0.8 wt%, Table 7). Sample B5660 is different from all other samples because about 4 vol-% pyrrhotite (ferrimagnetic type) occur together with ilmenite. Magnetite was not observed in this sample.

A retrograde alteration of the cordierite-bearing rocks is commonly observed. Ilmenite is most abundant and some hematite occurs. Grain sizes do generally not exceed 100 µm. Titanite-

leucoxene lamellae within ilmenite are alteration products. Similar to ilmenite from the biotite zone, ilmenite shows no significant hematite component and MnO contents range between 1.7 and 2.8 wt% (Table 7).

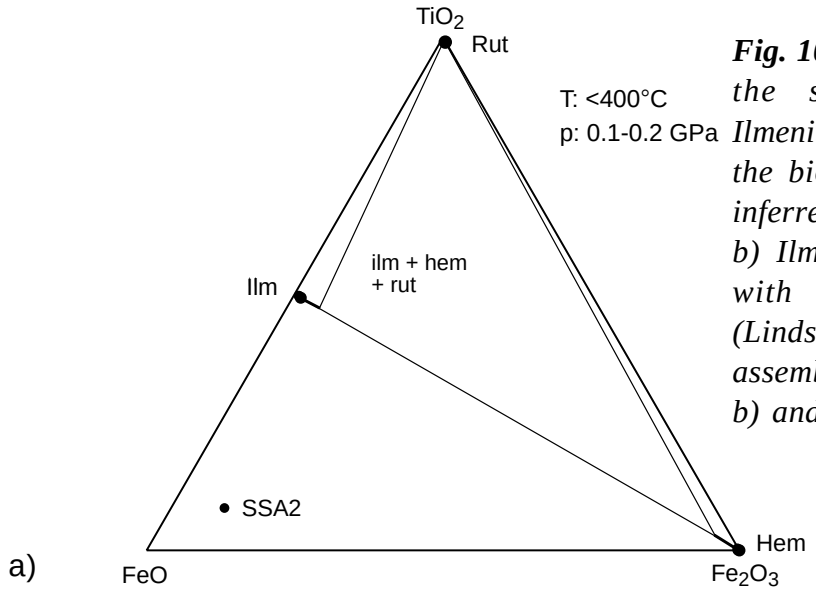

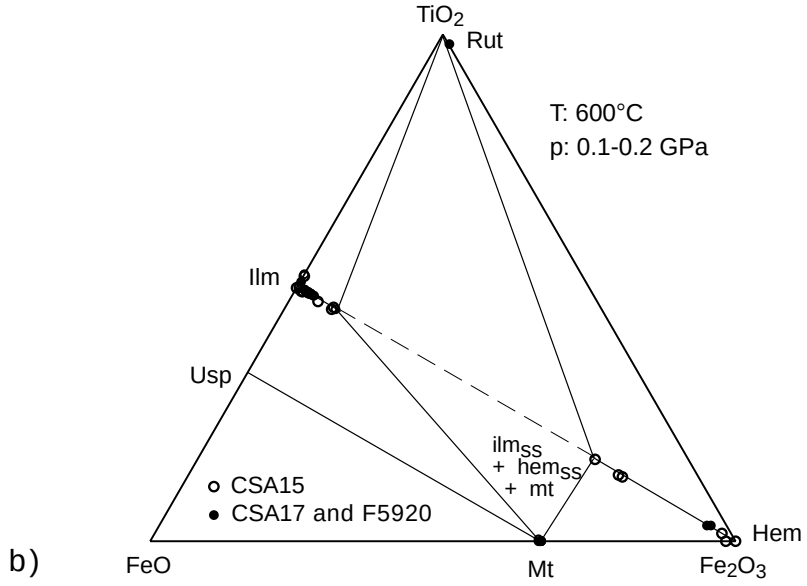

Fig. 10. *Compositional relationships in the system FeO-TiO_2-Fe_2O_3. a) Ilmenite, hematite and rutile (Rut) from the biotite zone with phase relations inferred from natural occurrences and b) Ilmenite-hematite$_{ss}$ (Ilm_{ss}, Hem_{ss}) with experimental phase relations (Lindsley, 1991) composition of oxide assemblages from a) biotite zone, and b) andalusite-cordierite and transition*

	Northern profile								
zone	bio		and-crd			trans		crd-kf	
sample	SSA1	SSA2	SSA15	CSA9	CSA12	CSA17	CSA15	CSA13	Lok23
T_{low}	-173	para	para	para			-170	para	
	-146				-149	-149	-149		
T_{trans}	150	390	420						
T_c	305		560				338		
	590	590	590	(580)	590	580	580		575
k (10^{-6} SI)	2782	462	353	528	28000	17500	10273	511	760
oxide	hm, il,	hm, rt	goe, il	hm, il	mt, il	mt, il,	mt, ilhm,	il, rt	il
assemblage	mt,					hm, rt	hm, il		

	Southern profile			
zone	and-	trans		crd-kfs
sample	F5920	P9	P18	B5660
Tl_{ow}	-169	-166	para	-172
	-148			
T_{trans}				
T_c	550	545	(550)	320
	580	580		580
k (10^{-6} SI)	16260	11733	350	2020
oxide	mt, il	mt, il(2)	il,hm	po, il,
assemblage				(mt?)

Table 9. *Characteristic temperatures from κ(T)-curves, oxide assemblages and bulk susceptibilities (in 10^{-6} SI units). Oxide assemblage as observed by reflected microscopy.*

8. Temperature-dependent magnetic susceptibility and its application for ferromagnetic phase identification

The results of the magnetic measurements are shown in Table 9. Within the *biotite zone*, bulk susceptibilities are between 200 and 500 x 10^{-6} SI units (Table 9 and Fig. 1). These low values indicate that paramagnetic (Fe-bearing silicates and ilmenite) or antiferromagnetic minerals (hematite) are mainly responsible for the magnetic susceptibility. Only a few samples (like SSA1) with detrital magnetite show higher susceptibilities. The large scatter in the bulk

susceptibilities within the *andalusite-cordierite* and *transition zones* (between 300 and 28000 x 10^{-6} SI units) can

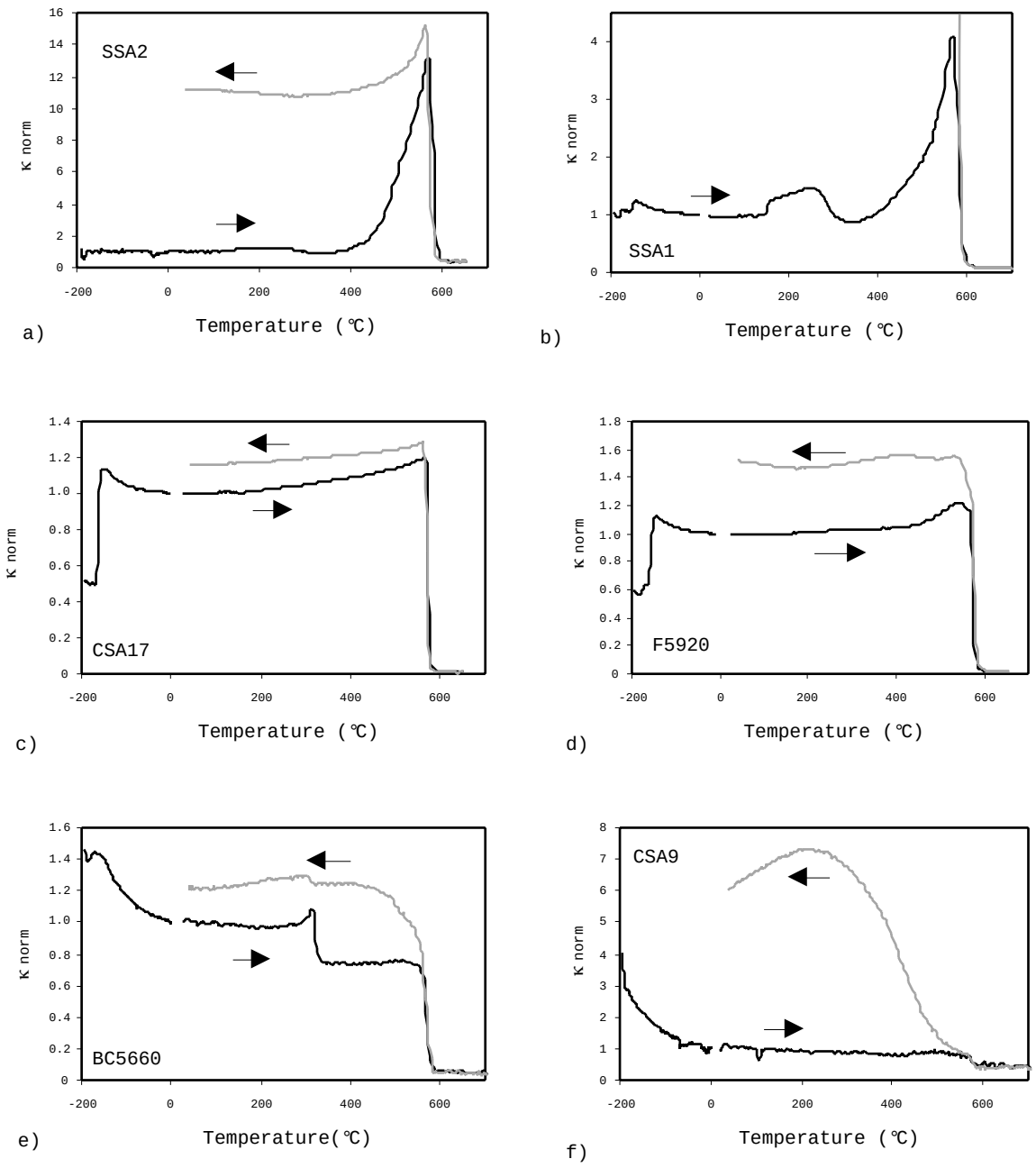

Fig. 11. *Normalised susceptibility vs. temperature cycles (-200 – 700°C) from different zones: a) and b) from biotite zone, c) and d) from andalusite-cordierite zone, e) from cordierite-K-feldspar zone and f) shows a retrograde sample (susceptibilities were normalised to room temperature, arrows indicate heating and cooling curve).*

be explained by a varying amount of magnetite. Within sample LOK23 from the *cordierite-K-feldspar zone* the bulk susceptibility is only slightly higher relative to rocks with only para- and antiferromagnetic minerals. The bulk susceptibility of 2020 x 10^{-6}SI units from sample B5660 can be explained by abundant pyrrhotite. Retrograded rocks show bulk susceptibilities with low values (350-530 x 10^{-6} SI units).

Thermomagnetic cycles from –192° to 700°C were performed in order to characterise the magnetic phases (Fig. 11). Within the *biotite zone* most samples show paramagnetic behaviour during heating up to 390°C. Above this temperature a strong increase in susceptibility was observed and a phase with a Curie temperature of 590°C formed, which is probably magnetite. During the cooling run this phase remains sTable (Fig. 11a). Sample SSA1 (Fig. 11b) shows a very complex behaviour with two kinks in susceptibility at low temperatures (-173°, -146°C), a transition temperature at 150°C and two Curie temperatures (T_c) at 305° and 590°C, respectively. The changes in susceptibility at –146°C (Vervey transition) and 590°C indicate magnetite. The change at around –170°C that also occurs in samples from the higher grade metamorphic zones (see below), can be attributed to Fe^{3+}-bearing ilmenite with about 4 mol% of the Fe_2O_3 component. This is indeed the mean composition analysed by EMP for this sample (Table 7). The transition temperature at 150°C and the T_c at 305°C cannot be explained by the phases that occur at room temperature and must be related to phase transitions during the heating run. Since it was not possible in our samples to identify hematite by the Curie temperature (685°C), it is likely that hematite transforms into magnetite during heating in argon. The strong increase in magnetic susceptibility above 300°C seems to be related to this transformation. Microscopic investigations and BSE images revealed that two types of magnetite, one in single domain (<1.6 μm) and the

other in multidomain state, occur in the sample. The domain size of magnetite controls the shape of the susceptibility curve; single domains cause a strong increase in susceptibility before reaching the Curie temperature (Hopkinson effect). The occurrence of the Vervey transition at –146°C can be related to multidomain magnetite grains; single domain magnetite does not show this transition (Muxworthy 1999).

Within the *andalusite-cordierite* and *transition zones*, ferrimagnetic behaviour dominates the thermomagnetic curves. Three types of cycles occur. (1) A "tooth"-shape of the thermomagnetic curve that results from the change of susceptibility at –150°C and 590°C (Fig. 11c) is characteristic for magnetite in a multi-domain state. The high magnetite content masks all other features. (2) Beside the typical magnetite-indicating temperatures, a change in susceptibility occurs at a temperature of –170° and 550°C (Fig. 11d). (3) Sample CSA15 shows a curve similar to Fig. 11d, but the Curie temperature is 340°C instead of 550°C. Both samples (F5920 and CSA 15) contain ilmenite-hematite$_{ss}$, magnetite and ilmenite. Sample CSA 15 also shows some hematite. Estimations of the titanohematite composition from the Curie temperature provide $hm_{62}il_{38}$ in case of T_C = 340°C (sample CSA15) and $hm_{86}il_{14}$ for T_C = 550°C (sample F5920), but EMP analyses give a composition of $hm_{72}il_{28}$ (Table 7). The inconsistency between the compositions derived from the Curie temperature and from EMP for Ti-bearing hematites in sample F5920 and CSA 15 may indicate that this phase is unsTable during heating. Zapletal (pers. comm.) found Curie temperatures between 300° and 400°C as well as about 550°C which are typical for maghemite, the oxidised variety of magnetite. Our analyses of Ti-bearing hematite are within the field, in which metasTable titanomaghemites occur. Therefore we relate these Curie temperatures to unsTable Ti-bearing hematite compositions.

Although no magnetite was observed optically in the *cordierite-K-feldspar zone*, thermomagnetic studies indicate small amounts of it (Table 9). The heating curve of sample B5660 (Fig. 11e) shows one broad peak between –170 and –150°C which may indicate Fe^{3+}-bearing ilmenite together with magnetite. During heating to 0°C the susceptibility decreases as it is typical for paramagnetic phases. The heating course displays a Curie temperature at 320°C indicating ferrimagnetic pyrrhotite and T_c of magnetite at 580°C. This is the only sample that contains pyrrhotite beside magnetite.

Retrograde alteration of the cordierite-bearing rocks causes a decomposition of the ferrimagnetic components. The thermomagnetic cycles (Fig. 11f) show paramagnetic behaviour up to about 420°C followed by an increase in susceptibility (comparable to sample SSA2 from the biotite zone), and a Curie temperature at 580°C or a little bit lower (550°C). A small irregularity between –70° and –10°C is probably related to the Morin transition in hematite. Hematite was also observed optically. Our investigations suggest that hematite can be observed in thermomagnetic cycles only if no other ferrimagnetic phase masks the very small changes in susceptibility related to hematite.

9. Discussion and conclusions

The present data clearly show a relationship between metamorphic assemblage and magnetic susceptibility. As stated by Rochette (1987) metamorphic reactions among silicates have no significant effect on susceptibility as long as the amount of paramagnetic iron remains constant. This observation is confirmed by the fact that the most important factor controlling magnetic susceptibility is the occurrence and abundance of ferrimagnetic magnetite. Our samples range in

bulk FeO_{tot} content between 4.4 and 9.6 wt%, corresponding to a calculated paramagnetic susceptibility between 280 and 600 x 10^{-6} Si units. These values are similar in all metamorphic zones and they are consistent with measured susceptibilities for samples, in which only paramagnetic minerals control the susceptibility (e.g. sample SSA15 or P18; Table 1 and Table 9). In the quartzite sample SSA2, with the lowest FeO_{tot} content (1.3 wt% corresponding to a paramagnetic susceptibility of 80 x 10^{-6} SI units), the measured value of 460 x 10^{-6} SI units is much higher and indicates the influence of antiferromagnetic hematite. As soon as antiferromagnetic hematite or ferrimagnetic magnetite appear in the rock, susceptibility values are higher than the calculated paramagnetic portion. Therefore, if physico-chemical conditions change and ferrimagnetic minerals are able to form at the expense of para- or antiferromagnetic minerals, the magnetic susceptibility will change dramatically. Since the bulk rock composition is similar in the majority of our samples (Table 1), changes in mineral assemblages and in the composition of Fe-bearing phases are assumed to be controlled by the physical conditions during metamorphism, and not by bulk composition.

Within the biotite zone, biotite and Fe-bearing white mica as well as ilmenite, rutile and hematite control the paramagnetic/antiferromagnetic susceptibility, ranging between 200 and 500x10^{-6} SI units. Locally, magnetite-bearing detrital components lead to an increase in the magnetic susceptibility to values higher than 2000x10^{-6} SI units.

The prograde contact metamorphic assemblages from the biotite to the andalusite-cordierite zone do not induce significant changes in the chemical composition of paramagnetic biotite and white mica (Table 2 and Table 5). The susceptibility values scatter between 300 and 28.000 x 10^{-6} SI units, indicating a heterogeneous distribution of magnetite as the most important

ferrimagnetic mineral. As the FeO_{tot} contents in biotite remain constant, we conclude that magnetite appears at the expense of hematite due to the temperature increase (compare Fig. 8 for hematite-magnetite-buffer line). Changes of the relative oxygen fugacity due to silicate-oxide reactions play a minor role in the formation of magnetite during prograde contact metamorphism.

Further temperature increase in the cordierite-K-feldspar zone results in a decrease of magnetic susceptibility, indicating a decomposition of magnetite, which was identified only by thermomagnetic methods. It is no longer visible microscopically. Traces of magnetite are sufficient to explain the difference between calculated paramagnetic (560 x 10^{-6} SI units) and measured susceptibilities (760 x 10^{-6} SI units) of sample LOK23 (Tables 1 and 9). The decomposition of magnetite within this zone is accompanied by an increase of X_{Fe} in biotite from the biotite and andalusite-cordierite zones (0.56) to the cordierite-K-feldspar zone (0.69). Increasing X_{Fe} in biotite is generally interpreted as an indicator of decreasing oxygen fugacity (e.g. Lindsley et al., 1990). Looking at the distribution coefficients (K_D;) between the Fe-bearing silicates, K_D values of 0.54 for biotite-white mica pairs from the andalusite-cordierite and transition zone are similar to K_D values of 0.53 for cordierite-biotite pairs from the transition and cordierite-K-feldspar zone (Table 6). The K_D values of these prograde assemblages (samples CSA17, P9) suggest that a redistribution of Fe and Mg between Fe-Mg silicates is a more reasonable explanation for the changes of X_{Fe} in biotite than a decrease in oxygen fugacity. The observed increase of the hematite component in ilmenite (up to 12 vol-%) together with a strong decrease of magnetite in the cordierite-K-feldspar zone shows the importance of a redox reaction for the decomposition of magnetite. This could be the reaction 2 sillimanite + biotite +quartz + 2 magnetite + 0.5 O_2 = 2 K-feldspar + cordierite + 3 hematite. Therefore, it can be concluded that

high temperature contact metamorphism (in this study about 730°C) reduces magnetic susceptibility, whereas lower temperatures (550-650°C) support the formation of a magnetic magnetite isograde.

The local abundance of pyrrhotite within the cordierite-K-feldspar zone (sample B5660) probably documents the influence of a late, 30 m wide monzonitic dyke that intruded nearby. This sample also displays lower temperatures for the Na-in-cordierite thermometer, suggesting a reequilibration at lower temperatures (about 570°C, see Table 3). The presence of pyrrhotite indicates that not only heat transfer but also influx of a reducing fluid, which supplied sulphur, was involved.

Some of the investigated samples are effected by strong retrograde alteration as documented by the formation of chlorite and / or white mica. This alteration is often accompanied by a low magnetic susceptibility in all contact metamorphic zones (see samples CSA9, CSA13 and P18 in Table 9) masking the earlier magnetic isograde within the andalusite-cordierite and transition zone. Ilmenite + hematite or ilmenite + rutile, growing at the expense of magnetite, form the retrograde assemblage. This assemblage is comparable to that from the biotite zone. Only in samples with an incomplete alteration (sample F5920), magnetite is still preserved. Chlorite-geothermometry provides alteration temperatures ranging from 280° to 420°C. According to the thermodynamic model of Walshe (1986) the redox conditions of the alterating fluid changed from more oxidising at higher temperatures towards more reducing conditions at lower temperatures. This is in good agreement with the oxide assemblages and is also reflected by the ilmenite chemistry, which displays end member composition (Table 7).

Concluding, it can be stated that the changes in magnetic mineralogy shown in this study are related to:

(1) an increase of temperature within the andalusite-cordierite zone leading to the formation of magnetite;

(2) a further increase of temperature within the cordierite-K-feldspar zone, apparently related to increasing log $f(O_2)$ conditions (formation of hematite-bearing ilmenite and decomposition of magnetite);

(3) decreasing temperatures during retrograde metamorphism that are generally related to more reducing conditions (Fig. 8).

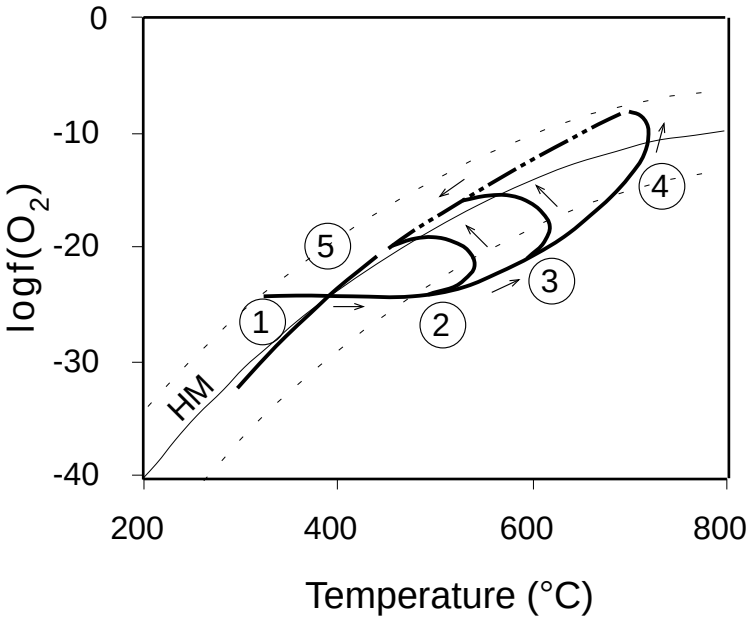

***Fig. 12**. Schematically path of log f(O_2) – T evolution within the contact aureole up to high-grade conditions and its retrograde overprint. Numbers 1-4 refer to biotite, andalusite-cordierite, transition and cordierite-K-feldspar zone, and number 5 to the retrograde conditions. For the hatched part of the retrograde path no data are available from this study.*

A schematic pathway of the prograde and retrograde T-log $f(O_2)$ evolution is given in Fig. 12.

It is obvious from this study that only small changes in oxygen fugacity across the hematite-magnetite buffer are sufficient to cause significant changes in the magnetite abundance and to modify the magnetic signal of a rock. The JBP pluton belongs to the magnetite-bearing plutonic

subprovince of the Cordilleran magmatic arcs (for definition of magnetite-series plutons, see Gastil et al. 1990 and references therein) that is characterised by distinct magnetic anomalies. From our investigations it can be concluded that contact metamorphic aureoles, as long as they are not strongly altered, contribute significantly to magnetic anomalies. Therefore, the geometry of magnetite-series plutons mapped only with aeromagnetic methods must be treated carefully, because a possible magnetic signal from the aureole can be taken for the pluton itself and may lead to a misinterpretation of the pluton's size.

Gastil et al. (1990) observed magnetite destruction at the Sierra San Pedro Martir pluton in the Southern part of the Peninsula Ranges batholith similar to the decomposition of magnetite we observed in the innermost aureole of the JBP. These authors explain the magnetite loss by an interaction of the pluton with water-rich, low-f(O_2) fluids late in the cooling history. The fact that metamorphic minerals in the contact aureole of the JBP such as cordierite and andalusite are often replaced by white mica and chlorite also suggests an increasing activity of H_2O that probably can be related to the cooling of the pluton. The loss of magnetite in the andalusite-cordierite and transition zones is probably related to water-rich reducing fluids at a late stage of plutonic cooling. In the present case, the magnetite decomposition starts already under more oxidising conditions in the cordierite-K-feldspar zone during a late stage of high-grade metamorphism. This implies that fluids played an important role not only during cooling of the pluton but also during the emplacement. Therefore, fluids probably influenced the rheology of the aureole rocks and controlled the emplacement of the JBP. On the other hand, the similar X_{Fe}-values between biotite and its retrograde alteration product chlorite (Table 6) from the various zones indicate isochemical conditions during fluid flow, and therefore these fluids did not have a

strong metasomatic effect on the aureole rocks. This phenomenon might either be explained by the small amounts of fluids active during the emplacement of the JBP, or by high flow velocities, which would restrict fluid-rock interactions.

Acknowledgements

This research was supported by the Graduiertenkolleg 273 “fluid-rock interactions” to C. Dietl. Special thanks go to D. Lattard, R.O. Greiling and R. Marioth for constructive advice and comments. We acknowledge H.P. Meyer for assistance with obtaining electron microprobe analyses.

References

Bateman, P.C., 1992. Plutonism in the central part of the Sierra Nevada batholith, California: US Geol. Survey Prof. Paper, 1483: 186 pp.

Bailey, S.W., 1986. Hydrous phyllosilicates: Rev. Mineral., 19: 464 pp.

Cathelineau, M., 1988. Cation site occupancy in chlorites as a function of temperature: Clay Minerals, 23: 471- 485.

De Caritat, P., Hutcheon I. and Walshe J.L., 1993. Chlorite geothermometry: a review: Clays and clay minerals, 41: 219-239.

Dietl, C., 1999. Emplacement of the Joshua Flat-Beer Creek Pluton (White Inyo Mountains, California): a story of multiple material transfer processes. In: Castro, A., Fernandez, C. and Vigneresse, J. L., (Editors), Understanding granites: Integrating new and classical techniques: Geological Society, London, Special Publications, 168: 161-176.

Ernst, W.G., 1996. Petrochemical study of regional/contact metamorphism in metaclastic strata of the central White-Inyo Range, eastern California: Bull. Geol. Soc. Am., 108: 1528-1548.

Gastil, G., Diamond, J., Knaack, C., Walawender, M., Marshall M., Boyles, C., Chadwick, B. and Erskine B., 1990. The problem of the magnetite/ilmenite boundary in southern and Baja California . In Anderson, J.L., (Editor), The nature and origin of Cordilleran magmatism. Geol. Soc. Am., 174: 19-32.

Gillespie, J. G., 1979, U-Pb and Pb-Pb ages of primary and detrital zircons from the White Mountains, eastern California: Geol. Soc. Am. Abstr. Prog., 11 (30): 79.

Haggerty, S.E., 1991. Oxide textures – a mini-atlas: Rev. in Mineralogy, 25: 129-137.

Holdaway, M.J., 1971. Stability of andalusite and the aluminium silicate phase diagram: Am. J. Sci., 271: 97-131.

Hrouda, F., 1994. A technique for the measurement of thermal changes of magnetic susceptibility of weakly magnetic rocks by the CS-2 apparatus and KLY-2 Kappabridge: Geophys. J. Int., 118: 604-612.

Jowett, E.C., 1991. Fitting iron and magnesium into the hydrothermal chlorite geothermometer: GAC/AGC - MAC/AMC - SEG, program with abstracts, 16: A62.

Kalt, A., Altherr, R. and Ludwig, T., 1998. Contact metamorphism in pelitic rocks on the island of Kos (Greece, Eastern Aegean Sea): a test for the Na-in-cordierite thermometer: J. Petrol., 39: 663-688.

Kranidiotis, P. and MacLean, W. H., 1987. Systematics of chlorite alteration at the Phelps Dodge Massive Sulphide Deposit, Matagami, Quebec: Econ. Geol., 82: 1898-1911.

Le Breton, N. and Thompson, A.B., 1988. Fluid absent (dehydration) melting of biotite in metapelites in the early stages of crustal anatexis: Contrib. Mineral. Petrol., 99: 226-237.

Lindsley, D.H., 1991. Experimental studies of oxide minerals: Rev. in Mineralogy, 25: 69-106.

Mason, B. and Moore, C.B., 1985. Grundzüge der Geochemie. Enke, Stuttgart, 350 pp.

Massonne, H.-J. and Schreyer, W., 1987. Phengite geobarometry based on the limiting assemblage with K-feldspar, phlogopite, and quartz: Contrib. Mineral. Petrol., 96: 212-224.

McKee, E.H. and Conrad, J.E., 1996. A tale of ten plutons – Revisited: Age of granitic rocks in the White Mountains, California and Nevada: Bull. Geol. Soc. Am., 108: 1515-1527.

Mirwald, P.W., 1986. Ist Cordierit ein Geothermometer? : Fortschr. Mineral., 64 (1): 119.

Muxworthy, A.R., 1999. Low-temperature susceptibility and hysteresis of magnetite: Earth Planet. Sci. Lett., 169: 51-58.

Nelson, C.A., Hall, C.A., Jr. and Ernst, W.G., 1991. Geologic history of the White-Inyo Range. In: Hall, C.A.,Jr., (Editor), Natural history of the White-Inyo Range, California. Univ. Cal. Nat. Hist. Guides, 55, pp. 42-74.

Patiño Douce, A.E., 1994. Titanium substitution in biotite: an empirical model with applications to thermometry, O_2 and H_2O barometries, and consequences for biotite stability: Chem. Geol., 108: 133-162.

Patiño Douce, A.E., Johnston, A.D. and Rice, J.M., 1993. Octahedral excess mixing properties in biotite: a working model with application to geobarometry and geothermometry: Am. Mineral., 78: 113-131.

Pouchou, J.L. and Pichoir, F., 1984. A new model for quantitative X-ray microanalysis; Part I: Application to the analysis of homogeneous samples: La Recherche Aérospatiale, 3: 167-192.

Robigou, V., 1986. Metamorphism in the Cambrian Campito Formation, White-Inyo Mountains, California. In Hall, C.A., Jr., and Young, D.V., (Editors), Natural history of the White-Inyo

Range, eastern California and western Nevada and high altitude physiology. Univ. Cal. WMRS Symposium, 1, Los Angeles, pp. 27-36.

Rochette, P., 1987. Metamorphic control of the magnetic mineralogy of black shales in the Swiss Alps: toward the use of "magnetic isograde": Earth Planet. Sci. Lett., 84: 446-456.

Shive, P.N. and Fountain, D.M., 1988a. Magnetic mineralogy in an archean crustal cross section: implications for crustal magnetisation: J. Geophys. Res., 93: 12177-12186.

Shive, P.N., Frost, B.R. and Peretti, A., 1988b. The magnetic properties of metaperidotitic rocks as a function of metamorphic grade: implications for crustal magnetic anomalies: J. Geophys. Res., 93: 12187-12195.

Stein, E., 2000. Zur Platznahme von Granitoiden - Vergleichende Fallstudien zu Gefügen und Platznahmemechanismen aus den White-Inyo Mountains, California, USA und dem Bergsträßer Odenwald. Geotekt. Forsch., 93: 330 pp.

Stern, T.W., Bateman, P.C., Morgan, B.A., Newell, M.F., and Peck, D.L., 1981. Isotopic U-Pb ages of zircon from the granitoids of the central Sierra Nevada, California: U.S. Geological Survey Professional Paper, 1185: 17 pp.

Sylvester A.G., Miller C.F. and Nelson C.A., 1978. Monzonites of the White-Inyo Range, California, and their relation to the calc-alkalic Sierra Nevada batholith. Geol. Soc. Am. Bull., 89: 1677-1687

Symmes, G.H. and Ferry, J.M., 1995. Metamorphism, fluid flow and partial melting in pelitic rocks from the Onawa contact aureole, central Maine, USA: J. Petrol., 36: 587-612.

Walshe, J. L., 1986. A six-component chlorite solid solution model and the conditions of chlorite formations in hydrothermal and geothermal systems: Econ. Geol., 81: 681-703.

Warner, R.D. and Wasilewski, P.J., 1995. Magnetic petrology of lower crust and upper mantle xenoliths from McMurdo Sound, Antarctica: Tectonophysics, 249: 69-92.

The diapiric emplacement and related magmatic fabrics of the porphyritic Ludwigshöhe granite, Central Odenwald (Germany)

Die diapirische Platznahme des porphyrischen Ludwigshöhe-Granits, Mittlerer Odenwald (Deutschland), und damit verbundene magmatische Gefüge

Carlo Dietl[1] & Eckardt Stein[2].

[1)] Geologisch-Paläontologisches Institut, Universität Heidelberg

[2)] Institut für Mineralogie , TU Darmstadt

With 7 Figures

Received

Revised version accepted

Summary

The Ludwigshöhe pluton is a 1.5 by 2.5 km, oval-shaped, NE-SW oriented, distinct body of a medium-grained porphyritic granite with large euhedral to lensoid K-feldspar phenocrysts and pancake shaped microdioritic enclaves.

The granite shows a well developed NE-SW striking, steeply inclined foliation defined by mafic minerals, the phenocrysts, and the enclaves. All phenocrysts have an orthorhombic symmetry with respect to the foliation. Monoclinic shear sense criteria are absent. Shape orientation analysis of enclaves, K-feldspar phenocrysts, magmatic hornblende and plagioclase and strain analyses (R_f/Φ) result in uniaxial, oblate ellipsoids, plotting in the field of apparent flattening of the Flinn diagram.

In thin section no penetrative plastic deformations of both the feldspars, hornblende and biotite can be observed. Twinning in feldspars occurs parallel to their

flat faces, which are oriented parallel to the magmatic foliation. Quartz, growing in interstitial positions, shows penetrative plastic deformations starting under HT-late magmatic/early solid-state conditions and end under LT conditions during sinistral shear deformations, responsible for an oblique orientation of the quartz-c-axes fabric.

AMS studies as well as cathodoluminescence investigations and quartz c-axes textures support the interpretation of flattening processes under a NW-SE directed compressive strain regime, during the magmatic stage and/or emplacement of the granites.

Zusammenfassung

Der Ludwigshöhe-Pluton ist ein 1.5 km breiter und 2.5 km langer, ovaler, NE-SW-orientierter, mittelkörniger Granit mit großen, idiomorphen bis linsenförmigen Kalifeldspat-Einsprenglingen und oblaten mikrodioritischen Enklaven.

Der Granit zeigt eine deutliche NE-SW-streichende, steilstehende Foliation, die durch die Einregelung der mafischen Minerale, der Kalifeldspat-Einsprenglinge und der Enklaven definiert wird. Alle Einsprenglinge besitzen orthorhombische Symmetrie in Bezug zur Foliation. Monokline Schersinnindikatoren fehlen. Formregelungsanalysen an Enklaven, Kalifeldspat-Einsprenglingen, magmatischer Hornblende und Plagioklas sowie Strainanalysen (R_f/Φ) ergeben uniaxiale, oblate Ellipsoide, die im Plättungsfeld des Flinn-Diagramms plotten.

Im Dünnschliff kann keine durchgreifende, plastische Verformung, weder der Feldspäte, noch von Hornblende oder Biotit, beobachtet werden. Feldspäte sind generell parallel zu ihren Flachseiten verzwillingt und liegen mit ihren Langachsen parallel zur magmatischen Foliation. Quarz wächst im allgemeinen in Zwickelräumen, er zeigt penetrative, plastische Verformung. Sie beginnt unter HT-Bedingungen nahe dem Solidus und endet unter LT-Bedingungen und sinistraler Scherung. Diese Scherdeformation ist verantwortlich für die Schiefregelung des Quarz-c-Achsen-Gefüges.

AMS- und Kathodolumineszenz-Untersuchungen, sowie Quarz-c-Achsen-Messungen unterstützen die Interpretation, daß Plättung unter einem NW-SE-gerichteten, einengenden Strainregime die gefügeprägende Rolle während der Platznahme des Ludwigshöhe-Plutons spielte.

Key words

Odenwald, Flasergranitoid zone, magmatic fabrics, anisotropy of magnetic susceptibility, shape orientation analyses, quartz c-axis measurements

Introduction

Generally magmatic rocks are characterized by an isotropic fabric. However, from orogenic belts all over the world igneous rocks with a more or less pronounced planar fabric are wellknown. They might be generated either by solid-state deformation during and/or after their emplacement or by magmatic processes within the magma chamber. Especially the latter tells a lot about the emplacement history of plutons.

The Crystalline Odenwald (Fig. 1) in the southwestern part of Germany is composed of calk-alkaline plutons and to a smaller amount of amphibolite-facies metasediments. It is the largest continous outcrop of the Mid German Crystalline Rise, which according to *Kossmat* (1927) forms the northern rim of the Variscan Saxothuringian Zone (compare Fig. 1 in *Stein* same vol.). The Crystalline Odenwald and the so called Northern Phyllite Zone at the southern rim of the Rhenohercynian Zone are interpreted by *Krohe* (1991) as a paired metamorphic belt. *Anderle* et al. (1990) describe a HP-LT-metamorphism for the Northern Phyllite Zone (6 kbars, 300 °C), whereas metamorphism is of HT-LP-type in the Odenwald (*Willner* et al. 1991). Geochemical investigations point to a subduction-related, I-type nature of the granitoid plutons, therefore the Mid German Crystalline Rise is regarded as a magmatic arc above a south dipping subduction zone (*Henes-Klaiber* 1992, *Kreher* 1994). Hornblende and biotite K/Ar-cooling ages (*Kreuzer* and *Harre* 1975, *Kirsch* et al. 1988) tie the intrusion

of the plutons in a range between 363 Ma for the northern and 320 Ma for the southern Odenwald.

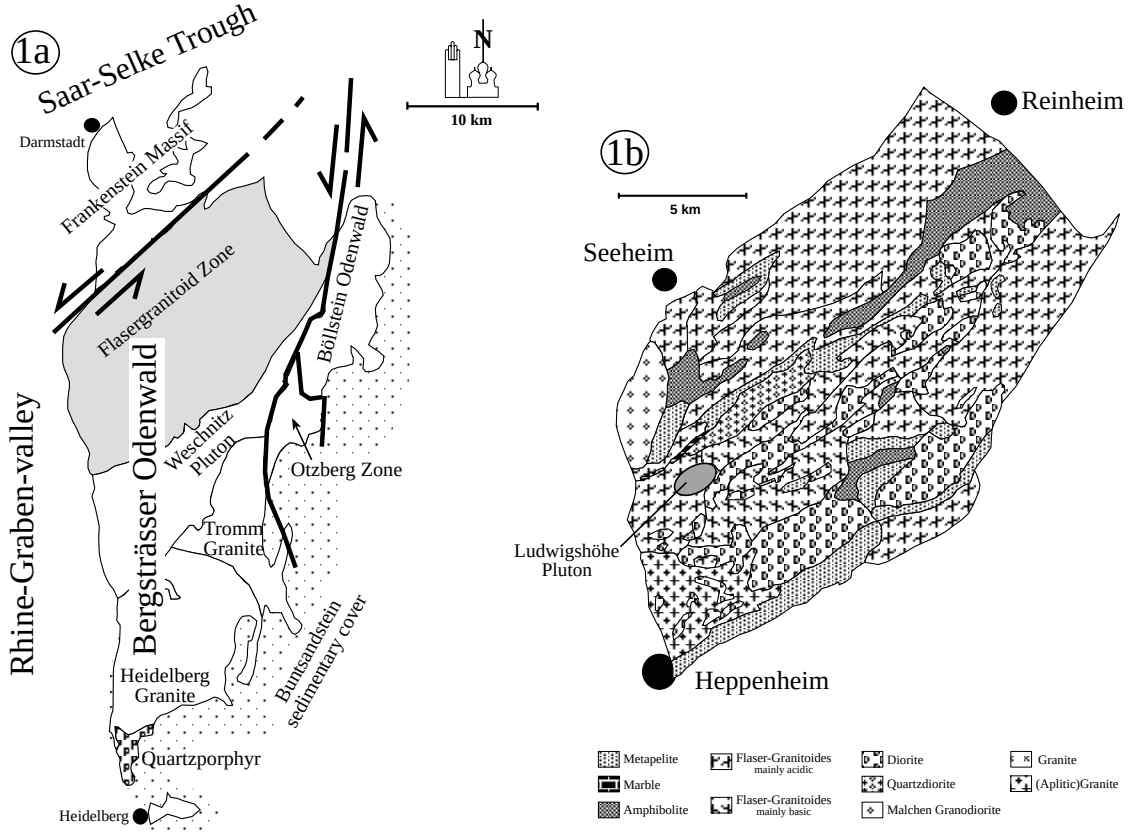

Fig. 1: *Overview map of the Crystalline Odenwald and a close up view of the Flasergranitoid Zone with the Ludwiugshöhe granite and its neighbouring plutons.*

A zone of special interest is the so called Flasergranitoid Zone in the central Odenwald (Fig. 1), which is characterized by an intimate association of gabbros, diorites, granodiorites and granites, because most of these rocks show a pronounced planar fabric. Its origin is still in discussion either as tectonic due to a syntectonic intrusion into a transtensional regime (*Krohe* 1994), or as magmatic due to the successive emplacement of different plutons (*Stein* 1996, 2000). *Krohe* (1994) describes a polyphase structural imprint in all the rocks and interpreted a syntectonic emplacement of the magmatites during a late stage of a crustal scale transtensional extension regime. In this paper, the Ludwigshöhe granite stands as an excellent example for magmatic fabrics which provide a lot of information for the diapiric emplacement of the granitoids in the Odenwald area and additionally related mechanisms.

The investigated Ludwigshöhe granite in the central Odenwald area is a small but distinct granitic blister in midst of quartzdioritic, dioritic and granodioritc intrusions (Fig. 1), which shows a well developed planar fabric. Different studies at the granite and the microdioritic enclaves as well, like a precise description of their macro- and microscopic fabrics, cathodoluminescence microscopy, strain analyses resp. shape orientation analyses at quartz, K-feldspars, plagioclase, biotite und hornblende and at the microdioritic enclaves, quartz-c-axes measurements, and AMS-investigations were carried out, to decifer as much as possible about its origin and to derive in a second, more global step the emplacement history and mechanism of this granite.

Mesostructures and microfabrics

The porphyritic Ludwigshöhe granite is situated at the western margin of the Flasergranitoid Zone. From the lithological context this acidic blister builds up a very distinct, elliptical, NE-SW striking pluton, sized about 1.5 • 2.5 km, in midst of more basic to intermediate diorites and granodiorites.

The granite is a homogeneous, medium grained rock (Figs. 2a, 2b), consisting of plagioclase (An_{25-30}) (38 Vol.-%), quartz (23 Vol.-%), K-feldspar (21 Vol.-%), biotite (12 Vol.-%), hornblende, chlorite, epidote, ilmenite, magnetite, hematite and titanite, zircon, apatite and prehnite, with large (up to several cm) euhedral to lensoid K-feldspar phenocrysts, a typical composition of I-type granitoids (*White* et al. 1986).

Like most of the plutons in this zone, it is characterized by a pervasive, NE-SW trending, steeply dipping planar fabric, which can be described as a magmatic foliation, due to the alignment of mafic minerals (biotite, hornblende) and of the K-feldspar-phenocrysts. This foliation lies parallel to the long diameter of the granite's elliptic shape and parallel to the regional strike direction of the planar and linear structures, derived from the Variscan orogeny. Locally, a magmatic banding made up by mafic schlieren can be observed and, where visible, is oriented parallel to the magmatic foliation. However, a concentric pattern of both, foliation and banding can not be verified due to poor exposure at both ends of the elliptical pluton.

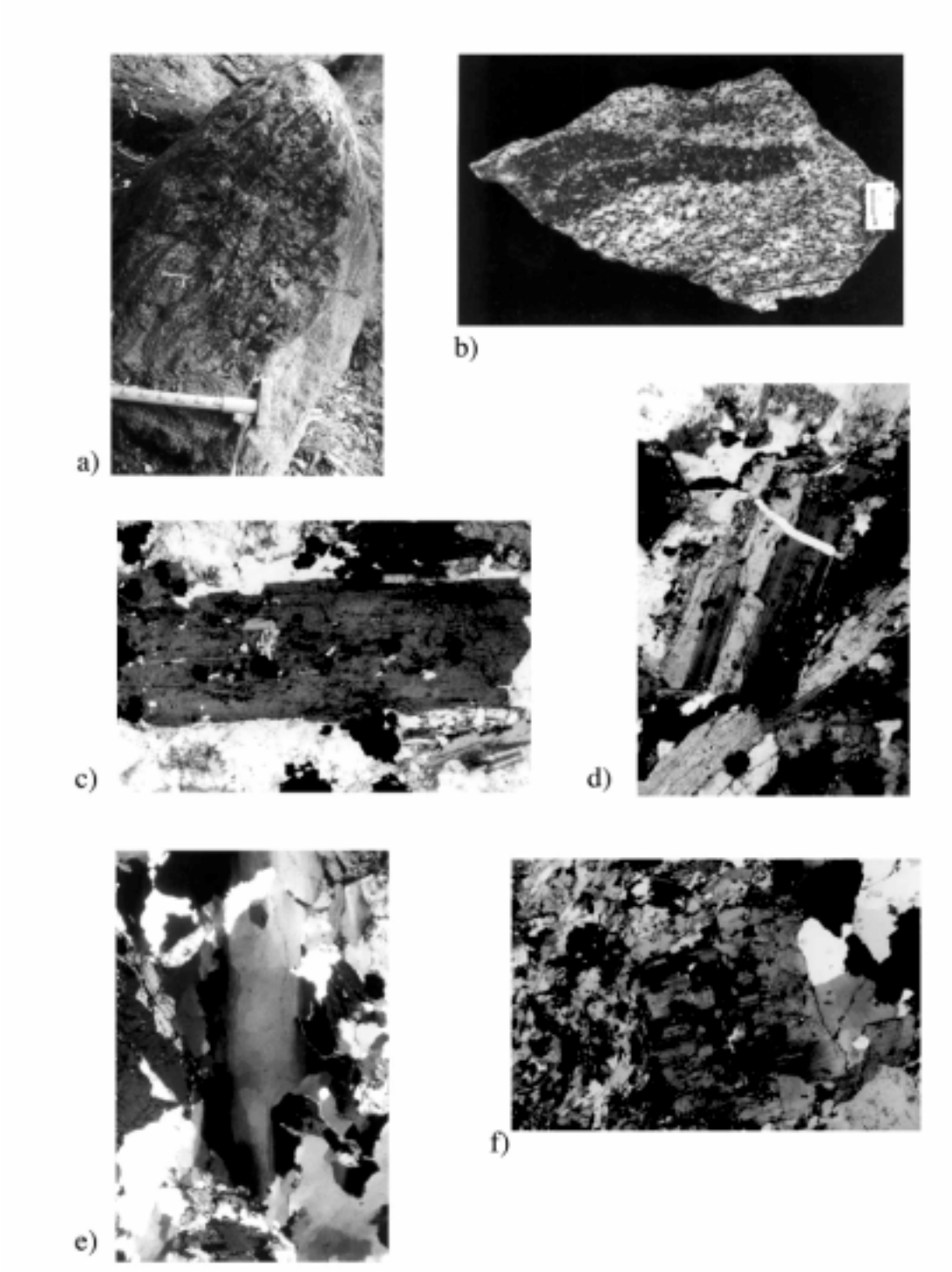

Fig. 2: *Photographs of the Ludwigshöhe granite: a) Outcrop of the porphyritic Ludwigshöhe granite; b) Polished slice of the porphyritic Ludwigshöhe granite including a microdioritc enclave; c) Microphotograph of the contact between granite and enclave: biotite crystals of the enclave wrap around plagioclase of the granite indicating the magmatic nature of this contact; the plagioclase dissolves potassium-feldspar (XPL; long side: 3,4 mm); d) Hornblende with inclusions of magnetite, biotite and plagioclase give hints to the crystallization sequence in the Ludwigshöhe granite (PPL; long side: 3,9 mm); e) Plagioclase, broken and healed with quartz (XPL; long side: 3,9 mm); f) Quartz with deformation lamellae as well as subgrains with chess board patterns in the center and partly recrystallizing at its rims (XPL; long side: 3,9 mm).*

Although the phenocrysts show a good preferred shape orientation, they cannot be used as shear sense indicators, because mostly they are euhedral or at least subhedral, but in any case their symmetry is orthorhombic with respect to the foliation. The occurence of subhedral, lensoid phenocrysts is rather due to crystal growth than to ductile deformations, because no recrystallization fabrics can be observed. *Vernon* (1986) interpreted this as a strong argument for a magmatic origin, because euhedral K-feldspar phenocrysts can not develop under metamorphic conditions. No other monoclinic fabrics and kinematic markers like σ- or δ-clasts were observed.

This planar fabric is pronounced by finegrained, pancake shaped, microdioritic enclaves (Figs. 2a, 2b), which mainly consist of plagioclase (An_{25-30}) (46 Vol.-%), biotite (32 Vol.-%) and hornblende (14 Vol.-%). Furthermore quartz (3 Vol.-%), K-feldspar (1 Vol.-%), titanite (1 Vol.-%), apatite, zircon, ore minerals, epidote, and prehnite are accessory phases. These enclaves are especially abundant (30 to 40 Vol.-%) in the northern part, where the granite bounds against the fine- to medium-grained Felsberg quartzdiorite (Fig. 1). This quartzdiorite has the same modal composition as the enclaves, and is consequentely interpreted as source from which those enclaves probably are derived by magma-mingling processes. The enclaves' sizes range from a few centimeters to some dezimeters. All their long axes are oriented parallel to the foliation, dipping to the SW.

From the minerals‘ habit and from mineral inclusions within the different constituents a typical magmatic crystallization succession: ore minerals ➜ plagioclase ➜ biotite ➜hornblende ➜ K-feldspar ➜ quartz can generally be derived for the granite. According to a changing amount of available water during the crystallization process biotite and hornblende may have formed alternatively during multiple stages (Fig. 2c).

The parallel orientation of the mafic minerals is not indicative for a solid-state or a magmatic fabric by itself. Furthermore it must be proven, whether it is due to a crystalplastic deformation or not. *Paterson* et al. (1989) give a detailed description of distinctive criteria for magmatic fabrics, which are particularly valid for diapirs. They

list a number of elements, the combination of which is clearly indicative for the magmatic origin of the entire fabric:

(1) Schlieren and enclaves of mafic, finegrained material in a more felsic host rock are regarded as result of magma mingling (incomplete magma mixing). Commonly interfaces between wall rock and inclusions are lobate. According to experimental work of *Blake* and *Campell* (1986) this points to an origanally liquid-liquid contact and unstable flow at the magma-magma-interface.

(2) Early crystallized minerals and xenoliths are oriented parallel to a layering due to magmatic flow and/or deformation of the melt.

(3) Twinning lamellae of the feldspars and hornblende are parallel to the mineral´s flat faces, due to their preferred orientation in the melt prior to twinning, which is typical for growth twins.

(4) The symmetry of most fabric elements (individual crystals, schlieren, enclaves etc.) is orthorhombic, because no crystalplastic simple shear deformation can be recorded in magma (characterized by a power law rheology) above the rheological critical melt percentage of c. 25% melt (RCMP, *Arzi* 1978).

(5) No mineral(stretching)lineations occur, because they again require crystalplastic, ductile deformation.

(6) Fabrics developed under flattening strain, typical for a diapir (*Schmeling* et al. 1988).

In the Ludwigshöhe granite samples, no penetrative, ductile, solid-state deformation can be observed in the foliation forming minerals hornblende, biotite and K-feldspar. This is another strong argument against solid-state deformation and supports a magmatic origin of the planar fabric. Biotite just displays undulose extinction but no polygonization. Plagioclase and K-feldspar only show brittle deformations like cracks along preexisting crystallographic traces, often healed with quartz (Fig. 2d). Such healing and consequently the fractures could have developed already during the magmatic state. The lack of freely in the matrix floating feldspar fragments with disrupted zonation patterns argues against penetrative hypersolidus brittle deformation of the feldspars. Twinning is common in both the feldspars as

Albite- and Perikline-twins in plagioclase and Karlsbad-twins in K-feldspar as well as in hornblende. Twins mostly are oriented parallel to the minerals‘ flat faces and, therefore, parallel to the magmatic foliation and banding, which sensu *Paterson* et al. (1989) is indicative for a magmatic development.

Quartz is the only mineral, which displays penetrative, ductile deformation structures, ranging from undulose extinction, deformation bands, deformation lamellae and subgrains to a penetrative recrystallized fabric (Fig. 2e). All these microfabrics can develop in a crystal mush between the RCMP and the solidus as HT ”solid-state“ fabrics under high strain rates, or due to subsolidus, solid-state deformations during a late stage in a temperature range between 300 °C (quartz recrystallization) and about 350 °C (biotite undulose extinction) (*Voll* 1960). The most important deformation mechanism in quartz is prism-<a>-glide, which according to *Kruhl* (1996) is typical for deformation in a medium temperature regime (T < 575 °C, P = 0 kbar; T < 800 °C, P 10 kbars). Additionally, relictic subgrains with a chessboard pattern can be observed, pointing to a combined prism-<c>- and basal-<a>-glide. *Kruhl* (1996) interpretes this as a high temperature deformation mechanism (T > 575 °C, P = 0 kbar; T > 800 °C, P 10 kbars). Summarizing, all these observations clearly prove a crystalplastic deformation of quartz. The chessboard pattern on the one hand probably developed under high temperature conditions, perhaps during the transition from magmatic to solid-state conditions (*Kruhl* 1996). Our own pressure data, obtained from Al-in-hornblende barometry (*Schmidt* 1992, *Anderson* and *Smith* 1995) support this idea: pressures range from 4.1 to 4.5 kbars (*Stein* and *Dietl* 2000, same volume). Related temperatures which are necessary to form chessboard patterns are c. 680 °C, derived from the quartz fabric thermobarometer by *Kruhl* (1996), i.e. close to the wet granitic solidus. The most obvious quartz fabric on the other hand may have either developed together with this chessboard pattern under higher temperatures and higher strain rates, or late as result of low temperature solid-state deformations.

Cathodoluminescence investigations

Since quartz is one of the most deformation-sensitive rock forming minerals, whose luminescence colours reflect its magmatic or metamorphic origin (*Zinkernagel* 1978), first priority of cathodoluminescence investigations was given to this mineral. *Zinkernagel* (1978) describes blue or violet colours which are related to a HT-magmatic origin and reddish to brown colours indicating a LT-metamorphic imprint. *Götze* (1996) interpretes 0-dimensional lattice defects as being responsible for the luminescence of quartz. *Yacobi* and *Holt* (1990) distinguishes an initial and a final luminescence, respectively, the first caused by the already existing lattice defects, the latter resulting from lattice defects due to the interaction of the electron beam with the sample.

Cathodoluminescence investigations at quartz of the granite and the enclaves just show blue initial luminescence colours changing to stable violet final colours after a few seconds. This supports a high temperature crystallization, probably in a magmatic state (*Zinkernagel* 1978, *Sprunt* and *Nur* 1979), without any intense LT-metamorphic overprint. Thinking of the conspicious ”solid-state“ quartz fabric, this clearly indicates the HT-magmatic origin. Since quartz just fills out interstitial positions, it must have crystallized late during the magmatic stage and consequently its fabrics develops close to the solidus, either during the latest magmatic state or during the earliest subsolidus state.

Both the feldspars show a concentric zonation with euhedral, in case of plagioclase An-rich cores. They dissolve antiperthitic respectively perthitic, which again points to a magmatic or to a granlulitic origin. Since no granulites have been described from the Odenwald so far, a subsolidus nature of these fabrics can be excluded Given the very different luminescence colours of the leucocratic minerals, cathodoluminescence investigations make a good preferred shape orientation of plagioclase parallel to the foliation in both the granite and the enclaves visible.

Besides, some other fabrics also point to an early high temperature, probably magmatic history. At the granite/enclave contact the finegrained quartzdioritic enclave material flows ductilely around medium to coarse-grained K-feldspar phenocrysts and

matrix minerals of the granite, displaying a good example for a hypersolidus deformation during the magmatic state (Fig. 2f).

Strain/shape orientation analyses

The strain/shape orientation analyses were carried out with a VIDS image analysis and the program VIDS V, using the R_f/Φ-method (*Ramsey* and *Huber* 1983). The computer program RS PLOT, which is based on the geological strain analysis of *Lisle* (1985) was used for data processing and their evaluations. The triaxial strain ellipsoids were calculated by the computer program TRISEC.

The R_f/Φ-method (*Ramsay* 1967) resp. the modified method after *Lisle* (1985) is a good tool to determine deformations of elliptical markers in heterogeneously strained rocks as well as possible preexisting orientations. For a lot of these markers have a predeformational eccentricity (shape factor), their final shapes or axial ratios do not consequently coincide with the shape and orientation of the strain ellipsoid, but are due to a combination of the shape factor and the superimposed strain (*Lisle* 1985). Two theoretical end members of elliptical markers are possible: (1) randomly oriented markers with the same shape factor, and (2) parallel oriented markers with a random shape factor. According to *Lisle* (1985) asymmetric R_f/Φ-plots with a low symmetry index (I_{sym}) are characteristic for a preexisting preferred orientation of the elliptical markers.

Strain analyses, or more precisely, shape orientation analyses were carried out seperately for the matrix minerals quartz, plagioclase, biotite, hornblende, and the K-feldspar phenocrysts in three perpendicular oriented thin sections and polished slices of the granite as well as of the enclaves. Usually, the March-method (*March* 1932) is used for strain measurements at hornblendes and micas, because these minerals do not really fulfill the basic requirements of the R_f/Φ-method. In our case no deviatoric- or volume strain should be determined, we just focus on the shape orientations of magmatic

minerals, therefore the Rf/Φ-method is an applicable tool. For comparison with these results, the enclaves' shapes were used as strain ellipsoids as well. As microfabrics and mineral dependent inclusions proved, the investigated minerals crystallized during different stages of the magma´s solidification history, therefore they display different increments of the magmatic strain history. Though quartz shows a strong crystalloplastic solid-state deformation, including subgrain rotation and recrystallization, it was possible to use it for a minimum strain estimation, because cathodoluminescence made the old magmatic grains visible again.

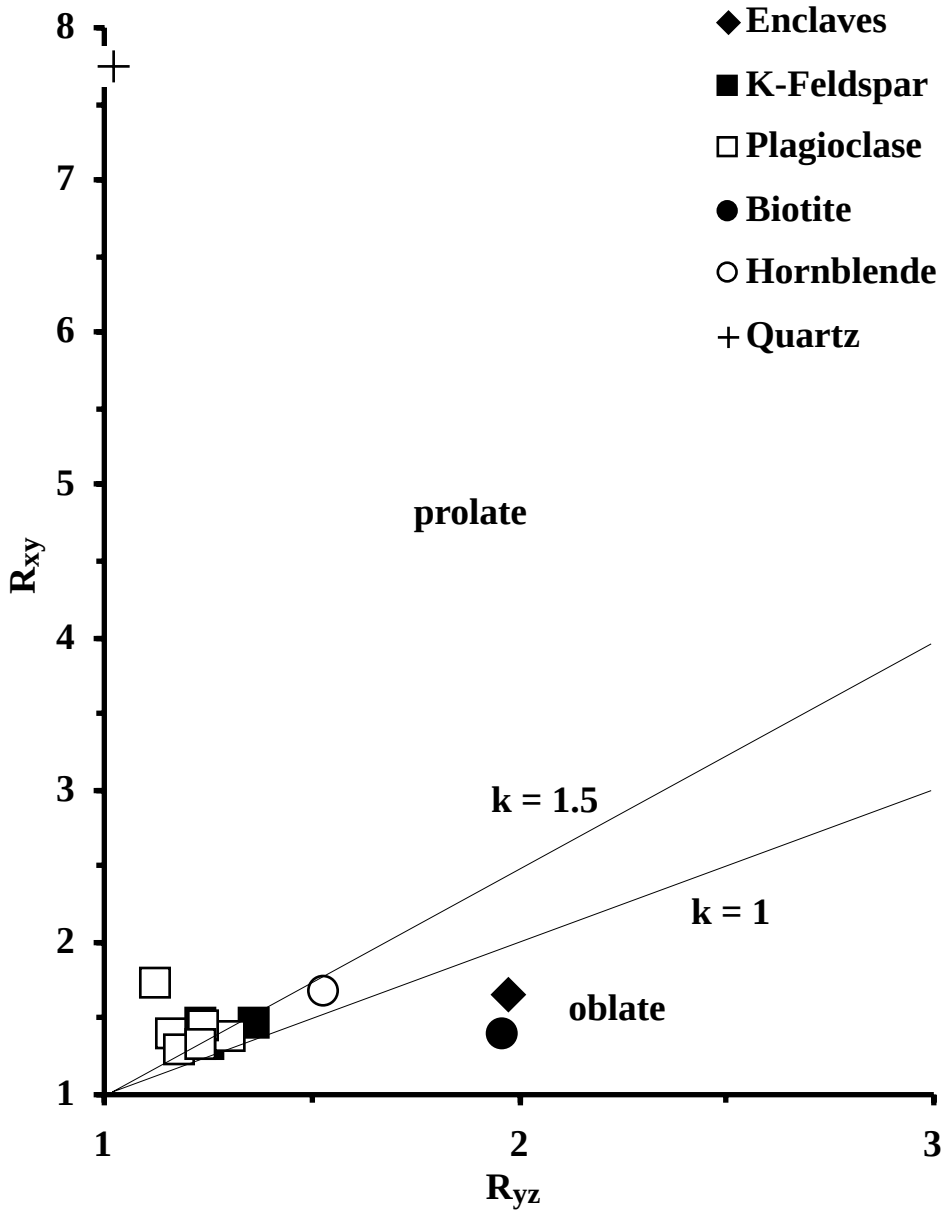

Fig. 3: *Flinn-diagram for the strain/shape orientation ellipsoids of the porphyritic Ludwigshöhe pluton.*

1. Shape orientation of K-feldspar phenocrysts

Due to their euhedral shape the K-feldspar phenocrysts are interpreted to crystallize in the

presence of a high percentage of melt well above the RCMP and therefore early in the soldification history (*Vernon* 1986), but late in the crystallisation sequence of the constituents of the Ludwigshöhe granite. Therefore they might display the entire magmatic and subsequent solid-state strain increments. On the other hand their euhedral shapes with an only weak brittle to ductile overprint along crystallographic traces, like twins or microcracks, give rise to an intense shape oriention during the magmatic state without a later, strong solid-state imprint. The K-feldspar phenocrysts are characterized by low symmetry indices, pointing to an already preexisting, preferred orientation. Their shape orientation ratios are low and range between R_s=1.3 and R_s= 1.7, which nearly coincide with the shape factor of average euhedral K-feldspars. The xy-planes of the finite shape orientation ellipsoids either dip steeply to the SE (152/64), which generally is parallel to the magmatic foliation. All their ellipsoid axes are well defined, λ_1 as the magmatic lineation is moderately plunging to the ENE (083/36), λ_2 is moderately plunging to the SW (216/43), and λ_3 as pole to the xy-plane either plunges gently to the NW (332/26). All the shape orientation ellipsoids are prolate, plotting in the constrictional field of the Flinn diagram, with K-values ranging from 1.32 to 2.04.

2. Shape orientation of plagioclase

Mostly the plagioclases of the granite and of the enclaves are euhedral as well. According to their scarce mineral inclusions they are also interpreted as early crystallized phases, during the solidification of the granite, displaying a comparable history of strain increments. Generally their shape orientation data show a bigger spread than those of the K-feldspars. The finite shape orientations of plagioclase in the granite as well as in the enclaves are characterized by low symmetry indices, again pointing to a preexisting fabric. Their shape factor ratios are slightly different in the granite (R_s=1.3 to R_s= 1.6) and the enclaves (R_s=1.3 to R_s= 6.2). All the finite shape orientation

ellipsoids are prolate, their K-values range from 1.32 to 6.17, plotting in the field of apparent constriction. Their xy-planes are steeply dipping either to the ESE (118/40), generally lying parallel to the weak, macroscopic ”foliation”. λ_1 as the magmatic lineation plunges steeply to the ESE (104/39), λ_2 gently to the SW (199/07), and λ_3 as pole to the xy-plane of the finite ellipsoid plunges steeply to the NW (298/50).

3. Shape orientation of hornblende

The hornblende measurements show a low symmetry index (I_{sym} = 0.1), which again is interpreted as a strong ”predeformational”, preferred orientation, caused by magmatic flow. The finite ellipsoid is prolate as well, with an K-value = 1.28. The axes of the shape orientation ellipsoid as well as the xy-plane show very similar orientations to the plagioclase ellipsoids. λ_1 is moderately NE plunging (070/28), λ_2 steeply SW (234/61), and λ_3 shallowly NW (336/07). The resulting, steeply SE dipping xy-planes (156/83) again lie parallel to the visible foliation.

4. Shape orientation of quartz

The quartz measurements were carried out at cathodoluminescence microphotographs, which made the originally magmatic quartz grains visible again. The results show a low symmetry index (I_{sym} = 0.19) as well, pointing to a predeformational, preferred orientation (*Lisle* 1985). This might be due to magmatic flow, which is recorded by all the constituents. The observed, penetrative deformations of quartz, described above, are responsible for the prolate shape of the finite strain ellipsoid and the extremely high K-value of 335.13. The xy-plane of the finite ellipsoid is oriented parallel to the magmatic foliation and dips moderately to the SE (131/38) with λ_1 moderately plunging to the ESE (101/34), λ_2 gently to the SSW (201/15), and λ_3 steeply to the NW (311/52).

5. Shape orientation of biotite

The symmetry index for the shape orientation ellipsoid of biotite is very low, again indicating a predeformational preferred orientation of the biotites. The orientation of the main ellipsoid axes are λ_1 = 146/73, λ_2 = 040/05, and λ_3 = 309/16, resulting in a xy-plane steeply dipping to the SE (129/74). The shape orientation ellipsoid has a K-value = 0.42, which reflects the typical habit of mica with its oblate shape.

6. Shape orientation of the enclaves

Three perpendicular photos of enclaves in a klippe are used for strain measurements, two of them result in R_S-values of 2.0 , the third one has a R_S-value of 2.4. Again, as for the investigated minerals, the symmetry index is low, probably due to a predeformational orientation into a magmatic flow fabric. With a K-value = 0.68 the ellipsoid plots in the Flinn diagram in the field of apparent flattening. The xy-plane of the strain ellipsoid lies parallel to the magmatic foliation and dips steeply to the SE (144/56) with λ_1 = 121/54, λ_2 = 227/11, and λ_3 = 324/34.

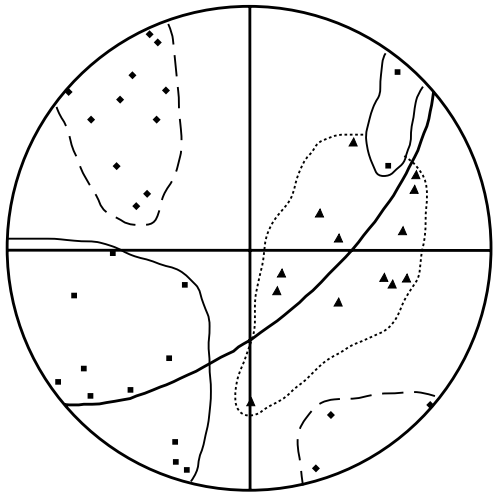

13 ellipsoids

Fig. 4: *Stereoplot with the axis and the mean plane of the strain/ shape orientation ellipsoids (x-axis = ▲ inside the hatched line; y-axis = ■ inside the drawn line; z-axis = ◆ inside the dashed line).*

The shape orientation ellipsoids of the different minerals plot in different fields of the Flinn diagram, due to their habits. While hornblende, plagioclase, K-feldspar and quartz mostly are prolate, plotting in the field of apparent constriction, biotite shows oblate ellipsoids, which plot in the field of apparent flattening. Generally all the measured K-values range in between 1.3 and 2.6, only quartz has a significant higher one (K = 355.13), due to its penetrative, ductile deformations (Fig. 3). Derived from empirical data, it can be assumed that K-values 1.5 are rather controlled by the mineral´s shape than by

deformations, because such a weak deformation will not develop a pronounced solid-state deformation fabric. The ellipsoids of the microdioritic enclaves are oblate, indicating a synmagmatic flattening during the ascent or emplacement of the granite. The xy-planes of all ellipsoids lie parallel to the average magmatic foliation, which may be explained by the fact, that both are of the same magmatic origin (Fig. 4).

The anisotropy of the magnetic susceptibility (AMS)

According to *Hrouda* (1982) and *Bouchez* (1997) the measurement of the AMS is a good tool to prove weak fabrics, e.g. magmatic foliations and lineations or to compare intensities and orientations of magmatic fabrics. The magnetic susceptibility κ determines the degree of magnetization M for a given material under the influence of an external magnetic field H according to the equation:

$$M = \kappa \cdot H$$

with: M [Ampere/meter]; H [A/m]; κ dimension-less [SI]

Generally a combination of 5 different types of magnetism determine the AMS of rocks: dia-, para-, ferro-, antiferro and ferrimagnetism (for a detailed description see *Tarling* and *Hrouda* 1993). Only para- and ferrimagnetism are of particular interest for geological purposes. Paramagnetic susceptibility is positive and ranges between 10^{-5} and 10^{-6} SI as well. Typical paramagnetic rock forming minerals contain several weight % of Fe, Ni, Co, like hornblende, biotite and ilmenite (at room temperature). Ferrimagnetic minerals are characterized by antiparallel magnetic momentums with different intensities, resulting in a susceptibility range from 10^{-2} to 10^{1} SI. Typical examples are magnetite and pyrrhotine**.**

The magnetic susceptibility of minerals is an anisotropic property, which either depends on the orientation and length of the crystallographic axes (crystal anisotropy), or on the mineral´s shape (form anisotropy). All dia-, para- and some ferromagnetic minerals have a crystal-anisotropy controlled magnetic susceptibility, whereas cubic ferrimagnetic minerals (e.g. magnetite) are form anisotrope.

The AMS is a symmetric second order tensor. The eigen values of the tensor matrix κ_{11}, κ_{22} and κ_{33} are the main susceptibilities and represent -similar to the strain ellipsoid- the 3 orthogonal main axes of the AMS ellipsoid k_X k_y k_z. Long (k_X) and intermediate (k_Y) axes spread out the magnetic foliation plane, while k_X represents the magnetic lineation. To standardize the description of AMS ellipsoids *Hrouda* (1982) defined following parameters: (1) foliation factor $F = k_y / k_z$; (2) lineation factor $L = k_x / k_y$; (3) anisotropy factor $P = k_x / k_z$; (4) corrected anisotropy factor $P' = \sqrt[2]{2(\ln\kappa_{max} - \ln\bar{\kappa})^2 + 2(\ln\kappa_{int} - \ln\bar{\kappa})^2 + 2(\ln\kappa_{min} - \ln\bar{\kappa})^2}$, with $\bar{\kappa}$ = mean susceptibility; (5) form factor T = (ln F - ln L)/(ln F - ln L). P respectively P´ stands for the grade of anisotropy of the magnetic fabric as a result of the strain intensity, caused by deformations in solid or magmatic state., using the degree of ellipticity, which is defined by the main axes of the AMS ellipsoid, while T describes the ellipsoids shape. It is oblate for T values > 0 and prolate for T values < 0. P´ describes the degree of anisotropy

The most useful graphical depiction to describe and interprete AMS data is the Jelinek diagram (*Jelinek* 1981), in which P´ (x-axis direction) is plotted against the form factor T (y-axis).

AMS measurements were carried out with a Kappabridge KLY-2 (*Jelinek* 1980) at the Geology Department of Heidelberg University under following conditions:
(1) room temperature T = 20 °C; (2) magnetic field H = 300 A/m (weak magnetic field); (3) sample cylinders with a height of 2.08 cm and a diameter of 2.54 cm have an approximate sample volume of about 10 cm^3.

Magnetic susceptibility is measured in 15 positions and the AMS ellipsoid is calculated with the ANISO14g computer program (*Jelinek* 1977).

In total 33 samples of granite and enclaves were measured. Due to their lithological composition they were divided into 4 groups: enclaves (15 cylinders), schlieren (4 cylinders) granite (7 cylinders) granite with schlieren (7 cylinders).

The AMS data of the different samples display two data sets with respect to the measured mean susceptibility: the first one from a quartzdioritic enclave yields a $\bar{\kappa}$-

value of $6 \cdot 10^{-4}$ SI, which is typical for a susceptibility, just controlled by paramagnetic minerals. Referring to thin-section observations and to microprobe analyses hornblende, biotite, ilmenite and hematite but no magnetite are responsible for the magnetic susceptibility in this enclave. The second set is characterized by a two magnitudes higher mean susceptibility, with average values ranging from $1 \cdot 10^{-2}$ to $8 \cdot 10^{-4}$ SI, which cannot be explained with paramagnetic minerals exclusively. Besides biotite, hornblende, titanite, ilmenite and hematite up to 1 weight-% Ti-magnetite can be proven in the samples of the granite and the schlieren by microprobe analyses, which sustainably influence or even dominate the magnetic susceptibilities and cause the high $\overline{\kappa}$ –values.

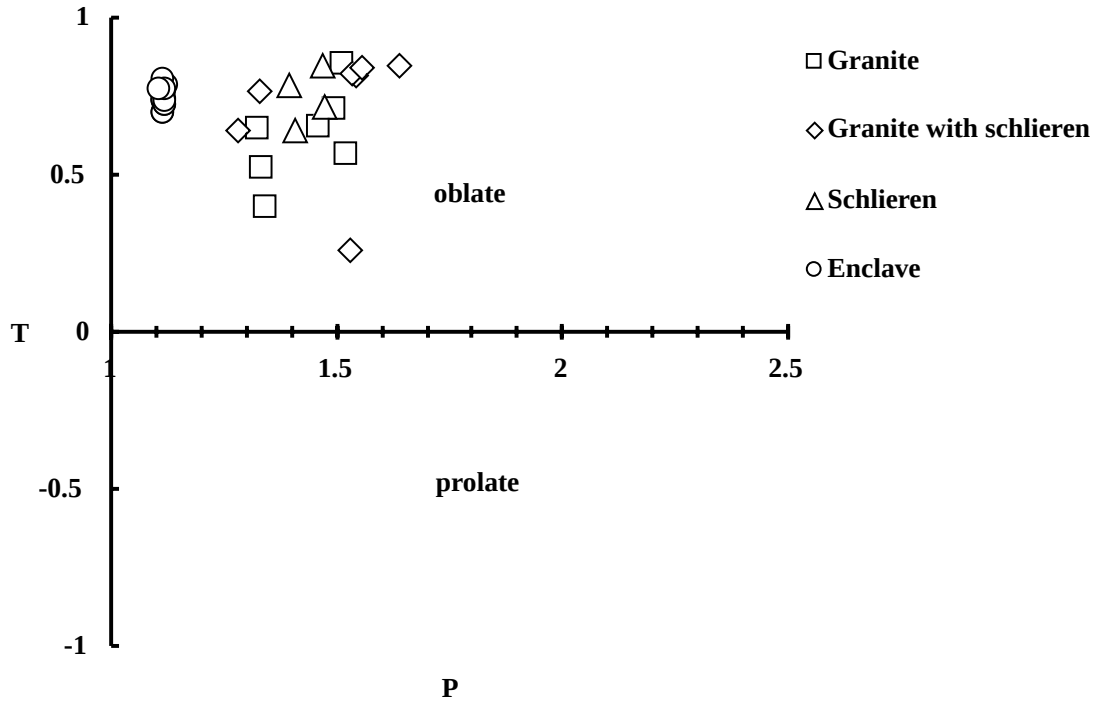

Fig. 5: *Jelinek diagram for the porphyritic Ludwigshöhe pluton.*

Plotted in the Jelinek diagram (Fig. 5) (*Jelinek* 1981) all the samples of the porphyritic Ludwigshöhe granite have oblate AMS ellipsoids, as well as oblate shape orientation and strain ellipsoids, which developed during flattening processes under a coaxial strain. With respect to the anisotropy factor P´, again all the samples verify the above described seperation into two data sets: granite and schlieren yield P´ values between 1.27 and 1,.63, the special quartzdioritic enclave of about 1.1. According to

Hrouda (1982) AMS fabrics in magmatic rocks with P´ 1.1 are due to magmatic flow, whereas magnetic fabrics with P´ 1.1 develop during magmatic or solid-state deformations. Referring to Hrouda´s interpretation, the AMS of the enclave represents a flow fabric, whereas the higher P´ in the granite and the schlieren should be due to deformations. Because no penetrative ductile solid-state lattice deformations can be proven in the foliation forming minerals, the AMS fabric should be mostly caused by deformations in the magmatic state.

Another important factor, which influences the anisotropy factor (P'), does not only depend on magmatic or solid-state deformations, but is mainly controlled by the magnetic mineralogy, described by the mean susceptibility $\overline{\kappa}$. The enclave, just containing paramagnetic minerals as carrier of the susceptibility with a $\overline{\kappa}$ = $6 \cdot 10^{-4}$ SI, shows much smaller P´ values than the magnetite bearing granite and schlieren with $\overline{\kappa}$ = $1 \cdot 10^{-2}$ to $8 \cdot 10^{-4}$ SI.

In the stereo net projection (Fig. 6) the main AMS ellipsoid axes k_x, k_y and k_z of all samples are well defined, k_x as magnetic lineation gently plunges to the ENE or WSW, k_y steeply to the S and k_z again gently to the NNW (and in 3 cases to the SSE). The derived average magnetic foliation of all the AMS ellipsoids strikes ENE-WSW, steeply dipping to the SSE. Obviously it lies (sub-)parallel to the mesoscopic magmatic foliation and the xy-plane of the finite shape orientation ellipsoids.

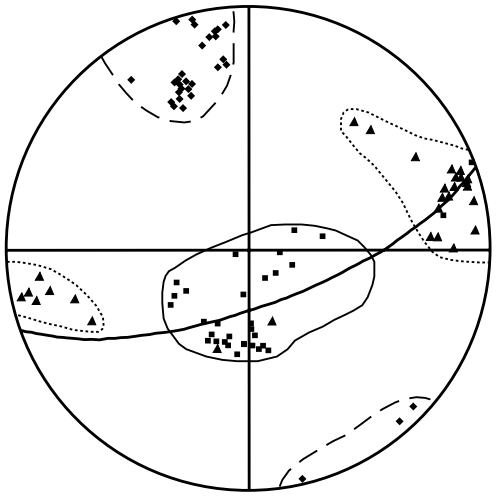

33 ellipsoids

Fig. 6: *Stereoplot with the axis and the mean plane of the AMS ellipsoids (x-axis = ▲ inside the hatched line; y-axis = ■ inside the drawn line; z-axis = ◆ inside the dashed line).*

Quartz-c-axes measurements

900 measurements were carried out at recrystallized quartz grains of the porphyritc Ludwigshöhe granite on a four axial ZEISS-U-stage at 3 sets of 3 perpendicular thin

sections. The data are plotted in one stereo net with respect to the main axes of the average shape orientation ellipsoid, as shown in Fig. 7. The N-S direction corresponds to the z-axis of the reference ellipsoid, its E-W direction to the x-axis.

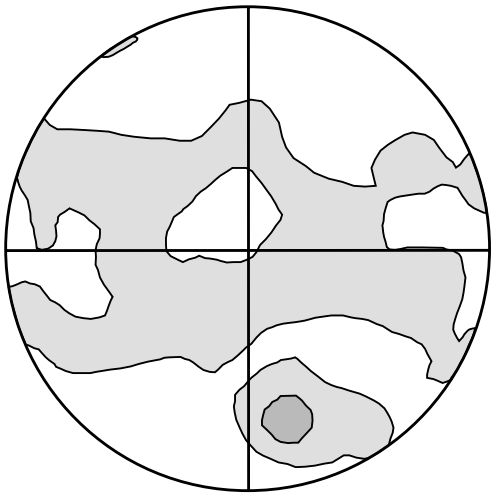

Fig. 7: *Quartz-c-axis patterns in the porphyritic Ludwigshöhe granite applied to the xz plane of the mean strain ellipsoid (x-axis: E-W, z-axis: N-S); number of measurements: 900; maximum density: 3.67 %.*

The porphyitic Ludwigshöhe granite shows only very weak quartz-c-axes patterns, representing pseudo-two-girdle distributions (*Sander* 1950), subordinate a maximum V distribution (*Sander* 1950) occurs. The cone axes of both small circle distributions are shifted against each other by an angle of about 30°. Compared with the shape orientation and AMS ellipsoids the pseudo-two-girdle pattern is nearly coaxial to the xy-plane and magnetic foliation, respectively.

Two different models yield reasonable interpretations for the quartz-c-axis patterns like those, measured at samples of the Ludwigshöhe granite:

- Internal rotation of the crystal lattice by dislocation creep and the activation of preferrred slip systems on prism and basal planes (”easy glide”),
- Stress oriented crystal growth.

According to the first one pseudo-two-girdle distributions develop during an axisymmetric shortening (*Carter* et al. 1964, *Green* et al. 1970, *Tullis* et al. 1973) under flattening conditions (*Schmid* and *Casey* 1986). The opening angle of this small circle distribution increase with increasing temperature and decreasing strain rate (*Tullis* et al. 1973, *Kruhl* 1998). Same authors derive pseudo-two-girdle distributions from a combined basal and prism glide. Point maxima are typical quartz-c-axes fabrics, which develop during shear deformations (*Vollbrecht* 1981).

Under a stress field crystals adjust their axis of maximum compressibility parallel to the maximum compressive stress (*Kamb* 1959, *Brace* 1960).

According to these models, the pseudo-two-girdle quartz-c-axes fabric of the Ludwigshöhe granite must be interpreted as result of an axisymmetric shortening under flattening conditions. Consequently, this quartz-c-axes fabric developed under the same stress regime, which is responsible for the magmatic foliation defined by the shape orientation of biotite, hornblende and K-feldspar phenocrysts, and to a lesser amount of plagioclase, quartz and the enclaves as well as the magnetic fabrics. Since opening angles of c-axes-patterns depend on temperature and strain rate, the 140° angle in the Ludwigshöhe granite argues for low strain rates and temperatures close to the wet granitic solidus of c. 680 °C. According to *Kruhl* (1998) an opening angle of 140° is related to a temperature of at least 800 °C. This correlates very well with the results of the cathodoluminescence investigations. Despite this quartz–c-axes fabric is just derived from recrystallized quartz grains it yields similar temperatures as the chessboard patterns, which implies that both quartz fabrics are cogenetic. Furthermore chessboard patterns as well as pseudo-two-girdle distributions are due to a combined prism-<c>- and basal-<a>-glide. (*Tullis* et al. 1973, *Lister* et al. 1978, *Kruhl* 1996). From all the described observations and results it must be concluded that the quartz fabric is closely related to all the other subfabrics, and therefore to the emplcement of the Ludwigshöhe granite.

Only the observed maximum V fabric with its obliquity with respect to the pseudo-two-girdle fabric can probably be explained by postmagmatic solid-state deformation under a sinistral shear movement, which is wellknown from other solid-state deformations and quartz fabrics all over the Flasergranitoid Zone (*Stein* 1996, 2000).

Summary of the results:

- The Ludwigshöhe pluton is an I-type granite,
- inclusion relations point to a normal magmatic crystallization succesion,
- antiperthitic dissolving indicates a magmatic origin of plagioclase,

- blue initial and violet final cathodoluminescence colours, quartz-c-axis patterns and chessboard microfabrics prove the high temperature probably magmatic nature of quartz,
- the observed twinning parallel to the flat faces of feldspars and hornblende as well as the pancake shaped enclaves and their highly ductile behaviour at the contact to the granite are typical magmatic fabrics,
- quartz is the only mineral showing ductile ”solid-state“ fabrics, which mostly are interpreted as result of HT-deformation close to the solidus and only sobordinately of LT-overprint,
- the orientation of plagioclase, hornblende and biotite in a planar fabric is not the result of a penetrative ductile solid-state deformation,
- the visible planar fabric is a magmatic foliation parallel to a weak magmatic banding,
- all investigated fabrics were developed under the same NW-SE directed stress field in a flattening regime. Flattening is typically associated with the rise of a diapiric pluton (*Schmeling* et al. 1988).

Conclusions and discussion

According to thin section observations and microprobe investigations the mineral assemblage of the porphyritic Ludwigshöhe granite is typical for an I-type granite, which originated due to subduction processes at the northern margin of the Saxothuringian as part of a magmatic arc (e.g. *Henes-Klaiber* 1992, *Kreher* 1994). Plutons in the Flasergranitoid Zone intruded during a short period of time and are associated intimately with each other (*Stein* 2000). The Ludwigshöhe granite with its distinct lithology and its microdioritic enclaves is a good example for the close relationship between different plutons: As described above, the enclaves can be derived from the adjacent Felsberg quartzdiorite and were preserved by magma mingling processes of the granitic and the quartzdioritic magma, due to viscosity contrasts between them.

Microfabric observations and shape orientation analyses of plagioclase, K-feldspar, biotite and hornblende do not prove any crystalplastic, just brittle deformations of those minerals. According to the criteria of *Paterson* et al. (1989), all these subfabrics are due to magmatic deformations. Shape orientation analyses indicate, that the affecting strain generally was low, because the axial ratios of the finite ellipsoids display the undeformed habits of the investigated minerals. The alignement of minerals developed under the same NW-SE directed strain field.

Only quartz displays ductile ”solid-state“ deformations like undulose extinction, deformation bands and lamellae, subgrains and penetrative grainsize reduction by dynamic recrystallization. The ductile quartz fabric mostly developed at the solidus just before or immediately after the complete solidification of the granite and therefore is labeled as ”solid-state“. This is proven by the pseudo-two-girdle distribution as main quartz-c-axes fabric, the chessboard pattern and the blue to violet luminescence colours which characterize a contemperaneous high temperature, probably magmatic development under axisymmetric conditions.

All the AMS ellipsoids and the strain ellipsoids of the enclaves are oblate, i.e. result from coaxial flattening. Summing up the results of the Jelinek diagram and the stereo net projection, it is obvious that potential flow fabrics (preserved in the enclave) and unequivocal magmatic deformation fabrics developed during coaxial flattening under the same NW-SE to NNW-SSE oriented strain field, contemperaneously with the magmatic foliation and the shape orientation fabrics of the investigated minerals and enclaves.

The outlined results bear important implications for the emplacement of the calc-alcaline plutons of the Bergsträsser Odenwald with special respect to the Flasergranitoid Zone. *Krohe* (1991, 1994) interpretes the abundant planar fabrics within the magmatic rocks as ductile to brittle shear zones of all scales and postulates at least the Flasergranitoid Zone as a major transtensional strike slip zone, in which all the plutons were emplacemed synkinematically. This would imply a complete continuous fabric development ranging from hypersolidus to brittle conditions.

Resulting from all our observations, however, just a late magmatic or early HT-”solid state“ history is recorded in the Ludwigshöhe granite. Only the maximum V quartz-c-axes pattern may point to a weak ductile LT-imprint, which does not support the interpretation of *Krohe*. We suggest a diapiric emplacement of the Ludwigshöhe granite, which may be supported to a minor amount by a forceful inflation of the diapir by ballooning. During this process the planar flattening fabrics of the Ludwigshöhe developed in a late magmatic state. Microdioritic enclaves, which are especially abundant at the northern contact to a quartzdiorite result from magma mingling processes during the diapiric emplacement of the granite. After the complete solidification of the pluton late solid-state shearing, which reactivated the magmatic anisotropy may be responsible for ductile lattice deformations of quartz and brittle to ductile of biotite or plagioclase.

Concluding, the Ludwigshöhe granite stands as an excellent example for the preservation of hypersolidus and near solidus fabrics.

Acknowledgements

Research was funded by the DFG (Deutsche Forschungsgemeinschaft). Special thanks go to J. Kolb for thin section preparation, to Dr. F. Gerullis, who provided the computer program RS PLOT, used for the shape orientation analyses, to Dr. H. de Wall (Heidelberg University) for her introduction to the Kappabridge KLY-2 as well as to Prof. Dr. J. Kruhl and PD. Dr. U. Altenberger for their helpful and constructive reviews.

References

Anderle, HJ, Massonne, HJ, Meisl, S, Omcken, O, Weber, K (1990) Southern Taunus Mts. In: Field-Guide to pro-conference excursion: Mid-German Crystalline Rise & Rheinisches Schiefergebirge. IGCP 233, Terranes in the Circum-Atlantic Paleozoic Orogens, Conference on Paleozoic Orogens in Central Europe - Geology and Geophysics: pp 125-148.

Anderson, JL, Smith, DR (1995) The effects of temperature and f_{O2} on the Al-in-hornblende barometer. Am Mineral 80: 549-559

Arzi, AA (1978) Critical phenomena in the rheology of partially melted rocks. Tectonophysics 44: 173-184

Blake, S, Campell, IH (1986) The dynamics of magma-mixing during flow in volcanic conduits Contrib Mineral Petrol 94: 72-81

Bouchez, JL (1997) Granite is never isotropic: an introduction to AMS studies of granitic rocks. In: *Bouchez, JL, Hutton, DHW, Stephens, WE* (eds) Granite: from segregation of melt to emplacement fabrics. Kluwer Academic Publishers, Dordrecht Boston London, pp 95-112

Brace, WF (1960) Orientation of anisotropic minerals in a stress field: discussion. Mem Geol Soc Am 79: 9-20

Carter, NL, Christie, JM, Griggs, DT (1964) Experimental deformation and recrystallisation of quartz. J Geol 72: 687-733.

Green, HW, Griggs, DT & Christie, JM (1970) Syntectonic and annealing recrystallisation of fine-grained quartz-aggregates. In: *Paulitsch, P* (ed) Experimental and natural rock deformation. Springer, Berlin Heidelberg New York Tokyo, pp 272-335

Götze, J (1996) Kathodolumineszenz von Quarz – Grundlagen und Anwendung in den Geowissenschaften. Aufschluss 47: 215-223

Henes-Klaiber, U (1992) Zur Geochemie der variszischen Granitoide des Bergsträßer Odenwaldes. Unpubl dissertation, TU Karlsruhe, 264 pp

Hrouda, F (1982) Magnetic anisotropy of rocks and its application in geology and geophysics. Geophys Surv 5: 37-82

Jelinek, V (1977) The statistical theory of measuring anisotropy of magnetic susceptibility of rocks and its application. Geofyzika Brno, 88 pp

Jelinek, V (1980) Kappabridge KLY-2. A precision laboratory bridge for measuring magnetic susceptibility of rocks (including anisotropy). Geofyzika Brno, Leaflet

Jelinek, V (1981) Characterization of the magnetic fabric of rocks. Tectonophysics 79: 63-67

Kamb, WB (1959) Theory of preferred crystal orientation developed by crystallisation under stress. J Geol 67: 153-170

Kirsch H , Kober B, Lippolt H J (1988) Age of intrusion and rapid cooling of the Frankenstein gabbro (Odenwald, SW-Germany) evidenced by $^{40}Ar/^{39}Ar$ and single-zircon $^{207}Pb/^{206}Pb$ measurements. Geol Rdsch 77: 693-711

Kossmat, F (1927) Gliederung des varistischen Gebirgsbaues. Abh Sächs Geol L-Anst 1: 1-39

Kreher, B (1994) Petrologie und Geochemie der Gabbrointrusionen des Frankensteins (Odenwald). Geol Jb Hessen 122: 81-122

Kreuzer H, Harre W (1975) K/Ar-Altersbestimmungen an Hornblenden und Biotiten des Kristallinen Odenwalds.- In: *Amstutz GC, Meisl S, Nickel E* (EDS.) Mineralien und Gesteine im Odenwald. Aufschluß Sonderbd 27: 71-77

Krohe, A (1991) Emplacement of synkinematic plutons in the Variscan Odenwald (Germany) controlled by transtensional tectonics. Geol Rdsch 80: 391-409

Krohe, A (1994) Verformungsgeschichte in der mittleren Kruste eines magmatischen Bogens - der variszische Odenwald als Modellregion. Geotekt Forsch 80: 1-147

Kruhl, JH (1996) Prism- and basis-parallel subgrain boundaries in quartz: a microstructural geothermobarometer. J Metamorph Geol 14: 581-589

Kruhl, JH (1998) Reply: Prism- and basis-parallel subgrain boundaries in quartz: a microstructural geothermobarometer. J Metamorph Geol 16: 142-146

Lisle, RJ (1985) Geological strain analysis: A manual for the R_f/Φ method. Pergamon Oxford, 99 pp

Lister, GS, Paterson, MS, Hobbs, BE (1978) The simulation of fabric development and its application to quartzite: the model. Tectonophysics 45: 107-158

March A (1932) Mathematische Theorie der Regelung nach der Korngestalt bei nichtaffiner Deformation. Z Kristallographie 81: 285-297

Paterson, S, Vernon, RH, Tobisch, OT (1989) A review of criteria for the identification of magmatic and tectonic foliations in granitoids. J Struc Geol 11: 349-363

Ramsay, JG (1967) Folding and fracturing of rocks. McGraw-Hill New York, 562 pp

Ramsay, JG, Huber, MI (1983) The techniques of modern structural geology. Vol. I: Strain analyses. Academic Press, London, 307 pp

Sander, B (1950) Einführung in die Gefügekunde der geologischen Körper. II. Teil. Springer, Wien, 409 pp

Schmeling, H, Cruden, AR, Marquart, G (1988) Finite deformation in and around a fluid sphere moving through a viscous medium: Implications for diapiric ascent. Tectonophysics 149: 17-34.

Schmid, SM, Casey, M (1986) Complete fabric analysis of some commonly observed quartz c-axis patterns. Mineral and Rock Deformation: Laboratory Studies The Paterson Volume. Geophys Monograph 36: 263-286

Schmidt, MW (1992) Amphibole composition in tonalite as a function of pressure: an experimental calibration of the Al-in-hornblende barometer. Contrib Mineral Petrol 110: 304-310

Sprunt, ES, Nur, A (1979) Microcracking and healing in granites: new evidence from cathodoluminescence. Science 205: 495-497

Stein, E (1996) Untersuchungen zur Genese der Flasergranitoid Zone des zentralen Odenwaldes - Magmatische und/oder tektonische Gefüge. Z geol Wiss 24: 573-583

Stein, E (2000) Zur Platznahme von Granitoiden - Vergleichende Fallstudien zu Gefügen und Platznahmemechanismen aus den White-Inyo Mountains, California, USA und dem Bergsträßer Odenwald. Geotekt Forsch 93: 1-330

Stein, E & Dietl, C (this volume) Hornblende thermobarometry at granitoids from the Central Odenwald (Germany).

Tarling, DH, Hrouda, F (1993) The magnetic anisotropy of rocks. Chapman and Hall, London, 217 pp

Tullis, J, Christie, JM, Griggs, DT (1973) Microstructures and preferred orientations of experimentally deformed quartzites. Bull Geol Soc Amer 84: 297-314

White, AJR, Clemens, JD, Holloway, JR, Silver, LT, Chappel, BW, Wall, VJ (1986) S-type granites and their probable absence in southwestern North America. Geology 14: 115-118

Willner, AP, Massonne, HJ, Krohe, A (1991) Tectono-thermal evolution of a part of a Variscan magmatic arc: the Odenwald in the Mid-German Crystalline Rise. Geol Rdsch 80: 369-389

Vernon, RH (1986) K-feldspar megacrysts in granites; phenocrysts, not porphyroblasts. Earth Sci Rev 23/1: 1-63

Voll, G.(1960) New work on petrofabrics. Liv a Man Geol J 2/3: 503-567

Vollbrecht, A (1981) Tektogenetische Entwicklung der Münchberger Gneismasse (Quarzkorngefüge-Untersuchungen und Mikrothermie an Flüssigkeitseinschlüssen). Gött Arb Geol Paläont 24, 122 pp

Yacobi, BG, Holt, DB (1990) Cathodoluminescence microscopy of inorganic solids. Plenum Press, New York, 292 pp

Zinkernagel, U (1978) Cathodoluminescence of quartz and its application to sandstone petrology. Contrib Sediment 8: 1-69

Authors´ adresses:

Carlo Dietl

Geologisch-Paläontologisches Institut, Universität Heidelberg, Im Neuenheimer Feld 234, D-69120 Heidelberg

Eckardt Stein

Institut für Mineralogie , TU Darmstadt, Schnittspahnstr. 9, D-64287 Darmstadt

Implications of hornblende thermobarometry at granitoids for the meaning of shear zones in the Bergsträßer Odenwald (Germany)

Hornblende-Thermobarometrie an Granitoiden des Mittleren Odenwaldes (Deutschland)

Eckardt Stein[1] & Carlo Dietl[2]

[1)] Institut für Mineralogie , TU Darmstadt

[2)] Geologisch-Paläontologisches Institut, Universität Heidelberg

With 6 Figures and 2 Tables

Received

Revised version accepted

Summary

The three major units of the Bergsträßer Odenwald (Frankenstein complex, Flasergranitoid zone and southern Bergsträßer Odenwald) are, according to literature, separated by two major shear zones. The aim of the present paper is to evaluate the importance of these sutures by comparing own new hornblende geothermobarometry data from five plutons of the Flasergranitoid zone with published PT data from the entire Bergsträßer Odenwald. Furthermore radiometric, geochemical and structural data from the literature were also used for this purpose. Temperatures were calculated with the amphibole-plagioclase thermometer and range from 600 to 800°C. Determinations of the intrusion depth, using the Al-in-hornblende barometer show most plutons to intruded in a pressure range from about 4 to 6 kbars (13 to 20 km). These data as well as radiometric, geochemical and structural data from the Flasergranitoid zone and the southern Bergsträßer Odenwald do not allow to postulate a major suture zone between these two “units“, while comparison of similar data from the Flasergranitoid zone and the Frankenstein complex verify the importance of this shear zone. Moreover, our PT data show, that the HT-LP metamorphism in the Bergsträßer Odenwald can also be interpreted as contact metamorphism and not necessarily as regional metamorphism.

Zusammenfassung

Die drei Haupteinheiten des Bergsträßer Odenwaldes (Frankensteinkomplex, Flasergranitoidzone uns südlicher Bergsträßer Odenwald), werden, nach der Literatur, durch zwei bedeutende Scherzonen voneinander getrennt. Ziel der vorliegenden Arbeit ist es, die wirkliche Bedeutung dieser beiden Suturen herauszuarbeiten. Dazu wurden eigene, neue Hornblende-Geothermobarometrie-Daten, die an fünf Plutonen der Flasergranitoidzone ermittelt wurden, mit bereits publizierten PT-Daten aus dem gesamten Bergsträßer Odenwald verglichen. Zudem wurden radiometrische, geochemische und

strukturgeologische Datensätze aus der Literatur für diesen Zweck benutzt. Kristallisationstemperaturen wurden mit Hilfe des Amphibol-Plagioklas-Thermometers errechnet und liegen zwischen 600 und 800°C. Die Bestimmung der Intrusionstiefe mit dem Al-in-Hornblende-Barometer ergab für die meisten Plutone Drücke im Bereich von 4 bis 6 kbar (13 bis 20 km). Diese , sowie radiometrische, geochemische und strukturgeologische Daten aus der Flasergranitoidzone und dem südlichen Bergsträßer Odenwald geben keinen Hinweis auf eine wichtige Suturzone zwischen diesen beiden „Einheiten“, wohingegen der Vergleich ähnlicher Daten aus der Flasergranitoidzone und dem Frankensteinkomplex die Bedeutung der Scherzone zwischen diesen beiden Einheiten hervorhebt. Unsere PT-Daten zeigen außerdem, daß die HT-LP-Metamorphose im Bergsträßer Odenwald nicht notwendigerweise als regionalmetamorphose interpretiert werden muß, sondern ebenso gut als Kontaktmetamorphose interpretiert werden kann.

Key words

Bergsträßer Odenwald, Flasergranitoid zone, amphibole-plagioclase thermometer, Al-in-hornblende barometer, shear zones, HT-LP metamorphism

Regional setting of the Odenwald

Introduction

The crystalline Odenwald, as part of a magmatic arc along the northern margin of the Saxothuringian is the largest exposure of crystalline rocks within the so-called mid-German Crystalline High. To the west it is bound by the Rhine-graben valley, to the north by the Saar-Selke trough and to the south and east it is covered by mesozoic sediments (compare Fig. 3, *Stein* this volume). The crystalline Odenwald can be divided morphologically and geologically into two parts: the smaller Böllstein gneissdome to the east and the Bergsträßer Odenwald to the west. Both are interpreted as magmatic arcs, the first of pre- to

early Variscan age (*Altenberger* and *Besch* 1993), the latter of mid- to late Variscan age (*Henes-Klaiber* 1992, *Kreher* 1994) and are separated by a major Variscan shear zone, the so-called Otzberg zone (*Hess* and *Schmidt* 1989). The Bergsträßer Odenwald, which is the subject of the present paper, consists of about 90 % calc-alkaline magmatic rocks, and just about 10 % metasediments forming narrow and distinct, NE-SW trending bands, which separate the igneous complexes. *Willner* et al. (1991) distinguish three units in the Bergsträßer Odenwald: the Frankenstein complex in the north (unit 1), the central Flasergranitoid zone (unit 2) and the southern Bergsträßer Odenwald (unit 3), which, according to several authors (e.g.*Henes-Klaiber* 1992, *Krohe* 1994, *Altherr* et al. 1999) are also parted by two important shear zones. The aim of our study was to evaluate the geotectonic importance of the postulated sutures by applying several hornblende geothermobarometers to rocks from the Flasergranitoid zone and comparison of our data with published PT data from the entire Bergsträßer Odenwald. Moreover, we used radiometric, geochemical and structural data from the literature for this purpose.

The magmatic rocks of the Bergsträßer Odenwald

Most of the igneous rocks of the Frankenstein complex and the adjacent Bergsträßer Odenwald show I-type signatures with a typical subduction related geochemistry, characterized by negative anomalies of Nb, Ta and Ti (*Henes-Klaiber* 1992). Especially radiometric data point to a different intrusion and cooling history from north to south. $^{207}Pb/^{206}Pb$-dating on single zircons (362 ±9 ma) as well as $^{40}Ar/^{39}Ar$-dating on hornblende (363 ±7 ma) and plagioclase (359 ±3 ma) of gabbros from the Frankenstein complex are interpreted as intrusion ages with a very rapid subsequent cooling history (*Kirsch* et al. 1986). Low Sr-initials (0.703) point to a mantle derived gabbroic magma (*Kirsch* et al. 1986). Radiometric data from intermediate to felsic plutonic rocks of the central and southern Bergsträßer Odenwald give evidence for a different intrusion history: the oldest data are obtained from a granodiorite of the northern parts K/Ar hornblende: 340 ma; K/Ar biotite: 330-327 ma). For the rest of the central and southern Bergsträßer Odenwald the

results are quite homogeneous, but 5-10 ma younger (K/Ar hornblende: 330-335 ma; K/Ar biotite: 323-325 ma) (*Kreuzer* and *Harre* 1975). Moreover, according to geochemical data, these felsic rocks can be derived from metaluminous crustal protoliths (*Altherr* et al. 1999).

The metamorphic rocks of the Bergsträßer Odenwald

The magmatic rocks are seperated by four narrow, several hundred meters to about 1 kilometer wide zones of metamorphic rocks, consisting of gneisses, micaschists, graphite-bearing quartzites, marbles, calcsilicate rocks and amphibolites. Characteristic mineral assemblages with sillimanite, andalusite and cordierite in metapelitic rocks and wollastonite in metacarbonates indicate a HT-LP metamorphic imprint in amphibolite-facies with average peak-conditions at about 3-4 kbars and 600-650 °C (*Okrusch* 1995). This implies a geothermal gradient of about 50 °C/km. Differences in the metamorphic history between the Frankenstein complex, characterized by anticlockwise PT paths, and clockwise ones in the rest of the Bergsträßer Odenwald were firstly described by *Willner* et al. (1991).

$^{235}U/^{207}Pb$- and $^{238}U/^{206}Pb$-datings on zircons of metasementary rocks of the central (336-337 ma) and of the southern Bergsträßer Odenwald (342 ma, 332 ma) are referred to as thermal peak of the regional metamorphism (*Todt* et al. 1995). The subsequent cooling history is derived from K/Ar*- and $^{40}Ar/^{39}Ar$ data of hornblende (343-335ma*; 334 ma) and biotite (328-317 ma*; 330 ma), worked out by *Kreuzer* and *Harre** (1975) and *Rittmann* (1984).

The geology of the Flasergranitoid zone

A zone of special interest is the so-called Flasergranitoid zone in the central Bergsträßer Odenwald, which is characterized by an intimate association of gabbros, diorites, granodiorites and granites (Fig. 1). In the northern part of the Flasergranitoid zone predominantly felsic granites are exposed, alternating with metasediments, whereas in the south basic diorites with even a few gabbros prevail with about 60 Vol.-% (*Stein* 2000). This trend is portrayed even more detailed by hornblende-diorites most abundant in the

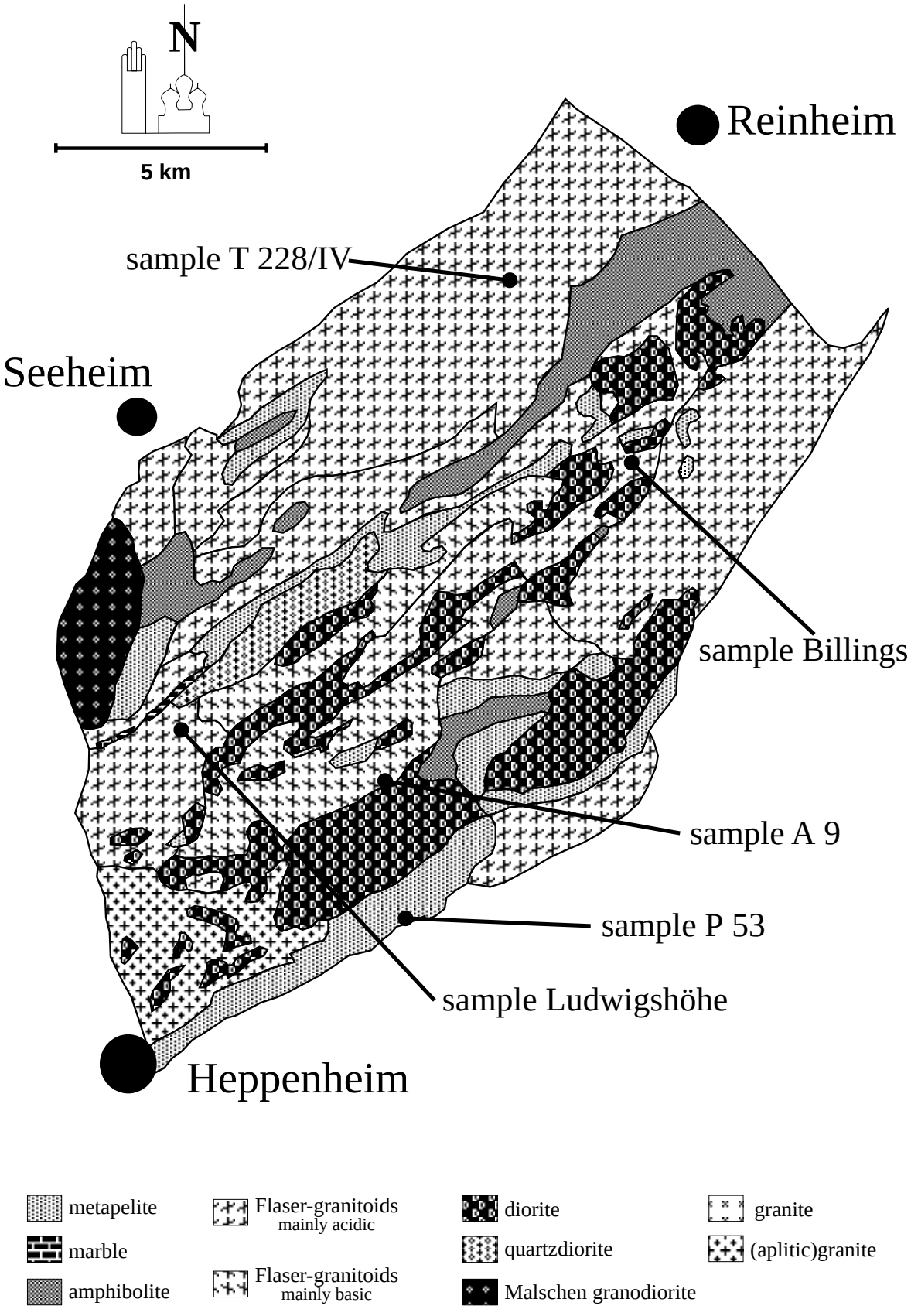

Fig. 1: *Geologic map of the Crystalline Odenwald with the sampled plutons.*

Hauptdioritzug (southern Flasergranitoid zone) with a gradual shift to biotite-diorites in the north. Therefore it can be stated, that the basicity of the magmatic rocks within the Flasergranitoid zone continuously decrease from south to north. This trend completely contradicts the general zonation of the Bergsträßer Odenwald with more basic rocks to the north and more felsic to the south (*Stein* 2000).

Most of the magmatic rocks show a pronounced planar fabric, the origin of which is still in discussion, either as tectonic, due to a syntectonic intrusion in a transtensional regime (*Krohe* 1994), or as magmatic, due to the successive emplacement of different plutons, called nested diapirs (*Stein* 2000). Another obvious trend concerns the fabric development within the magmatic rocks. In the south with the most intimate association of basic, intermediate and felsic intrusives together with metamorphic rocks clearly magmatic fabrics, like magmatic layering, magmatic foliations and magmatic lineations predominate, which are only locally overprinted by solid-state deformations (*Stein* 2000). In the northern part with its mostly granitic lithologies again magmatic fabrics occur. However, they are strongly obliterated by solid-state fabrics, concentrated in discrete ductile shear zones up to several meters thick, which are restricted to a 1.5 km wide array along the border to the Frankenstein complex. These shear zones show all possible transitions from mylonites to ultramylonites with sinistral and dextral transport directions side by side (*Stein* 2000). Sinistral strike slip zones are wellknown from all over the Bergsträßer Odenwald and described in detail from the Melibocus massif (*Altenberger* et al., this volume), but the dextral ones are especially abundant at this northern rim.

Willner et al. (1991) and *Krohe* (1994) describe, as already stated above, an important strike-slip zone as border between the Flasergranitoid zone and the south adjacent Weschnitz pluton. Therefore they divide the central and the southern part of the Bergsträßer Odenwald into two independent tectono-metamorphic units (“unit 2“ and “unit 3“), although the structural and PT data, obtained from both parts, do not significantly differ. *Henes-Klaiber* (1992) applies this model to her geochemical investigations, and derives different crustal thicknesses as possible magma sources and a continous increase of the

intrusion depth from the central toward the southern Bergsträßer Odenwald with a considerable vertical displacement at this boundary. On the first view he emplacement mechanisms seem to be quite different north and south of this border. In the southern “unit 3“ the calc-alkaline intrusions occur as large, diapiric plutons like the granodiorite of the Weschnitz pluton and the granites of Tromm and Heidelberg, whereas in the Flasergranitoid zone (“unit 2“) most of them form an intimate and complex association (*Stein* 2000).

A brief classification of the intrusives of the Flasergranitoid zone

In the Flasergranitoid zone of the central Bergsträßer Odenwald *Stein* (2000) distinguishes at least four different types of intrusions:

(1) Round to elliptical plutons with homogeneous lithologies and a clear distinction to their neighbouring rocks. They are characterized by more or less isotropic fabrics with magmatic euhedral habits of the main constituents, partly as magmatic phenocrysts, which besides quartz do not show any imprint of solid-state deformations. Typical examples are the larger Melibocus pluton and the smaller Ludwigshöhe granite.

(2) Again round to elliptical plutons with a concentric structure. They show a normal zoning with diorites at their outer shells and granites in the cores. They are characterized by magmatic fabrics with increasing intensities from the inner toward the outer parts. The most penetrative fabrics occur at lithological boundaries and decrease continuously toward the centers of the intrusions. This is also true for solid-state deformations, so that the older diorites at the outer shells are overprinted strongest by solid-state fabrics, whereas the younger granites in the core in most cases do not show any solid-state imprint. Such configurations are explained as forceful intrusions by ballooning. One of the best examples in the Flasergranitoid zone is the outcrop Billings.

(3) Ballooning-like plutons with a clear reverse zonation, with undeformed diorites in their cores and granites with intense magmatic fabrics and solid-state overprint at their

margins. This intrusion mechanism characterizes nested diapirs, which are typical for the southern part of the Flasergranitoid zone. Good examples are known from the quarry Seemann in Hochstädten or from the boundary region to the Weschnitz pluton, where samples A 9 and P 53 were from.

(4) Dykes.

Short description of the samples

The Ludwigshöhe granite (for location see Fig. 1) is characterized as light, weakly textured, medium to coarse-grained, porphyritic granite with about 2 cm large euhedral K-feldspar phenocrysts. Furthermore it contains schlieren and dark, fine-grained, microdioritic enclaves with amphibolitic or dioritic composition. They are especially abundant with about 40 Vol.-% at its northwestern margin, at the boundary to the neighbouring Felsberg quartz-diorite. The granite consists of the assemblage plagioclase An 25 (38 vol.-%), quartz (23 vol.-%), K-feldspar (21 vol.-%), biotite (12 vol.-%), hornblende (5 vol.-%) and the accessories epidote, ilmenite, magnetite, hematite, titanite, zircon and monazite.

Four main lithologies occur in the outcrop Billings (for location see Fig. 1), diorites, granodiorites, granites and porphyrs. The diorites are the only ones to fullfill the required assemblages for geothermobarometry. They are characterized by an intense, steeply inclined (326/54), magmatic foliation, which is weakly overprinted by solid-state deformations. The diorite is medium to coarse-grained with large euhedral plagioclases and hornblendes, which are parallel-oriented with their long axes within the foliation plane (332/59). The diorite consists of plagioclase An 25-40 (60-65 vol.-%), hornblende (15 vol.-%), biotite (10 vol.-%), K-feldspar, quartz and chlorite (5 vol.-% each) and zircon, ilmenite, hematite, calcite and titanite.

Krohe (1994) and *Willner* et al. (1991) interpret most of the intrusions in the entire Odenwald as syntectonic, during an intense shearing under extensional or transtensional conditions. They describe examples from the northern parts of the Flasergranitoid zone. On the contrary *Stein* (2000) observed older magmatic fabrics, which are intensively oblitered

by successive solid-state deformations under strike-slip movements. Sample T 228 IV (for location see Fig. 1) stands as example for this part of the Flasergranitoid zone. It is of granodioritic composition and shows abundant micrographic fusion of quartz and K-feldspar, growing into several cm-large plagioclase phenocrysts and myrmekites. The complete assemblage contains quartz, K-feldspar, plagioclase (An 28-33), green hornblende, ti-rich biotite, titanite, ilmenite, apatite, zircon.

Sample A 9 (for location see Fig. 1) comes from a "Flasergranodiorite" north of the Hauptdioritzug. It is characterized by a strong magmatic foliation, which is steeply inclined (318/51). The granodiorite consists of plagioclase An 25-40 (35 vol.-%), quartz (30 vol.-%), hornblende (15 vol.-%), biotite (10 vol.-%), K-feldspar, and chlorite (5 vol.-% each) and zircon, ilmenite, hematite, calcite and titanite.

Sample P 53 (for location see Fig.1) is a granodiorte from the southernmost edge of the Flasergranitoid zone, where it is associated with the metamorphic rocks of the Silbergrubenkopf area. It consists of plagioclase An 25-30 (35 vol.-%), hornblende (25 vol.-%), quartz (20 vol.-%), biotite (10 vol.-%), K-feldspar, and chlorite (5 vol.-% each) and zircon, ilmenite, hematite, apatite and titanite.

Amphiboles

As we have seen earlier, all the samples contain mineral assemblages, with a certain amount of amphiboles, which can be used as good pressure and temperature indicators in igneous rocks. Therefore several plutons of the Flasergranitoid zone were sampled, to gain insight into the magmatic history of the Central Odenwald area.

Care was taken to examine only unzoned and unaltered amphiboles of a clear magmatic origin to get undisturbed PT data for the intrusion of the individual plutons.

Nomenclature of amphiboles

According to *Leake* et al. (1997) amphiboles are classified due to their chemical compositions respectively on the number of cations on certain lattice positions. The mineral

formula calculations are based on 23 oxygens, standardized on 13 cations (without Ca, Na and K).

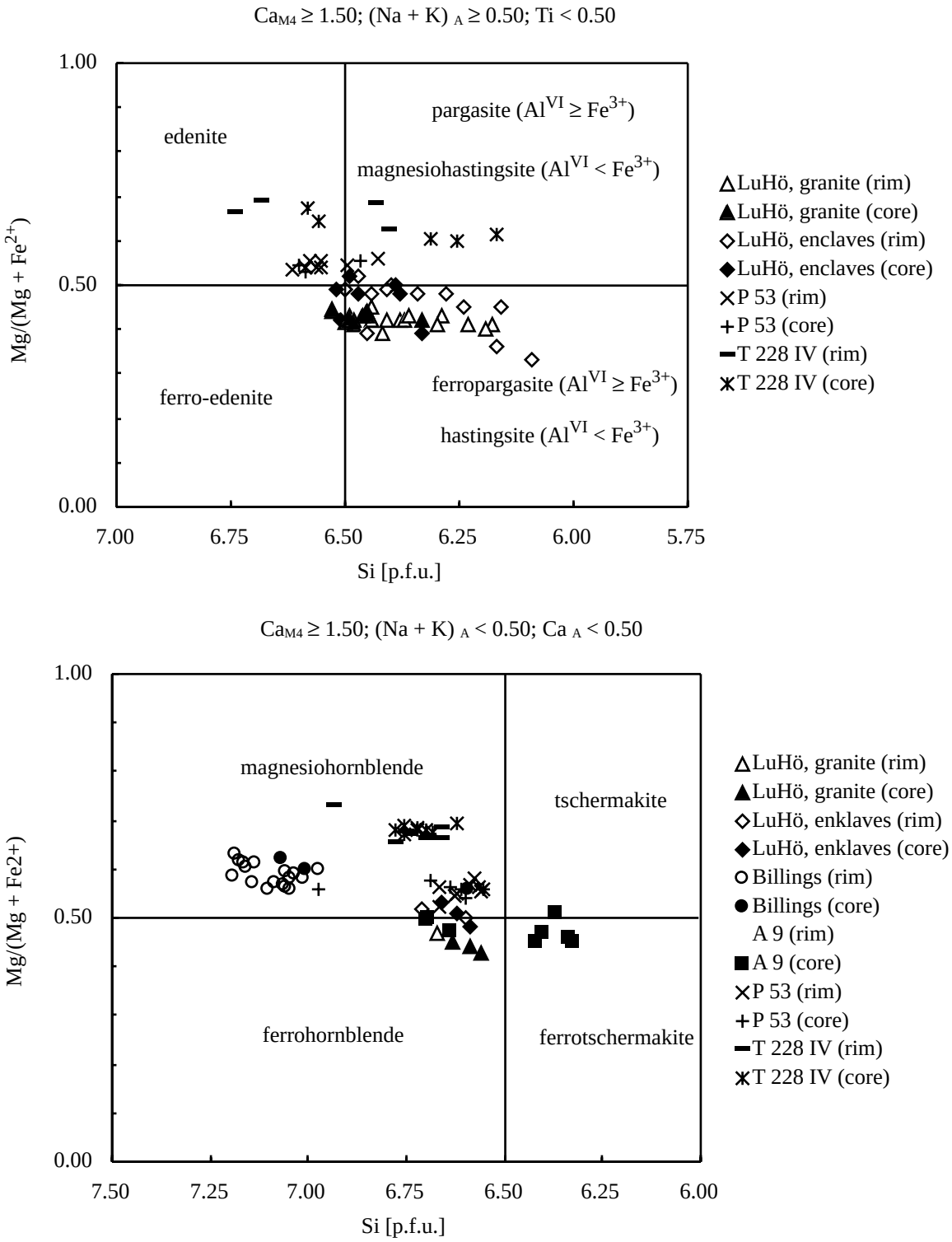

Fig. 2: *Classification of amphiboles from the investigated plutons according to the nomenclature of Leake (1997), LuHö: Ludwigshöhe.*

All the investigated hornblendes plot in the field of calcic amphiboles, which is defined by (Ca + Na) on M_4 1,00 with Na < 0,50, and Ca on M_4 1,50 (*Leake* et al. 1997). Within the calcic amphiboles *Leake* et al. (1997) distinguish 4 groups, characterized by:

a) $(Na + K)_A$ 0,50 and Ti < 0,50;

b) $(Na + K)_A$ 0,50 and Ti 0,50;

c) $(Na + K)_A$ < 0,50 and Ca_A < 0,50;

d) $(Na + K)_A$ < 0,50 and Ca_A 0,50.

The hornblendes of the examined plutons belong either to group ”a)” or ”c)” with a distinct relation to individual plutons and lithologies (see also Fig. 2): The porphyritic Ludwighshöhe granite as well as its microdioritic enclaves for the most part contain hastingsites accompanied by a small number of ferroedenites, ferropargasites and ferrohornblendes in the granite, and some ferroedenites, magnesiohastingsites, magnesio- and ferrohornblendes in the enclaves. All hornblendes of the diorites and granodiorites from the Billings quarry are magnesiohornblendes. Most of the amphiboles from sample A 9 are ferrohornblendes, but also some ferrotschermakites and one tschermakite occur. Hornblendes in sample P 53 have magnesiohornblenditic composition, but also edenites, pargasites and magnesiohastingsites occur. In the granodioritic porphyry (sample T 228 IV) mainly magnesiohornblendes are found, but also some edenites and magnesiohastingsites.

Calcic amphiboles are typical for I-type intrusives (*Chappel* and *White* 1974, *Wyborn* et al. 1981, *White* and *Chappel* 1983, *Clemens* and *Wall* 1984), supporting the results of *Henes-Klaiber* (1992).

For their compositions generally are calcic, all the different amphiboles in the following text will simply be adressed as hornblendes or amphiboles.

Thermobarometry

Amphiboles are the most useable minerals for geothermobarometric applications in calc-alkaline igneous rocks, because they occur in nearly all calc-alkaline intrusives, regardless

if mafic, intermediate or felsic compositions. They are stable over a wide P-T-range from 1 - 23 kbar and 400 - 1150 °C (Blundy and Holland 1990), which is true for all the magmatic rocks of the Bergsträßer Odenwald. A lot of those geothermobarometers are based on the Al-content of hornblende, the Al-in-hornblende-barometer (Hammarstrøm and Zen 1986, Hollister et al. 1987, Johnson and Rutherford 1989, Thomas and Ernst 1990, Schmidt 1992, Anderson and Smith 1995), for example, refers to the total Al-content of hornblende. The amphibole-plagioclase-thermometer (Blundy and Holland 1990, Holland and Blundy 1994) is controlled by the number of Si- and Al-cations on the tetraeder positions.

Factors influencing the Al-content of hornblende

The intensive parmeters pressure, temperature, oxygen fugacity, as well as the whole rock composition and the coexisting phases determine the Al-content of hornblende. According to *Hollister* et al. (1987) the tschermak substitution $Si + R^{2+} = Al^{IV} + Al^{VI}$ is pressure-sensitive. Increasing pressure intensifies the reaction and the Al-content in the hornblende lattice increases, too. Other reactions, like the edenite substitution $Si + vac^{A} = Al^{IV} + (K + Na)^{A}$ and reactions involving Ti, e.g. $Ti + R^{2+} = 2\ Al^{VI}$ and $Ti + Al^{IV} = Al^{VI} + Si$, are rather controlled by temperature (*Anderson* and *Smith* 1995). The higher the temperature, the better the efficiancy of the edenite substitution, resulting in an increasing Al-content of hornblende.

Besides these important substitutions the oxygen fugacity plays a decisive role, it controls the Fe-# {Fe/(Mg + Fe)} and $Fe^{3+}/(Fe^{2+} + Fe^{3+})$-ratios: The lower the oxygen fugacity is, the more Fe (especially Fe^{2+}) is present. *Spear* (1981) and *Anderson* and *Smith* (1995) classify a Fe-# in the range from 0 to 0.6 as high, between 0.6 and 0.8 as medium and up to 1 as low oxygen fugacity. The relationship of substitution reactions involving Al and of the oxygen fugacity is based on the fact, that a low oxygen fugacity favors the insertion of Fe^{2+} in the hornblende lattice. High amounts of Fe^{2+} with respect to Fe^{3+} preferently favors the substitution of Mg by Al during the tschermak substitution. A low oxygen fugacity therefore leads to high Al-contents of hornblende, which pretend

artificially high crystallization pressures. Therefore *Anderson* (1997) recommends just to use hornblendes with a Fe-# 0.65 for geobarometry. But on the other hand a high oxygen fugacity leads to a preferred incorporation of Fe^{3+} into the lattice, which preferably substitutes Al. This can keep the Al-content of hornblende low, again faking an artificial low pressure. *Anderson* and *Smith* (1995) therefore recommend just to use amphiboles with a $Fe^{3+}/(Fe^{2+} + Fe^{3+})$-ratio 0.25 for barometric analyses. The general disadvantage with both these criteria with respect to oxygen fugacity during the growth of hornblende and its derived usability as tool for geothermobarometry is, that they are just based on stoichiometric calculations and not on direct measurements of the Fe^{3+}- and Fe^{2+}-contents. Therefore Fe-# and $Fe^{3+}/(Fe^{2+} + Fe^{3+})$-ratios can not stand as the only criteria, determining the oxygen fugacity.

Possible futher objectives may be derived from the rock composition. According to *Ishihara* (1977) magnetite-bearing igneous rocks (so called "magnetite series") point to crystallization conditions under a high oxygen fugacity, whereas ilmenite-bearing ("ilmenite series") rather are due to a low oxygen fugacity. Moreover the abundance of titanite indicates a high f_{O2}.

Generally it can be concluded, that hornblendes crystallizing under a high oxygen fugacity give better and more reasonable results for geothermobarometry than those growing under low f_{O2}.

Factors influencing the Al-content of the investigated hornblendes

Both, the Tschermak- and the Edenite-substitution play important roles for the compositions of amphiboles of all the investigated plutons, indicating, that temperature and pressure have influenced the hornblende compositions of the Flasergranitoid zone.

The role of the oxygen fugacity during the hornblende crystallization is much more difficult to evaluate. As we have seen earlier, both criteria of *Anderson* (1997) and *Anderson* and *Smith* (1995) vigorously influence the amphiboles compositions and due to our considerations, both are true for most of the Odenwald plutons. The only exception are

hornblendes of the Ludwigshöhe pluton, where porphyritic granite and microdioritic enclaves were sampled and investigated. Results from this locality partly show too low $Fe^{3+}/(Fe^{2+} + Fe^{3+})$-ratios and a too high Fe-#.

On the other hand the porphyritic Ludwigshöhe granite stands as example for the very few magnetite-bearing granitoids of the Flasergranitoid-Zone. This composition points to a high oxygen fugacity and therefore crystallization conditions, which are suitable for the geobarometric investigations are taken into account. Generally all other sampled rocks, even some enclaves in the Ludwigshöhe granite, are characterized by the occurence of ilmenite -no magnetite- as accessorial oxide phase with small amounts of titanite, i. e. they probably crystallized under low to medium f_{O2} conditions.

Because all the amphiboles of all plutons fullfill at least one criteria for a high oxygen fugacity, all samples are used for geothermobarometry.

The amphibole-plagioclase-thermometer

General comments

Although the amphibole-plagioclase thermometer is a little bit obsolete among some petrologists, there is, due to the rock composition of the calc-alkaline intrusives, no other chance to determine its temperatures. Furthermore, according to our experience, the resulting temperatures correlate very good with independently determined temperatures at metamorphic rocks, i.e. using the garnet-biotite thermometer.

Blundy and *Holland* (1990) and *Holland* and *Blundy* (1994) published three different calibrations for their amphibole-plagioclase-thermometer: two based on the edenite-tremolite-reaction:

4 quartz + edenite = albite + tremolite,

one based on the edenite-richterite-reaction:

edenite + albite = richterite + anorthite.

Blundy and *Holland* (1990) first proposed a very simple, empirical thermometer on the basis of the edenite-tremolite-reaction, which could be applied only to quartz-bearing, intermediate to felsic igneous rocks with plagioclase An 0.92 and Si 7.8 atoms p.f.u. in hornblende. This thermometer is calibrated for a range between 500 °C and 1100 °C. It already takes into account, that the Al-content of hornblende does not only depend on temperature, but also on pressure. The thermometer can be described is by the following formula:

$$T[\pm 311K] = \frac{0.677P[kbar] - 48.98}{-0.0429 - 0.0083144 \ln\left\{\left(\frac{Si-4}{8-Si}\right) X_{Ab}^{Plag}\right\}}$$

with Si-atoms p. f. u. in hornblende and X_{Ab} in plagioclase in decimal units.

The formula presented in this paper has already been changed slightly from the original version, for it has been adopted to the plagioclase compositions, observed in the 5 plutons, just ranging from albite to andesine.

For this calibration resulted in too high temperatures for some lithologies (e. g. *Poli* and *Schmidt* 1992), *Holland* and *Blundy* (1994) recalibrated the amphibole-plagioclase-thermometer. They extended the data base to all components, which take part in the edenite-tremolite-reaction. Moreover they considered a non-ideality instead of an ideality, as it was the case for the first calibration. These changes enables an application of this thermometer A (*Holland* and *Blundy* 1994) to quartz-bearing metabasites. It now is:

$$T[\pm 313K] = \frac{-76.95 + 0.79P[kbar] + 39.4X_{Na}^{A} + 22.4X_{K}^{A} + (41.5 - 2.89P[kbar])X_{Al}^{M2}}{-0.0650 - 0.0083144 \ln\left(\frac{27X_{vac}^{A} X_{Si}^{T1} X_{Ab}^{Plag}}{256 X_{Na}^{A} X_{Al}^{T1}}\right)}$$

Additionally they calibrated a second version, thermometer B, which is based on the edenite-richterite-reaction (*Holland* and *Blundy* 1994), and which is applicable also to quartz-free magmatites:

$$T[\pm 313K] = \frac{81.44 - 33.6X_{Na}^{M4} - (66.88 - 2.92P[kbar])X_{Al}^{M2} + 78.5X_{Al}^{T1} + 9.4X_{Na}^{A}}{0.0721 - 0.0083144 \ln\left(\frac{27X_{Na}^{M4}X_{Si}^{T1}X_{An}^{Plag}}{64X_{Ca}^{M4}X_{Al}^{T1}X_{Ab}^{Plag}}\right)}$$

Although these two new thermometers can be used for a wide range of lithologies, they have one main disadvantage, they take too many components into account, which all influence the calculated temperature, and which therefore can all act as sources of error.

Again the presented formulas of thermometers A and B has slightly been changed, because they are also adopted to the An -contents of the used plagioclases.

Application of the amphibole-plagioclase-thermometer to the Ludwigshöhe and Billings plutons

As a preliminary calibration all those three different thermometers need an independent pressure estimation. Pressures determined by *Willner* et al. (1991) from outcrops close to the sampled plutons were used for this purpose (see also Tab. 1).

Willner et al. (1990)				this paper		
outcrop	P [kbars]	T [°C]	close to	outcrop	P [kbars]	T [°C]
-	-	-		T 228 IV	2.9 - 4.1	-
Helgengrund	4.4 - 4.6	560 - 660		Ludwigshöhe	4.1 - 6.2	626 - 787
Felsberg	3.8 - 4.7	550				
Rimdidim	2.7	625		Billings	1.9 - 3.0	605 - 697
Mühlberg quarry	3.0	-				
Kolmbach	-	700		A 9	4.5 - 6.0	-
Gadernheim	2.5 - 4.3	600 - 610				
Silbergrubenkopf	2.0 - 4.9	600 - 625		P 53	4.3 - 5.7	-
Oberhambach	2.7	625				

Tab. 1: *Comparison of PT data determined by Willner et al. (1991) and PT data from this study.*

This is only true for the Ludwigshöhe and Billings plutons, where pressures of PT-data from metamorphic wallrocks can be correlated with the intrusion of the plutons. Unfortunately no hornblende-plagioclase-pairs of sample P 53 were investigated, although at least one pressure value of the neighbouring Silbergrubenkopf (4.9 kbar) lie on the prograde branch of the PT-path and seems to correlate with the intrusion of the granitoids

(*Willner* et al. (1991). Pressures of the PT-data of Gadernheim, close to our sample A 9, are just displaying the retrograde development of originally MP-rocks. For no PT-data of metamorphic rocks of this region exist, no independent pressures from a directly regional context could be assumed for sample T 228 IV.

Hornblende							**Plagioclase**			
Sample	**T228IV**	**LH,g**	**LH,e**	**Billings**	**A9**	**P53**		**LH,g**	**LH,e**	**Billings**
	n = 25	n = 28	n = 26	n = 20	n = 23	n = 26		n = 38	n = 37	n = 1
SiO_2	45.13	42.04	42.19	48.41	43.30	44.26	SiO_2	61.65	60.83	60.60
Al_2O_3	8.93	10.43	10.53	7.63	10.68	10.23	Al_2O_3	25.84	26.75	28.48
TiO_2	1.62	1.18	1.10	0.90	1.11	0.96	Fe_2O_3	0.15	0.26	0.11
Cr_2O_3	0.03	0.03	0.01	0.01	0.02	0.06	SrO	0.00	0.00	0.00
MnO	0.41	0.83	0.66	0.46	0.59	0.48	MnO	0.02	0.02	0.04
MgO	12.62	7.26	8.18	11.63	8.18	10.06	MgO	0.01	0.01	0.01
FeO	11.27	17.36	16.39	14.49	16.17	14.54	TiO_2	0.01	0.02	0.00
Fe_2O_3	3.97	4.91	4.51	1.50	4.42	3.43	CaO	5.60	5.97	8.14
CaO	11.97	11.60	11.90	12.32	11.81	12.06	Na_2O	8.24	8.12	6.95
Na_2O	1.54	1.29	1.18	0.79	1.09	1.17	K_2O	0.32	0.20	0.19
K_2O	0.96	1.19	1.24	0.62	0.87	1.12	BaO	0.06	0.02	0.00
	98.44	**98.11**	**97.88**	**98.78**	**98.24**	**98.36**		**101.90**	**102.27**	**104.51**
T spaces							Z spaces			
Si	6.63	6.43	6.43	7.07	6.53	6.60	Si	10.76	10.60	10.35
Al	1.37	1.57	1.57	0.93	1.47	1.40	Al	5.31	5.49	5.73
T	*8.00*	*8.00*	*8.00*	*8.00*	*8.00*	*8.00*	Fe^{3+}	0.02	0.03	0.01
M1 - M3 spaces							*Z*	*16.09*	*16.12*	*16.10*
Al	0.18	0.31	0.32	0.38	0.42	0.39	X spaces			
Ti	0.18	0.14	0.13	0.10	0.13	0.11	Sr	0.00	0.00	0.00
Fe^{2+}	1.39	2.22	2.09	1.77	2.04	1.81	Ti	0.00	0.00	0.00
Fe^{3+}	0.44	0.57	0.52	0.16	0.50	0.38	Mn	0.00	0.00	0.01
Cr	0.00	0.00	0.00	0.00	0.00	0.01	Mg	0.00	0.00	0.00
Mn	0.05	0.11	0.09	0.06	0.08	0.06	Ca	1.05	1.11	1.49
Mg	2.76	1.66	1.86	2.53	1.84	2.23	Na	2.79	2.74	2.30
M1- bis M3	*5.00*	*5.00*	*5.00*	*5.00*	*5.00*	*5.00*	K	0.07	0.05	0.04
M4 spaces							Ba	0.00	0.00	0.00
Ca	1.88	1.90	1.94	1.92	1.91	1.93	*X*	*3.91*	*3.91*	*3.84*
Na	0.12	0.10	0.06	0.07	0.09	0.07	*spaces*	**20.01**	**20.03**	**19.94**
M4	*2.00*	*2.000*	*2.000*	*2.000*	*2.000*	*2.000*	**Cations**			
A spaces							Mol-%			
Na	0.32	0 .28	0.29	0.15	0.22	0.27	An	26.84	28.58	38.88
K	0.18	0.23	0.24	0.12	0.17	0.21	Ab	71.33	70.28	60.04
A	*0.50*	*0.52*	*0.53*	*0.27*	*0.39*	*0.48*	Or	1.83	1.14	1.08
Cations	**15.50**	**15.52**	**15.53**	**15.27**	**15.39**	**15.48**		**100.00**	**100.00**	**100.00**
Mg-#	0.67	0.43	0.47	0.59	0.47	0.55				
Mg value	0.60	0.37	0.42	0.57	0.42	0.50				
Fe^{3+}-#	0.24	0.20	0.20	0.09	0.20	0.17				

Tab. 2: *Average hornblende and plagioclase compositions of the investigated igneous rocks (LH,g: Ludwigshöhe, granite; LH,e: Ludwigshöhe, enclave).*

The pressures derived from PT-data, determined by *Willner* et al. (1991) at the Felsberg and the Helgengrund localities, close to the Ludwigshöhe pluton range from 4.4 kbars to 4.6 kbars, Again PT-data of the same authors of the Rimdidim outcrop, close to the Billings pluton with 2.7 kbars are used as database. With these independent pressure estimations the three different amphibole-plagioclase-thermometers were calibrated and applied to the the porphyritic Ludwigshöhe granite, its enclaves and the Billings pluton.

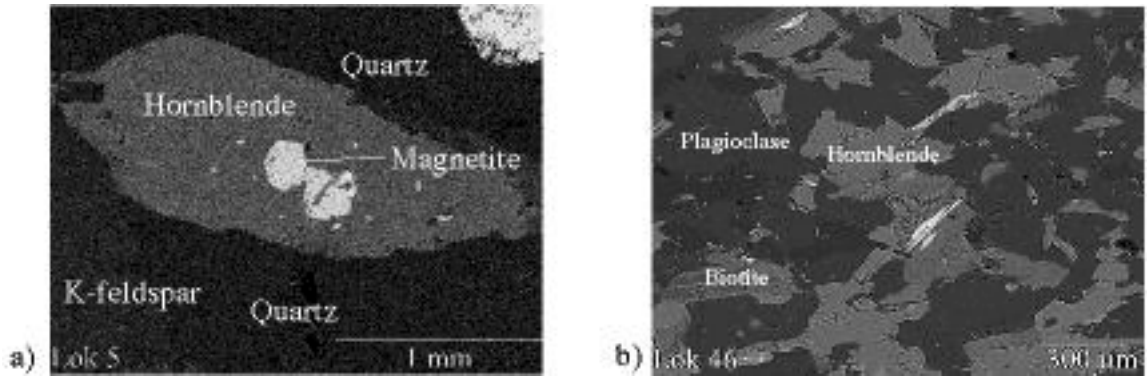

Fig. 3: *BSE photographs of typical structural and petrographic relationships between a) hornblende, K-feldspar and quartz in the porphyritic Ludwigshöhe granite and b) hornblende, biotite, plagioclase, and quartz in its microdioritic enclaves.*

Temperatures were calculated for individual hornblende-plagioclase-pairs of the different samples (4 from the porphyritic Ludwigshöhe granite, 16 from its enclaces and 2 from the Billings pluton), from which average temperatures for each locality were derived. The average plagioclase and hornblende compositions are listed in Tab. 2, typical structural relations between hornblende and plagioclase are shown in Fig. 3.

As obvious in Fig. 4, temperatures calculated with the 1990 thermometer (*Blundy* and *Holland* 1990) are significantly higher than those computed with both 1994 calibrations. Amphiboles and cogenetic plagioclases of the porphyritic Ludwigshöhe granite crystallized at temperatures of about 768 ±27 °C, the enclaves at 787 ±37 °C and the Billings pluton at 697 ±2 °C. All temperatures lie above the granitic wet solidus.

Using thermometer A (*Holland* and *Blundy* 1994) significantly lower temperatures are determined: for the porphyritic Ludwigshöhe granite T = 704 ±47 °C, for the Ludwigshöhe enclaves T = 743 ±24 °C and for the Billings pluton T = 643 ±10 °C. Even

lower temperatures were calculated, using thermometer B (*Holland* and *Blundy* 1994): for the Ludwighshöhe granite T = 626 ±65 °C, for its microdioritic enclavceT = 660 ±29 °C and for the Billings pluton T = 605 ±19 °C. But these data implie, that the resulting temperatures for all the three investigated magmatic rocks are far below the granitic solidus.

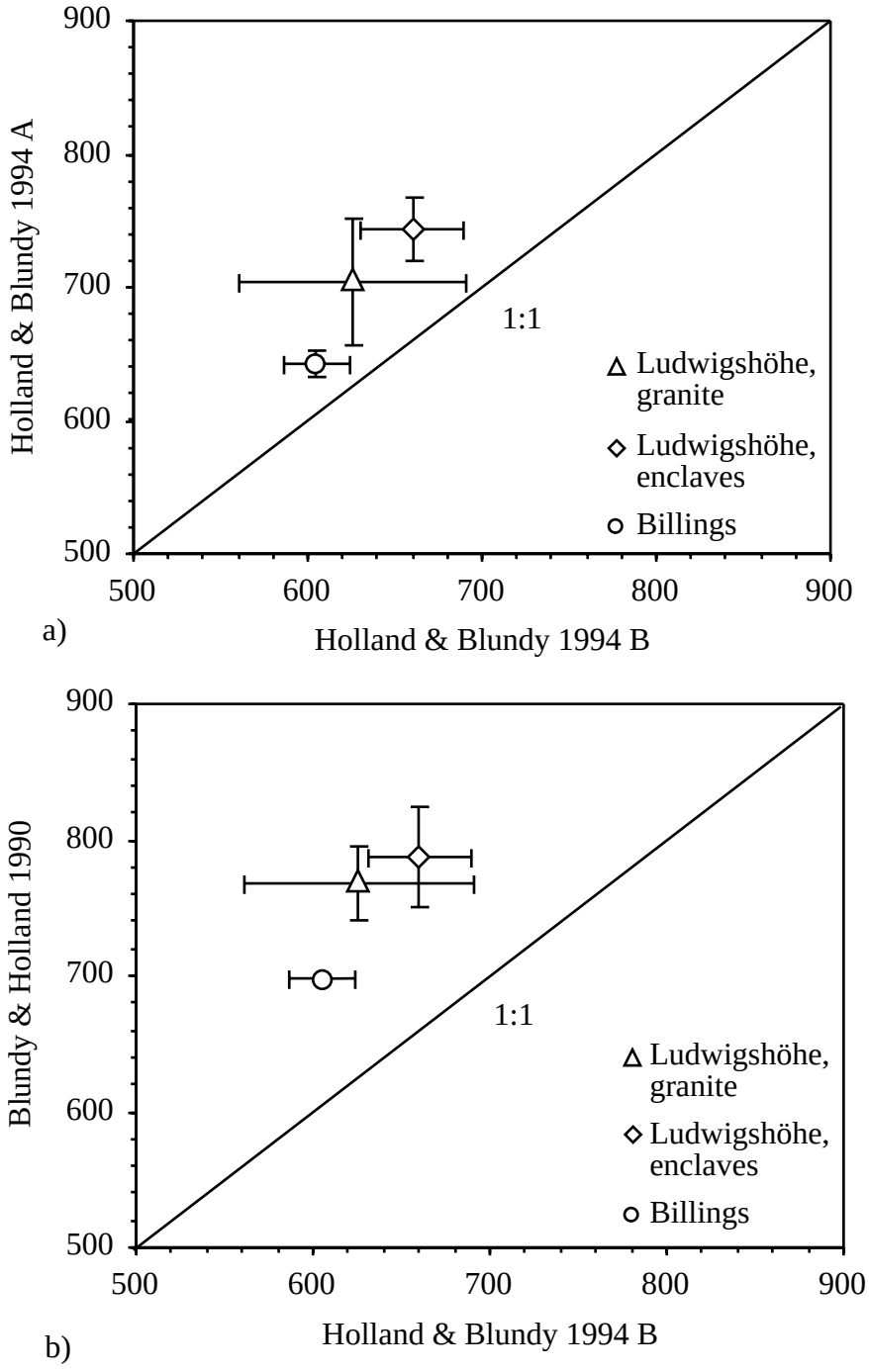

Fig. 4: *Comparison of the crystallization temperatures of hornblende plagioclase pairs from the Ludwigshöhe and Billings plutons, respectively determined with the three calibrations of the amphibole-plagioclase-thermometer: a) Holland & Blundy (1994) thermometer A on the x-axis versus Holland & Blundy (1994) thermometer A on the y-axis; b) Holland & Blundy (1994) thermometer B on the x-axis versus Blundy & Holland (1990) on the y-axis. It is clear from these two graphs, that the Blundy & Holand (1990) calibration yields the highest temperatures and thermometer B of Holland & Blundy (1994) the lowest, in some cases even unrealistical low values (below the wet granitic solidus).*

The Al-in-hornblende-barometer

General comments

Hammarstrøm and *Zen* (1986) were the first to state a relationship between the Al_{tot}-content of amphiboles and the confining pressure, under which those amphiboles had been crystallizing. As data base serve a lot of microprobe measurements of amphiboles from granitoids, the intrusion depth of which have been calculated independently at 2 kbars respectively 8 kbars. Resulting from this, they formulated a first empirical geobarometer:

$$P[\pm 3kbars] = -3.92 + 5.03Al_{tot}$$

Hollister et al. (1987) confirmed this correlation and empirically extended the barometer to granitoids, which crystallized at pressures between 4 and 6 kbars. At the same time they reduceded the errorbar of the barometer with their recalibrated formula:

$$P[\pm 1kbar] = -4.76 + 5.64Al_{tot}$$

A first experimental calibration of this barometer was carried out by *Johnson* and *Rutherford* (1989) at temperatures between 720 °C and 780 °C, taking a CO_2 - H_2O mixture with two different compositions (CO_2 : H_2O = 50 : 50 and 75 : 25) as fluid phase, to reach pressures between 2 and 8 kbars. Their formula reads as follows:

$$P[\pm 0.5kbar] = -3.46 + 4.23Al_{tot}$$

Thomas and *Ernst* (1990) carried out further experiments, using a pure H_2O fluid at 750 °C under a pressure range of 6 to 12 kbars. They achieved similar results as *Johnson* and *Rutherford*, at least for a pressure range between 6 and 8 kbars.

Schmidt (1992) calibrated his experimental barometer at temperatures between 655 °C and 700 °C under water saturated conditions in the pressure range from 2.5 to 13 kbars. His Al-in-hornblende-barometer reads:

$$P[\pm 0.6kbar] = -3.01 + 4.76Al_{tot}$$

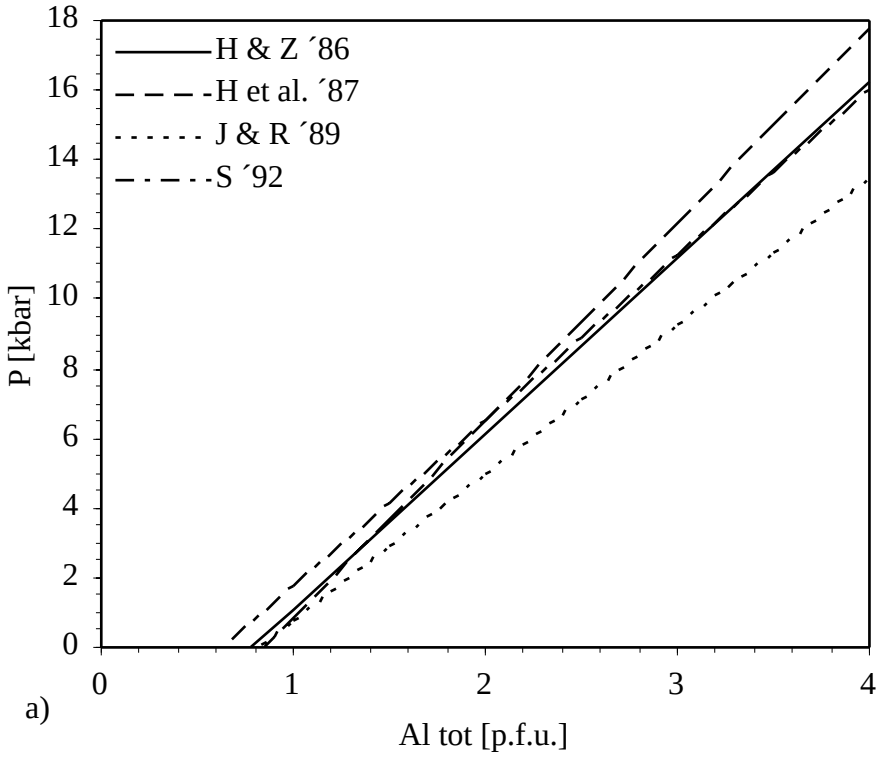

a)

Fig. 5 a: *The four most important temperature independent calibrations of the Al-in-hornblende-barometer: H & Z ´86: Hammarstrøm & Zen (1986); H et al. ´87: Hollister et al. (1987); J & R ´89: Johnson & Rutherford (1989); S ´92: Schmidt (1992).*

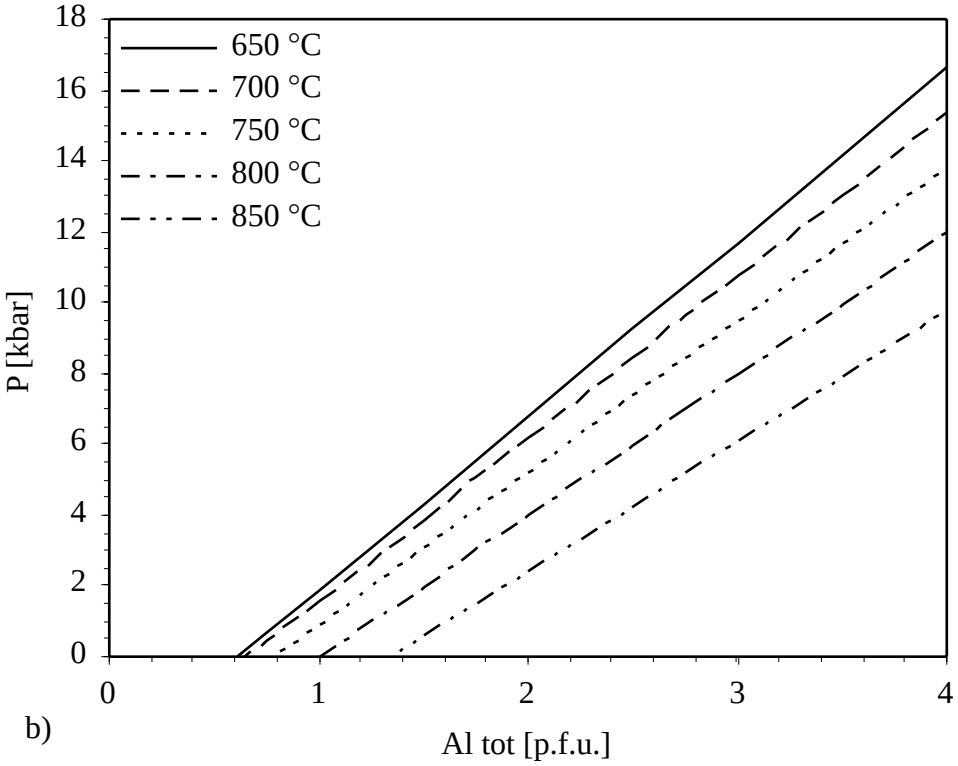

b)

Fig. 5 b: *The calibration of the Al-in-hornblende-barometer by Anderson & Smith (1995) applied to several temperatures.*

As stated earlier, at high temperatures the Edenite-substitution causes a rising amount of Al^{IV}-content in the hornblende lattice (*Anderson* and *Smith* 1995), therefore pressures determined on the base of the Al_{tot}-content of hornblendes seem to be higher as they really are. This temperature dependency may lead to different results for the individual Al-in-hornblende-barometers. But, as shown in Fig. 5, all the different introduced calibrations yield similar pressures as results, therefore this temperature dependency can be excluded.

According to the cited authors several prerequisites have to be fullfilled strictly for a correct application of the barometers:

(1) the assemblage quartz, plagioclase, K-feldspar, hornblende, biotite, titanite and magnetite/ilmenite has to be present contemperaneously with melt,

(2) the barometer can be applied only to rocks which crystallized in a pressure range between 2 and 13 kbars,

(3) plagioclase coexisting with hornblende should range between An_{25} and An_{35},

(4) hornblende should have crystallized near the granitic solidus,

(5) the Si-activity of the melt must have been 1, i. e. it must have been SiO_2 -saturated, because the Al-content of hornblende is directly related to its Si-content and therefore also to the Si-activity of the entire system,

(6) amphibole should coexist with K-feldspar, because its activity also influences the Al-content of hornblende,

(7) due to the last three prerequisites only hornblende in contact with quartz and/or K-feldspar should be measured.

(8) Taking all these preconditions into account, the Al content of hornblende should only be controlled by the pressure dependent Tschermak substitution and therefore it can be used as a good barometer.

But already *Blundy* and *Holland* (1990) emphasized, that temperature plays a more important role for the Al-content of amphiboles as the above cited authors conceded. *Anderson* and *Smith* (1995) therefore presented a new formulation of the Al in hornblende

barometer, which considers all the three intensive parameters pressure, temperature and oxygen fugacity, which are responsible for the Al content of hornblendes.

Their recalibration is based on the amphibole-plagioclase-thermometer of *Blundy* and *Holland* (1990) and the pressure term of *Schmidt* (1992), but additionally they introduce a correction term for temperature. Involving the temperature sensitive edenite substitution into the barometer, enables pressure calculations even for igneous amphiboles, which did not crystallize at or close to the granitoids solidus. Oxygen fugacity limits the new Al-in-hornblende-barometer of *Anderson* and *Smith* (1995), for they restricted its application to hornblendes, which crystallized under a high f_{O2}. Recommended by the authors the Fe-# and the $Fe^{3+}/(Fe^{3+}+Fe^{2+})$ ratio serve as measure of the f_{O2}, with a Fe-# 0.65 and a $Fe^{3+}/(Fe^{3+}+Fe^{2+})$ ratio 0.25, because all experimental calibrations of their Al-in-hornblende-barometer were carried out under medium to high oxygen fugacities. The new formula of *Anderson* and *Smith* (1995) reads as follows:

$$P[\pm 0.6kbar] = -3.01 + 4.76Al_{tot} - \left\{\frac{(T[°C] - 675)}{85}\right\} \times \left\{0.53Al_{tot} + 0.005294 \times (T[°C] - 675)\right\}$$

Application of the Al-in-hornblende-barometer to the investigated plutons

All five introduced calibrations of the Al-in-hornblende-barometer (*Hammarstrøm* and *Zen* 1986, *Hollister* et al. 1987, *Johnson* and *Rutherford* 1989, *Schmidt* 1992, *Anderson* and *Smith* 1995) were used to the above mentioned plutons of the Flasergranitoid zone (Fig. 1). The calibration of *Anderson* and *Smith* (1995) can only be applied to the Ludwigshöhe and Billings plutons, because just for these two plagioclase analyses are available, which are necesarry for the temperature- and temperature-correction terms based on the amphibole-plagiocase-thermometer of *Blundy* and *Holland* (1990). The temperature correction is carried out, using average temperatures for each individual pluton (Billings; Ludwigshöhe granite and enclaves).

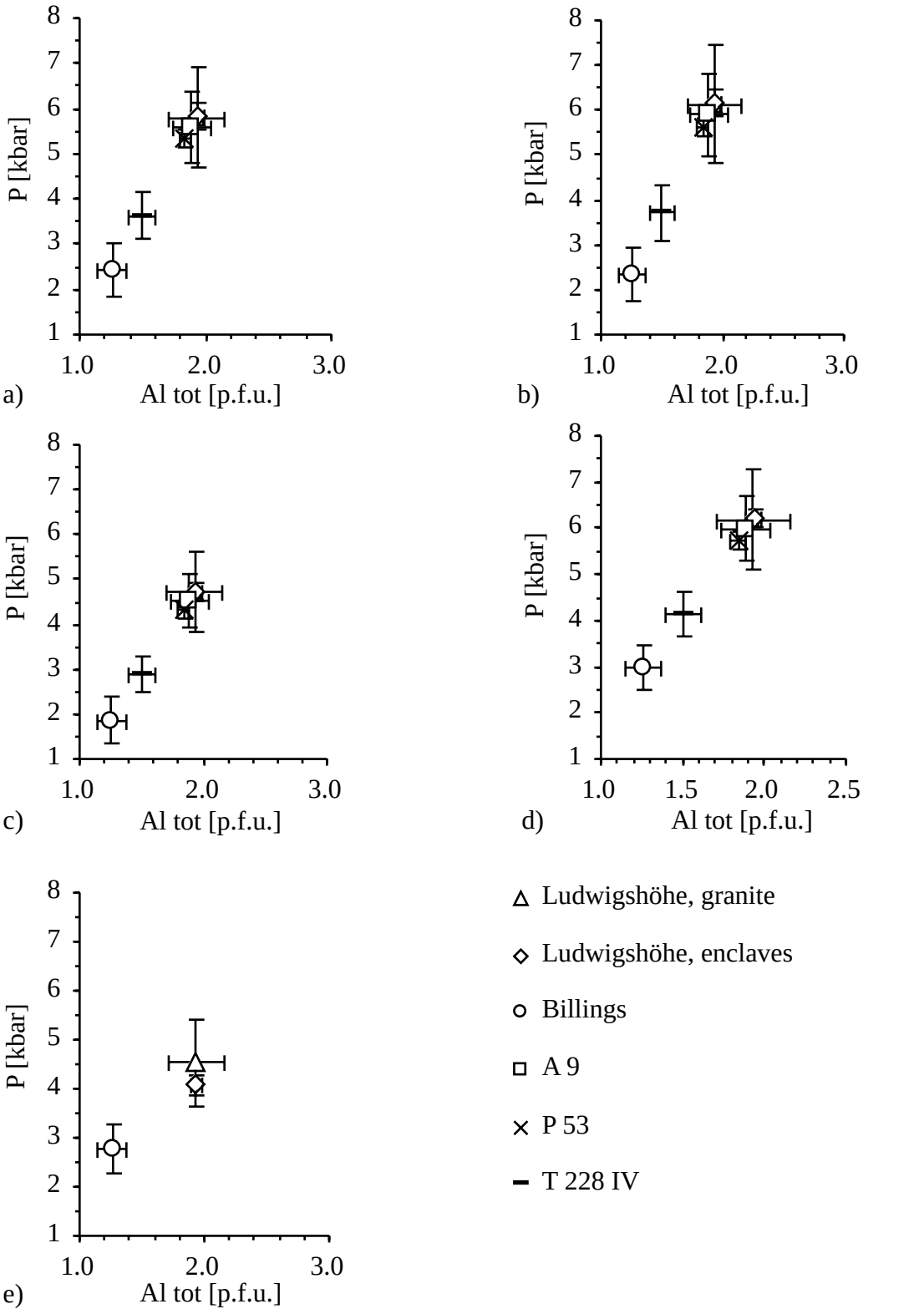

Fig. 6: *All five calbrations of the Al-in-hornblende-barometer applied to the six sample fractions: a) Hammarstrøm & Zen (1986); b) Hollister et al. (1987); c) Johnson & Rutherford (1989); d) Schmidt (1992); e) Anderson & Smith (1995).*

For the investigated plutons following pressures are determined (for a graphical compilation of all data see also Fig. 6):

Sample T 228 IV:

9 amphibole rim measurements from the granodioritic porphyry of sample T 228 IV (for an average analysis see Tab. 2) yield an average Al_{tot} = 1.501 ±0.106, or expressed in pressure data: 3.6 ± 0.5 kbars (*Hammarstrøm* and *Zen* 1986), 3.7 ± 0.6 kbars (*Hollister* et al. 1987), 2.9 ± 0.4 kbars (*Johnson* and *Rutherford* 1989) and 4.1 ± 0.5 kbars (*Schmidt* 1992). Because no plagioclase compositions were measured for the granodioritic porphyry, pressures were not temperature-corrected according to *Anderson* and *Smith* (1995).

Ludwigshöhe pluton:

For pressure determination at the Ludwigshöhe pluton in total 17 hornblende measurements could be used, 13 from the porphyritic granite itself and 4 from enclaves and schlieren. The microprobe analyses are obtained from amphibole rims either with quartz or with k- feldspar. The structural relationship of hornblende and quartz/K-feldspar is displayed in Fig. 3a. Average Al_{tot}-contents of hornblendes are 1.931 ±0.222 for the granite and 1.936 ±0.050 for the enclaves. Consequentely, pressures without applying the temperature correction term calculated for the Ludwigshöhe pluton range from 4.7 to 6.2 kbars. Both sample fractions, the porphyritic granite as well as the enclaves yield the same average pressure for each calibration. The lowest pressure (4.7 ± 0.9 kbars) is calculated with the calibration of *Johnson* and *Rutherford* (1989), the highest (6.2 ± 1.1 kbars) with the calibration of *Schmidt* (1992). The other two give intermediate values with 5.8 ±1.1 kbars (*Hammarstrøm* and *Zen* 1986) and 6.1 ± 1.3 kbars (*Hollister* et al. 1987). Since the amphibole-plagioclase-thermometer of *Blundy* and *Holland* (1990) yields temperatures, which are significantly above the solidus (granite: 768 °C, enclaves: 787 °C), a temperature correction, according to *Anderson* and *Smith* (1995), seems to be reasonable. This correction generally leads to a pressure decrease, values of 4.5 ± 0.9 kbars for the granite and 4.1 ± 0.2 kbars for the enclaves are determined, which correlate with those computed

with the calibration of *Johnson* and *Rutherford* (1989). This result, obtained with the *Anderson* and *Smith* calibration seems to fit quite good, because *Johnson* and *Rutherford* (1989) calibrated their experiments at temperatures between 720 and 780 °C, and this is exactly the temperture range, where hornblendes of the Ludwigshöhe pluton crystallized.

Billings pluton:

In the sample from the Billings pluton 7 measurements of hornblendes sharing their grain boundaries with quartz were carried out. The average Al_{tot}-content is 1.259 ±0.111. Derived pressures range from 1.9 ± 0.5 kbars (*Johnson* and *Rutherford* 1989) to 3.0 ± 0.5 kbars (*Schmidt* 1992). Again the results of the amphibole-plagioclase-thermometry with obtained temperatures of about 697 °C prove, that the amphiboles crystallized well above the solidus and that again the temperature correction of the *Anderson* and *Smith* (1995) calibration is necessary. According to their calibration the billings pluton cooled at a confining pressure of 2.8 ± 0.5 kbars.

Samples A 9 and P 53

For the samples A 9 and P 53 (A 9: Neunkirchener Komplex; P 53: close to the Heppenheimer Schieferzug), no plagioclase microprobe analyses were carried out. Therefore only the 4 non temperature corrected calibrations can be applied to these samples. In total 7 hornblende measurements of sample A 9 and 8 of P 53 fulfill the requirements for the Al-in-hornblende-barometry, stated above (for an average analysis see Tab. 2). Both yield similar average Al_{tot}-values with 1.889 ±0.151 for A 9 and 1.839 ±0.042 for P 53, resulting in similar pressure data. The pressures range from 5.6 ± 0.8 to 6.0 ± 0.7 kbars for sample A 9 and from 5.3 ± 0.2 to 5.7 ± 0.2 kbars for sample P 53, using those barometers calibrated at lower temperatures. Only the *Johnson* and *Rutherford* (1989) barometer gives lower pressures at 4.5 ± 0.6 kbars for sample A 9 and 4.3 ± 0.2 kbars for sample P 53.

Conclusions

Determinations of the intrusion depth of several plutons in the Flasergranitoid zone, using the Al-in hornblende geobarometer show, that the analyzed plutons intruded in a pressure range from about 2.5 kbars to 6 kbars, which correlates with intrusion depth of about 8 to 19.5 km. Compared with the data of *Henes-Klaiber* (1992) neither a regional distribution pattern within the Flasergranitoid zone, nor any correlations with the different intrusion types and mechanisms can be derived from these data. But at least two important conclusions can be drawn, the first one concerns the southern boundary between the Flasergranitoid zone and the Weschnitz pluton, the second puts attention at the northern border as well.

Two very close to each, just about 2 km apart lying samples, one from the northern edge of the Weschnitz pluton with 5.7 kbars (*Henes-Klaiber* 1992) and one from the southernmost edge of the Flasergranitoid zone ranging from 5.3 to 5.7 kbars show very similar results, so that the demanded vertical displacement (*Henes-Klaiber* 1992) can not be proven. This result and interpretation is supported by several other data sets listed by *Stein* (2000):

(1) Radiometric dating by *Kreuzer* and *Harre* (1975), *Rittmann* (1984) and *Todt* et al. (1995) indicates no time gap between the intrusions in the central and southern Bergsträßer Odenwald, respectively, nor a significant time difference between the peak metamorphism in both these “units“.

(2) No major difference in the geochemical signatures of plutons from the central and southern Bergsträßer Odenwald was reported (*Altherr* et al. 1999).

(3) Fabrics in the southernmost Flasergranitoid zone do not point to an extended overprint of magmatic fabrics by solid state deformation as it should be expected in a major shear zone.

(4) Not even the generally more homogeneous character of the plutons in the southern Bergsträßer Odenwald compared to the Flasergranitoid zone is a good

argument for different origin of these "units" and for the tectonic character of the boundary between both, because in the Flasergranitoid zone, next to many small intrusions of a wide range of compositions, also big, homogeneous plutons such as the Melibocus granodiorite occur.

On the other hand our PT data together with PT data from the Frankenstein complex (*Kreher* 1994) indicate clearly different intrusion depth for the Frankenstein gabbro on the one hand and the plutons of the Flasergranitoid on the other hand. Therefore, our data support the idea of a major tectonic boundary, probably a strike-slip shear zone with a vertical component, between these two units. Radiometric, geochemical and structural data also point to such a suture zone:

(1) The Frankenstein gabbro intruded at c. 360 ma (*Kirsch* et al. 1986), 20 ma before pluton emplacement in the Flasergranitoid zone started *Kreuzer* and *Harre* (1975).

(2) The Frankenstein gabbro is interpreted as the product of mantel melting (*Kirsch* et al. 1986), while all plutons in the adjacent southern part of the Bergsträßer Odenwald have a crustal signature (*Altherr* et al. 1999).

(3) Solid state fabrics overprinting and almost obliterating magmatic fabrics were observed in the felsic granites of the Neutsch complex in the northern Flasergranitoid zone (Stein 2000).

Consequentely, this northern boundary between the Frankenstein complex and the Flasergranitoid zone is interpreted to be an important strike-slip zone, which is responsible for the fabric development, which originally is due to the magmatic event. This anisotropy is reactivated under the strike-slip movement, which started already under amphibolite-facies conditions but in a compressional stressfield.

In our context the model of *Stein* (2000) is favored, who proposed three units in the Odenwald: The Böllstein Odenwald, the Frankenstein complex and the Bergsträßer Odenwald, which may have a common sedimentation and early tectono-metamorphic history with a MP-metamorphic imprint at about 400-375 ma. Afterwards those units were

seperated and suffered independent tectono-magmatic and tectono-metamorphic histories each. For PT-data of the metamorphic rocks and the intrusion depths of the magmatic rocks, as well as their radiometric ages, fit very good together, the pervasive LP-metamorphism in the Bergsträßer Odenwald is interpreted as dynamic contact-metamorphism. Finally all the three units were juxtaposed again at two important strike-slip zones.

Acknowledgements

Research was funded by the DFG. Microprobe analyses were carried out at the Material Sciences Department of the TU Darmstadt and guided by S. Weinbruch. Special thanks go to J. Reinhardt and D. Scheuvens for lively discussions and helpful comments, as well as to W. Schubert for his very constructive review.

References

Altenberger, U, Besch, T (1993) The Boellstein Odenwald; evidence for pre- to early Variscan plate convergence in the Central European Variscides. Geol Rdsch 82: 475-488

Altenberger, U, Oberhänsli, R, Stein, E, Moghni, M (this volume) Geochemistry, tectonic setting and geodynamic significance of late orogenic dikes in the Melibocus Massif, Bergstraesser Odenwald.

Altherr, R, Henes-Klaiber, U, Hegner, E, Satir, M, Langer, C (1999) Plutonism in the Variscan Odenwald (Germany): from subduction to collision. Int Journ Earth Sciences 88: 422-443

Anderson, JL (1997) Status of thermobarometry in granitic batholiths. Trans Roy Soc Edinb: Earth Sci 87: 125-138

Anderson, JL, Smith, DR (1995) The effects of temperature and f_{O2} on the Al-in-hornblende barometer. Am Mineral 80: 549-559

Blundy, JD, Holland, TJB (1990) Calcic amphibole equilibria and a new amphibole-plagioclase geothermometer. Contrib Mineral Petrol 104: 208-224

Chappel, BW, White, AJR (1974) Two contrasting granite types. Pacific Geol 8: 173-174

Clemens, JD, Wall, VJ (1984) Origin and evolution of a peraluminous silicic ignimbrite suite: The Violet Town Volcanics. Contrib Mineral Petrol 88: 354-371

Hammarstrom, JM, Zen, E-an (1986) Aluminium in hornblende: An empirical igneous geobarometer. Am Mineral 71: 1297-1313

Henes-Klaiber, U (1992) Zur Geochemie der variszischen Granitoide des Bergsträßer Odenwaldes. Unpubl dissertation, TU Karlsruhe, 264 pp

Hess, JC, Schmidt, G (1989) Zur Altersstellung der Kataklastite im Bereich der Otzberg-Zone, Odenwald. Geol Jb Hessen 117: 69-77

Holland, T, Blundy , J (1994) Non-ideal interactions in calcic amphiboles and their bearing on amphibole-plagioclase thermometry. Contrib Mineral Petrol 116: 433-447

Hollister, LS, Grissom, GC, Peters, EK, Stowell, HH, Sisson, VB (1987) Confirmation of the empirical correlation of Al in hornblende with pressure of solidification of calc-alkaline plutons. Am Mineral 72: 231-239

Ishihara, S (1977) The magnetite-series and ilmenite-series. Min Geol 27: 293-305

Johnson, MC, Rutherford, MJ (1989) Experimental calibration of the aluminium-in-hornblende geobarometer with applications to Long Valley caldera (California) volcanic rocks. Geology 17: 837-841

Kirsch H , Kober B, Lippolt HJ (1988) Age of intrusion and rapid cooling of the Frankenstein gabbro (Odenwald, SW-Germany) evidenced by $^{40}Ar/^{39}Ar$ and single-zircon $^{207}Pb/^{206}Pb$ measurements. Geologische Rundschau 77/3: 693-711

Kreher, B (1994) Petrologie und Geochemie der Gabbrointrusionen des Frankensteins (Odenwald). Geol Jb Hessen 122: 81-122

Kreuzer H, Harre W (1975) K/Ar-Altersbestimmungen an Hornblenden und Biotiten des Kristallinen Odenwalds.- In: *Amstutz GC, Meisl S, Nickel E* (EDS.) Mineralien und Gesteine im Odenwald. Aufschluß Sonderbd 27: 71-77

Krohe A (1994) Verformungsgeschichte in der mittleren Kruste eines magmatischen Bogens. Geotekt Forsch 80: 1-147

Leake, BE, Woolley, AR, Arps, CES, Birch, WD, Gilbert, MC, Grice, JD, Hawthorne, FC, Kato, A, Kisch, HJ, Krivovichev, VG, Linthout, K, Laird, J, Mandarino, J, Maresch, WV, Nickel, EH, Rock, NMS, Schumacher, JC, Smith, DC, Stephenson, NCN, Ungaretti, L, Whittaker, EJW, Youzhi, G (1997) Nomenclature of amphiboles. Report of the Subcommittee on Amphiboles of the International Mineralogical Association Commission on New Minerals and Mineral Names. Eur J Mineral 9: 623-651

Okrusch M (1995): Metamorphic Evolution.- In: *Dallmeyer RD, Franke W, Weber K* (eds.) Pre-Permian Geology of Central and Eastern Europe. Springer, Heidelberg, 201-213

Poli, S, Schmidt, MW (1992) A comment on "Calcic amphibole equilibria and a new amphibole-plagioclase geothermometer" by JD Blundy and TJB Holland (Contributions to Mineralogy and Petrology 1990, vol 104, p 208-224). Contrib Mineral Petrol 111: 273-282

Rittmann, KL (1984) Argon in Hornblende, Biotit und Muskovit bei der geologischen Abkühlung - $^{40}Ar/^{39}Ar$-Untersuchungen. Unpubl. PhD thesis, University of Heidelberg, 278 pp

Schmidt, MW (1992) Amphibole composition in tonalite as a function of pressure: an experimental calibration of the Al-in-hornblende barometer. Contrib Mineral Petrol 110: 304-310

Spear, FS (1981) Amphibole-plagioclase equilibria: an empirical model for the reaction albite + tremolite = edenite + 4 quartz. Contrib Mineral Petrol 77: 355-364

Stein, E (2000) Zur Platznahme von Granitoiden - Vergleichende Fallstudien zu Gefügen und Platznahmemechanismen aus den White-Inyo Mountains, California, USA und dem Bergsträßer Odenwald. Geotekt Forsch 93: 1-330

Thomas, WM, Ernst, WG (1990) The aluminium content of hornblende in calc-alkaline granitic rocks: A mineralogic barometer calibrated experimentally to 12 kbars. In: *Spencer, RJ, Chou, IM* (eds) Fluid-mineral interactions: a tribute to H.P. Eugster. Geochem Soc Spec Publ 2: 59-63

Todt WA, Altenberger U, Raumer JF von (1995) U-Pb data on zircons for the thermal peak of metamorphism in the Variscan Odenwald, Germany. Geol Rundsch 84: 466-472

White, AJR, Chappel, BW (1983) Granitoid types and their distribution in the Lachlan Fold Belt, southeastern Australia. Mem Geol Soc Am 159: 21-34

Willner, AP, Massonne, HJ, Krohe, A (1991) Tectono-thermal evolution of a part of a Variscan magmatic arc: the Odenwald in the Mid-German Crystalline Rise. Geol Rdsch 80: 369-389

Wyborn, D, Chappel, BW, Johnston, RM (1981) Three S-type volcanic suites from the Lachlan Fold Belt, southeast Australia. In: Granites and rhyolites. J Geophys Res 86: 10335-10348

Authors‘ adresses:

PD. Dr. Eckardt Stein

Institut für Mineralogie , TU Darmstadt, Schnittspahnstr. 9, D-64287 Darmstadt

Carlo Dietl

Geologisch-Paläontologisches Institut, Universität Heidelberg, Im Neuenheimer Feld 234, D-69120 Heidelberg

Data appendix

Here all data are listed, which were not presented in detailed in the individual chapters. The single microprobe and XRF analyses can be found on the CD ROM attached to the copy of the thesis, which is stored in the library of the Geological-Palaeontological Department of the University of Heidelberg.

Structural field measurements in and around the Joshua Flat – Beer Creek - Pluton

For location of the individual areas see attatched map. Planar fabrics are given as “dip direction / dip angle”, linear fabrics as “trend / plunge”.

Magmatic foliation (lineations in brackets); *data from R. B. Miller and T. Fink in italics*

Deep Springs College
247/80

Soldier Pass
136/70
181/72
125/74
152/47
333/75
035/65
218/40

Deep Springs Fault Zone
201/58 (248/55)
201/52
198/44
167/47
201/52
158/45
200/50
286/85 (203/68)
220/48
198/66
233/77
186/63
159/48
148/48
184/70 (268/70)
244/64
044/62
202/66
195/72
241/78
226/75
239/76
312/64
049/85 (342/79)
227/73 (300/65)
013/54
016/72
062/83 (133/74)
025/70 (341/45)
233/87 (266/74)
037/73
066/78
068/74
028/76
030/65
006/72
034/75
040/60
070/54
060/50
060/58
046/65
045/44
054/52

Corral Springs Area
074/71
070/70
025/48
103/83
303/84
047/90
061/68
028/56
078/64

Buckhorn Springs Area
050/67
019/56
032/63
048/56
020/82

Mount Nunn
260/85
220/90
240/82
244/80
030/85
236/85
038/84
045/85
030/78

A-Canyon
246/60
230/86
254/60
242/62
096/52
040/83
226/74
042/66
032/76 (302/58)
040/72
057/80 (336/72)
076/62
063/60 (083/66)
051/74
064/62 (028/55)
010/76
082/65 (014/35)
Solid state Foliation
054/70 (034/66)
356/55
029/78 (062/70)
048/76 (024/73)

B-Canyon
249/68
090/70
242/78
034/46
052/68
049/57 (105/49)
025/80
061/72
071/65
052/70
272/76
079/73
070/80
060/60 (023/68)
044/70
242/70 (310/62)
200/45
235/64
032/72

E-Canyon
069/80
066/56
072/62
074/66
068/85 (357/58)

050/60
036/70
051/76
075/70
064/70
083/86
035/74
289/77
252/86
264/85
069/72 (319/55)
054/62

G-Canyon
267/66 (177/38)
250/62
240/63 (295/43)
238/68
214/72
223/60
218/59
188/83
192/88
211/86 (308/65)
183/72
230/74
263/85 (260/65)
028/73 (297/44)
214/64

H-Canyon
261/82
263/78
180/90
030/85
276/86
277/90 (205/52)
054/80
239/70 (359/58)
094/82
020/88
229/60
227/82
105/83 (022/70)
234/85
033/70
054/60
058/54

I-Canyon
336/73
249/76
230/65
243/80
074/80
030/85
210/87
220/70
246/85
240/63
178/87
176/65
200/70
206/74
202/65
045/88
180/63
200/65
206/54
143/13
207/84
176/71
178/47 (253/17)
192/65 (262/45)
224/69
016/89
193/45
344/87
199/43
206/78
199/55 (261/30)
204/52 (272/13)

Birch Creek
248/68
236/42
244/58
232/76 (177/52)
253/81 (173/74)
250/70
239/83
251/72
226/62 (284/70)
235/55
264/80
278/76 (260/63)
265/58
254/70 (009/28)
252/79
268/72
257/68
272/60
260/73
260/68
072/77
086/80
072/88
088/87
242/80
040/87
100/85
237/76
072/67
263/80
234/82
059/80
101/90
101/82
260/76
092/78
063/64
300/60
140/80 (179/77)

Beer Creek
040/64
094/74
226/65 (300/50)
210/55
200/72
222/62
272/45
252/65
235/70
298/65
248/63
284/40 (225/30)
228/88
120/90
272/68
254/82
222/61
216/72
244/58
258/65
252/68
282/84
029/61
082/76
223/75
235/61
242/67
254/59
262/75
248/61
280/55
100/58
095/76

Index Finger
247/74
249/67
255/65
234/66 (270/65)
226/76 (155/65)
232/49
247/73
262/68 (327/55)
297/88
237/65
232/45
222/76
220/74
224/84
232/86
249/87
261/62
275/42
252/69
241/60

260/82
252/72
262/66
256/70
258/87 (190/60)
249/73 (204/50)
218/58
052/85
220/73 (182/71)
172/73
223/58
266/76
255/82
116/63
273/58
283/85
260/88
056/87
239/67
259/55
242/72
253/74
234/68
250/83
242/74
248/78
303/78
314/80
239/87
251/68

242/60
259/65
057/73

Crystal Peak Area
282/74
030/60
042/72 (111/72)
042/80
030/77
055/82
237/85 (194/72)
063/85
258/68
082/76
140/72
044/82
036/80
057/86
057/88
055/85
222/77
252/85 (158/44)
062/83 (152/57)
255/60
246/60
255/80
258/82
247/88

252/88
272/82
070/84 (149/50)
077/86
065/47
051/63
055/79
228/77 (161/50)
080/83
073/70
226/75 (198/46)
194/60

Northern End of the Area
228/75
245/76
000/57
199/85
226/73
266/85
237/85
191/85
170/78
198/74
210/50
212/60
250/64
234/84
245/30

228/38
230/50
212/64
222/62
227/55
205/53
035/82
040/77
219/85
243/73
237/62
235/76
224/90
032/85
208/76
244/85
057/76 (354/55)
233/82
046/88
243/65
264/70
236/76
234/73
260/58
264/70
226/75

Solid state foliation within the pluton (lineations in brackets); *data from R. B. Miller and T. Fink in italics*

Birch Creek
241/79 (325/32)
256/89
255/79
035/83
028/70 (274/34)

260/65
086/87
283/67 (323/61)
257/81 (335/53)
092/78
051/90 (321/23)

272/77 (324/69)
253/78 (324/48)
259/83 (292/30)
246/84 (338/56)
260/85 (308/42)
228/74 (295/52)

223/62 (351/45)
236/82 (002/42)
090/90 (000/32)
245/88

Magmatic banding

Soldier Pass
165/35

Deep Springs Fault Zone
051/58
068/58
213/82
202/74
026/60
100/35
030/65
040/60
070/54
060/50
060/58
046/65

Corral Springs Area
070/70
066/66
160/65

Mount Nunn
220/90
158/85
172/70
180/85
178/58

A-Canyon
246/60
230/86
254/60
242/62
076/62
063/60
212/57

B-Canyon
246/55
249/68
034/46
052/68
049/57
052/70
272/76
070/80
060/60
044/70
242/70

E-Canyon
069/80
066/56
072/62
074/66
068/85
050/60
036/70
051/76
187/64
289/77
252/86

G-Canyon
194/56
025/87
183/72
162/27
185/26
178/26

I-Canyon
180/60
220/62
212/47
191/65
176/71
178/47
262/45
246/15
199/55

H-Canyon
262/65
054/80
239/70

Birch Creek
257/68
272/60
066/73
320/43
288/70
264/73
244/80
280/67
270/80
240/70
260/68
259/65
072/88
092/60
085/67
084/55
230/65
100/85
072/67

Index Finger
247/74
249/67
255/65
234/66
247/73
220/74
224/84
232/86
241/60
195/79
302/45
218/58
035/88
232/76
072/76
241/80
312/78

Crystal Peak Area
030/77
036/80
057/86
057/88
055/85
066/88
246/60
255/80
045/18
106/86
056/75
065/47
220/52
060/84

Norther End of the Area
220/83
230/80
238/79
236/72
223/75
228/80
084/80
264/81
070/88
080/75
231/85
226/73
248/63
226/72
225/77
236/78
235/77
046/84
243/85
170/78
198/74
210/50
212/60
250/64
210/60
234/84
212/48
216/40
259/72
244/35
252/52
240/47
243/55

232/35
208/50
223/43
204/55
246/70
212/64
222/62

227/55
214/88
043/82
223/85
228/86
243/73
237/62

235/76
224/90
032/85
048/82
028/80
238/78
266/75

236/76
234/73
273/83
192/76
201/55
230/77
258/88

Axes of magmatic folds (axial planes in brackets)

Deep Springs Fault Zone
102/42
097/34
358/35
180/58
226/69

Corral Springs Area
315/64

B-Canyon
301/67 (071/65)

G-Canyon
088/47
068/59
059/40

H-Canyon
172/45 (227/82)
118/60 (032/73)

I-Canyon
177/67
251/52 (344/87)
078/63

Birch Creek
003/44 (272/86)

Beer Creek
182/00

Northern End of the Area
209/65 (273/73)
170/25 (088/43)
160/45 (046/84)

Foliation s_1 (lineations in brackets); ***data from S. R. Paterson, R. B. Miller and T. Fink in italics***

Corral Springs Area
276/80
055/88
059/70
038/62
076/70
078/80
038/65
064/66
058/72
060/70

Buckhorn Springs Area
038/58
039/56
034/58
038/45
043/50 (356/35)
018/47
051/32
050/50
061/47

025/58
022/45 (044/38)
030/66
045/45
036/72
044/45
042/68
046/80 (324/45)
052/82 (327/42)
044/70
052/82 (130/50)
070/58
068/59 (075/62)
065/46 (096/43)
054/66 (110/58)
052/59
048/56
054/48
004/18
062/70
048/70
042/52 (091/42)
030/76
034/80

050/60
041/58 (343/38)
042/60
048/54
045/56
044/58
046/50
038/56 (317/19)
230/66 (328/27)
046/31
040/37
048/67
052/45
041/50
050/43
026/45
045/40
084/47
080/38
211/34

Prospect
015/82
206/84

213/69
200/73
200/55 (169/52)
221/56
223/62
229/62
236/76 (300/66)
236/74
242/60
248/70
240/50 (273/43)
232/60 (282/50)
241/50
238/71 (276/70)
235/69 (270/64)
238/85 (312/79)
235/78 (268/78)
237/86 (318/78)
233/85
233/67
239/70
242/66
240/70
239/65

242/80 (304/84)
253/75 (264/75)
236/84 (256/78)
245/80 (273/80)
248/66
236/73
252/45
249/85
243/45
227/58
217/54 (182/47)
242/33 (262/30)
224/27 (235/23)
020/46
011/50
049/44
060/77
073/74
054/65 (332/28)
230/88
233/86
066/55
043/45
274/70
340/28 (324/23)
050/67
037/56

B-Canyon
056/46 (026/42)
088/34 (016/15)
054/40 (040/40)
018/21 (010/21)
050/35 (028/32)
056/82 (322/53)
238/82
236/86 (318/54)
021/82 (292/62)
242/76
037/77
055/83 (292/62)
044/87 (315/65)
035/74
227/88
224/84
046/86
226/82
248/87
225/66
060/84
247/89
074/69 (106/86)
070/54 (061/46)
077/66
045/65 (036/65)
239/80
079/83
084/74
054/88
246/85
236/86
256/84
070/85
216/44
047/86
241/66
160/83
079/79

C-Canyon
049/73
050/57
035/67
036/58
051/80
029/64
046/59
046/54
050/52
040/53 (078/47)
046/57
071/50
078/52
080/50
072/52
059/57
046/55
069/54
068/49
084/60
084/45
081/50
063/48
081/43 (089/45)
085/42 (094/47)
084/45
083/47
076/38
078/40
094/25
081/28
062/32 (074/29)
043/25
050/28
042/25 (110/12)
048/42
041/51
050/32
101/21 (098/19)
138/16
112/25
184/32
166/27
138/12
110/25 (105/24)
122/13 (098/12)
146/80
343/82
331/75
344/82
350/78
342/74
342/73
341/75
042/20
032/38
004/25
023/04
020/10 (060/01)
344/30
346/38
312/25
342/16
315/09
352/50
334/70
340/45
329/72
356/63
348/47
345/58

D-Canyon
038/37
050/40
045/38
056/35
042/42
040/42
022/36
033/44 (066/37)
040/42
070/35
048/46
051/56
044/53
034/43

F-Canyon
340/45
010/40
166/82
176/88
170/87
166/80 (094/40)
166/76
350/83
172/80 (097/57)
350/75 (265/16)

?-Canyon
343/77
352/75
343/85
353/54
350/75 (273/32)
347/75
353/63
004/46
355/46
016/32
024/36 (349/32)

Sams Spring Area
115/65
114/64
114/63
108/80
112/68
109/68
108/50 (170/25)
116/43
111/41
129/57
122/57

111/75
118/54
123/57
121/50
124/57
119/58
122/63
120/62
125/70
116/62
132/45
138/45
134/41
136/45
157/40
135/42
136/46
145/46
142/42
130/44 (208/07)
128/43 (208/07)
110/57
112/63
107/56 (194/08)
116/63
102/60
103/73
100/63
099/64
127/52
140/54
121/50
122/58
119/56
131/54
122/60
120/58
121/57
119/57
122/53
112/60
120/56
121/55
117/46
110/53
116/59 (032/05)
117/52
117/51
116/53
131/42
120/50
125/42
126/51
111/57
117/46
133/47
099/72
094/66
103/66
113/55
102/64
123/52
116/58
115/48
114/53
119/53
121/48
115/50
117/54
115/53
107/53
114/49
116/50 (130/47)
112/51
115/45
106/57
112/80
106/76
124/56
119/55
119/58
126/62 (204/28)
137/52
206/36
128/58
126/54
126/58
125/66
123/55
124/59

Cuna Spring Area

122/45
100/58
136/35
126/48 (158/37)
126/50 (137/45)
127/45
127/78
133/33
130/40 (110/37)
119/60 (115/55)
129/50
150/42
152/32 (201/22)
128/40
180/20
135/36
119/25
120/48
145/36 (165/26)
117/57
124/70
125/58
139/62
125/62
125/66
105/53
148/49
278/30 (347/30)
271/74 (342/47)
271/76 (342/47)
146/40
127/88
142/40 (105/33)
080/79
110/76
109/80 (140/77)
064/83 (123/72)
067/83 (122/60)
104/76
268/80 (211/63)
085/84 (179/63)
249/62
260/78
098/88
251/83 (335/48)
103/90
102/85
308/75
114/77
108/81
105/80
118/89 (041/50)
108/78 (154/75)
097/68
028/53
112/87
123/86
098/75
274/87 (356/77)
234/85
276/62
277/60
288/78
140/34
171/44
141/40
116/71 (185/18)
101/85 (204/30)
130/52
114/36
103/27
109/36
097/60
134/32
135/52 (178/38)
124/69 (196/42)
116/77 (197/28)
177/40 (168/42)
155/60 (208/34)

The Elephant and adjacent hills

082/54
(098/605)
081/44 (146/30)
294/65
303/45
335/14
045/25
079/38
269/85
290/72
061/47 (132/25)
075/43 (132/27)
262/70
300/23
090/76
062/44
081/30 (149/10)
070/43 (139/17)
079/75
085/46

094/55
108/52
080/44
108/45
106/38 (170/10)
069/45 (160/04)
054/53
064/42 (134/20)
045/43
008/69
024/53
079/52
079/42
061/37 (160/07)
072/42
062/45
080/57
084/57
098/65
087/62
081/55
065/45
073/57
038/45
090/74
070/79 (155/23)
093/70
066/68
079/54
086/50
088/42
054/54 (336/21)
065/51
080/44
091/45
088/50
079/42
061/42
050/47
068/70 (146/25)
085/83
074/75
049/34
050/32
039/35
055/42 (133/08)
060/69
072/60
103/53
267/72
047/27 (339/07)
074/28 (330/03)
105/40 (130/40)
079/51
120/31
087/31 (146/17)
062/15
225/57
237/26 (135/40)
238/60 (134/09)
086/40 (015/05)
099/80
102/51
214/45
166/46
101/85 (182/11)
101/72
084/87 (188/30)
112/71

Birch and Beer Creek
246/86
265/55
045/65
072/86
240/82
246/72
262/78
259/86
274/75 (mit Linear 325/71)
288/75
284/58
186/65
282/78
245/50
238/45
234/54
235/33 (283/22)
231/72
258/83 (346/60)
251/82 (328/75)
250/67
268/60 (332/36)
250/70
264/70
101/60 (024/18)
271/58
252/67
262/65
283/67 (321/63)
271/74 (320/62)
262/74 (290/68)
265/75 (347/45)
268/53 (286/55)
266/53
274/35 (256/32)
276/48
257/47
258/68
282/55
279/68
253/88
259/70
268/79
257/76
268/79
257/77
254/54
250/81
233/84
257/81
253/73 (327/44)
244/70 (306/65)
238/78 (270/62)
078/86
260/85 (328/69)
258/64
253/83
283/76 (295/74)

Foliation s_2 (lineations in brackets); *data from S. R. Paterson in italics*

Sams Spring Area
260/82
279/45
280/43
259/65
267/63
072/69
295/42
292/32
097/72
296/65 (259/58)

Cuna Spring Area
266/84
122/85
347/46
108 62
135 58

The Elephant
076/42
063/68
288/83
278/86
339/55
070/43 (139/17)
066/64
062/66
250/65

Birch and Beer Creek
106/38
262/73

Fold axes (axial planes in brackets); *data from S. R. Paterson, R. B. Miller and T. Fink in italics*

Corral Springs Area
172/21 (055/88)

Buckhorn Springs Area
058/34 (050/50)
311/28 (096/88)
315/25
105/40
311/02
121/09
132/62
354/50 (052/59)
028/68
092/62 (054/48)
092/41
092/60

Prospect
143/60
151/70
184/70
145/64
132/40 (200/73)
148/44 (200/55)
135/32
143/38
150/42
045/67 (337/82)
326/57 (070/70)

B-Canyon
021/25 (088/34)
049/30 (054/40)
326/45
310/27 (009/74)
(210/90)
(100/90)
318/45
324/45
312/25
128/70
148/70
129/45
012/66
351/65
296/72
336/57
343/03
356/40
166/70 (070/85)

C-Canyon
025/25
055/25
263/17

D-Canyon
084/27
095/45
326/46
070/50

F-Canyon
064/50 (340/45)

?-Canyon
052/85
(isoklinal mit FAF = 353/63)
048/88
(isoklinal wie oben)

Sams Spring Area
186/45 (140/45)
106/60 (173/75)
190/35 (267/72)

Cuna Spring Area
074/35
200/45
204/07
062/30
012/03
193/19 (099/72)
029/60 (087/89)
107/66
032/31 (122/85)
032/38 (354/53)
044/57
046/47 (346/54)
008/38 (290/72)
(268/74)
(266/66)
(278/66)
(265/80)

The Elephant and adjacent hills
024/30 (288/83)
356/09 (270/69)
008/33 (284/65)
282/32 (303/45)
054/51
028/42 (327/80)
030/34 (134/32)
106/10
120/35 (090/22)
151/10 (040/35)
164/09
(166/85)
(185/61)
(085/30)
(089/50)
(099/53)
(103/82)
(275/80)
(098/75)
(102/76)

Birch and Beer Creek
310/42
350/40
334/24
321/20
324 24
180/80
035/37
146/08 (238/45)
310/25 (231/72)
195/55 (270/67)
306/42 (253/61)
357/50 (282/73)
164/18 (082/34)
175/15 (106/84)
359/43 (257/67)
331/35 (278/55)
303/45 (262/73)
318/31 (238/77)
322/20 (233/72)
326/07 (242/71)
326/31 (259/50)
332/13 (243/54)
339/13 (258/60)
324/14 (234/75)
334/24 (241/74)

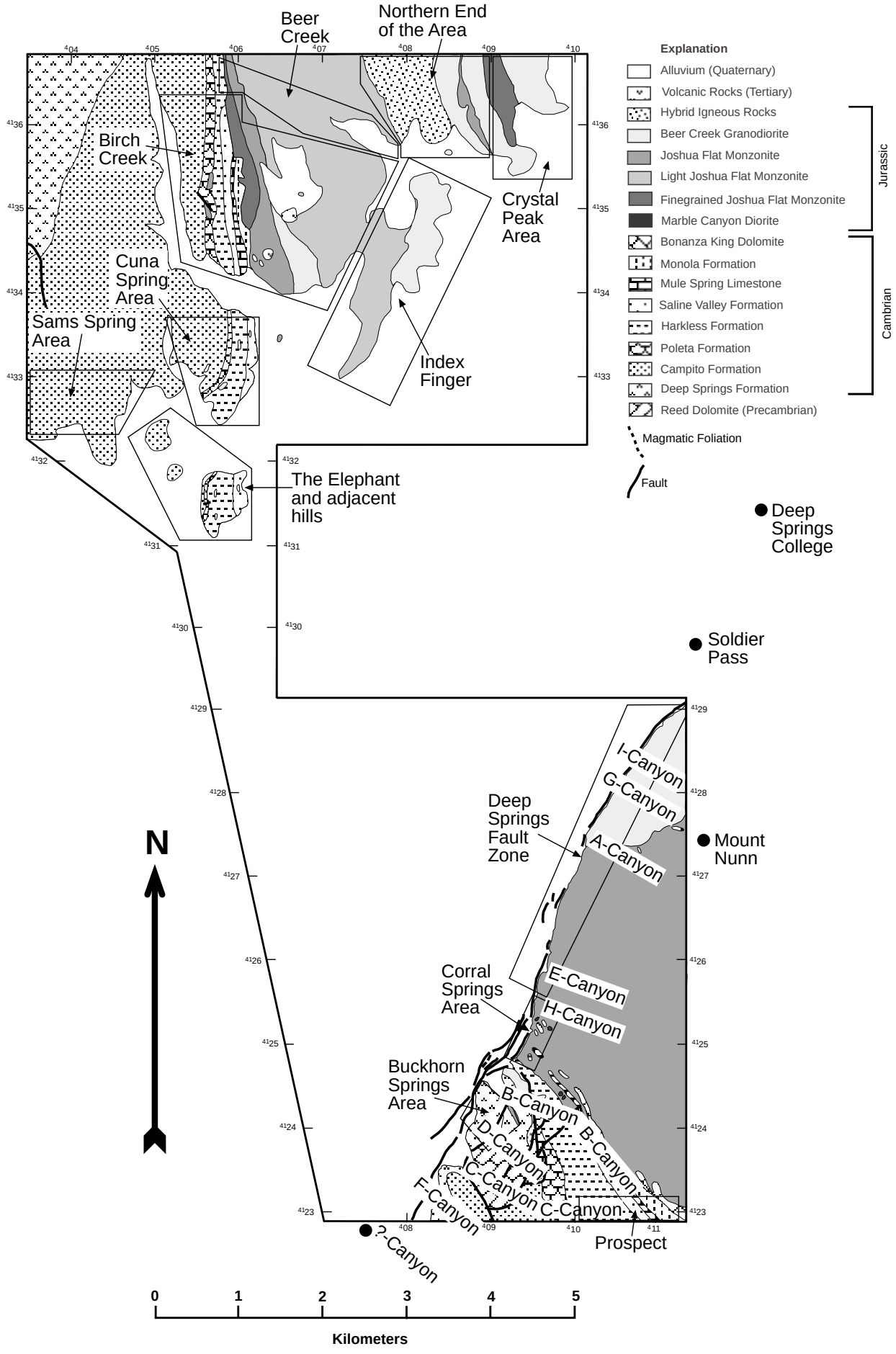
Beer Creek
Northern End of the Area
Birch Creek
Crystal Peak Area
Cuna Spring Area
Sams Spring Area
Index Finger
The Elephant and adjacent hills
Deep Springs College
Soldier Pass
Mount Nunn
Deep Springs Fault Zone
Corral Springs Area
Buckhorn Springs Area
I-Canyon
G-Canyon
A-Canyon
E-Canyon
H-Canyon
B-Canyon
D-Canyon
C-Canyon
F-Canyon
?-Canyon
Prospect
N
0 1 2 3 4 5
Kilometers
Explanation
Alluvium (Quaternary)
Volcanic Rocks (Tertiary)
Hybrid Igneous Rocks
Beer Creek Granodiorite
Joshua Flat Monzonite
Light Joshua Flat Monzonite
Finegrained Joshua Flat Monzonite
Marble Canyon Diorite
Bonanza King Dolomite
Monola Formation
Mule Spring Limestone
Saline Valley Formation
Harkless Formation
Poleta Formation
Campito Formation
Deep Springs Formation
Reed Dolomite (Precambrian)
Jurassic
Cambrian
Magmatic Foliation
Fault

AMS measurements in the Joshua Flat – Beer Creek – Pluton

The most important parameters of the AMS ellipspod, such as the shape factor T, the corrected anisotropy factor P' the average magnetic susceptibility κ, as well as the orientation of the magnetic foliation (dip direction / dip angle) and lineation (trend / plunge) together with their standard deviation and eigen values, respectively, are presented here for both the Beer Creek Granodiorite (BCG) and the Joshua Flat Monzonite (JFM).

BCG samples	N-S coords.	E-W coords.	n	Ave. T	St. dev.	Ave. P'	St. dev.
DSC1	4136600	0413751	2	0.420	0.022	1.084	0.001
C5632	4133450	0413000	2	-0.270	0.035	1.085	0.014
DSFZ1	4127485	0410150	3	0.078	0.229	1.068	0.003
DSFZ5.1	4128950	0411355	3	0.715	0.160	1.095	0.003
DSFZ5.2	4128950	0411355	3	0.611	0.034	1.116	0.004
DSFZ6	4128710	0411135	8	0.335	0.186	1.119	0.008
DSFZ7	4128395	0410770	10	0.640	0.113	1.073	0.009
DSFZ10	4127990	0410600	9	0.660	0.104	1.143	0.011
DSFZ11	4127800	0410410	8	0.779	0.132	1.126	0.010
A5180	4127530	0410170	1	0.369	0.000	1.078	0.000
A5340	4127460	0410280	10	0.672	0.072	1.126	0.022
G5460.1	4127960	0410710	5	0.498	0.114	1.158	0.009
G5460.2	4127960	0410710	5	0.245	0.068	1.285	0.009
G5680	4127910	0410850	10	0.429	0.045	1.129	0.008
G6000	4127820	0411010	10	0.553	0.107	1.142	0.008
I5100	4128390	0410715	6	0.705	0.044	1.106	0.004
I5180	4128350	0410760	6	0.454	0.191	1.075	0.004
I5300	4128350	0410790	12	0.610	0.094	1.058	0.002
I5340.1	4128350	0410860	5	0.752	0.040	1.104	0.005
I5340.2	4128350	0410860	2	0.665	0.032	1.086	0.005
ZF1	4135275	0408480	4	0.494	0.028	1.152	0.019
ZF5	4135030	0408130	3	0.345	0.026	1.212	0.007
ZF9.1a	4134055	0408140	6	0.502	0.227	1.192	0.015
ZF9.1b	4134055	0408140	8	0.855	0.074	1.156	0.009
ZF9.2	4134055	0408140	4	-0.845	0.121	1.105	0.005
ZF19	4134605	0407990	4	0.524	0.024	1.172	0.002
ZF22.1	4134825	0408110	7	0.505	0.095	1.195	0.006
ZF22.2	4134825	0408110	5	0.179	0.036	1.209	0.011
ZF23	4135095	0408135	7	0.138	0.058	1.151	0.017
CPG2	4136205	0409800	2	0.488	0.099	1.086	0.007
CPG10	4135665	0409390	1	-0.292	0.000	1.049	0.000
CPG18	4136480	0409260	4	0.558	0.032	1.068	0.008
CPG19	4136675	0409210	3	0.181	0.124	1.070	0.003
NEG8	4136120	0408810	7	0.530	0.198	1.090	0.023
NEG21	4135940	0408325	4	0.252	0.054	1.199	0.013
NEG22	4135905	0408380	5	0.556	0.044	1.249	0.010
NEG27	4136445	0408700	3	0.417	0.079	1.086	0.004
Average				**0.405**	**0.328**	**1.135**	**0.060**

BCG samples	Ave. κ (SI)	St. dev.	Mag. Fol.	Eigenvalue	Mag. Lin.	Eigenvalue
DSC1	2.01E-01	8.45E-03	275/43	0.9987	274/43	0.9973
C5632	1.32E-01	7.13E-02	318/53	0.9929	228/00	0.9803
DSFZ1	1.56E-01	1.12E-02	032/21	0.9932	046/20	0.9990
DSFZ5.1	1.94E-01	1.25E-02	220/86	0.9637	167/79	0.8785
DSFZ5.2	4.18E-01	1.47E-02	220/86	0.9637	167/79	0.8785
DSFZ6	2.38E-01	1.61E-02	222/64	0.9912	180/56	0.9493
DSFZ7	2.33E-01	1.54E-02	057/65	0.9893	010/55	0.9031
DSFZ10	2.61E-01	1.17E-02	359/27	0.9818	035/22	0.9724
DSFZ11	2.40E-01	1.68E-02	228/84	0.9939	206/85	0.8525
A5180	2.57E-01	0.00E+00	041/85	1.0000	352/82	1.0000
A5340	2.16E-01	4.09E-02	229/79	0.9915	161/62	0.9794
G5460.1	2.62E-01	1.78E-02	223/82	0.9958	201/81	0.9935
G5460.2	4.55E-01	1.60E-02	223/82	0.9958	210/81	0.9935
G5680	2.48E-01	1.21E-02	058/72	0.9953	344/42	0.9907
G6000	2.90E-01	1.48E-02	215/50	0.9982	216/50	0.9951
I5100	2.39E-01	1.21E-02	054/64	0.9965	015/58	0.9736
I5180	2.05E-01	1.18E-02	278/40	0.9933	216/20	0.9747
I5300	2.52E-01	1.16E-02	196/42	0.9904	194/42	0.9690
I5340.1	2.45E-01	2.41E-02	201/52	0.9961	134/27	0.9678
I5340.2	3.21E-01	4.50E-04	201/52	0.9961	134/27	0.9678
ZF1	2.40E-01	2.66E-02	238/59	0.9395	214/62	0.8962
ZF5	2.77E-01	9.41E-03	245/65	0.9984	246/65	0.9982
ZF9.1a	2.39E-01	1.07E-02	255/77	0.8715	273/74	0.8953
ZF9.1b	2.24E-01	1.16E-02	255/77	0.8715	273/74	0.8953
ZF9.2	3.54E-01	2.10E-02	255/77	0.8715	273/74	0.8953
ZF19	4.61E-01	1.52E-02	064/84	0.9984	035/83	0.9943
ZF22.1	3.44E-01	4.91E-02	281/66	0.9946	281/66	0.9938
ZF22.2	2.56E-01	9.57E-03	281/66	0.9946	281/66	0.9938
ZF23	2.27E-01	8.17E-03	250/84	0.9937	326/65	0.9932
CPG2	2.12E-01	1.24E-02	073/66	0.9361	038/62	0.9411
CPG10	1.04E-01	0.00E+00	157/56	1.0000	113/48	1.0000
CPG18	3.32E-01	1.05E-02	046/84	0.9960	134/20	0.9929
CPG19	7.26E-02	2.65E-03	057/77	0.9972	079/76	0.9648
NEG8	2.91E-01	2.24E-02	050/50	0.9672	321/01	0.9750
NEG21	3.23E-01	2.40E-02	248/78	0.9977	273/77	0.9948
NEG22	1.58E-01	2.44E-02	140/14	0.9992	106/12	0.9972
NEG27	1.22E-01	6.73E-03	096/78	0.9983	183/12	0.9934
Average	**2.58E-01**	**8.65E-02**	**237/79**	**0.6585**	**221/84**	**0.6344**

JFM samples	N-S coords.	E-W coords.	n	Ave. T	St. dev.	Ave. P'	St. dev.
DSFZ2	4127230	0410085	5	-0.623	0.139	1.202	0.012
DSFZ3	4127320	0410140	6	-0.132	0.080	1.235	0.009
DSFZ4.1	4126320	0409730	5	0.387	0.055	1.288	0.039
DSFZ4.2	4126320	0409730	1	0.415	0.000	1.230	0.000
DSFZ8	4126530	0409780	8	0.305	0.052	1.265	0.019
DSFZ9	4126840	0409950	12	-0.307	0.123	1.255	0.020
CoSA1	4125640	0409520	5	0.637	0.133	1.208	0.015
CoSA3	4125370	0409500	4	-0.040	0.045	1.201	0.017
CoSA4	4125280	0409490	7	-0.304	0.131	1.404	0.081
A5800	4127250	0410790	1	0.143	0.000	1.452	0.000
A6140	4127215	0410855	9	-0.007	0.062	1.593	0.041
B7000	4123200	0411070	5	0.357	0.222	1.083	0.010
E5180	4126080	0409710	7	0.466	0.241	1.207	0.036
E5340	4126060	0409850	9	0.422	0.112	1.270	0.048
E5540	4126070	0410020	4	0.446	0.029	1.360	0.023
E5840.1	4126030	0410210	8	0.406	0.112	1.364	0.041
E5840.2	4126030	0410210	1	0.145	0.000	1.209	0.000
H5250	4125500	0409585	8	0.072	0.123	1.276	0.044
H5520	4125550	0409750	8	0.232	0.361	1.262	0.018
H5800	4125580	0409950	10	0.113	0.304	1.025	0.004
H5860	4125560	0409970	7	0.321	0.122	1.217	0.024
P0	4123105	0411150	7	0.057	0.110	1.201	0.032
Lok1	4135760	0407900	1	0.826	0.000	1.280	0.000
Lok8	4136120	0406880	4	0.134	0.139	1.228	0.006
Lok12	4136445	0406015	1	-0.296	0.000	1.034	0.000
Lok17	4133060	0407215	1	-0.111	0.000	1.225	0.000
Lok18	4133465	0406480	5	-0.094	0.042	1.471	0.128
Lok24	4134370	0406190	1	0.659	0.000	1.060	0.000
TC5840	4134350	0406115	15	0.121	0.202	1.209	0.076
BC0	4135270	0406205	10	0.520	0.077	1.120	0.009
Pl1	4134780	0407470	6	0.342	0.141	1.162	0.018
Pl7.1	4134800	0406740	3	-0.345	0.010	1.126	0.013
Pl7.2	4134800	0406740	2	0.311	0.006	1.298	0.016
Pl8	4134810	0406600	11	0.090	0.111	1.064	0.003
ZF10	4133610	0407655	5	0.146	0.168	1.224	0.046
ZF13	4134150	0407800	11	0.435	0.084	1.177	0.009
ZF14	4135540	0407740	11	0.221	0.126	1.286	0.017
ZF15	4134470	0407800	11	0.516	0.213	1.184	0.035
CPG1	4136180	0409830	5	0.423	0.224	1.079	0.014
CPG12	4135875	0409225	4	0.643	0.073	1.112	0.029
CPG17	4136430	0409060	7	0.554	0.042	1.078	0.002
NEG1.1	4135990	0408535	11	0.795	0.092	1.098	0.010
NEG1.2	4135990	0408535	4	0.520	0.046	1.235	0.008
NEG3	4136050	0408700	10	0.423	0.128	1.145	0.014
NEG4	4136120	0408825	9	0.557	0.088	1.067	0.005
NEG5	4136245	0408680	8	0.493	0.220	1.072	0.006
NEG11	4136530	0408055	9	0.684	0.038	1.245	0.016
NEG13	4136360	0408015	6	0.644	0.125	1.140	0.014
NEG14	4136110	0408140	9	-0.379	0.223	1.120	0.014
NEG16	4135940	0408015	9	0.250	0.077	1.138	0.013
NEG17	4136590	0407580	3	0.559	0.056	1.338	0.026
NEG18	4136290	0407760	6	0.236	0.0.36	1.157	0.008
NEG20	4136235	0407925	9	0.308	0.061	1.264	0.012
Average				**0.374**	**0.280**	**1.161**	**0.078**

JFM samples	Ave. κ (SI)	St. dev.	Mag. Fol.	Eigenvalue	Mag. Lin.	Eigenvalue
DSFZ2	3.99E-01	2.01E-02	047/83	0.9771	321/28	0.9980
DSFZ3	1.88E-01	2.18E-02	219/86	0.9711	174/84	0.9507
DSFZ4.1	3.75E-01	6.31E-02	060/56	0.9734	332/03	0.9686
DSFZ4.2	4.89E-01	0.00E+00	049/59	1.0000	324/09	1.0000
DSFZ8	2.50E-01	1.91E-02	290/67	0.9992	340/56	0.9968
DSFZ9	3.95E-01	3.59E-02	029/67	0.9834	006/66	0.9971
CoSA1	6.35E-01	1.06E-01	078/61	0.9969	014/37	0.9364
CoSA3	4.08E-01	9.82E-03	026/55	0.9985	061/49	0.9979
CoSA4	3.01E-01	4.34E-02	031/76	0.9337	304/16	0.9671
A5800	4.32E-01	0.00E+00	039/80	1.0000	322/52	1.0000
A6140	2.81E-01	1.22E-01	050/59	0.9977	022/56	0.9968
B7000	4.27E-02	3.01E-02	238/57	0.9965	155/10	0.9964
E5180	4.91E-01	3.46E-02	069/79	0.9903	359/62	0.9301
E5340	3.23E-01	4.30E-02	194/53	0.9827	267/22	0.9589
E5540	3.81E-01	3.15E-02	111/60	0.9968	035/26	0.9960
E5840.1	3.64E-01	5.24E-02	073/58	0.9879	144/25	0.9875
E5840.2	2.11E-01	0.00E+00	083/63	1.0000	147/13	1.0000
H5250	8.32E-01	4.63E-02	182/16	0.9718	254/04	0.9765
H5520	4.83E-01	2.46E-02	241/58	0.9975	266/55	0.9969
H5800	5.58E-02	1.11E-02	085/90	0.9592	358/63	0.9743
H5860	6.09E-01	6.25E-02	060/51	0.9921	141/11	0.9754
P0	4.28E-01	4.84E-02	243/77	0.9797	266/78	0.9922
Lok1	2.53E-01	0.00E+00	029/54	1.0000	104/19	1.0000
Lok8	2.78E-01	1.53E-02	019/39	0.9986	001/38	0.9983
Lok12	5.78E-02	0.00E+00	257/70	1.0000	246/69	1.0000
Lok17	2.29E-01	0.00E+00	073/43	1.0000	129/28	1.0000
Lok18	1.99E-01	4.31E-02	263/82	0.8438	340/43	0.9443
Lok24	1.61E-03	0.00E+00	265/78	1.0000	270/78	1.0000
TC5840	6.12E-02	2.61E-02	083/60	0.9549	085/59	0.9621
BC0	1.77E-01	1.59E-02	220/56	0.9986	303/11	0.9955
Pl1	2.21E-01	1.12E-02	036/43	0.9909	315/08	0.9771
Pl7.1	4.53E-02	5.43E-03	073/90	0.9930	345/83	0.9928
Pl7.2	2.26E-01	6.10E-03	074/52	0.9971	048/49	0.9966
Pl8	8.52E-02	1.94E-02	064/87	0.9971	346/77	0.9963
ZF10	2.47E-01	2.78E-02	052/40	0.9950	326/03	0.9820
ZF13	2.32E-01	1.23E-02	049/61	0.9977	111/40	0.9887
ZF14	2.25E-01	1.86E-02	246/72	0.9918	254/72	0.9125
ZF15	1.39E-01	2.88E-02	249/43	0.9943	240/42	0.8957
CPG1	3.94E-01	7.85E-02	065/53	0.7740	011/23	0.8412
CPG12	2.95E-01	2.57E-02	076/59	0.8113	133/35	0.7287
CPG17	4.35E-01	1.17E-02	202/82	0.9996	134/69	0.9965
NEG1.1	3.21E-01	4.86E-02	067/81	0.9950	155/10	0.6680
NEG1.2	3.47E-01	2.74E-02	233/77	0.9986	298/63	0.9974
NEG3	2.04E-01	7.01E-02	239/85	0.9771	296/81	0.9443
NEG4	5.35E-02	1.09E-02	240/81	0.9975	309/66	0.9691
NEG5	2.13E-01	3.24E-02	295/60	0.9943	304/60	0.9973
NEG11	4.70E-01	1.81E-02	232/55	0.9976	269/49	0.9918
NEG13	2.63E-01	2.51E-02	216/59	0.9985	162/45	0.9841
NEG14	2.68E-01	1.19E-02	270/74	0.8683	214/65	0.9597
NEG16	4.07E-01	1.79E-02	228/80	0.9976	297/64	0.9955
NEG17	2.77E-01	2.02E-02	242/84	0.9972	278/83	0.9878
NEG18	2.38E-01	1.29E-02	219/73	0.9982	269/64	0.9941
NEG20	2.91E-01	9.49E-03	063/84	0.9986	007/79	0.9967
Average	**2.36E-01**	**1.20E-01**	**060/83**	**0.6854**	**324/66**	**0.5420**

Strain measurements for aureole rocks of the Joshua Flat – Beer Creek – Pluton

The presented data were determined with the computer program “TRISEC”.

SSA8

STRAIN ANALYSES AT CORDIERITE PORPHYROBLASTS (POLISHED SECTION)

N-S COORDINATE: 4132790; E-W COORDINATE: 0404710

SECTION 1 DIP 88 STRIKE 296 PITCH OF ELLIPSE LONG AXIS 94 ELLIPSE RATIO 1.900
SECTION 2 DIP 66 STRIKE 27 PITCH OF ELLIPSE LONG AXIS 149 ELLIPSE RATIO 1.500
SECTION 3 DIP 24 STRIKE 210 PITCH OF ELLIPSE LONG AXIS 33 ELLIPSE RATIO 1.430
1.0954687
51.4228707
2.4616210

PRODUCT OF ADJUSTMENT FACTORS 1.7160

SECTION 1 ADJUSTMENT ELLIPSE RATIO 1.197
SECTION 2 ADJUSTMENT ELLIPSE RATIO 1.197
SECTION 3 ADJUSTMENT ELLIPSE RATIO 1.197

MATRIX REPRESENTING ELLIPSOID

0.512 -0.214 0.145
-0.214 0.582 0.105
0.145 0.105 0.251

AXIS NUMBER 1 TREND 219 PLUNGE 51 LENGTH 3.044
AXIS NUMBER 2 TREND 43 PLUNGE 39 LENGTH 1.455
AXIS NUMBER 3 TREND 311 PLUNGE 2 LENGTH 1.144

X:Y:Z = 2.661: 1.272: 1.000 LODES PARAMETER = -0.508

ES VALUE = 0.874

TECTONIC CLEAVAGE AS DEFINED BY X:Y PLANE HAS STRIKE 41 AND DIP 88

SSA15

STRAIN ANALYSES AT CORDIERITE PORPHYROBLASTS (POLISHED SECTION)

N-S COORDINATE: 4132890; E-W COORDINATE: 0404390

SECTION 1 DIP 85 STRIKE 291 PITCH OF ELLIPSE LONG AXIS 118 ELLIPSE RATIO 1.910
SECTION 2 DIP 61 STRIKE 24 PITCH OF ELLIPSE LONG AXIS 44 ELLIPSE RATIO 1.960
SECTION 3 DIP 29 STRIKE 191 PITCH OF ELLIPSE LONG AXIS 21 ELLIPSE RATIO 1.900
1.1492901
10.4832473
2.1024245

PRODUCT OF ADJUSTMENT FACTORS 0.9494

SECTION 1 ADJUSTMENT ELLIPSE RATIO 0.983
SECTION 2 ADJUSTMENT ELLIPSE RATIO 0.983
SECTION 3 ADJUSTMENT ELLIPSE RATIO 0.983

MATRIX REPRESENTING ELLIPSOID

0.531 -0.353 0.035
-0.353 0.646 -0.305
0.035 -0.305 0.457

AXIS NUMBER 1 TREND 52 PLUNGE 33 LENGTH 2.909
AXIS NUMBER 2 TREND 186 PLUNGE 47 LENGTH 1.483
AXIS NUMBER 3 TREND 305 PLUNGE 24 LENGTH 0.971

X:Y:Z = 2.996: 1.527: 1.000 LODES PARAMETER = -0.228

ES VALUE = 0.851

TECTONIC CLEAVAGE AS DEFINED BY X:Y PLANE HAS STRIKE 35 AND DIP 66

SSA18

STRAIN ANALYSES AT CORDIERITE PORPHYROBLASTS (POLISHED SECTION)

N-S COORDINATE: 4132990; E-W COORDINATE: 0404220

SECTION 1 DIP 64 STRIKE 21 PITCH OF ELLIPSE LONG AXIS 124 ELLIPSE RATIO 1.810
SECTION 2 DIP 72 STRIKE 120 PITCH OF ELLIPSE LONG AXIS 62 ELLIPSE RATIO 2.150
SECTION 3 DIP 30 STRIKE 231 PITCH OF ELLIPSE LONG AXIS 150 ELLIPSE RATIO 1.780
1.1844395
2.2418704
4.4502049

PRODUCT OF ADJUSTMENT FACTORS 1.3467

SECTION 1 ADJUSTMENT ELLIPSE RATIO 1.104
SECTION 2 ADJUSTMENT ELLIPSE RATIO 1.104
SECTION 3 ADJUSTMENT ELLIPSE RATIO 1.104

MATRIX REPRESENTING ELLIPSOID

0.648 -0.207 0.383
-0.207 1.674 -0.456
0.383 -0.456 0.762

AXIS NUMBER 1 TREND 170 PLUNGE 45 LENGTH 1.830
AXIS NUMBER 2 TREND 35 PLUNGE 35 LENGTH 1.097
AXIS NUMBER 3 TREND 287 PLUNGE 25 LENGTH 0.715

X:Y:Z = 2.558: 1.533: 1.000 LODES PARAMETER = -0.090

ES VALUE = 0.686

TECTONIC CLEAVAGE AS DEFINED BY X:Y PLANE HAS STRIKE 17 AND DIP 65

CSA 12

STRAIN ANALYSES AT CORDIERITE PORPHYROBLASTS (POLISHED SECTION)

N-S COORDINATE: 4132545; E-W COORDINATE: 0405930

SECTION 1 DIP 13 STRIKE 297 PITCH OF ELLIPSE LONG AXIS 116 ELLIPSE RATIO 1.820
SECTION 2 DIP 77 STRIKE 103 PITCH OF ELLIPSE LONG AXIS 92 ELLIPSE RATIO 4.240
SECTION 3 DIP 87 STRIKE 194 PITCH OF ELLIPSE LONG AXIS 86 ELLIPSE RATIO 1.700
18.8583483
1.0278552
4.5686047

PRODUCT OF ADJUSTMENT FACTORS 2.3103

SECTION 1 ADJUSTMENT ELLIPSE RATIO 1.322
SECTION 2 ADJUSTMENT ELLIPSE RATIO 1.322
SECTION 3 ADJUSTMENT ELLIPSE RATIO 1.322

MATRIX REPRESENTING ELLIPSOID

0.471 -0.312 0.031
-0.312 0.585 -0.035
0.031 -0.035 0.066

AXIS NUMBER 1 TREND 137 PLUNGE 87 LENGTH 3.981
AXIS NUMBER 2 TREND 40 PLUNGE 0 LENGTH 2.181
AXIS NUMBER 3 TREND 310 PLUNGE 3 LENGTH 1.086

X:Y:Z = 3.667: 2.008: 1.000 LODES PARAMETER = 0.073

ES VALUE = 0.899

TECTONIC CLEAVAGE AS DEFINED BY X:Y PLANE HAS STRIKE 40 AND DIP 87

E2

STRAIN ANALYSES AT CORDIERITE PORPHYROBLASTS (POLISHED SECTION)

N-S COORDINATE: 4131415; E-W COORDINATE: 0405990

SECTION 1 DIP 78 STRIKE 359 PITCH OF ELLIPSE LONG AXIS 135 ELLIPSE RATIO 1.670
SECTION 2 DIP 28 STRIKE 112 PITCH OF ELLIPSE LONG AXIS 67 ELLIPSE RATIO 1.570
SECTION 3 DIP 60 STRIKE 262 PITCH OF ELLIPSE LONG AXIS 113 ELLIPSE RATIO 1.490
2.3656827
4.8994660
1.1893623

PRODUCT OF ADJUSTMENT FACTORS 1.3918

SECTION 1 ADJUSTMENT ELLIPSE RATIO 1.117
SECTION 2 ADJUSTMENT ELLIPSE RATIO 1.117

SECTION 3 ADJUSTMENT ELLIPSE RATIO 1.117

MATRIX REPRESENTING ELLIPSOID

0.624 -0.025 0.241
-0.025 1.242 -0.250
0.241 -0.250 0.620

AXIS NUMBER 1 TREND 163 PLUNGE 48 LENGTH 1.691
AXIS NUMBER 2 TREND 25 PLUNGE 34 LENGTH 1.125
AXIS NUMBER 3 TREND 280 PLUNGE 22 LENGTH 0.862

X:Y:Z = 1.962: 1.305: 1.000 LODES PARAMETER = -0.209

ES VALUE = 0.518

TECTONIC CLEAVAGE AS DEFINED BY X:Y PLANE HAS STRIKE 10 AND DIP 68

E17

STRAIN ANALYSES AT CORDIERITE PORPHYROBLASTS (POLISHED SECTION)

N-S COORDINATE: 4131610; E-W COORDINATE: 0405970

SECTION 1 DIP 57 STRIKE 329 PITCH OF ELLIPSE LONG AXIS 98 ELLIPSE RATIO 1.510
SECTION 2 DIP 80 STRIKE 66 PITCH OF ELLIPSE LONG AXIS 116 ELLIPSE RATIO 2.000
SECTION 3 DIP 35 STRIKE 171 PITCH OF ELLIPSE LONG AXIS 14 ELLIPSE RATIO 2.230
1.2198274
1.8327789
5.5493469

PRODUCT OF ADJUSTMENT FACTORS 2.7334

SECTION 1 ADJUSTMENT ELLIPSE RATIO 1.398
SECTION 2 ADJUSTMENT ELLIPSE RATIO 1.398
SECTION 3 ADJUSTMENT ELLIPSE RATIO 1.398

MATRIX REPRESENTING ELLIPSOID

0.279 -0.097 0.185
-0.097 0.861 -0.045
0.185 -0.045 0.279

AXIS NUMBER 1 TREND 184 PLUNGE 44 LENGTH 3.285
AXIS NUMBER 2 TREND 19 PLUNGE 45 LENGTH 1.508
AXIS NUMBER 3 TREND 281 PLUNGE 8 LENGTH 1.062

X:Y:Z = 3.093: 1.420: 1.000 LODES PARAMETER = -0.379

ES VALUE = 0.944

TECTONIC CLEAVAGE AS DEFINED BY X:Y PLANE HAS STRIKE 11 AND DIP 82

Quartz-c-axes measurements at samples from the aureole of the Joshua Flat - Beer Creek - Pluton

300 c-axes were measured in each of the ten samples. The data obtained were plotted in a stereonet with reference to the lineation and foliation of the individual samples. The N-S direction of the stereonet corresponds to the pole of the foliation and the E-W direction to the lineation.

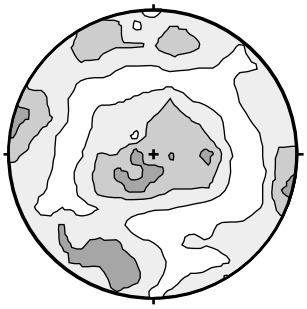

SSA1
N-S coordinate: 4132516
E-W coordinate: 0403560
Maximum density: 4.67

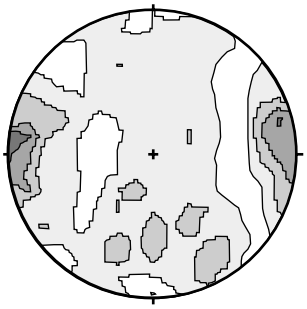

SSA12
N-S coordinate: 4132745
E-W coordinate: 0404640
Maximum density: 5.33

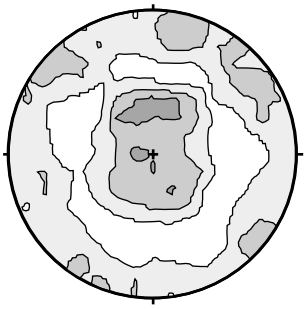

SSA20
N-S coordinate: 4132990
E-W coordinate: 0404110
Maximum density: 5.00

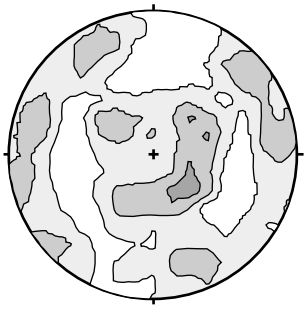

CSA1
N-S coordinate: 4133040
E-W coordinate: 0405465
Maximum density: 5.00

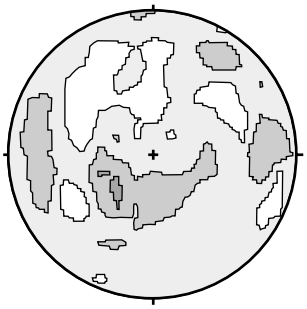

CSA2
N-S coordinate: 4133095
E-W coordinate: 0405545
Maximum density: 4.00

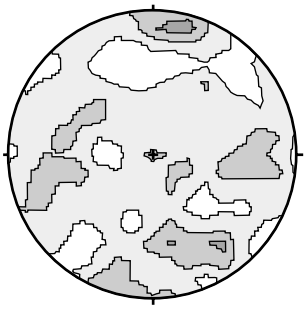

CSA9
N-S coordinate: 4132900
E-W coordinate: 0405775
Maximum density: 4.33

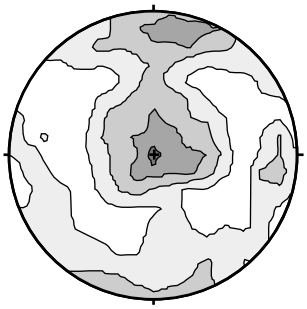

CSA13
N-S coordinate: 4133145
E-W coordinate: 0406160
Maximum density: 5.00

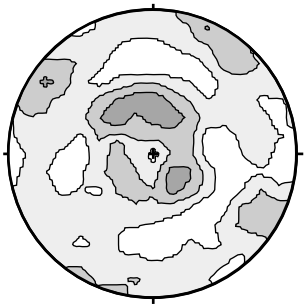

CSA15
N-S coordinate: 4133065
E-W coordinate: 0406160
Maximum density: 4.33

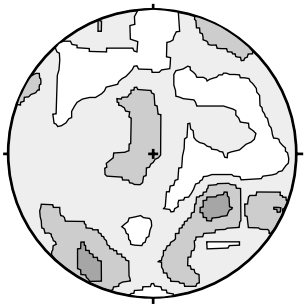

CSA17
N-S coordinate: 4133080
E-W coordinate: 0406015
Maximum density: 5.00

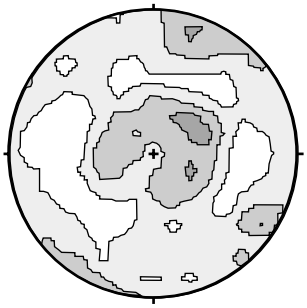

CSA20
N-S coordinate: 4133180
E-W coordinate: 0405960
Maximum density: 3.67

Infra-red spectroscopy measurements for aureole rocks of the Joshua Flat - Beer Creek - Pluton

Infra-red spectra were determined for channel volatiles in cordierite crystals from three locations:
P9 (N-S coordinate: 4123050; E-W coordinate: 0410440),
BC5660 (N-S coordinate: 4124380; E-W coordinate: 0409620),
Lok23 (N-S coordinate: 4135130; E-W coordinate: 0405910).

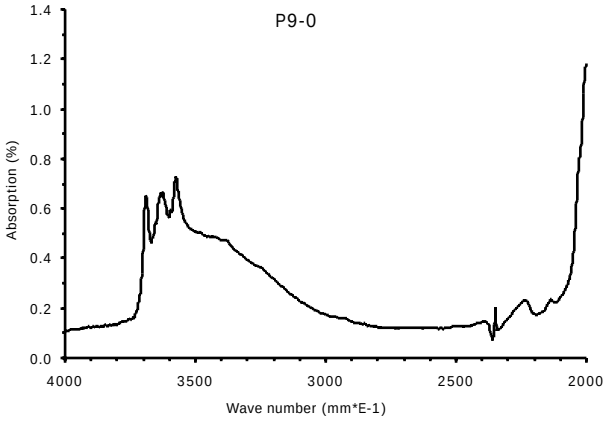

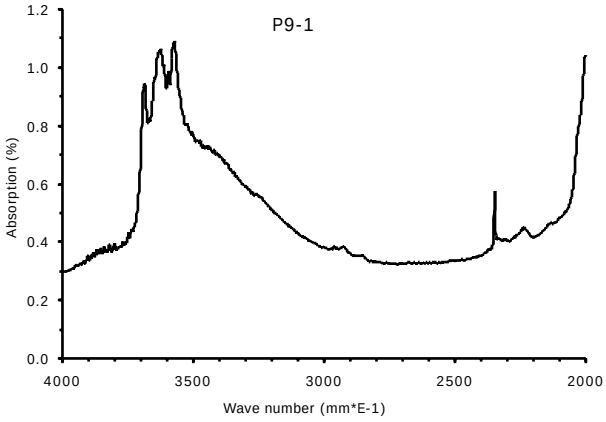

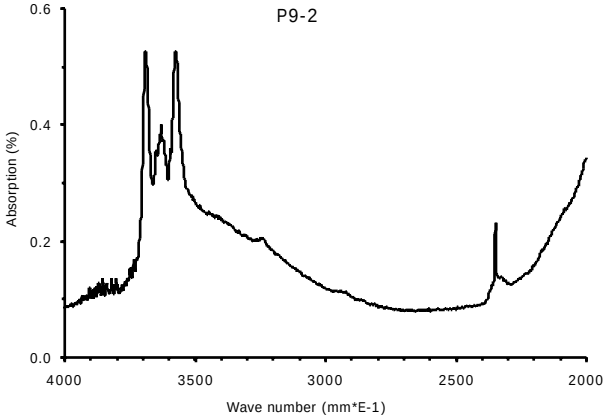

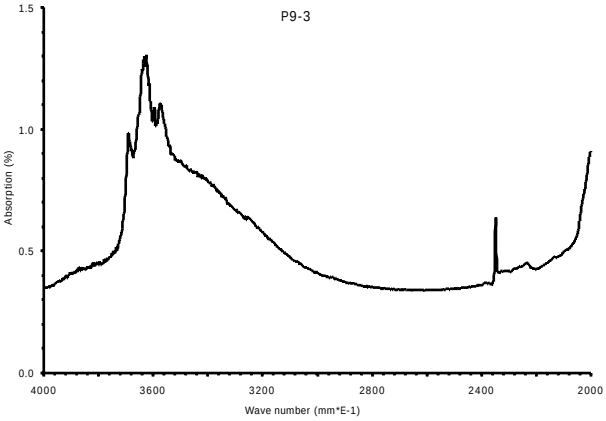

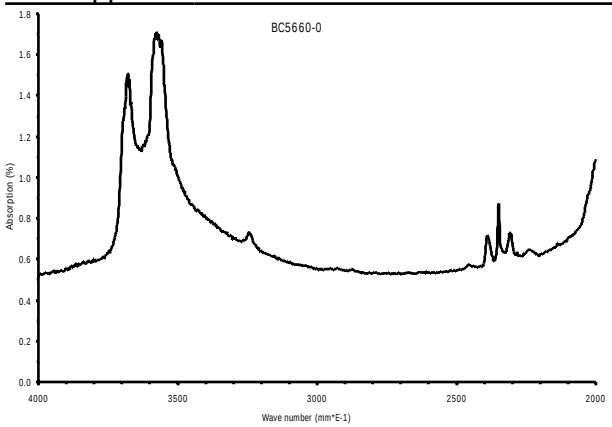
BC5660-0
Absorption (%)
Wave number (mm*E-1)

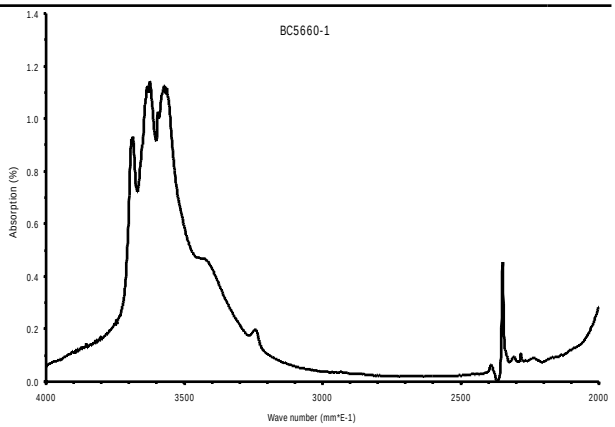
BC5660-1
Absorption (%)
Wave number (mm*E-1)

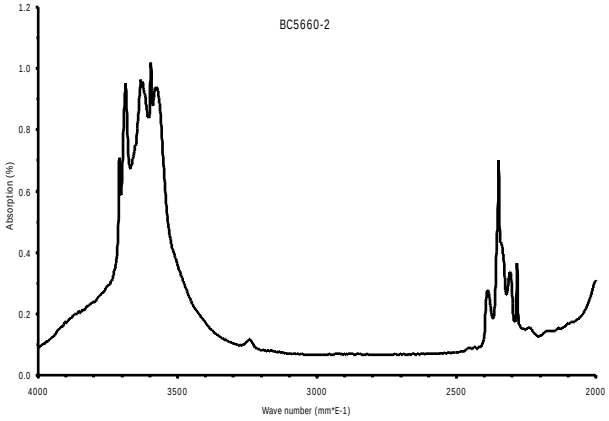
BC5660-2
Absorption (%)
Wave number (mm*E-1)

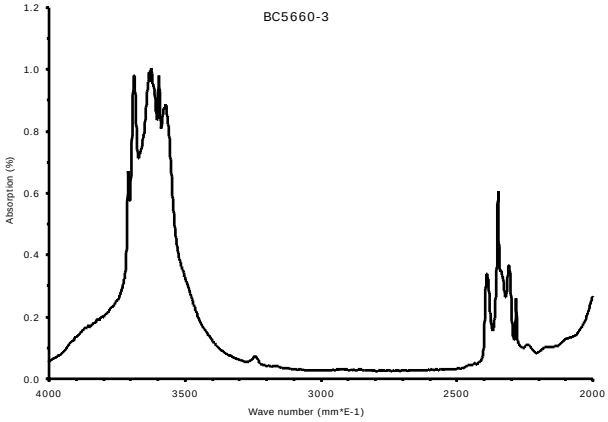
BC5660-3
Absorption (%)
Wave number (mm*E-1)

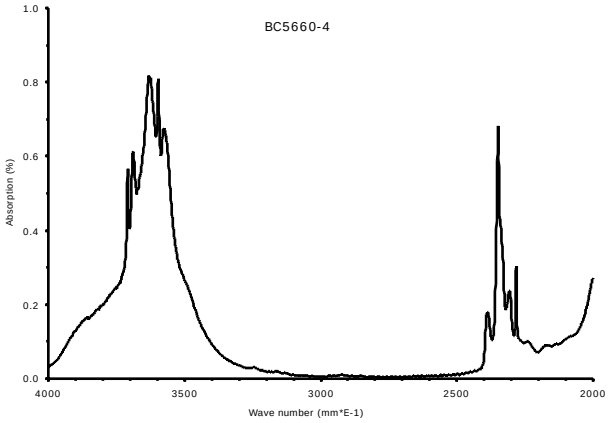
BC5660-4
Absorption (%)
Wave number (mm*E-1)

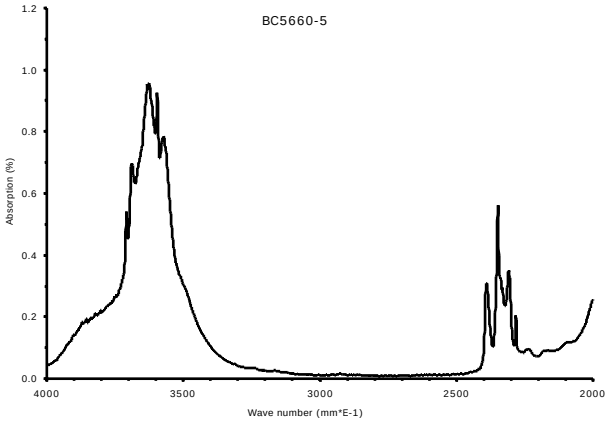
BC5660-5
Absorption (%)
Wave number (mm*E-1)

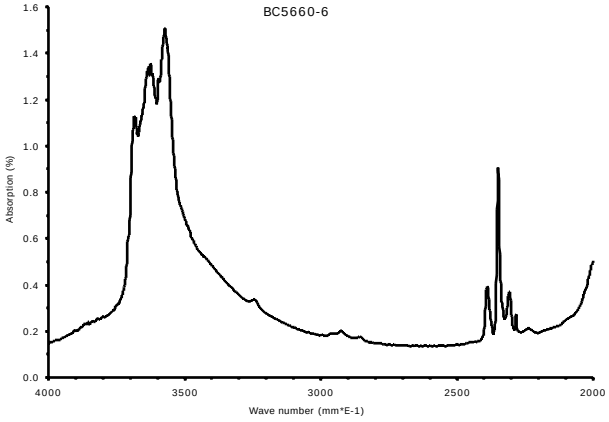
BC5660-6
Absorption (%)
Wave number (mm*E-1)

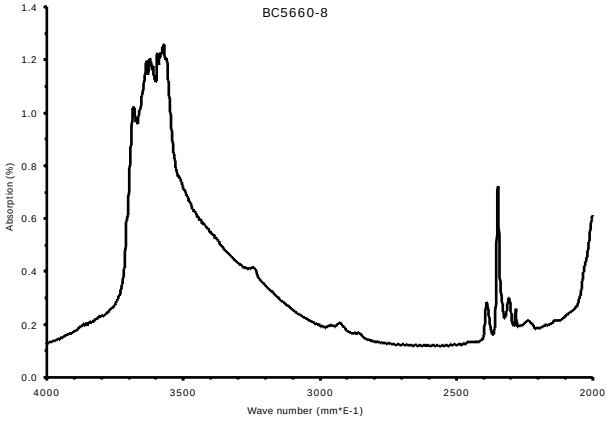
BC5660-8
Absorption (%)
Wave number (mm*E-1)

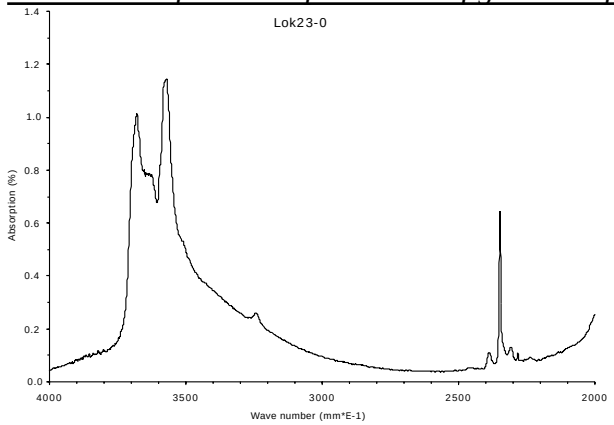
Lok23-0
Absorption (%)
Wave number (mm*E-1)

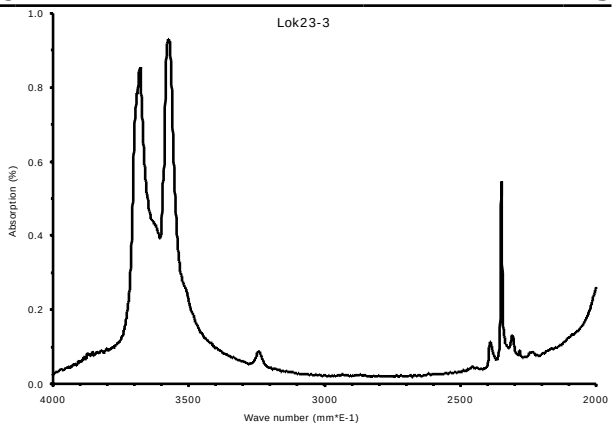
Lok23-3
Absorption (%)
Wave number (mm*E-1)

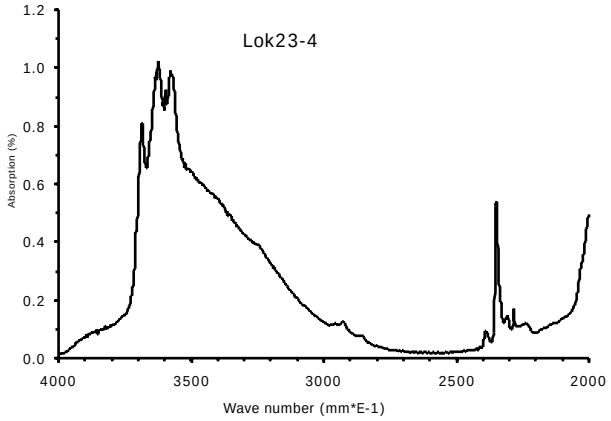
Lok23-4
Absorption (%)
Wave number (mm*E-1)

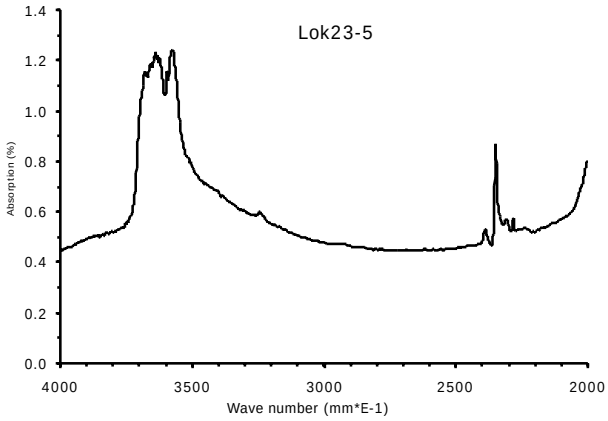
Lok23-5
Absorption (%)
Wave number (mm*E-1)

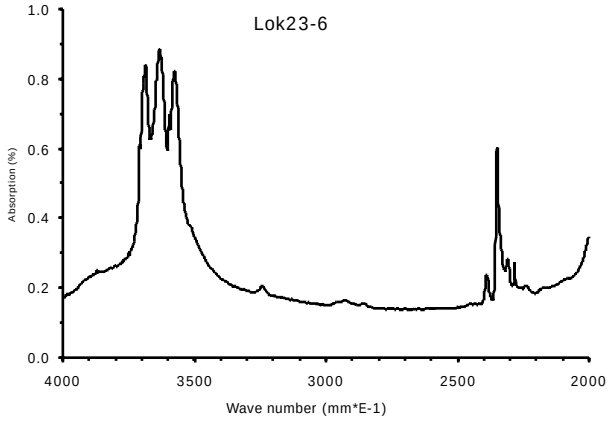
Lok23-6
Absorption (%)
Wave number (mm*E-1)

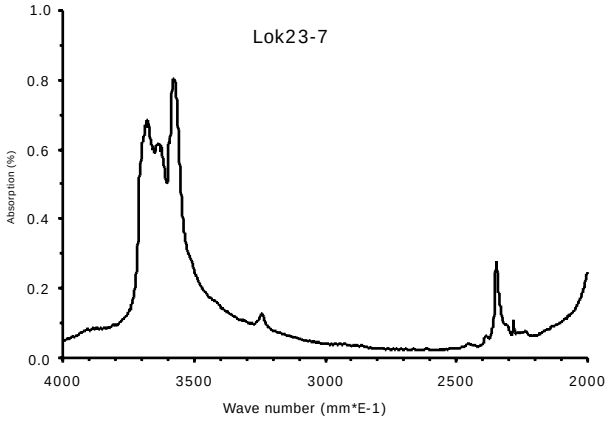
Lok23-7
Absorption (%)
Wave number (mm*E-1)

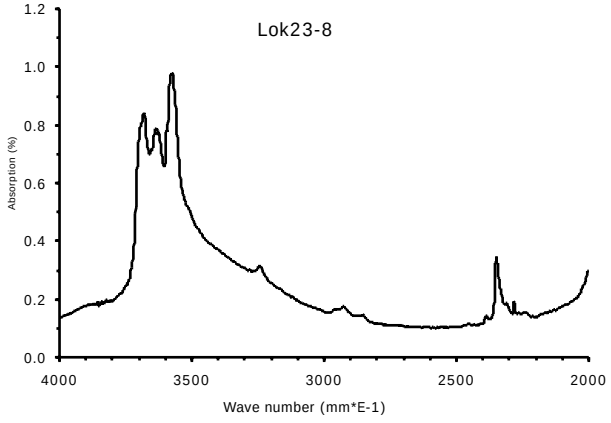
Lok23-8
Absorption (%)
Wave number (mm*E-1)

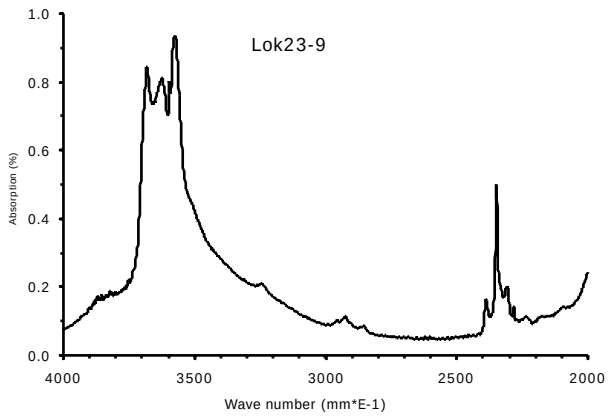
Lok23-9
Absorption (%)
Wave number (mm*E-1)

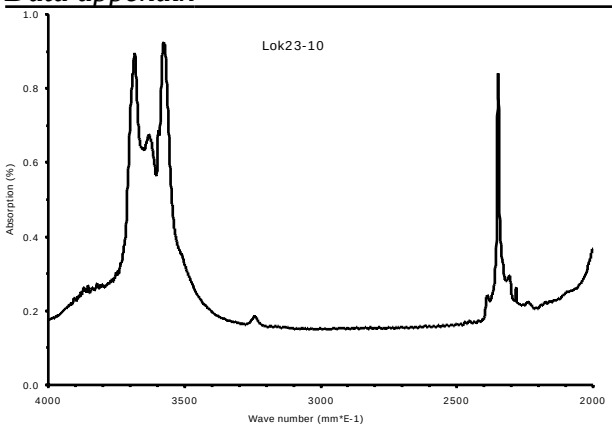
Lok23-10
Absorption (%)
Wave number (mm*E-1)

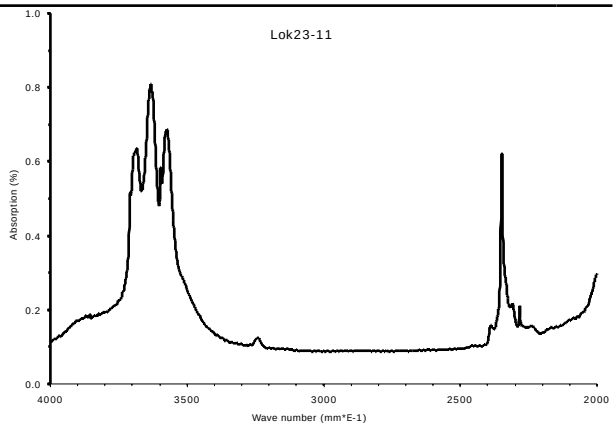
Lok23-11
Absorption (%)
Wave number (mm*E-1)

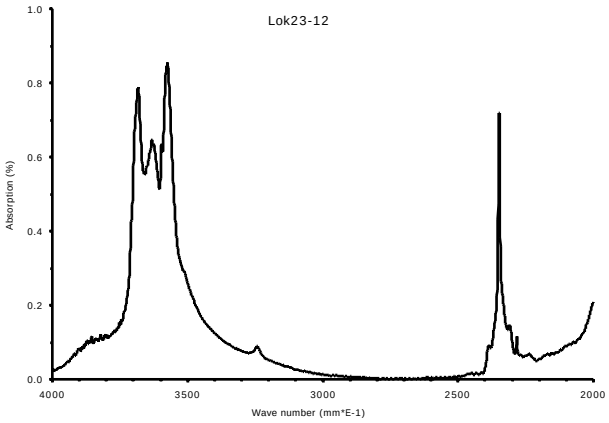
Lok23-12
Absorption (%)
Wave number (mm*E-1)

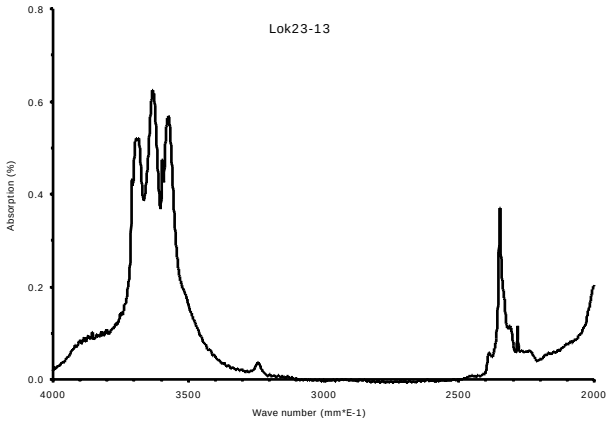
Lok23-13
Absorption (%)
Wave number (mm*E-1)

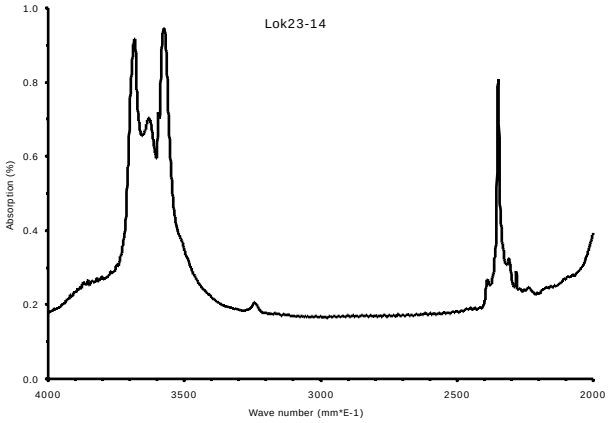
Lok23-14
Absorption (%)
Wave number (mm*E-1)

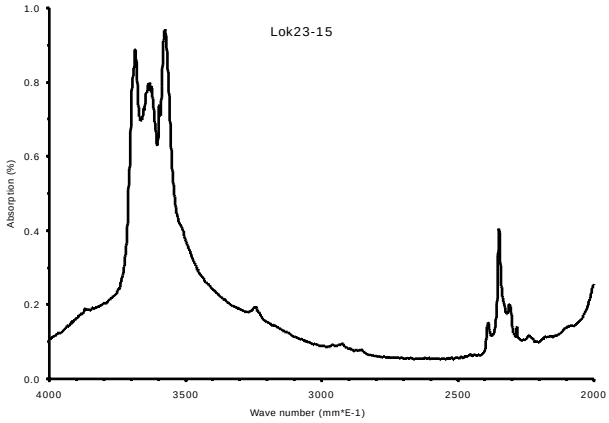
Lok23-15
Absorption (%)
Wave number (mm*E-1)

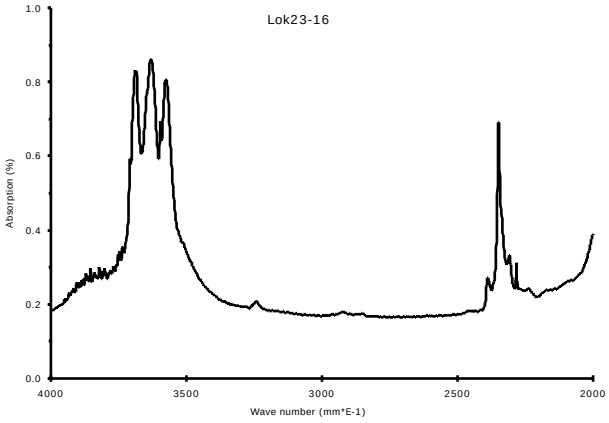
Lok23-16
Absorption (%)
Wave number (mm*E-1)

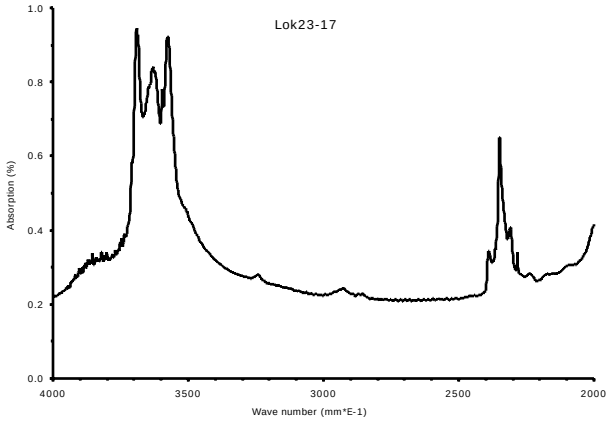
Lok23-17
Absorption (%)
Wave number (mm*E-1)

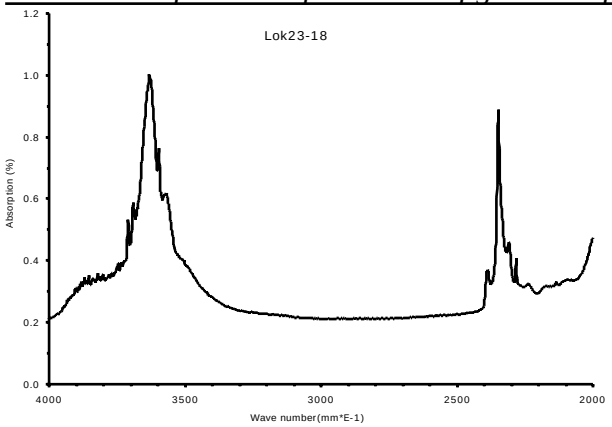
Lok23-18
Absorption (%)
Wave number(mm*E-1)

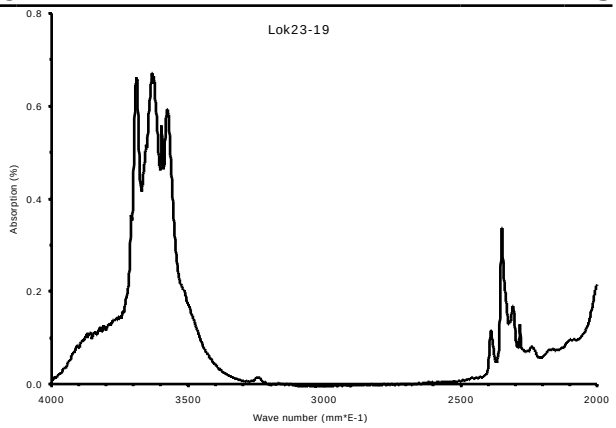
Lok23-19
Absorption (%)
Wave number (mm*E-1)

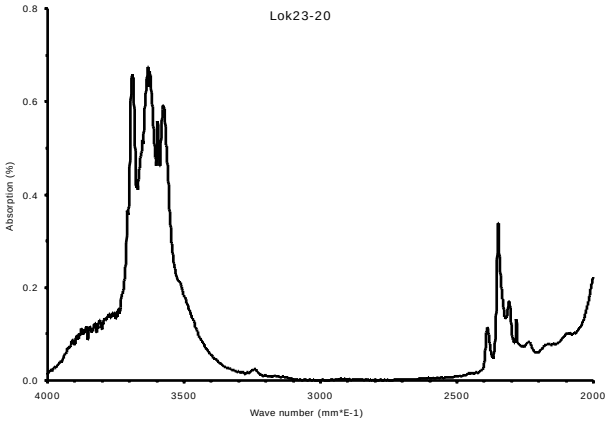
Lok23-20
Absorption (%)
Wave number (mm*E-1)

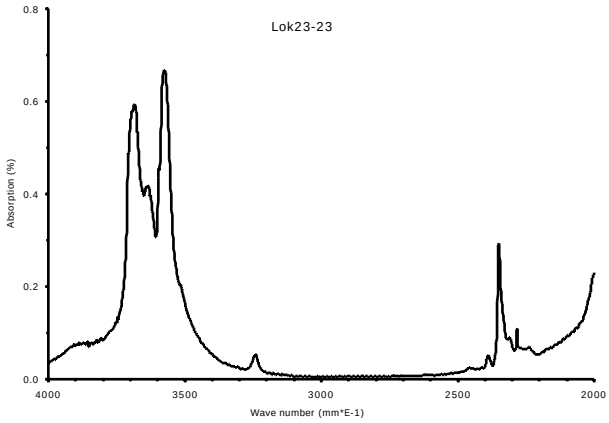
Lok23-23
Absorption (%)
Wave number (mm*E-1)

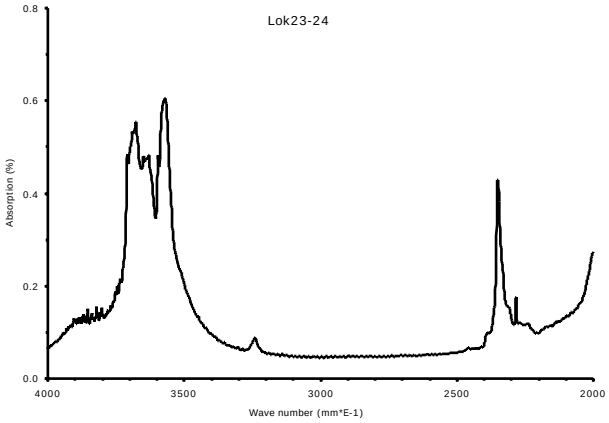
Lok23-24
Absorption (%)
Wave number (mm*E-1)

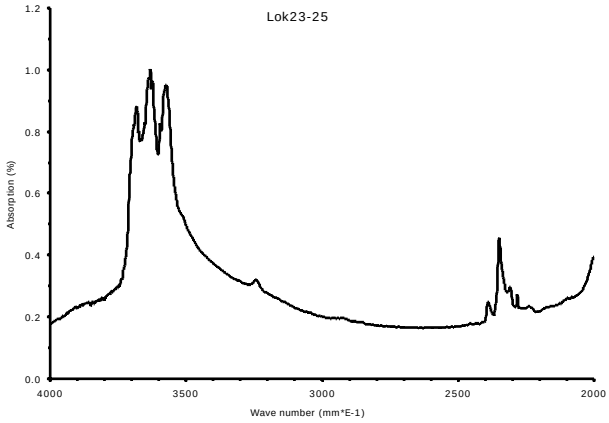
Lok23-25
Absorption (%)
Wave number (mm*E-1)

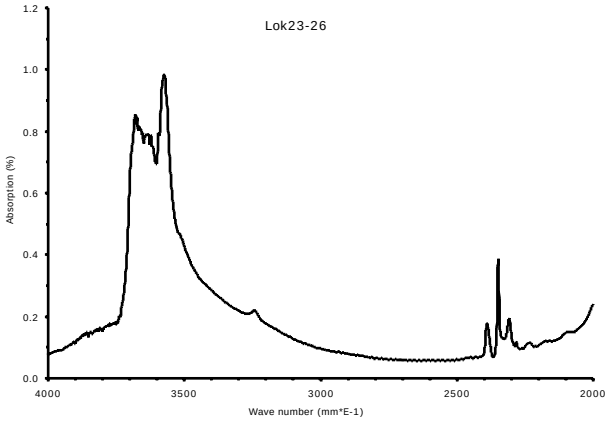
Lok23-26
Absorption (%)
Wave number (mm*E-1)

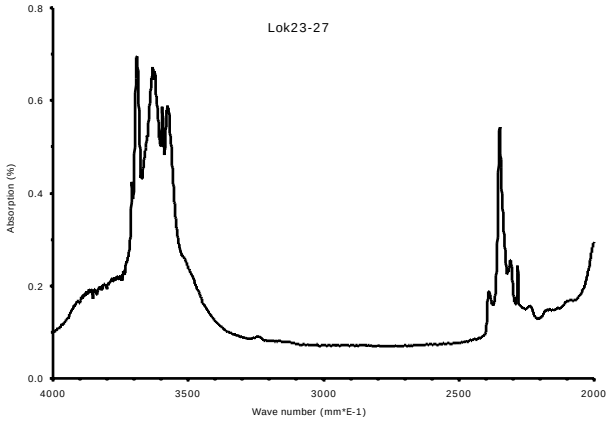
Lok23-27
Absorption (%)
Wave number (mm*E-1)

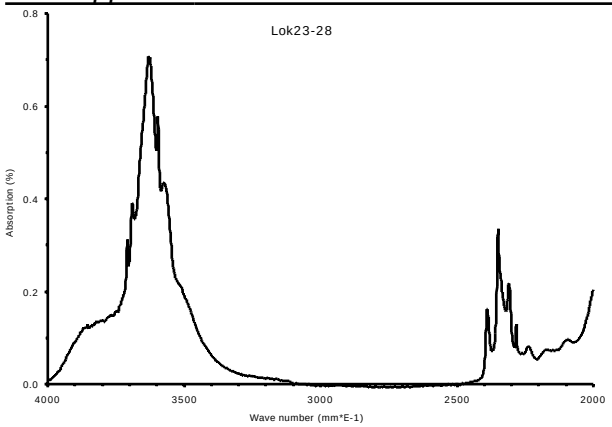
Lok23-28
Absorption (%)
0.0
0.2
0.4
0.6
0.8
4000
3500
3000
2500
2000
Wave number (mm*E-1)

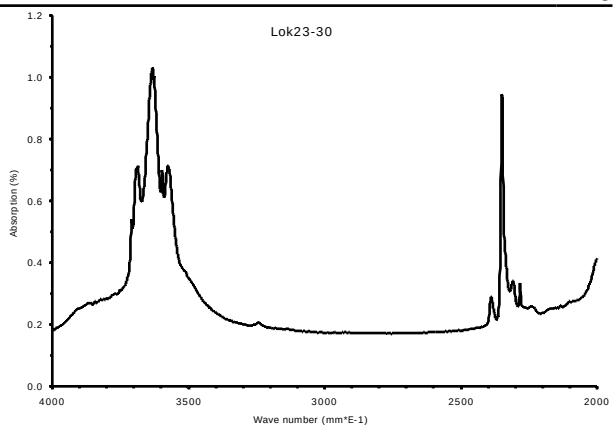
Lok23-30
Absorption (%)
0.0
0.2
0.4
0.6
0.8
1.0
1.2
4000
3500
3000
2500
2000
Wave number (mm*E-1)

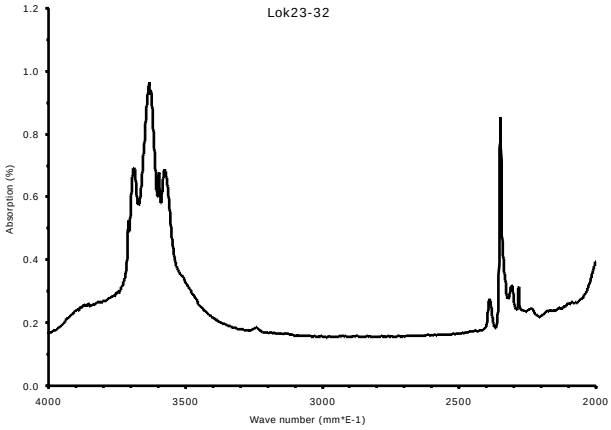
Lok23-32
Absorption (%)
0.0
0.2
0.4
0.6
0.8
1.0
1.2
4000
3500
3000
2500
2000
Wave number (mm*E-1)

AMS measurements in the Ludwigshöhe–Pluton

The most important parameters of the AMS ellipspod, such as the shape factor T, the corrected anisotropy factor P' the average magnetic susceptibility κ, as well as the orientation of the magnetic foliation (dip direction / dip angle) and lineation (trend / plunge) together with their standard deviation and eigen values, respectively, are presented here for the four sample factions "granite", "granite with schliere" (g. w. schliere), "schliere" and "enclave".

	N-S coords.	E-W coords.	n	Ave. T	St. dev.	Ave. P'	St. dev.
Granite							
Lok5.1	5507670	3475290	7	0.624	0.145	1.425	0.089
G. w. schliere							
Lok5.2	5507670	3475290	7	0.716	0.211	1.485	0.130
Schliere							
Lok5.3	5507670	3475290	4	0.749	0.088	1.433	0.039
Enclave							
Lok46	5507100	3474670	15	0.767	0.059	1.112	0.010

	Ave. κ (SI)	St. dev.	Mag. Fol.	Eigenvalue	Mag. Lin.	Eigenvalue
Granite						
Lok5.1	4.36E-01	2.58E-01	162/79	0.9483	251/12	0.7255
G. w. schliere						
Lok5.2	4.08E-01	2.71E-01	161/77	0.8821	072/08	0.7085
Schliere						
Lok5.3	2.52E-01	1.85E-02	170/78	0.9976	082/12	0.9527
Enclave						
Lok46	6.56E-03	1.63E-04	157/61	0.9951	074/13	0.9892

Strain measurements for the Ludwigshöhe-Pluton

The presented data were determined with the computer program “TRISEC”.

LOK5.1 GRANITE

STRAIN ANALYSES AT K-FELDSPAR PHENOCRYSTS (POLISHED SECTION)

N-S COORDINATE: 5507670; E-W COORDINATE: 3475290

SECTION 1 DIP 74 STRIKE 345 PITCH OF ELLIPSE LONG AXIS 126 ELLIPSE RATIO 1.600
SECTION 2 DIP 31 STRIKE 103 PITCH OF ELLIPSE LONG AXIS 152 ELLIPSE RATIO 1.500
SECTION 3 DIP 64 STRIKE 247 PITCH OF ELLIPSE LONG AXIS 139 ELLIPSE RATIO 1.500
2.2876043
3.6752040
1.1688138

PRODUCT OF ADJUSTMENT FACTORS 2.3287

SECTION 1 ADJUSTMENT ELLIPSE RATIO 1.325
SECTION 2 ADJUSTMENT ELLIPSE RATIO 1.325
SECTION 3 ADJUSTMENT ELLIPSE RATIO 1.325

MATRIX REPRESENTING ELLIPSOID

0.630 -0.101 0.070
-0.101 0.355 -0.166
0.070 -0.166 0.435

AXIS NUMBER 1 TREND 83 PLUNGE 36 LENGTH 2.129
AXIS NUMBER 2 TREND 216 PLUNGE 43 LENGTH 1.446
AXIS NUMBER 3 TREND 332 PLUNGE 26 LENGTH 1.177

X:Y:Z = 1.809: 1.229: 1.000 LODES PARAMETER = -0.305

ES VALUE = 0.477

TECTONIC CLEAVAGE AS DEFINED BY X:Y PLANE HAS STRIKE 62 AND DIP 64

LOK5.1 GRANITE

STRAIN ANALYSES AT PLAGIOCLASE CRYSTALS (THIN SECTION)

N-S COORDINATE: 5507670; E-W COORDINATE: 3475290

SECTION 1 DIP 74 STRIKE 345 PITCH OF ELLIPSE LONG AXIS 119 ELLIPSE RATIO 1.300
SECTION 2 DIP 31 STRIKE 103 PITCH OF ELLIPSE LONG AXIS 39 ELLIPSE RATIO 1.300
SECTION 3 DIP 64 STRIKE 247 PITCH OF ELLIPSE LONG AXIS 159 ELLIPSE RATIO 1.350
2.2876043
3.6752040
1.1688138

PRODUCT OF ADJUSTMENT FACTORS 0.8430

SECTION 1 ADJUSTMENT ELLIPSE RATIO 0.945
SECTION 2 ADJUSTMENT ELLIPSE RATIO 0.945
SECTION 3 ADJUSTMENT ELLIPSE RATIO 0.945

MATRIX REPRESENTING ELLIPSOID

0.952 0.011 0.126
0.011 0.772 -0.361
0.126 -0.361 0.941

AXIS NUMBER 1 TREND 104 PLUNGE 39 LENGTH 1.459
AXIS NUMBER 2 TREND 216 PLUNGE 7 LENGTH 1.032
AXIS NUMBER 3 TREND 332 PLUNGE 298 LENGTH 0.892

X:Y:Z = 1.636: 1.156: 1.000 LODES PARAMETER = -0.410

ES VALUE = 0.418

TECTONIC CLEAVAGE AS DEFINED BY X:Y PLANE HAS STRIKE 28 AND DIP 40

LOK5.1 SCHLIERE

STRAIN ANALYSES AT PLAGIOCLASE CRYSTALS (THIN SECTION)

N-S COORDINATE: 5507670; E-W COORDINATE: 3475290

SECTION 1 DIP 74 STRIKE 345 PITCH OF ELLIPSE LONG AXIS 112 ELLIPSE RATIO 1.450
SECTION 2 DIP 31 STRIKE 103 PITCH OF ELLIPSE LONG AXIS 37 ELLIPSE RATIO 1.400
SECTION 3 DIP 64 STRIKE 247 PITCH OF ELLIPSE LONG AXIS 154 ELLIPSE RATIO 1.400
2.2876043
3.6752040
1.1688138

PRODUCT OF ADJUSTMENT FACTORS 0.8114

SECTION 1 ADJUSTMENT ELLIPSE RATIO 0.933
SECTION 2 ADJUSTMENT ELLIPSE RATIO 0.933
SECTION 3 ADJUSTMENT ELLIPSE RATIO 0.933

MATRIX REPRESENTING ELLIPSOID

0.999 0.034 0.112
0.034 0.747 -0.445
0.112 -0.445 0.843

AXIS NUMBER 1 TREND 102 PLUNGE 42 LENGTH 1.735
AXIS NUMBER 2 TREND 196 PLUNGE 5 LENGTH 1.000
AXIS NUMBER 3 TREND 291 PLUNGE 48 LENGTH 0.892

X:Y:Z = 1.946: 1.122: 1.000 LODES PARAMETER = -0.654

ES VALUE = 0.643

TECTONIC CLEAVAGE AS DEFINED BY X:Y PLANE HAS STRIKE 21 AND DIP 42

LOK5.1 GRANITE

STRAIN ANALYSES AT QUARTZ CRYSTALS (THIN SECTION)

N-S COORDINATE: 5507670; E-W COORDINATE: 3475290

SECTION 1 DIP 74 STRIKE 345 PITCH OF ELLIPSE LONG AXIS 106 ELLIPSE RATIO 1.700
SECTION 2 DIP 31 STRIKE 103 PITCH OF ELLIPSE LONG AXIS 28 ELLIPSE RATIO 2.050
SECTION 3 DIP 64 STRIKE 247 PITCH OF ELLIPSE LONG AXIS 170 ELLIPSE RATIO 1.700
2.2876043
3.6752040
1.1688138

PRODUCT OF ADJUSTMENT FACTORS 0.5316

SECTION 1 ADJUSTMENT ELLIPSE RATIO 0.810
SECTION 2 ADJUSTMENT ELLIPSE RATIO 0.810
SECTION 3 ADJUSTMENT ELLIPSE RATIO 0.810

MATRIX REPRESENTING ELLIPSOID

1.198 0.128 0.139
0.128 0.442 -0.582
0.139 -0.582 0.910

AXIS NUMBER 1 TREND 101 PLUNGE 34 LENGTH 7.064
AXIS NUMBER 2 TREND 201 PLUNGE 15 LENGTH 0.910
AXIS NUMBER 3 TREND 311 PLUNGE 52 LENGTH 0.870

X:Y:Z = 8.124: 1.047: 1.000 LODES PARAMETER = -0.956

ES VALUE = 2.366

TECTONIC CLEAVAGE AS DEFINED BY X:Y PLANE HAS STRIKE 41 AND DIP 38

LOK5.2 ENCLAVES

STRAIN ANALYSES AT MICRODIORITIC ENCLAVES (PHOTOGRAPHS)

N-S COORDINATE: 5507670; E-W COORDINATE: 3475290

SECTION 1 DIP 74 STRIKE 345 PITCH OF ELLIPSE LONG AXIS 92 ELLIPSE RATIO 2.000
SECTION 2 DIP 40 STRIKE 84 PITCH OF ELLIPSE LONG AXIS 87 ELLIPSE RATIO 2.000
SECTION 3 DIP 48 STRIKE 264 PITCH OF ELLIPSE LONG AXIS 164 ELLIPSE RATIO 2.400
1.5627974
9.5667722
1.5801322

PRODUCT OF ADJUSTMENT FACTORS 0.3459

SECTION 1 ADJUSTMENT ELLIPSE RATIO 0.686
SECTION 2 ADJUSTMENT ELLIPSE RATIO 0.686
SECTION 3 ADJUSTMENT ELLIPSE RATIO 0.686

MATRIX REPRESENTING ELLIPSOID

1.849 -0.690 1.019
-0.690 1.239 -0.851
1.019 -0.851 1.220

AXIS NUMBER 1 TREND 121 PLUNGE 54 LENGTH 1.827
AXIS NUMBER 2 TREND 227 PLUNGE 11 LENGTH 1.103
AXIS NUMBER 3 TREND 324 PLUNGE 34 LENGTH 0.560

X:Y:Z = 3.261: 1.969: 1.000 LODES PARAMETER = 0.146

ES VALUE = 0.803

TECTONIC CLEAVAGE AS DEFINED BY X:Y PLANE HAS STRIKE 54 AND DIP 56

LOK5.2 GRANITE

STRAIN ANALYSES AT K-FELDSPAR PHENOCRYSTS (POLISHED SECTIONS)

N-S COORDINATE: 5507670; E-W COORDINATE: 3475290

SECTION 1 DIP 74 STRIKE 345 PITCH OF ELLIPSE LONG AXIS 68 ELLIPSE RATIO 1.500
SECTION 2 DIP 79 STRIKE 142 PITCH OF ELLIPSE LONG AXIS 70 ELLIPSE RATIO 1.600
SECTION 3 DIP 18 STRIKE 269 PITCH OF ELLIPSE LONG AXIS 143 ELLIPSE RATIO 1.600
1.0513370
4.1278337
5.1885498

PRODUCT OF ADJUSTMENT FACTORS 1.1762

SECTION 1 ADJUSTMENT ELLIPSE RATIO 1.056
SECTION 2 ADJUSTMENT ELLIPSE RATIO 1.056
SECTION 3 ADJUSTMENT ELLIPSE RATIO 1.056

MATRIX REPRESENTING ELLIPSOID

1.324 -0.367 0.155
-0.367 1.104 -0.385
0.155 -0.385 0.642

AXIS NUMBER 1 TREND 83 PLUNGE 59 LENGTH 1.541
AXIS NUMBER 2 TREND 220 PLUNGE 24 LENGTH 1.038
AXIS NUMBER 3 TREND 319 PLUNGE 19 LENGTH 0.763

X:Y:Z = 2.020: 1.361: 1.000 LODES PARAMETER = -0.124

ES VALUE = 0.521

TECTONIC CLEAVAGE AS DEFINED BY X:Y PLANE HAS STRIKE 49 AND DIP 71

LOK5.2 GRANITE

STRAIN ANALYSES AT PLAGIOCLASE CRYSTALS (THIN SECTIONS)

N-S COORDINATE: 5507670; E-W COORDINATE: 3475290

SECTION 1 DIP 74 STRIKE 345 PITCH OF ELLIPSE LONG AXIS 28 ELLIPSE RATIO 1.600
SECTION 2 DIP 79 STRIKE 142 PITCH OF ELLIPSE LONG AXIS 109 ELLIPSE RATIO 1.400
SECTION 3 DIP 18 STRIKE 269 PITCH OF ELLIPSE LONG AXIS 138 ELLIPSE RATIO 1.400
1.0513370
4.1278337
5.1885498

PRODUCT OF ADJUSTMENT FACTORS 0.8347

SECTION 1 ADJUSTMENT ELLIPSE RATIO 0.942
SECTION 2 ADJUSTMENT ELLIPSE RATIO 0.942
SECTION 3 ADJUSTMENT ELLIPSE RATIO 0.942

MATRIX REPRESENTING ELLIPSOID

1.037 -0.303 0.318
-0.303 0.768 -0.037
-0.318 -0.037 0.734

AXIS NUMBER 1 TREND 44 PLUNGE 38 LENGTH 1.568
AXIS NUMBER 2 TREND 268 PLUNGE 43 LENGTH 1.126
AXIS NUMBER 3 TREND 154 PLUNGE 24 LENGTH 0.863

X:Y:Z = 1.818: 1.305: 1.000 LODES PARAMETER = -0.108

ES VALUE = 0.440

TECTONIC CLEAVAGE AS DEFINED BY X:Y PLANE HAS STRIKE 244 AND DIP 66

LOK5.2 SCHLIERE

STRAIN ANALYSES AT PLAGIOCLASE CRYSTALS (THIN SECTIONS)

N-S COORDINATE: 5507670; E-W COORDINATE: 3475290

SECTION 1 DIP 74 STRIKE 345 PITCH OF ELLIPSE LONG AXIS 92 ELLIPSE RATIO 1.450
SECTION 2 DIP 79 STRIKE 142 PITCH OF ELLIPSE LONG AXIS 77 ELLIPSE RATIO 1.300
SECTION 3 DIP 18 STRIKE 269 PITCH OF ELLIPSE LONG AXIS 145 ELLIPSE RATIO 1.350
1.0513370
4.1278337
5.1885498

PRODUCT OF ADJUSTMENT FACTORS 1.4705

SECTION 1 ADJUSTMENT ELLIPSE RATIO 1.137
SECTION 2 ADJUSTMENT ELLIPSE RATIO 1.137
SECTION 3 ADJUSTMENT ELLIPSE RATIO 1.137

MATRIX REPRESENTING ELLIPSOID

0.963 -0.121 0.100
-0.121 0.853 -0.096
0.100 -0.096 0.506

AXIS NUMBER 1 TREND 127 PLUNGE 76 LENGTH 1.458
AXIS NUMBER 2 TREND 235 PLUNGE 4 LENGTH 1.134
AXIS NUMBER 3 TREND 326 PLUNGE 14 LENGTH 0.965

X:Y:Z = 1.510: 1.175: 1.000 LODES PARAMETER = -0.217

ES VALUE = 0.318

TECTONIC CLEAVAGE AS DEFINED BY X:Y PLANE HAS STRIKE 56 AND DIP 76

LOK5.2 SCHLIERE

STRAIN ANALYSES AT BIOTITE CRYSTALS (THIN SECTIONS)

N-S COORDINATE: 5507670; E-W COORDINATE: 3475290

SECTION 1 DIP 74 STRIKE 345 PITCH OF ELLIPSE LONG AXIS 94 ELLIPSE RATIO 1.750
SECTION 2 DIP 79 STRIKE 142 PITCH OF ELLIPSE LONG AXIS 77 ELLIPSE RATIO 2.200
SECTION 3 DIP 18 STRIKE 269 PITCH OF ELLIPSE LONG AXIS 145 ELLIPSE RATIO 2.400
1.0513370
4.1278337
5.1885498

PRODUCT OF ADJUSTMENT FACTORS 1.8445

SECTION 1 ADJUSTMENT ELLIPSE RATIO 1.226
SECTION 2 ADJUSTMENT ELLIPSE RATIO 1.226
SECTION 3 ADJUSTMENT ELLIPSE RATIO 1.226

MATRIX REPRESENTING ELLIPSOID

1.255 -0.790 0.375
-0.790 1.605 -0.423
0.375 -0.423 0.487

AXIS NUMBER 1 TREND 146 PLUNGE 73 LENGTH 1.773
AXIS NUMBER 2 TREND 40 PLUNGE 5 LENGTH 1.267
AXIS NUMBER 3 TREND 309 PLUNGE 16 LENGTH 0.645

X:Y:Z = 2.750: 1.965: 1.000 LODES PARAMETER = 0.335

ES VALUE = 0.674

TECTONIC CLEAVAGE AS DEFINED BY X:Y PLANE HAS STRIKE 39 AND DIP 74

LOK5.3 GRANITE

STRAIN ANALYSES AT K-FELDSPAR PHENOCRYSTS (POLISHED SECTIONS)

N-S COORDINATE: 5507670; E-W COORDINATE: 3475290

SECTION 1 DIP 74 STRIKE 345 PITCH OF ELLIPSE LONG AXIS 62 ELLIPSE RATIO 1.700
SECTION 2 DIP 66 STRIKE 101 PITCH OF ELLIPSE LONG AXIS 61 ELLIPSE RATIO 1.400
SECTION 3 DIP 43 STRIKE 220 PITCH OF ELLIPSE LONG AXIS 52 ELLIPSE RATIO 1.450
1.3648370
1.8351125
2.4304739

PRODUCT OF ADJUSTMENT FACTORS 0.4067

SECTION 1 ADJUSTMENT ELLIPSE RATIO 0.741
SECTION 2 ADJUSTMENT ELLIPSE RATIO 0.741
SECTION 3 ADJUSTMENT ELLIPSE RATIO 0.741

MATRIX REPRESENTING ELLIPSOID

1.251 -0.161 0.104
-0.161 0.828 -0.121
-0.104 -0.121 0.554

AXIS NUMBER 1 TREND 63 PLUNGE 63 LENGTH 1.448
AXIS NUMBER 2 TREND 255 PLUNGE 26 LENGTH 1.087
AXIS NUMBER 3 TREND 163 PLUNGE 5 LENGTH 0.873

X:Y:Z = 1.658: 1.244: 1.000 LODES PARAMETER = -0.136

ES VALUE = 0.377

TECTONIC CLEAVAGE AS DEFINED BY X:Y PLANE HAS STRIKE 253 AND DIP 85

LOK5.3 GRANITE

STRAIN ANALYSES AT PLAGIOCLASE CRYSTALS (THIN SECTIONS)

N-S COORDINATE: 5507670; E-W COORDINATE: 3475290

SECTION 1 DIP 74 STRIKE 345 PITCH OF ELLIPSE LONG AXIS 135 ELLIPSE RATIO 1.450
SECTION 2 DIP 66 STRIKE 101 PITCH OF ELLIPSE LONG AXIS 76 ELLIPSE RATIO 1.400
SECTION 3 DIP 43 STRIKE 220 PITCH OF ELLIPSE LONG AXIS 168 ELLIPSE RATIO 1.450
1.3648370
1.8351125
2.4304739

PRODUCT OF ADJUSTMENT FACTORS 1.3666

SECTION 1 ADJUSTMENT ELLIPSE RATIO 1.110

SECTION 2 ADJUSTMENT ELLIPSE RATIO 1.110
SECTION 3 ADJUSTMENT ELLIPSE RATIO 1.110

MATRIX REPRESENTING ELLIPSOID

0.583 -0.118 0.297
-0.118 0.966 -0.169
-0.297 -0.169 0.754

AXIS NUMBER 1 TREND 179 PLUNGE 37 LENGTH 1.670
AXIS NUMBER 2 TREND 59 PLUNGE 33 LENGTH 1.143
AXIS NUMBER 3 TREND 302 PLUNGE 35 LENGTH 0.921

X:Y:Z = 1.812: 1.240: 1.000 LODES PARAMETER = -0.276

ES VALUE = 0.472

TECTONIC CLEAVAGE AS DEFINED BY X:Y PLANE HAS STRIKE 32 AND DIP 55

LOK46 ENCLAVE

STRAIN ANALYSES AT PLAGIOCLASE CRYSTALS (THIN SECTIONS)

N-S COORDINATE: 5507100; E-W COORDINATE: 3474670

SECTION 1 DIP 74 STRIKE 345 PITCH OF ELLIPSE LONG AXIS 91 ELLIPSE RATIO 1.400
SECTION 2 DIP 66 STRIKE 146 PITCH OF ELLIPSE LONG AXIS 99 ELLIPSE RATIO 1.400
SECTION 3 DIP 89 STRIKE 247 PITCH OF ELLIPSE LONG AXIS 161 ELLIPSE RATIO 1.400
60.3615479
11.6902404
1.0039716

PRODUCT OF ADJUSTMENT FACTORS 0.8017

SECTION 1 ADJUSTMENT ELLIPSE RATIO 0.929
SECTION 2 ADJUSTMENT ELLIPSE RATIO 0.929
SECTION 3 ADJUSTMENT ELLIPSE RATIO 0.929

MATRIX REPRESENTING ELLIPSOID

0.900 -0.220 -0.032
-0.220 0.521 -0.107
-0.032 -0.107 0.612

AXIS NUMBER 1 TREND 66 PLUNGE 25 LENGTH 1.645
AXIS NUMBER 2 TREND 240 PLUNGE 65 LENGTH 1.229
AXIS NUMBER 3 TREND 335 PLUNGE 2 LENGTH 0.999

X:Y:Z = 1.646: 1.230: 1.000 LODES PARAMETER = -0.169

ES VALUE = 0.376

TECTONIC CLEAVAGE AS DEFINED BY X:Y PLANE HAS STRIKE 65 AND DIP 88

LOK46 ENCLAVE

STRAIN ANALYSES AT HORNBLENDE CRYSTALS (THIN SECTIONS)

N-S COORDINATE: 5507100; E-W COORDINATE: 3474670

SECTION 1 DIP 74 STRIKE 345 PITCH OF ELLIPSE LONG AXIS 96 ELLIPSE RATIO 1.750
SECTION 2 DIP 5 STRIKE 146 PITCH OF ELLIPSE LONG AXIS 101 ELLIPSE RATIO 2.000
SECTION 3 DIP 89 STRIKE 247 PITCH OF ELLIPSE LONG AXIS 154 ELLIPSE RATIO 1.700
60.3615479
11.6902404
1.0039716

PRODUCT OF ADJUSTMENT FACTORS 0.9236

SECTION 1 ADJUSTMENT ELLIPSE RATIO 0.974
SECTION 2 ADJUSTMENT ELLIPSE RATIO 0.974
SECTION 3 ADJUSTMENT ELLIPSE RATIO 0.974

MATRIX REPRESENTING ELLIPSOID

0.877 -0.277 0.022
-0.277 0.330 -0.134
0.022 -0.134 0.373

AXIS NUMBER 1 TREND 70 PLUNGE 28 LENGTH 2.565
AXIS NUMBER 2 TREND 234 PLUNGE 61 LENGTH 1.531
AXIS NUMBER 3 TREND 336 PLUNGE 7 LENGTH 0.999

X:Y:Z = 2.567: 1.531: 1.000 LODES PARAMETER = -0.096

ES VALUE = 0.690

TECTONIC CLEAVAGE AS DEFINED BY X:Y PLANE HAS STRIKE 66 AND DIP 83